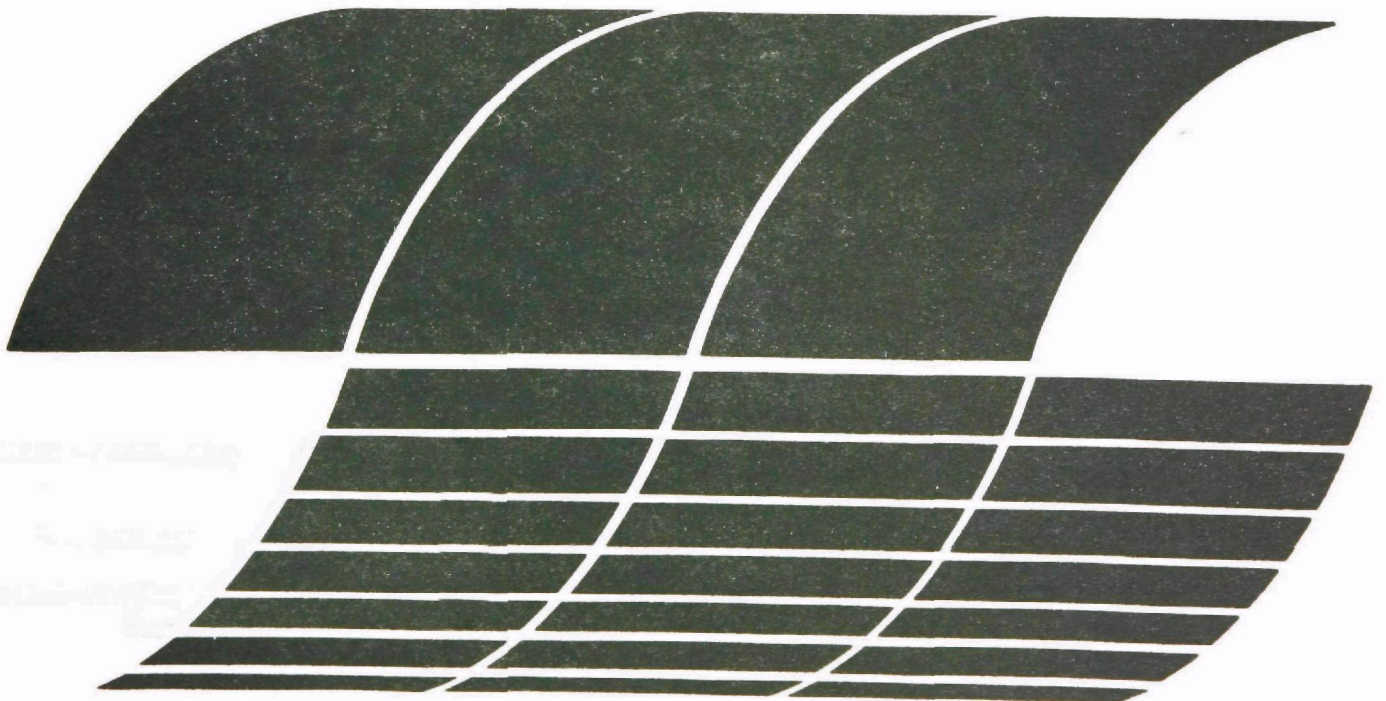




# Mobile Bed Flux Force/Condensation Scrubbers

Interagency  
Energy/Environment  
R&D Program Report



## **RESEARCH REPORTING SERIES**

Research reports of the Office of Research and Development, U.S. Environmental Protection Agency, have been grouped into nine series. These nine broad categories were established to facilitate further development and application of environmental technology. Elimination of traditional grouping was consciously planned to foster technology transfer and a maximum interface in related fields. The nine series are:

1. Environmental Health Effects Research
2. Environmental Protection Technology
3. Ecological Research
4. Environmental Monitoring
5. Socioeconomic Environmental Studies
6. Scientific and Technical Assessment Reports (STAR)
7. Interagency Energy-Environment Research and Development
8. "Special" Reports
9. Miscellaneous Reports

This report has been assigned to the INTERAGENCY ENERGY-ENVIRONMENT RESEARCH AND DEVELOPMENT series. Reports in this series result from the effort funded under the 17-agency Federal Energy/Environment Research and Development Program. These studies relate to EPA's mission to protect the public health and welfare from adverse effects of pollutants associated with energy systems. The goal of the Program is to assure the rapid development of domestic energy supplies in an environmentally-compatible manner by providing the necessary environmental data and control technology. Investigations include analyses of the transport of energy-related pollutants and their health and ecological effects; assessments of, and development of, control technologies for energy systems; and integrated assessments of a wide range of energy-related environmental issues.

## **EPA REVIEW NOTICE**

This report has been reviewed by the participating Federal Agencies, and approved for publication. Approval does not signify that the contents necessarily reflect the views and policies of the Government, nor does mention of trade names or commercial products constitute endorsement or recommendation for use.

This document is available to the public through the National Technical Information Service, Springfield, Virginia 22161.

**February 1979**

# **Mobile Bed Flux Force/Condensation Scrubbers**

by

S.C. Yung, R. Chmielewski, and S. Calvert

Air Pollution Technology, Inc.  
4901 Morena Boulevard, Suite 402  
San Diego, California 92117

Contract No. 68-02-2124  
Program Element No. EHE624A

EPA Project Officer: Dale L. Harmon

Industrial Environmental Research Laboratory  
Office of Energy, Minerals, and Industry  
Research Triangle Park, NC 27711

Prepared for

U.S. ENVIRONMENTAL PROTECTION AGENCY  
Office of Research and Development  
Washington, DC 20460

## ABSTRACT

Fine particle collection in mobile bed scrubbers has been determined experimentally. Particle collection efficiency increased greatly as the gas phase pressure drop increased. With no water vapor condensation, the performance capability of a mobile bed scrubber is less than that of a gas-atomized spray scrubber with the same pressure drop. Compared to packed bed and sieve plate scrubbers, the mobile bed has better efficiency when the pressure drop is above 20 cm W.C. The presence of limestone in the scrubber liquid has no effect on particle collection.

When the mobile bed scrubber was used as a flux force/condensation scrubber it had better performance characteristics than sieve plate and spray scrubbers with condensation. However, its capability is inferior to a F/C system consisting of a condenser and venturi scrubber.

None of the design equations reported in the literature are adequate to predict the collection efficiency and pressure drop of the mobile bed scrubber. New correlations have been developed in this study to predict particle collection and pressure drop.

Liquid entrainment characteristics have also been determined experimentally in this study. This information may be used to design high efficiency entrainment separators for mobile bed scrubbers.

This report was submitted in partial fulfillment of contract number 68-02-2124, by Air Pollution Technology, Inc. under the sponsorship of the U.S. Environmental Protection Agency. This report covers the period from November 3, 1975 to November 3, 1978.

## CONTENTS

	<u>Page</u>
Abstract . . . . .	iii
Figures. . . . .	vi
Tables . . . . .	xii
Abbreviations and Symbols. . . . .	xv
Acknowledgment . . . . .	xix

### Sections

1. Summary and Conclusions . . . . .	1
Summary. . . . .	1
Conclusions. . . . .	16
2. Introduction. . . . .	19
3. Preliminary Studies . . . . .	22
Entrainment Measurements . . . . .	22
4. Mobile Bed F/C Scrubber Pilot Plant . . . . .	55
Mobile Bed F/C Scrubber Pilot Plant. . . . .	55
Instrumentation and Calibration. . . . .	67
Particle Generator . . . . .	68
Particulate Sampling System. . . . .	68
Data Reduction Methods . . . . .	70
5. Experiments . . . . .	75
Experimental Conditions Studied. . . . .	75
Experimental Procedures. . . . .	77
Experimental Results . . . . .	79
Discussions. . . . .	79

## CONTENTS (continued)

	<u>Page</u>
6. Mathematical Modeling . . . . .	122
Literature Search. . . . .	122
Comparison of Experimental Data with Predictions. . . . .	142
Mathematical Modeling. . . . .	148
F/C Scrubbing. . . . .	152
7. Evaluation of the Mobile Bed Scrubber . . . . .	174
Particle Scrubbing . . . . .	174
Mobile Bed as a F/C Scrubber . . . . .	176
Potential for Power Plant Application. . . . .	184
Mobile Bed Scrubber Design Recommendations . . . . .	188
8. Future Research Recommendations . . . . .	191
References . . . . .	198

### Appendices

A	DC-1 Drop Counter Entrainment Data. . . . .	202
B	Test Conditions and Particle Data . . . . .	210
C	Grade Penetration Curves for Cold Operation Mode. . . . .	217
D	Slurry Scrubbing Penetration Curves . . . . .	235
E	Grade Penetration Curves for F/C Runs . . . . .	237

## FIGURES

<u>Number</u>		<u>Page</u>
1	Cut/power relationship for scrubbers. . . . .	14
2	Mobile bed scrubber system for entrainment measurement . . . . .	23
3	Entrainment measurement sampling train. . . . .	29
4	Comparison between cascade impactor and DC-1 drop counter data . . . . .	33
5	Sketch of experimental equipment. . . . .	35
6	"Dry salt" particle size distribution. . . . .	36
7	Predicted drop size distribution as a function of water evaporated . . . . .	38
8	Measured wet size distributions, U. of W. impactor and series glass impactor. . . . .	39
9	Experimental setup for glass impactors. . . . .	41
10	Wet size distribution obtained with glass impactors . . . . .	42
11	Comparison between cascade impactor and DC-1 drop counter data. . . . .	44
12	Mass median drop diameter of entrainment from mobile bed scrubber (Drop counter data). . . . .	49
13	Cumulative entrainment loading (Drop counter data) . . . . .	50
14	Cumulative entrainment loading (Drop counter data) . . . . .	51
15	Cumulative entrainment loading (Drop counter data) . . . . .	52
16	Entrainment flow rate (Drop counter data) . . . . .	54

## FIGURES (continued)

<u>Number</u>		<u>Page</u>
17	Process flow diagram of mobile bed F/C scrubber system. . . . .	56
18	Mobile bed layout. . . . .	59
19	Mobile bed and entrainment separator . . . . .	60
20	Cooling tower framing and mobile bed sumps. . . . .	61
21	Quencher, furnace and blower vibration mounts. . . . .	62
22	Mobile bed platform and cooling tower piping elevation . . . . .	63
23	Mobile bed scrubber. . . . .	64
24	Powder redispersion particle generator . . . . .	69
25	Pressure drop across one stage of a mobile bed versus gas velocity with liquid velocity as parameter . . . . .	80
26	Experimental pressure drop of a 3-stage mobile bed with hardware screen support. . . . .	83
27	The variation of pressure drop with liquid- to-gas ratio and air velocity. . . . .	85
28	Effects of bed depth and number of stages on pressure drop. . . . .	86
29	Effect of packing diameter on pressure drop. . . . .	87
30	Pressure drop vs. superficial gas velocity for 3-stage mobile bed with plastic net support. . . . .	88
31	Pressure drop across four plastic net supports . . . . .	90
32	Pressure drop due to liquid holdup and weight of packing. . . . .	91



## FIGURES (continued)

<u>Number</u>		<u>Page</u>
33	Experimental grade penetration curves. . . . .	92
34	Experimental grade penetration curves. . . . .	93
35	Experimental grade penetration curves. . . . .	94
36	1-stage and 3-stage mobile bed scrubber performance. . . . .	96
37	Penetration curves from interstage sampling . . . . .	97
38	Experimental cut/power relationship for the mobile bed scrubber. . . . .	99
39	Comparison between published mobile bed performance data with present study. . . . .	100
40	The variation of bed expansion with liquid-to-gas ratio. . . . .	102
41	The variation of bed expansion with liquid-to-gas ratio. . . . .	103
42	Effect of packing diameter on bed expansion. . . . .	104
43	The variation of minimum fluidization velocity with liquid flow rate . . . . .	106
44	The variation of minimum fluidization velocity with packing sphere diameter. . . . .	107
45	Effects of slurry on pressure drop . . . . .	108
46	Slurry scrubbing test data . . . . .	109
47	F/C scrubbing pressure drop. . . . .	111
48	The variation of cut diameter with condensation ratio . . . . .	112
49	Penetration for 1.0 $\mu$ m diameter particle versus condensation ratio . . . . .	113

## FIGURES (continued)

<u>Number</u>	<u>Page</u>
50	The grown particle experimental setup . . . . . 118
51	The predicted and measured particle grown size distribution . . . . . 121
52	Typical pressure drop - flow characteristics in conventional packed towers . . . . . 124
53	Region of mobile bed operation mode . . . . . 126
54	Predicted and measured pressure drop (Chen and Douglas's correlation). . . . . 143
55	Predicted and measured pressure drop (Woźniak's correlation) . . . . . 144
56	Predicted and measured pressure drop (Kito et al.'s correlation) . . . . . 145
57	Predicted and measured pressure drop (Uchida et al.'s correlation) . . . . . 146
58	Measured and predicted pressure drop for a three stage mobile bed scrubber with hardware screen support, and each stage packed with 3.8 cm dia. spheres to a depth of 23 cm. . . . . 147
59	Comparison between measured and predicted mobile bed pressure drop. . . . . 150
60	Pressure drop through a single stage of a mobile bed obtained at EPA/TVA Shawnee plant . . . . . 151
61	Generalized F/C scrubber system . . . . . 154
62	Scrubber penetration for different scrubber stages . . . . . 166
63	Initial and grown particle size distribution. . . . . 168
64	The penetration curve for Runs No. FC-7 and FC-8 . . . . . 169

## FIGURES (continued)

<u>Number</u>	<u>Page</u>
65	The penetration curve for Runs No. FC-7 and FC-8. . . . . 170
66	Predicted and measured particle penetration for Run No. FC-23. . . . . 171
67	Predicted and measured penetration for 1.0 $\mu$ m diameter particle versus condensation ratio. . . . . 172
68	Predicted and measured variation of cut diameter with condensation ratio . . . . . 173
69	Cut/power relationship for scrubbers . . . . . 175
70	Comparison between mobile F/C and sieve plate F/C scrubber performance . . . . . 178
71	Comparison between mobile bed F/C and sieve plate F/C scrubber performance . . . . . 179
72	Comparison between mobile bed F/C and spray F/C scrubber performance . . . . . 181
73	Typical process design of a F/C scrubber system . . . . . 182
74	Typical fly ash distribution and grown size distribution . . . . . 186
75	Predicted mobile bed and F/C mobile bed scrubber performance . . . . . 187

## Appendices

C-1 through C-67	Experimental grade penetration curves. . . . .	218-234
D-1 through D-4	Experimental penetration curves. . . . .	236

# FIGURES (continued)

<u>Number</u>		<u>Page</u>
E-1	The penetration curve for Runs No. FC-1, FC-2, and FC-3 . . . . .	238
E-2	The penetration curve for Runs No. FC-4 and FC-5 . . . . .	238
E-3	The penetration curve for Run No. FC-6 . . . . .	238
E-4	The penetration curve for Runs No. FC-7 and FC-8 . . . . .	238
E-5	The penetration curve for Runs No. FC-9 and FC-10. . . . .	239
E-6	The penetration curve for Runs No. FC-11, FC-12, and FC-13 . . . . .	239
E-7	The penetration curve for Runs No. FC-14, FC-15, and FC-16 . . . . .	239
E-8	The penetration curve for Runs No. FC-17 and FC-20. . . . .	239
E-9	The penetration curve for Runs No. FC-18 and FC-19. . . . .	240
E-10	The penetration curve for Runs No. FC-21 and FC-22. . . . .	240
E-11	The penetration curves for Runs No. FC-23, FC-24 and FC-25. . . . .	240
E-12	The penetration curves for Runs No. FC-26 and FC-27. . . . .	240

## TABLES

<u>Number</u>		<u>Page</u>
1	Pressure Drop Correlations . . . . .	8
2	Cut/Power Relationships. . . . .	13
3	Drop Diameter Interval for DC-1 Drop Counter . . . . .	25
4	Preliminary Entrainment Measurement Scrubber Operating Conditions . . . . .	31
5	DC-1 Drop Counter Entrainment Data and Scrubber Operating Conditions . . . . .	46
6	List of Pilot Plant Components . . . . .	57
7	Flowrates and Conditions for Mobile Bed F/C Scrubber Pilot Plant . . . . .	58
8	Particle Count Results . . . . .	115
9	Particle Growth Data . . . . .	120

## Appendices

A-1	DC-1 Drop Counter Data for Run No. DC-1. . . . .	203
A-2	DC-1 Drop Counter Data for Run No. DC-2. . . . .	203
A-3	DC-1 Drop Counter Data for Run No. DC-3. . . . .	203
A-4	DC-1 Drop Counter Data for Run No. DC-4. . . . .	203
A-5	DC-1 Drop Counter Data for Run No. DC-5. . . . .	204
A-6	DC-1 Drop Counter Data for Run No. DC-6. . . . .	204
A-7	DC-1 Drop Counter Data for Run No. DC-7. . . . .	204
A-8	DC-1 Drop Counter Data for Run No. DC-8. . . . .	204
A-9	DC-1 Drop Counter Data for Run No. DC-9. . . . .	205

# TABLES (continued)

<u>Number</u>		<u>Page</u>
A-10	DC-1 Drop Counter Data for Run No. FC-10 . . . . .	205
A-11	DC-1 Drop Counter Data for Run No. FC-11 . . . . .	205
A-12	DC-1 Drop Counter Data for Run No. FC-12 . . . . .	205
A-13	DC-1 Drop Counter Data for Run No. FC-13 . . . . .	206
A-14	DC-1 Drop Counter Data for Run No. FC-14 . . . . .	206
A-15	DC-1 Drop Counter Data for Run No. FC-15 . . . . .	206
A-16	DC-1 Drop Counter Data for Run No. FC-16 . . . . .	206
A-17	DC-1 Drop Counter Data for Run No. FC-17 . . . . .	207
A-18	DC-1 Drop Counter Data for Run No. FC-18 . . . . .	207
A-19	DC-1 Drop Counter Data for Run No. FC-19 . . . . .	207
A-20	DC-1 Drop Counter Data for Run No. FC-20 . . . . .	207
A-21	DC-1 Drop Counter Data for Run No. FC-21 . . . . .	208
A-22	DC-1 Drop Counter Data for Run No. FC-22 . . . . .	208
A-23	DC-1 Drop Counter Data for Run No. FC-23 . . . . .	208
A-24	DC-1 Drop Counter Data for Run No. FC-24 . . . . .	208
A-25	DC-1 Drop Counter Data for Run No. FC-25 . . . . .	209
A-26	DC-1 Drop Counter Data for Run No. FC-26 . . . . .	209
A-27	DC-1 Drop Counter Data for Run No. FC-27 . . . . .	209
A-28	DC-1 Drop Counter Data for Run No. FC-28 . . . . .	209
B-1	Test Conditions and Particle Data. . . . .	211
B-2	Test Conditions and Particle Data. . . . .	211
B-3	Test Conditions and Particle Data. . . . .	211

# TABLES (continued)

<u>Number</u>		<u>Page</u>
B-4	Test Conditions and Particle Data. . . . .	212
B-5	Test Conditions and Particle Data. . . . .	213
B-6	Test Conditions and Particle Data. . . . .	213
B-7	Test Conditions and Particle Data. . . . .	214
B-8	Test Conditions and Particle Data. . . . .	214
B-9	Slurry Scrubbing Test Conditions and Particle Data. . . . .	215
B-10	F/C Scrubbing Test Conditions and Particle Data. . . . .	216
B-11	F/C Scrubbing Test Conditions and Particle Data. . . . .	216

## ABBREVIATIONS AND SYMBOLS

$A_p$	= cross-sectional area of scrubber, $\text{cm}^2$
$a$	= interfacial area of packing, $\text{cm}^2/\text{cm}^3$
$a_b$	= geometrical surface area of static bed per unit volume of static packing, $\text{cm}^2/\text{cm}^3$
$a_t$	= interfacial area for transfer volume of scrubber, $\text{cm}^2/\text{cm}^3$
$C'$	= Cunningham slip factor, dimensionless
$c$	= salt concentration in solution, $\text{g}/\text{cm}^3$
$c_p$	= particle mass loading, $\text{g}/\text{DNm}^3$
$c_{pi}$	= inlet particle mass loading, $\text{g}/\text{DNm}^3$
$c_{po}$	= outlet particle mass loading, $\text{g}/\text{DNm}^3$
$c_{pp}$	= heat capacity of particle, $\text{cal}/\text{g}^\circ\text{K}$
$c_{pt}$	= total particle loading, $\text{g}/\text{DNm}^3$
$D_c$	= column diameter, cm
$D_G$	= Diffusivity of water vapor in carrier gas, $\text{cm}^2/\text{s}$
$d_b$	= ball or packing diameter, cm
$d_d$	= drop diameter, $\mu\text{m}$ or cm
$d_{dM}$	= mass median drop diameter, $\mu\text{m}$ or cm
$d_{dN}$	= number median drop diameter, $\mu\text{m}$ or cm
$d_e$	= equivalent diameter of the grid opening, cm
$d_h$	= hole diameter, cm
$d_m$	= mass mean diameter, cm or $\mu\text{m}$
$d_{pa}$	= aerodynamic particle diameter, $\mu\text{m}$
$d_{pa_2}$	= grown aerodynamic particle diameter, $\mu\text{m}$
$d_{p1}$	= original physical particle diameter, $\mu\text{m}$
$d_{p2}$	= grown physical particle diameter, $\mu\text{m}$
$d_{pc}$	= cut diameter, $\mu\text{m}$
$d'_{pg}$	= physical geometric mass median diameter, cm
$d_w$	= hot wire diameter, cm
$F$	= foam density, dimensionless
$f_p$	= fraction of water vapor condensing on particles, fraction



$f_s$  = fractional open area of the supporting grid, fraction  
 $f_v$  = mole ratio of water vapor condensed, fraction  
 $G$  = gas mass velocity,  $\text{g}/\text{cm}^2\text{-s}$   
 $G_{mf}$  = minimum fluidization mass flow,  $\text{g}/\text{hr}\text{-cm}^2$   
 $g$  = acceleration of gravity,  $\text{cm}/\text{s}^2$   
 $H$  = packed column height or the distance between retaining grids, cm  
 $H_d$  = dynamic bed height, cm  
 $H_L$  = height of liquid column retained on the supporting grid, cm  
 $H_s$  = static bed height, cm  
 $H_1$  = humidity in the saturated inlet gas, g/g  
 $h_b$  = packing holdup,  $\text{cm}^3/\text{cm}^3$   
 $h_G$  = gas holdup,  $\text{cm}^3/\text{cm}^3$   
 $h_G$  = heat transfer coefficient,  $\text{kcal}/\text{cm}^2\text{-s-}^\circ\text{C}$   
 $h_L$  = liquid holdup in bed,  $\text{cm}^3/\text{cm}^3$   
 $h_{Lo}$  = liquid holdup based on fixed bed,  $\text{cm}^3/\text{cm}^3$   
 $h_{pG}$  = particle to gas heat transfer coefficient,  $\text{cal}/\text{cm}^2\text{-s-}^\circ\text{K}$   
 $h_{po}$  = packing holdup related to fixed bed,  $\text{cm}^3/\text{cm}^3$   
 $K_p$  = inertial impaction parameter, dimensionless  
 $k$  = constant characterizing the fraction of liquid being atomized, --  
 $k$  = thermal conductivity of gas,  $\text{cal}/\text{cm}^2\text{-s-}^\circ\text{K}/\text{cm}$   
 $k_G$  = mass transfer coefficient,  $\text{g}/\text{cm}^3\text{-s-atm}$   
 $k'_{pG}$  = particle to gas mass transfer coefficient,  $\text{gmol}/\text{cm}^2\text{-s-atm}$   
 $k'_G$  = mass transfer coefficient, gas to liquid,  $\text{gmol}/\text{cm}^2\text{-s-atm}$   
 $L$  = liquid mass velocity,  $\text{g}/\text{cm}^2\text{-hr-atm}$   
 $L_M$  = latent heat of vaporization for water,  $\text{cal}/\text{gmol}$   
 $M_1$  = molecular weight of water, g/mol  
 $M_2$  = molecular weight of nontransferring gas, g/mol  
 $m$  = total mass of particles, g  
 $N$  = total number of particles, #  
 $N_i$  = number of drops counted in the i'th bin, number  
 $n$  = number of mobile bed stages, --  
 $n_i$  = drop concentration corresponding to i'th bin, #/cm  
 $n_p$  = particle number concentration, #/cm<sup>3</sup>

$\overline{Pt}$  = overall penetration, fraction or percent  
 $Pt_c$  = penetration due to diffusiophoresis, fraction  
 $Pt_d$  = particle penetration for particle diameter,  $d_{pa}$ , fraction  
 $p_{BM}$  = mean partial pressure to nontransferring gas, atm  
 $p_G$  = water vapor partial pressure in bulk of gas bubble, atm  
 $p_{pi}$  = water vapor partial pressure at vapor liquid, interface, atm  
 $q'$  = condensation ratio, g/g  
 $r$  = distance in the direction of diffusion, cm  
 $r_p$  = particle radius, cm  
 $T_G$  = gas bulk temperature, °K  
 $T_L$  = temperature of liquid bulk, °K  
 $T_{pi}$  = particle interface temperature, °K  
 $t$  = time, s  
 $u_G$  = superficial gas velocity, cm/s  
 $u'_G$  = original entrainment velocity in wetted packing, cm/s  
 $u_{Gf}$  = flooding velocity, cm/s  
 $u_{Gi}$  = gas velocity in bed, cm/s  
 $u_{Gmf}$  = minimum fluidization velocity, cm/s  
 $u_{Gmfd}$  = minimum fluidization velocity of dry packing, cm/s  
 $u_L$  = superficial liquid velocity, cm/s  
 $u_{PD}$  = particle deposition by diffusiophoresis, cm/s  
 $V_s$  = volume of gas sampled, cm  
 $V_{si}$  = gas volume sampled by the i'th bin, cm<sup>3</sup>  
 $y$  = mole fraction water vapor, fraction  
 $Z$  = coordinate axis, cm

#### Latin

$\Delta P$  = pressure drop, cm W.C.  
 $\Delta P_b$  = pressure drop due to the weight of dry packing, cm W.C.  
 $\Delta P_c$  = column friction loss, cm W.C.  
 $\Delta P_f$  = supporting grid friction loss, cm W.C.  
 $\Delta P_L$  = pressure drop due to liquid froth retained on the supporting grid, cm W.C.  
 $\Delta P_{Lh}$  = pressure drop due to liquid holdup in bed, cm W.C.  
 $\Delta P_w$  = overall pressure drop across the scrubber, cm W.C.

$\rho_b$	= packing density, g/cm <sup>3</sup>
$\rho_G$	= gas density, g/cm <sup>3</sup>
$\rho_L$	= liquid density, g/cm <sup>3</sup>
$\rho_M$	= molar density of water, gmol/cm <sup>3</sup>
$\rho_p$	= particle density, g/cm <sup>3</sup>
$\rho_p$	= original particle density, g/cm <sup>3</sup>
$\rho_p$	= density of grown particle, g/cm <sup>3</sup>
$\rho_w$	= density of water, g/cm <sup>3</sup>
$\sigma_g$	= geometric standard deviation, dimensionless
$\sigma'_g$	= physical size geometric standard deviation, dimensionless
$\sigma_L$	= surface tension of liquid, dyne/cm
$\epsilon$	= porosity of static bed, fraction
$\epsilon_{mf}$	= voidage of bed at minimum fluidization velocity, dimensionless
$\mu_G$	= gas viscosity, g/cm <sup>2</sup> -s
$\mu_L$	= liquid viscosity, g/cm <sup>2</sup> -s
$\xi_f$	= experimental coefficient, dimensionless

## ACKNOWLEDGEMENT

Air Pollution Technology, Inc. wishes to express its appreciation to Mr. Dale Harmon, E.P.A. Project Officer; Dr. Leslie E. Sparks, E.P.A. previous Project Officer; and Mr. James Abbott, E.P.A. for excellent technical coordination and very helpful assistance in support of our technical effort.

## SECTION 1

### SUMMARY AND CONCLUSIONS

#### SUMMARY

A mobile bed scrubber is a three-phase contacting device which consists of several packed beds stacked inside a vessel shell. Gas flowing upward with a high velocity fluidizes the packing and liquid simultaneously flows downward through the column. The packing commonly used is 2.5 cm or 3.8 cm diameter lightweight spheres but other materials, such as lightweight plastic rings have been used (Levesh, 1968). The packing is supported and retained by nonflooding grids sufficiently far enough apart to permit turbulent and random motion of the spheres. The static packing depth is 15-60 cm (0.5 - 2 ft).

Mobile bed contactors have been used as gas absorption towers for many years. In recent years, they are also being used in the removal of sulfur dioxide and particulates from stack gases by a lime or limestone slurry. Fundamental studies on the mechanics of mobile beds such as hydrodynamics, pressure drop, liquid holdup, minimum fluidization velocity and axial liquid mixing have been conducted by a number of investigators. Prior to this work there had been no carefully performed study on the particle collection in a mobile bed scrubber.

The program which is reported here was undertaken in order to develop better information on the characteristics of the mobile bed scrubber performance and to point the way to the improvement of mobile bed scrubber design. Both experimental and theoretical investigations of mobile bed scrubber performance were made.

The objectives of this study were to:

1. Conduct an experimental study aimed at obtaining

- liquid entrainment data for the proper design of the entrainment separator.
2. Conduct an experimental study on particulate scrubbing in mobile bed scrubbers
  3. Determine the effects of lime or limestone slurry on mobile bed performance.
  4. Conduct an experimental study of flux force/condensation (F/C) scrubbing in mobile bed scrubbers.
  5. Develop engineering design equations.
  6. Evaluate mobile bed scrubbers.
  7. Develop specific research and development recommendations.

### Experimental Study

Two pilot plants were constructed. One was specifically for the study of liquid entrainment from mobile bed scrubbers. It had a maximum gas flow capacity of  $56.6 \text{ m}^3/\text{min}$  (2,000 CFM) and consisted of a single stage mobile bed scrubber, a blower, pump, supply and catch tank, and auxiliary equipment. The experiments were done with air and water at ambient temperatures. Measurements included entrainment loading and drop size distribution for various gas and liquid flow rate combinations. A hot wire anemometer and cascade impactor were used for drop sampling.

The second pilot plant was composed principally of a furnace, spray-type quencher, mobile bed scrubber, spray-type cooling tower, and two induced draft fans. The mobile bed scrubber could have a maximum of three stages housed in the scrubber shell and was designed for a maximum gas velocity of  $51 \text{ m}^3/\text{min}$  (1,800 CFM).

The pilot plant was operated in three modes: cold operation, slurry scrubbing, and F/C scrubbing. For cold operation the burner, furnace, quencher, and the cooling tower were idle. The air and water were at ambient conditions and no preconditioning was applied to either one. The effects on particle

collection efficiency of such factors as number of mobile bed stage, bed height, gas velocity, liquid-to-gas ratio, packing size, supporting grid types, and types of aerosol were determined experimentally. Particle measurements included the size distribution and concentration. Particle collection efficiency was calculated from particle data and was reported in terms of grade penetration curve.

Some experiments were made with limestone slurry in place of clear water and the effect of this change on particle collection efficiency was determined. Particle size distribution and concentration at the scrubber inlet and outlet were measured with cascade impactors. The particle penetration was computed and was related to:

1. Failure of the scrubber to collect particles.
2. Failure of the entrainment separator to collect entrained drops.
3. Particle generation by droplet evaporation.

Water condensation effects enhance fine particle scrubber collection efficiency and their influence on the mobile bed scrubber was studied. F/C scrubbing involves the saturation of the gas with water vapor and the subsequent inducement of condensation of water vapor on particles before the major collection mechanism occurs. Because condensation of water vapor on the particles increases their mass, they become more susceptible to collection by inertial impaction.

F/C scrubbing is applicable in situations where the gas is hot or where low cost waste steam is available. In the present study, hot gas was obtained by heating the air in the furnace with the natural gas burner. The gas was then saturated with water vapor in the spray quencher. Condensation of water vapor on particles was induced in the mobile bed scrubber by contacting the hot and humid gas with cold water. The improvement in collection efficiency depends on the amount of vapor condensed and the particle number concentration. These two parameters, along with the usual particle size distribution and

concentration measurements, were determined for all experiments.

### Experimental Findings

#### Liquid Entrainment -

The liquid entrainment loading measured with the hot wire anemometer was much lower than that measured with cascade impactors. Both devices measured the entrainment flow rate which increased with both the gas flow and liquid flow rates. At a constant superficial gas velocity the entrainment flow rate increased gradually with increasing liquid/gas ratio up to the flooding condition of the mobile bed. Further increases in the liquid/gas ratio beyond this value sharply increased the entrainment flow rate.

For a mobile bed scrubber operating under typical industrial conditions ( $u_G' = 2.7$  m/s and  $Q_L/Q_G = 6.7$  l/m<sup>3</sup>), the hot wire anemometer measured an entrainment flow rate of about 0.1 l/min-m<sup>2</sup>. The measured drop size distribution did not change much with operating conditions. The drop size distribution measured with the hot wire anemometer followed the log-normal distribution. The mass median diameter was about 250  $\mu$ m and the geometric standard deviation was 1.6.

#### Particle Collection -

Particle collection data for all experimental runs were reduced to plots of particle penetration versus particle diameter, commonly called grade penetration curve. Particle penetration depended only on the overall pressure drop across the scrubber and was independent of the number of scrubber stages. The grade penetration curve of a 1-stage mobile bed was the same as that of a 2-stage mobile bed if the overall pressure drops were the same.



Aerosol types had no significant effect on the scrubber collection efficiency.

A cut/power relationship has been established in this study for mobile bed scrubbers. It can be described by the following equation:

$$d_{pc} = 60.3 (\Delta P_w)^{-1.23} \quad (1)$$

where  $d_{pc}$  = scrubber performance cut diameter,  $\mu\text{m}$   
 $\Delta P_w$  = overall pressure drop across the scrubber, cm W.C.

The performance data obtained in this study are consistent with results obtained by other researchers.

#### Slurry Scrubbing -

The use of slurry as the scrubbing liquid did not affect the scrubber efficiency. A cut/power relationship for the mobile bed using slurry was identical to that determined in the cold operation mode. This indicates that increasing the liquid density by addition of limestone to the scrubber liquid does not influence the dependency of particle collection efficiency on pressure drop.

In some industrial scrubbers, the use of slurry is reported to result in lower efficiencies. This decrease in efficiency could be due to the failure of the entrainment separator to collect entrained slurry drops. In the present study, the tube bank entrainment separator had high efficiency and entrained solids were negligible.

#### F/C Scrubbing -

The use of F/C conditions greatly improved the collection efficiency for submicron particles. At a scrubber pressure drop of 13 cm W.C., the collection efficiency of the mobile bed scrubber with no F/C effect for 1  $\mu\text{m}$  diameter was less than 5%.

At the same pressure drop, the collection efficiency increased to 50% with a condensation ratio of 0.2 g/g.

Besides pressure drop, the collection efficiency of the mobile bed F/C scrubber also depended on condensation ratio and particle number concentration. High condensation ratio coupled with low particle number concentration resulted in larger grown particle size, which were more susceptible to collection by inertial impaction.

#### Pressure Drop -

The pressure drop characteristics, which represent most of the power requirement of the mobile bed, were determined experimentally in this study. The major findings are:

1. Retaining grid geometry has a profound effect on scrubber pressure drop. Under the same operating conditions, support with small openings and fractional open area caused a higher pressure drop. The higher pressure drop is probably due to the liquid froth retained on the grid.
2. Pressure drop increases with increasing static bed height, density of packing material, superficial gas velocity, and superficial liquid velocity; but it decreases with increasing packing size. For a fully fluidized mobile bed operating below flooding conditions, the dependence of pressure drop on gas velocity is small.
3. The measured pressure drop across the mobile bed with large opening supports agreed with those reported by Douglas and Snider (1963) and by Pollock, et al. (1967).

#### Engineering Design Equations

##### Pressure Drop -

For a fully fluidized mobile bed, the pressure drop is made up of the sum of those due to the dry retaining grids, the weight of the dry packings, the liquid holdup in the bed, liquid froth

retained on the grid, and the wall friction. Except for the grids with small openings and small fractional open area, the losses due to wall friction and supporting grid friction are small. There is also little liquid retained on the supporting grids. The pressure drop across the mobile bed then can be considered equal to the sum of the weight of the packing and the liquid holdup in the bed.

There are several empirical correlations reported in the literature for the prediction of pressure drop across a mobile bed. Table 1 lists four of the correlations for the calculation of pressure drop due to the weights of dry packing and liquid holdup. There are other correlations, mostly by Russian researchers, which contained constants which have to be determined experimentally for each application.

Predictions by these correlations were compared with the experimental data obtained in this study. The comparison revealed that predictions by Uchida, et al.'s correlation are much higher than that actually measured for the scrubber with large opening support grids. Predictions by Kito, et al.'s correlation and by Woźniak's correlation are better than Uchida, et al.'s correlation, but they still are higher than that measured.

Chen and Douglas' prediction agrees with the data for the scrubber with large opening support grids. However, Chen and Douglas' correlation did not predict the correct dependence of pressure drop on liquid flow rate. Compared to the experimental pressure drop data for the mobile bed with small opening supporting grids, Chen and Douglas' predictions are much lower.

Since predictions by the pressure drop correlations reported in the literature do not agree with the data obtained in this study, an empirical equation was developed through dimensional analysis. The agreement between predictions by this equation with data reported in the literature is good. The empirical equation is:

TABLE 1. PRESSURE DROP CORRELATIONS

Investigators	Correlation
Chen & Douglas (1969)	$\Delta P_w = (1-\epsilon) \rho_b H_s + h_{Lo} \rho_L H_s$ $h_{Lo} = 0.0944 d_b^{-0.5} L^{0.6} + 0.02$
Wozniak (1977)	$\Delta P_w = (1-\epsilon) \rho_b H_s + \Delta P_{Lh}$ $\Delta P_{Lh} = 476.54 \rho_G u_G^2 \left( \frac{H_s}{d_b} \right)^{0.4515} \left( \frac{d_b u_G \rho_G}{\mu_G} \right)^{1.798}$ $\left( \frac{d_b u_L \rho_L}{\mu_L} \right)^{0.8261}$
Kito, et al. (1976)	$\Delta P_w = (1-\epsilon) \rho_b H_s + h_{Lo} \rho_L H_s$ $h_{Lo} = 0.06 + 0.0316 \left( \frac{f d_e}{D'_c} \right)^{-0.84} d_b^{-0.84} \rho_b^{0.18} H_s^{-0.4} u_L$
Uchida, et al. (1977)	$\Delta P_w = (1-\epsilon) \rho_b H_s + \Delta P_{Lh}$ $\Delta P_{Lh} = 3317 \mu_L^{2.3} f_s^{-0.42} \left( \frac{d_e}{D_c} \right)^{-0.84} d_b^{-0.84} \rho_b^{0.18} H_s u_L$

$$\Delta P_w = n (\Delta P_b + \Delta P_{Lh} + \Delta P_L) + (n + 1) \Delta P_f + \Delta P_c \quad (2)$$

$$\Delta P_b = (1 - \epsilon) \rho_b H_s \quad (3)$$

$$\Delta P_{Lh} = 83.0 \rho_G u_G^2 \left( \frac{H_s}{d_b} \right)^{0.84} \left( \frac{d_b \rho_G u_G}{\mu_G} \right)^{-1.75} \left( \frac{d_b \rho_L u_L}{\mu_L} \right)^{0.96} \left( \frac{\rho_b}{\rho_L} \right)^{0.4} \quad (4)$$

$$\Delta P_L = 9.2 \times 10^{-9} \left( \frac{D_c}{f_s d_e} \right)^{2.6} u_G^{0.5} u_L^{2.0} \quad (5)$$

where:  $\Delta P_w$  = overall scrubber pressure drop, cm W.C.

$\Delta P_b$  = pressure drop due to weight of dry packing, cm W.C.

$\Delta P_{Lh}$  = pressure drop due to liquid holdup in bed, cm W.C.

$\Delta P_L$  = pressure drop due to liquid froth retained on grid, cm W.C.

$\Delta P_f$  = grid friction loss, cm W.C.

$\Delta P_c$  = column friction loss, cm W.C.

$D_c$  = column diameter, cm

$d_b$  = diameter of the packing, cm

$d_e$  = equivalent diameter of the grid opening, cm

$f_s$  = fractional open area of the retaining grid, dimensionless

$H_s$  = static bed height, cm

$n$  = number of mobile bed stages,

$u_G$  = superficial gas velocity, cm/s

$u_L$  = superficial liquid velocity, cm/s

$\rho_b$  = density of packing material, g/cm<sup>3</sup>

$\rho_G$  = gas density, g/cm<sup>3</sup>

$\rho_L$  = liquid density, g/cm<sup>3</sup>

$\epsilon$  = porosity of static bed, fraction

$\mu_G$  = gas viscosity, g/cm<sup>2</sup>-s

$\mu_L$  = liquid viscosity, g/cm<sup>2</sup>-s

" $\Delta P_f$ " and " $\Delta P_c$ " can be calculated by methods presented by Perry (1973).

## Particle Collection -

There is only one model available in the literature for particle collection in a mobile bed. It is a semi-empirical relationship presented by Bechtel Corporation in a June 1971 report on the Shawnee project for EPA and cited by Calvert, et al. (1972). This equation was based on the premise that particle collection is due to inertial impaction on balls.

Predictions of efficiency by this equation did not agree with performance data and were lower than measured. The Bechtel equation is not based on a realistic model of the particle collection mechanisms and does not account for the influence of the support grid. As mentioned earlier, the scrubber collection efficiency depends only on the pressure drop. The mobile bed scrubber with small opening supporting grids has higher pressure drop than the mobile bed with large opening supports. Consequently, the collection efficiency is higher for the mobile bed with small opening supports.

Particle collection in a mobile bed scrubber is partly due to inertial impaction on the atomized liquid drops. Thus, particle collection by this mechanism can be predicted if the atomized drop diameter and amount of liquid in drop form are known. However, the hydrodynamics of a three phase fluidized bed are extremely complex, and it was not possible to derive theoretical equations for predicting drop size and quantity of drops. Empirical approximations based on pressure drop relationships for gas atomized scrubbers were used to predict collection efficiency without success.

A new empirical equation was developed for predicting particle collection in a mobile bed scrubber. The equation developed in the present study is:

$$Pt_d = \exp \left[ -9.84 \times 10^{-4} (\Delta P_w)^{1.96} d_{pa}^{1.6} \right] \quad (6)$$

where:  $d_{pa}$  = aerodynamic particle diameter,  $\mu\text{m}$

$\Delta P_w$  = overall pressure drop, cm W.C.

$Pt_d$  = particle penetration for particle diameter " $d_{pa}$ ", fraction

In order to predict the particle collection efficiency of a mobile bed, one first predicts the pressure drop by means of equation (2) and then the performance cut diameter by means of equation (1) or (6). The penetration for other particle diameters can be calculated from equation (6).

In calculating the collection of one stage of a multi-stage scrubber, one first calculates " $Pt_d$ " for the multi-stage scrubber, and then calculates one stage penetration according to the following equation:

$$(Pt_1)^n = Pt_d \quad (7)$$

where  $Pt_1$  = penetration for one stage of a multi-stage scrubber, fraction

$n$  = number of stages, -

F/C Scrubbing-

The general theory on F/C scrubbing has been developed by Calvert, et al. (1973) and has been modified and simplified by Calvert and Gandhi (1977). By combining the theory for F/C scrubbing and the design equation for the mobile bed, the following equations were obtained which can be used to predict the particle collection performance of a F/C mobile bed scrubber.

Case 1: Condensation and particle growth occurred before the mobile bed scrubber.

$$Pt_d = \left[ 1 - \frac{0.85 q' (1 - f_p)}{0.62 + H_1} \right] \left[ \exp(-9.84 \times 10^{-4} \Delta P_w^{1.96} d_{pa_2}^{1.6}) \right] \quad (8)$$

where:

$$d_{pa_2} = d_{p_2} \left[ \left( 1 + \frac{0.165}{d_{p_2}} \right) \rho_{p_2} \right]^{0.5} \quad (9)$$

$$\rho_{p2} = \frac{f_p q' + 3.78 \times 10^{-10} n_p d_{p1}^3 \rho_{p1}^2}{f_p q' + 3.78 \times 10^{-10} n_p d_{p1}^3 \rho_{p1}} \quad (10a)$$

$$d_{p1} = \frac{0.165 + (0.0272 + 4 d_{pa}/\rho_{p1})}{2} \quad (10b)$$

$$d_{p2} = \left[ \frac{\rho_{p1}}{\rho_{p2}} (d_{p1} \times 10^{-4})^3 + \frac{6 f_p q'}{722 \pi n_p \rho_{p2}} \right]^{1/3} \times 10^4 \quad (10c)$$

where

- $d_{pa2}$  = grown aerodynamic particle diameter,  $\mu m$
- $d_{p2}$  = grown physical particle diameter,  $\mu m$
- $d_{pa}$  = original aerodynamic particle diameter,  $\mu m$
- $d_p$  = original physical particle diameter,  $\mu m$
- $f_p$  = fraction of water vapor condensing on particles, fraction
- $H$  = humidity in the saturated inlet gas, g/g
- $n_p$  = particle number concentration,  $\#/cm^3$
- $Pt_d$  = particle penetration for diameter,  $d_{pa}$ , fraction
- $q'$  = condensation ratio, g/g
- $\Delta P_w$  = overall pressure drop across mobile bed scrubber, cm W.C.
- $\rho_{p1}$  = initial particle density,  $g/cm^3$
- $\rho_{p2}$  = density of grown particle,  $g/cm^3$

Case 2: Condensation and particle growth occurred within the mobile bed scrubber.

$$Pt_d = \left[ 1 - \frac{0.85 q' (1 - f_p)}{0.62 + H_1} \right] \left[ \frac{\exp(-9.84 \times 10^{-4} \Delta P_w^{1.96} d_{pa}^{1.6})}{\left[ \exp(-9.84 \times 10^{-4} \Delta P_w^{1.96} d_{pa2}^{1.6}) \right]^{\frac{n-1}{n}}} \right]^{\frac{1}{n}} \quad (11)$$



where " $d_{pa_2}$ " is given by equation (9)

$n$  = number of mobile bed stages, -

For a " $f_p$ " of 0.15, which was determined experimentally, the predicted collection efficiency is slightly lower than that measured for large particles.

#### Evaluation of Mobile Bed Scrubber

Each scrubber type has a unique cut/power relationship which describes the dependency of scrubber performance on pressure drop. The cut/power relationships for other scrubber types are listed in Table 2 and plotted in Figure 1. The uniqueness of the cut/power relationship offers a simple method to evaluate the capabilities of different scrubber types.

TABLE 2. CUT/POWER RELATIONSHIPS

---

Gas-Atomized Scrubber:  $d_{pc} = 3.33 (\Delta P)^{-0.5}$

Packed Bed with 2.5 cm Rings:  $d_{pc} = 5.8 (\Delta P)^{-0.42}$

Sieve Plate with  $F = 0.4$  and  $d_h = 0.32$  cm:  $d_{pc} = 2.56 (\Delta P)^{-0.255}$

Note:  $d_{pc}$  = performance cut diameter,  $\mu m$

$\Delta P$  = pressure drop, cm W.C.

---

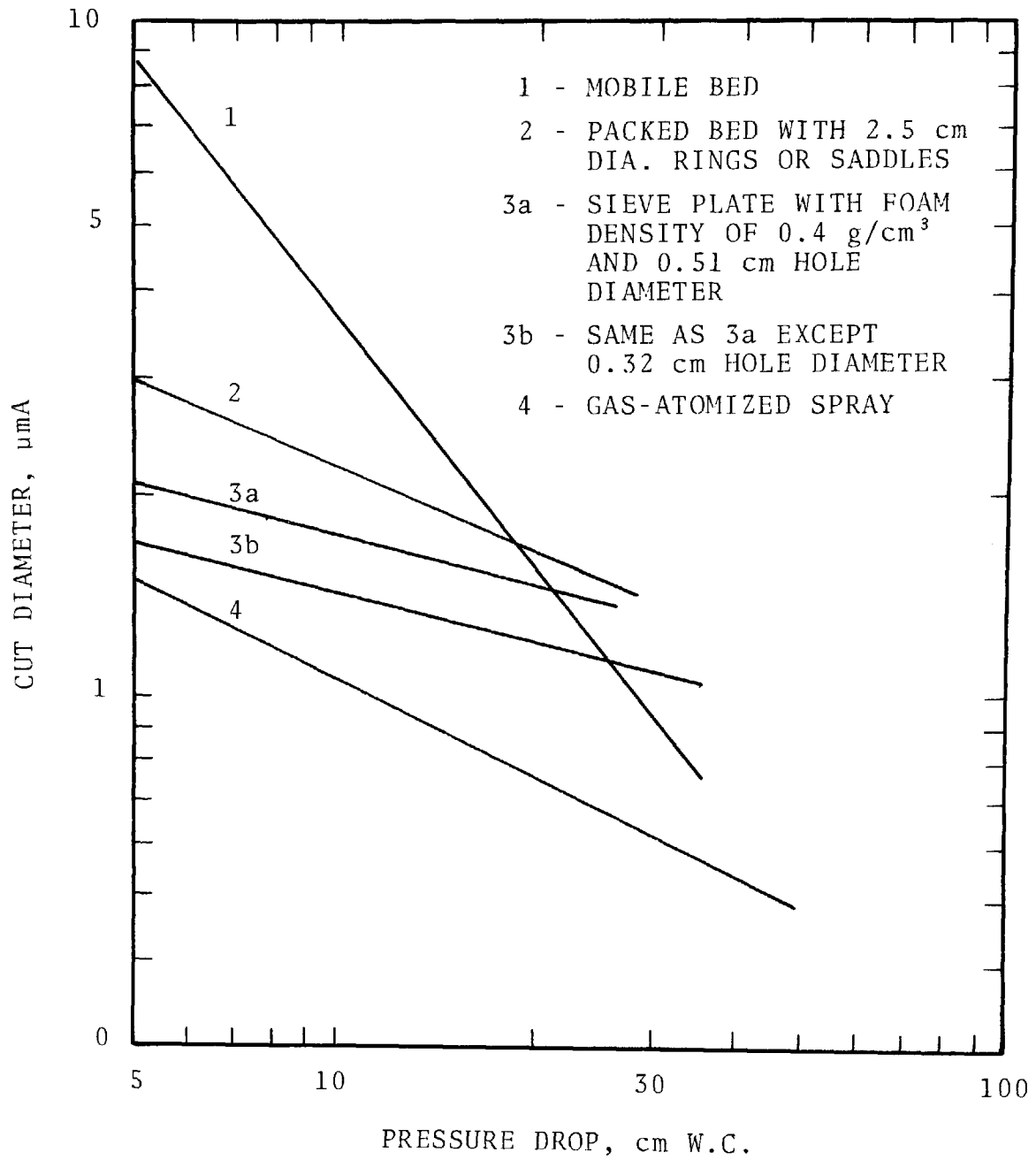


Figure 1. Cut/power relationship for scrubbers.

Of the four scrubber types (gas-atomized spray, mobile bed, packed bed, and sieve plates), the gas-atomized spray scrubber has the best performance capability because it can attain the smallest performance cut diameter with the same pressure drop. At a pressure drop of 20 cm W.C., the gas-atomized spray scrubber can achieve a performance cut diameter of 0.75  $\mu\text{m}$ . At the same pressure drop, the performance cut diameters are 1.6  $\mu\text{m}$ , 1.7  $\mu\text{m}$ , and 1.2  $\mu\text{m}$  for the mobile bed, packed bed, and sieve plate with 0.32 cm hole diameter, respectively. Industrial mobile beds usually operate at a pressure drop around 30 cm W.C. The performance cut diameter is approximately 0.9  $\mu\text{m}$  which is better than that of packed bed and sieve plate; but it is still larger than that of the venturi scrubber.

In F/C scrubbing, particle growth may be induced before or within the scrubber. A condenser is required if particle growth occurred before the scrubber. In this case, any type of particle scrubber may be used after the condenser to collect the grown particles. Since the gas-atomized scrubber has the best performance characteristics, it is the logical choice for this arrangement.

In the situation where condensation and particle growth are induced within the scrubber, the scrubber should have high heat and mass transfer capability. Suitable scrubbers include the mobile bed, sieve plate, packed bed, and spray.

The performance of the F/C sieve plate and F/C spray has been determined by Calvert, et al. (1975) through pilot plant studies. When comparing their results with the F/C mobile bed scrubber performance determined in this study, it shows that the F/C mobile bed has the best characteristics among the three.

The capital outlay for the three F/C scrubber systems is approximately the same. However, the mobile bed has the highest annual operating power cost because it has a larger cooling tower.

## CONCLUSIONS

The principal objectives of this study were achieved. The following conclusions can be drawn, based on evaluation of experimental results.

### Particle Collection

1. The particle collection capability of the mobile bed scrubber is a strong function of the gas phase pressure drop. The higher the pressure drop, the higher the collection efficiency will be. Any parameter that increases the scrubber pressure drop (except friction losses) will increase the scrubber collection efficiency. The cut/power relationship is given in equation (2).
2. Types of aerosol have no significant effect on the particle collection mechanisms and efficiency.
3. The use of limestone slurry does not affect the collection efficiency.
4. The performance capability of the mobile bed scrubber is less than that of the gas-atomized spray scrubber with the same pressure drop. Compared to the packed bed and sieve plate, the mobile bed has better performance capability when the pressure drop is above 20 cm W.C.

### F/C Scrubbing

1. The use of F/C effect improve the collection efficiency for submicron particles. The extent of improvement depends on the condensation ratio and particle number concentration. High condensation ratio combined with low particle number concentration leads to high collection efficiency.
2. The fraction of condensing vapor condensed on the particles was 0.15 for particle number concentrations of  $1 \times 10^7$  to  $5 \times 10^7/\text{cm}^3$ .

### Pressure Drop

The pressure drop across a fully fluidized mobile bed is made up of the sum of those due to the dry retaining grids, the weight of the dry packings, the liquid holdup in the bed, the liquid froth retained on the grid, and the wall friction. It increases with increasing static bed height, density of the packing material, superficial gas velocity, and superficial liquid velocity, but it decreases with increasing packing size. Retaining grid geometry has a significant effect on the pressure drop. The use of grids with small openings and small fractional area increases the liquid froth retention on the grid which in turn increases the pressure drop.

### Engineering Design Equations

The correlations reported in the literature for scrubber pressure drop and particle collection did not agree with data obtained in this study. New equations were derived for predicting scrubber pressure drop and particle collection. These equations compare favorably with available data reported in the literature, as well as data from this study.

### Potential as F/C Scrubber

1. As a F/C scrubber, the mobile bed scrubber can have better collection efficiency than sieve plate and spray scrubbers. The capital cost of a mobile bed F/C scrubber system is slightly higher than that for the spray F/C scrubber system, but it is slightly lower than that for the sieve plate system. The mobile bed F/C scrubber system has the highest annual power cost among the three systems. The overall annualized cost of the three F/C systems is about the same.

2. The condensation of water vapor on particles may be induced to occur before or within the scrubber. In the first arrangement, the venturi scrubber is a better choice as the particle scrubber. In the second arrangement, the mobile bed appears to be better.
3. Due to the low attainable condensation ratio, the mobile bed scrubber may be used as a  $\text{SO}_x$  and particle scrubber in power plant applications, but is not preferred as a F/C scrubber.

## SECTION 2

### INTRODUCTION

A mobile bed scrubber is a counter-current contacting tower in which beds of low density spheres are fluidized by the upward flowing gas and are irrigated by the downward flowing liquid. The spheres may typically be hollow plastic spheres of from 1 to 4 cm diameter and of density considerably below that of water. The beds are supported and retained by nonflooding grids.

Such a device was first described in the literature by Kielback in 1959 and later a modified version was developed by Douglas et al. (1963). The primary difference between the two versions of the mobile bed scrubber is that in the Kielback design, the distance between the lower and upper retaining grid is only slightly larger than the static bed height while in the configuration of Douglas et al., the static bed height is much less than the distance between grids and the bed is greatly expanded during operation.

In industry, Kielback's design is termed "floating bed scrubber" and the design by Douglas et al. is termed "turbulent contact absorber." Other names like "mobile bed scrubber," "fluidized packing contactor," and "fluidized bed scrubber" have been used to describe a packed tower operating in a fluidized state. In this report, the term "mobile bed scrubber" is adopted.

Mobile bed scrubbers have been used for scrubbing flue gas from coal-fired utility boilers. Experience with this application has pointed to the problem of liquid entrainment. Entrainment from mobile bed scrubbers has caused the plugging of entrainment separator and ductwork, failure of fan, and excessive emission of particulates.

Nearly 100% removal of entrained drops is essential for trouble-free operation of the scrubber system. Design of high efficiency entrainment separators requires knowledge of the entrained drop size distribution and concentration. Calvert et al. (1977) have started the measurement of entrainment from mobile bed scrubbers and have provided some information on drop size distribution and concentration. Their work is continued in this study.

Fundamental studies on the mechanics of mobile beds such as hydrodynamics, pressure drop, liquid holdup, minimum fluidization velocity, and axial liquid mixing have been conducted by a number of investigators. There is no carefully performed study on the particle collection in a mobile bed scrubber. Particle collection efficiency data reported in the literature varied as much as two orders of magnitude under similar operating conditions. A systematic pilot study was carried out to investigate the particle collection in a mobile bed scrubber.

Present day scrubbers are hampered by the large energy requirement for high removal efficiencies on particles in the size range of 0.1 to 2 microns in diameter. This is due to the decreased effectiveness of the inertial and diffusional collection mechanisms for particles in this size range. Flux force/condensation (F/C) effects resulting from water vapor condensation can greatly improve the collection efficiencies of low energy scrubbers for fine particles.

In this report, flux forces are defined as those caused by thermophoresis and diffusiophoresis, but not electrophoresis. Accordingly, we consider only those F/C scrubbers where particle removal from the gas is aided by temperature or vapor concentration gradients and particle growth is due to vapor condensation. These effects can result from the cooling of a hot, humid gas by contact with cold liquid, the condensation of injected steam, or other means.

The F/C sieve plate scrubber and F/C spray scrubber have been studied in detail by Calvert et al. (1975). The feasibility



of operating the mobile bed scrubber as a F/C scrubber is investigated in the present study.

This report presents the results of the experimental investigation of entrainment, particle collection, slurry scrubbing, and F/C scrubbing of mobile bed scrubbers. Mobile bed scrubber design recommendations and operating practices to ensure adequate fine particle collection are established from data analysis.

The economics and performance of F/C scrubbing using a mobile bed scrubber are evaluated and compared with the F/C spray scrubber and F/C sieve plate scrubber. The potential application of F/C mobile bed scrubbers in coal-fired power plants is evaluated.

### SECTION 3

#### PRELIMINARY STUDIES

Design of high efficiency entrainment separators requires knowledge of the entrained drop size distribution and concentration. Data on size distribution for drops smaller than 20  $\mu\text{m}$  diameter are especially important, for without it the design of high efficiency entrainment separators is impossible. A preliminary study was undertaken to provide data needed to design an efficient entrainment separator for the mobile bed F/C pilot plant.

#### ENTRAINMENT MEASUREMENTS

##### Equipment

A pilot plant was constructed to study the liquid entrainment. It consisted of a blower, a mobile bed scrubber, a knitted mesh entrainment separator, a scrubber sump tank, and a pump. Figure 2 shows the flow diagram of the setup.

The mobile bed scrubber was a single stage pilot-scale unit. It had a 45.7 cm (18 in.) square aluminum shell. The overall height of the scrubber was 3 m (10 ft), allowing 1 m for the fluidized bed plus 1.3 m of open column above the bed. Four flow straightening vanes were installed below the bed. Six Plexiglas windows, each of 15 cm x 40.6 cm, were installed on two adjacent sides of the column so that the action of the packing and entrainment flow pattern could be observed during operation. The packing used for the bed was 3.8 cm (1.5 in.) diameter hollow polyethylene spheres and the average weight of each sphere was 4.5 g. The depth of the static packed bed was 25.4 cm (10 in.). The retaining grids were made of hardware screen. The wire diameter was 0.16 cm and the openings were 1.1 cm x 2.4 cm.

Air and water were used for study. Air flow rates to the scrubber were measured through a pitot tube. The pitot tube

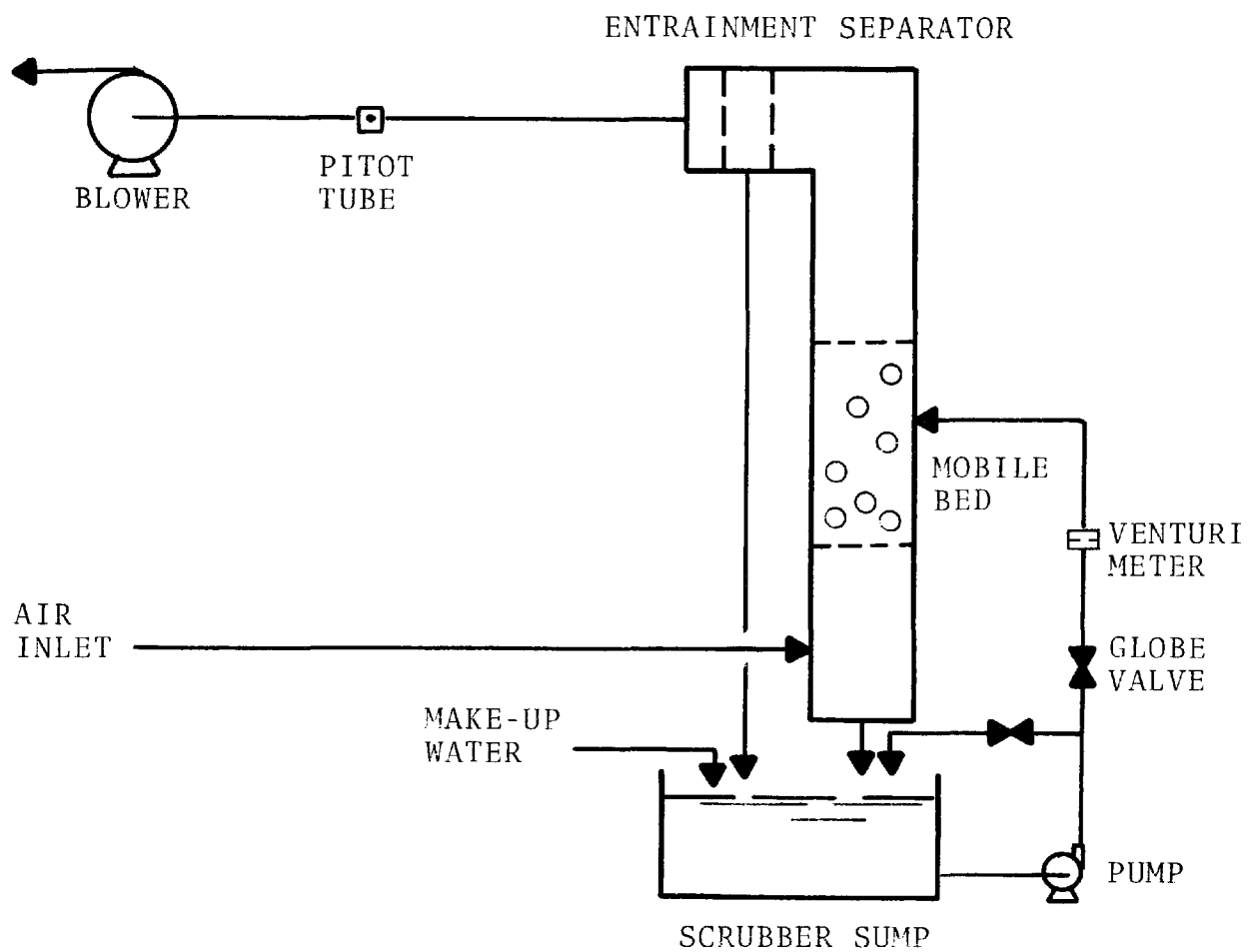


Figure 2. Mobile bed scrubber system for entrainment measurement.

was kept in one position after a complete traverse of the duct. Water flow rates were monitored with a calibrated venturi meter.

### Experimental Procedures

The purpose of the preliminary studies was to measure drop size distribution and concentration of entrainment from a mobile bed scrubber operating under fairly typical conditions. Air and water flow rates covered common operating ranges, especially those likely to cause heavy entrainment.

In starting the experiments, the water pump and blower were turned on and the flow rates were adjusted to desired levels. After steady conditions were obtained, entrainment drop samples were taken at a location 76 cm (30 in.) above the top retaining grids.

### Drop Sampling Methods

Drop size distribution and concentration were measured with a hot-wire anemometer and a cascade impactor.

#### Hot-Wire Anemometer -

The anemometer used in the study was the Model DC-1 Droplet Counter manufactured by KLD Associates. It consists of an electrically heated wire which is made of platinum and is 5  $\mu\text{m}$  in diameter and 1 mm in length. When the hot wire is placed in a liquid aerosol stream it will display fluctuations in voltage due to the cooling effects of the carrier stream and the liquid droplets. Each drop contacting the wire cools a wire length proportional to the drop diameter, reducing the wire electrical resistance proportionately. The wire forms one leg of an electric bridge which is imbalanced by this resistance change, thus generating a pulse. An electronic circuit analyzes, counts, and sorts the pulses into six channels or bins which have different drop diameter intervals. The diameter interval for each bin depends on the dc reference resistance network used. KLD calls this resistance network a "Ladder Network." The DC-1 drop counter is equipped with three "Ladder Networks." Table 3 shows the diameter interval for each bin for these three "Ladders."

TABLE 3. DROP DIAMETER INTERVAL FOR  
DC-1 DROP COUNTER

Bin No.	Ladder #1	Ladder #2	Ladder #3
1	1 - 1.5	1 - 2	1 - 3
2	1.5 - 2.25	2 - 4	3 - 9
3	2.25 - 3.4	4 - 8	9 - 27
4	3.4 - 5.0	8 - 16	27 - 81
5	5.0 - 7.5	16 - 32	81 - 243
6	> 7.5	> 32	> 243

Note: Diameters are in  $\mu\text{m}$ .

The drop counter can detect the existence of a drop only when the drop touches the hot wire (center of drop must be within one drop radius of wire and attached to the hot wire). Thus, a 10  $\mu\text{m}$  diameter drop must be closer to the wire than a 100  $\mu\text{m}$  diameter drop in order to be detected. Therefore, when the hot wire is placed in the gas stream, the gas volume sampled by the hot wire differs for different drop sizes and is expressed by the following formula:

$$V_s = u_G t l (2 d_d + d_w) \quad (12)$$

where  $d_d$  = drop diameter, cm  
 $d_w$  = hot wire diameter, cm  
 $l$  = hot wire length, cm  
 $t$  = sampling time, s  
 $u_G$  = gas velocity, cm/s  
 $V_s$  = gas volume sampled,  $\text{cm}^3$

The drop counter only counts and sorts the drops into six diameter intervals or bins. It does not give the exact size of each individual drop. For this reason, we assumed that drops in each bin had the same size and were equal to the arithmetic mean diameter of the bin. The drop number concentration corresponding to the bin is computed with the expression:

$$n_i = \frac{N_i}{V_{si}} \quad (13)$$

where  $n_i$  = drop concentration corresponding to ith bin,  
 $\#/\text{cm}^3$

$N_i$  = number of drops counted in the ith bin, number

$V_{si}$  = gas volume sampled by the ith bin,  $\text{cm}^3$

" $n_i$ " is also the number of entrainment drops per  $\text{cm}^3$  in the scrubber gas, which have diameters between the lower and upper

diameter limit of the bin. The total drop number concentration for all drop populations is the sum of all " $n_i$ 's"; i.e.

$$n = \sum_{i=1}^6 n_i \quad (14)$$

where  $n$  = total drop number concentration,  $\#/cm^3$

In obtaining a drop size distribution, the drop counter data were treated as cascade impactor data with each bin corresponding to a cascade impactor stage. The lower drop size limit of a bin was assumed to be equivalent to the impactor stage cut diameter. For example, if Ladder #3 is used for measurement, the drop number concentration or percent of total drops smaller than  $3 \mu m$ ; i.e. the lower limit of bin #2 is equal to the concentration in bin #1. The concentration smaller than  $9 \mu m$  or the lower limit of bin #3 is the sum of concentrations in bins #1 and 2. In general,

% by number smaller than  $d_{di}$

$$= \frac{\sum_{i=1}^{i-1} n_i}{n} \times 100\% \quad (15)$$

where  $d_{di}$  = lower diameter limit of bin #i, cm

To obtain entrainment volume concentration, one simply multiplies each bin's number concentration, " $n_i$ " by the size drop volume calculated from the bin's average drop size. Total entrainment volume is the sum of all bins. Cumulative entrainment volume versus drop size can be obtained by the same method as the derivation of cumulative number concentration.

### Cascade Impactor -

A few confirmatory measurements were performed with cascade impactors. The sampling system arrangement is illustrated in Figure 3.

Cascade impactors are usually used for size fractionation of particles smaller than  $20\text{ }\mu\text{m}$  in diameter. Calvert et al. (1977) reported that less than 1% of the mobile bed entrainment has a diameter smaller than  $10\text{ }\mu\text{m}$ . To prevent overloading the impactor by big drops, a side port probe/pre-cutter was used ahead of the impactor. The side port probe/pre-cutter was a 4.5 cm (1.75 in) I.D. Plexiglas tube with a 1.6 cm diameter hole drilled on the wall. When pulling a sample through the sampling system at a gas flow rate of 14  $\ell/\text{min}$  (0.5 CFM), the pre-cutter theoretically removes all drops larger than  $13\text{ }\mu\text{m}$  in diameter.

Early efforts to detect fine drops by cascade impactors were unsuccessful. It was found that fine drops evaporated even under a nearly saturated gas environment. It was also discovered that due to reduced pressure in the sampling system, drops collected on impactor stage collection plates evaporated. To alleviate this problem, sodium chloride was added to the water.

The salt has the effect of reducing the vapor pressure of the water and minimizing the evaporation of water from drops as they leave the mobile bed and travel to the sampling point.

The salt can also serve as a tracer. Once the drops are collected by the impactor stages, evaporation would still occur. If one assumes that evaporation does not occur before collection by impactor stages, the amount of salt collected on the impactor substrates allows the calculation of the size distribution and concentration of drops existing at the sampling point.



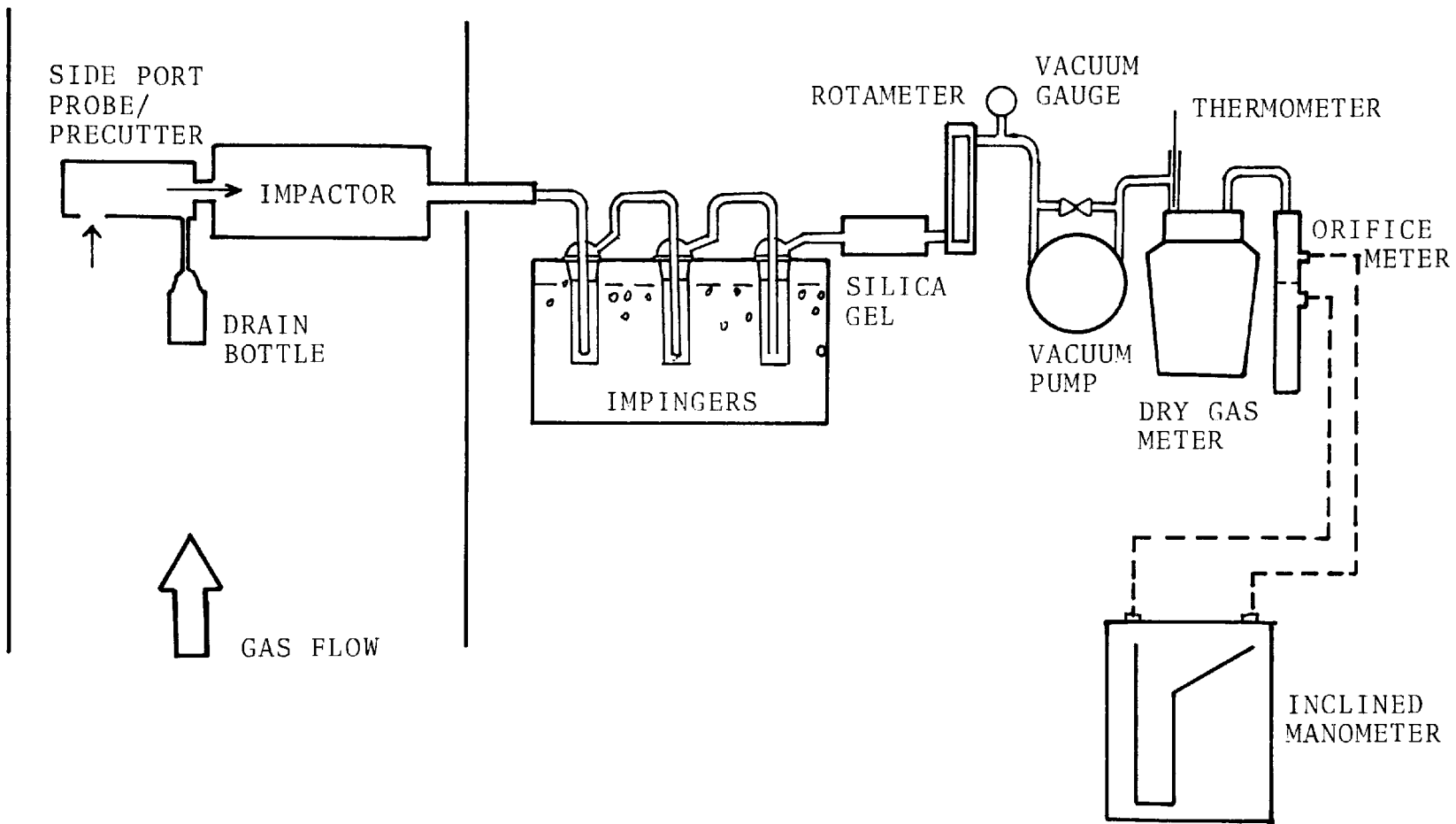


Figure 3. Entrainment measurement sampling train.

After the completion of a sampling run, the impactor substrates were soaked in a known volume of distilled water. The amount of sodium chloride leached out of the substrates was then determined with a chloride specific ion electrode.

The drop size distribution was calculated from each impactor stage catch, the cut diameter of the stage, and the sodium chloride concentration in the scrubber liquid. Summation of the pre-cutter catch and the impactor catch gives the entrainment mass flow rate.

#### Entrainment Data

##### Preliminary Runs -

Several exploratory runs were conducted with the DC-1 drop counter. It was found that due to the short sampling time capability of the counter (99.9 seconds or 999 drops, whichever comes first) and the irregular nature of entrainment generation, the agreement between runs was poor. However, if the average of ten runs was used to compute the drop size distribution, results would be consistent. Therefore, in subsequent entrainment measurements each run consisted of at least ten sets of data and the average of these was used for analysis.

Entrainment loadings were measured with the drop counter at several locations in the same scrubber cross section. Except at locations close to the scrubber wall, the entrainment loadings at different locations were close to each other. In subsequent measurements one point sampling was employed.

Seventeen runs corresponding to six different scrubber operating conditions were conducted to investigate whether there was a discrepancy in the measurement of entrainment between the DC-1 drop counter and the cascade impactors. The scrubber operating conditions are listed in Table 4. In all the runs, 12% by weight of sodium chloride solution was used as scrubber liquid.

TABLE 4. PRELIMINARY ENTRAINMENT MEASUREMENT  
SCRUBBER OPERATING CONDITIONS

Run No.	Measurement Device	Superficial Gas Velocity (m/s)	Gas Flow Rate (m <sup>3</sup> /min)	Liquid Flow Rate (ℓ/min)	Pressure Drop (cm W.C.)	Bed* Expansion (%)
1	Impactor	2.9	36.8	254	4.6	110
2	Impactor	2.9	36.8	254	4.6	110
3	Impactor	2.9	36.8	322	4.8	110
4	Impactor	2.9	36.8	322	4.8	120
5	Impactor	2.9	36.8	394	5.8	130
6	Impactor	3.4	42.5	299	5.2	130
7	Drop Counter	2.9	36.8	254	4.6	110
8	Drop Counter	2.9	36.8	254	4.6	110
9	Drop Counter	2.9	36.8	322	5.1	120
10	Drop Counter	2.9	36.8	322	5.1	120
11	Drop Counter	2.9	36.8	394	5.1	130
12	Drop Counter	2.9	36.8	394	5.1	130
13	Drop Counter	3.4	42.5	299	5.1	140
14	Drop Counter	3.4	42.5	299	5.1	140
15	Drop Counter	3.4	42.5	369	6.4	160
16	Drop Counter	3.4	42.5	369	6.4	160
17	Drop Counter	3.4	42.5	460	7.4	190

\*  
Bed Expansion =  $\frac{H_d - H_s}{H_s} \times 100\%$

Since the drop counter's manufacturer, KLD Associates, claims that suspended and dissolved solids will not affect the performance of the counter, the usage of sodium chloride solution offers an opportunity for checking the counter with the cascade impactor.

Figure 4 shows the comparison of the entrainment volumes measured by the drop counter and the cascade impactor. The entrainment volume measured by the drop counter is much less than that by the impactor. Cumulative entrainment volume curves, calculated from cascade impactor data, show a tendency to flatten out around  $10 \mu\text{m}$ . This is expected because of the side port probe/pre-cutter which was used. The pre-cutter has a theoretical cut diameter of about  $13 \mu\text{m}$ , which is close to the first and second stage cut diameters of the A.P.T. cascade impactor ( $13 \mu\text{m}$  for the first stage and  $9.8 \mu\text{m}$  for the second stage).

Another indication of the discrepancy between the two measurement methods is the overall entrainment volume. The DC-1 drop counter did not detect any drop larger than  $243 \mu\text{m}$  in diameter. Thus the overall entrainment volume measured with the drop counter, is equal to the cumulative volume at  $243 \mu\text{m}$ . For a superficial gas velocity of  $2.9 \text{ m/s}$  and a  $Q_L/Q_G$  equal to  $6.9 \ell/\text{m}^3$ , the entrainment volume is  $0.0245 \text{ ml/Nm}^3$ . However, for the same condition, the volume based on pre-cutter and impactor catch is  $1.6 \text{ ml/Nm}^3$ , which is 65 times higher than the drop counter result. Calvert, et al. (1977) reported some entrainment data from a mobile bed scrubber. They used the water balance technique to determine the volumetric entrainment flow rate. At a superficial gas velocity of  $2.9 \text{ m/s}$  and a  $Q_L/Q_G$  of  $6.9 \ell/\text{m}^3$ , the volumetric entrainment flow rate is about  $2 \ell/\text{m}^3\text{-min}$ , which corresponds to an entrainment loading of  $11.5 \text{ ml/Nm}^3$ . Calvert, et al.'s result is about 470 times higher than the drop counter data.

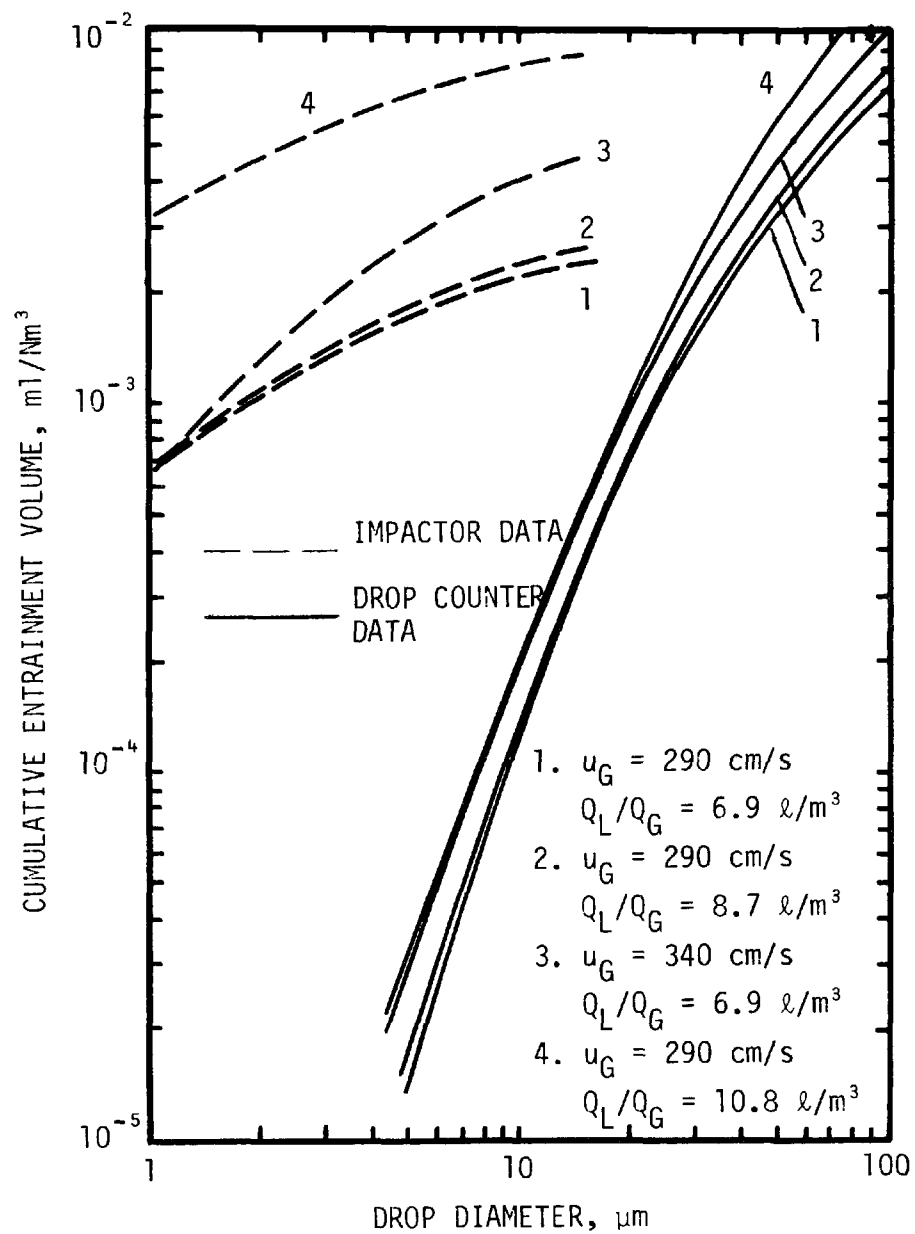


Figure 4. Comparison between cascade impactor and DC-1 drop counter data.

The DC-1 counter manufacturer was questioned on these discrepancies and it was found that they had the same experience. Salt solution was atomized and both the cascade impactor and the DC-1 drop counter were used to measure drop loading. They found that the loading by the cascade impactor was about ten times higher than by the DC-1.

#### Auxiliary Experiments -

In order to resolve the discrepancies between the two sampling devices, some auxiliary experiments were carried out. First, a small scale experiment was set up to duplicate the findings. A 5 weight % solution of sodium chloride was atomized with a Collison atomizer. Drop size distribution and loading were then measured with the drop counter and the cascade impactor simultaneously. The results confirmed the previous findings that the drop size distributions measured with the two devices were different.

It was suspected that even though evaporation of drops was not present before the cascade impactor, evaporation did occur inside the cascade impactor due to the pressure reduction from stage to stage. To study the evaporation of drops within the cascade impactor, the experimental apparatus shown in Figure 5 was built. A 5 weight % salt (NaCl) solution was atomized with a Collison atomizer. The gas is mixed with dilution air which passes through a conditioner which could either humidify or dry and heat the dilution air. The aerosol was then passed through an impactor to measure its size distribution. A specific ion probe for  $\text{Cl}^-$  was used to determine the mass of salt collected in these experiments.

The experiment consisted of two parts, and the first part involved drying the atomized aerosol by mixing it with dehumidified and heated dilution air. The size distribution obtained was that of the dry residual salt particles. Observation of the substrates indicated that no moisture was present for these runs. Figure 6 shows the size distribution obtained for the dry particle size.

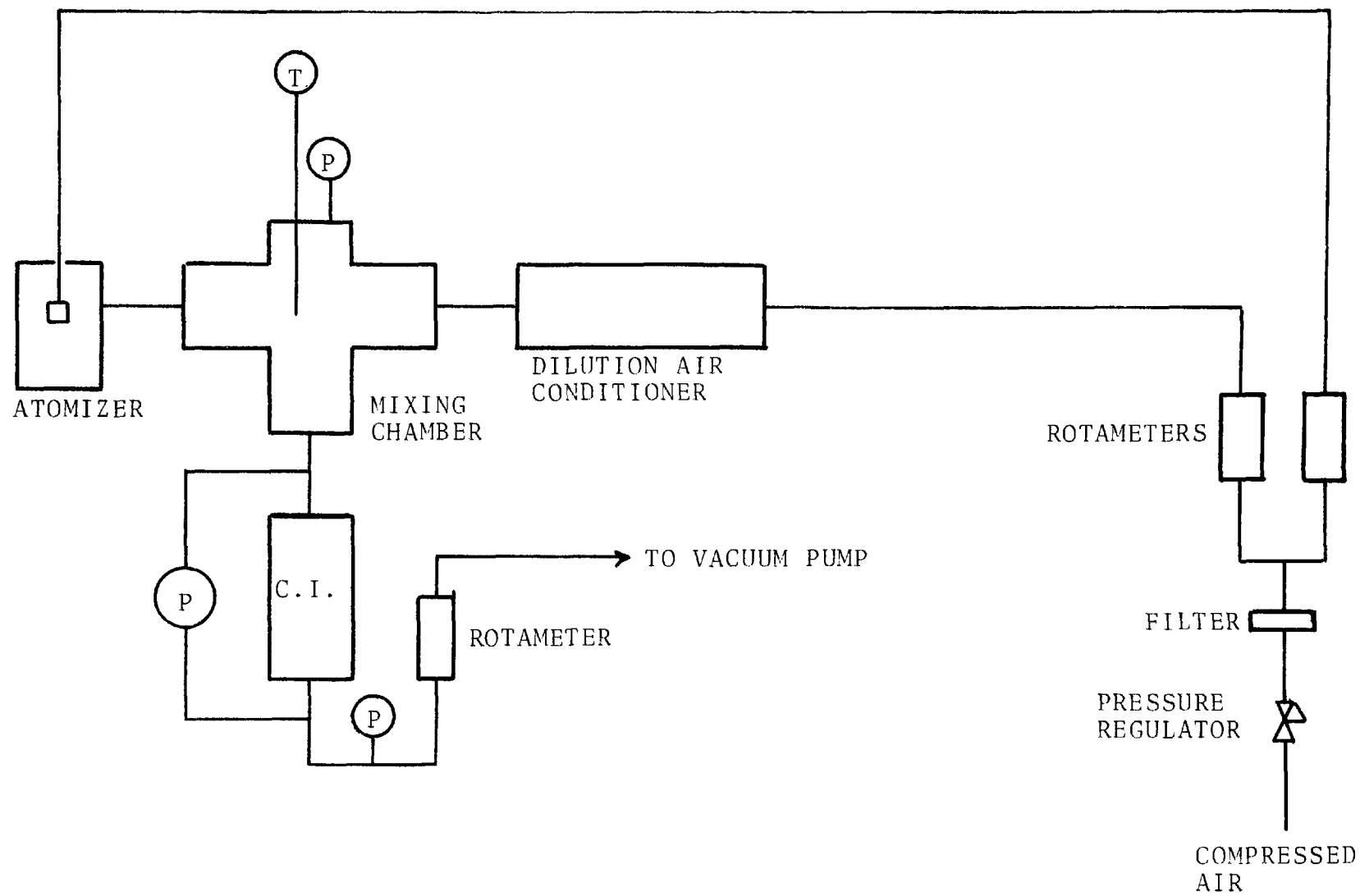


Figure 5. Sketch of experimental equipment.

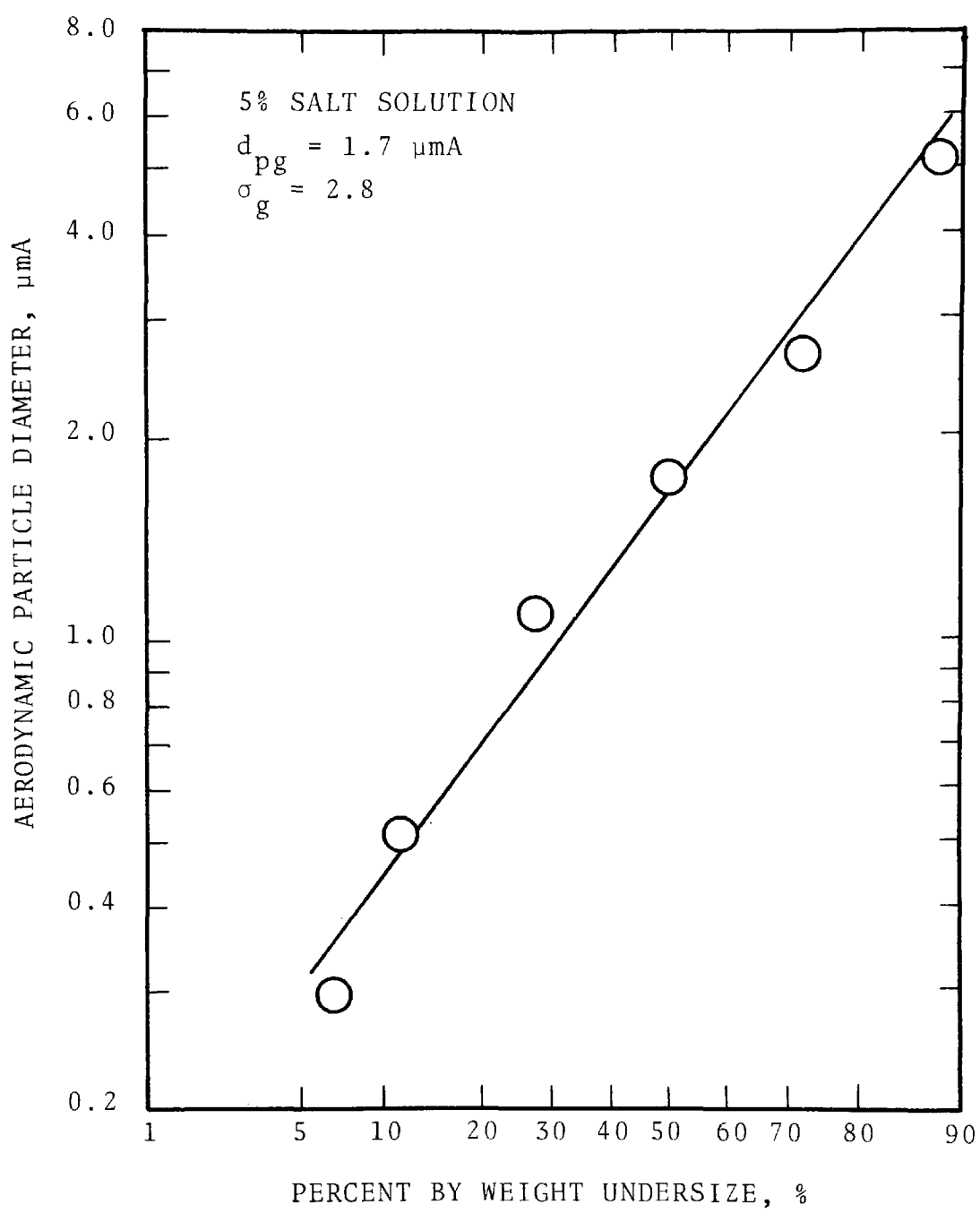


Figure 6. "Dry salt" particle size distribution.



The size distribution of the parent drops can be obtained from the size distribution of the residual salt particles since the initial salt concentration is known. The initial drop diameter is related to the salt particle diameter by the following equation:

$$d_d = d_p (\rho/c)^{1/3} \quad (16)$$

where:  $d_d$  = drop diameter, cm  
 $d_p$  = salt particle diameter, cm  
 $\rho$  = salt density, 2.16 g/cm<sup>3</sup>  
 $c$  = salt concentration in solution, g/cm<sup>3</sup>

This equation is good for diluted salt solutions where the density of the solution is close to that of pure water. The predicted drop size distribution from the atomizer is shown in Figure 7. Note that the aerodynamic diameter is shown and that conversion to physical diameter is required for application of equation (16). Also shown on this figure are lines which represent the size distribution which would exist if a given fraction of the water were evaporated from each of the drops. The upper curve shows the parent drop distribution while the lowest curve represents the measured dry size distribution.

The second part of the experiment involved measurement of the wet drop size distribution. For this case the dilution air was first saturated in a fritted disk bubbler so that particle drying would not occur. The results of several sampling runs with the University of Washington cascade impactor are shown in Figure 8. As can be seen, the wet size distribution, instead of being close to the predicted parent wet particle size distribution, is close to the size distribution of dried salt residues. This indicated that evaporation from particles occurred. Since the air was saturated with water vapor, evaporation from particles could not occur before the cascade impactor. Thus, it could

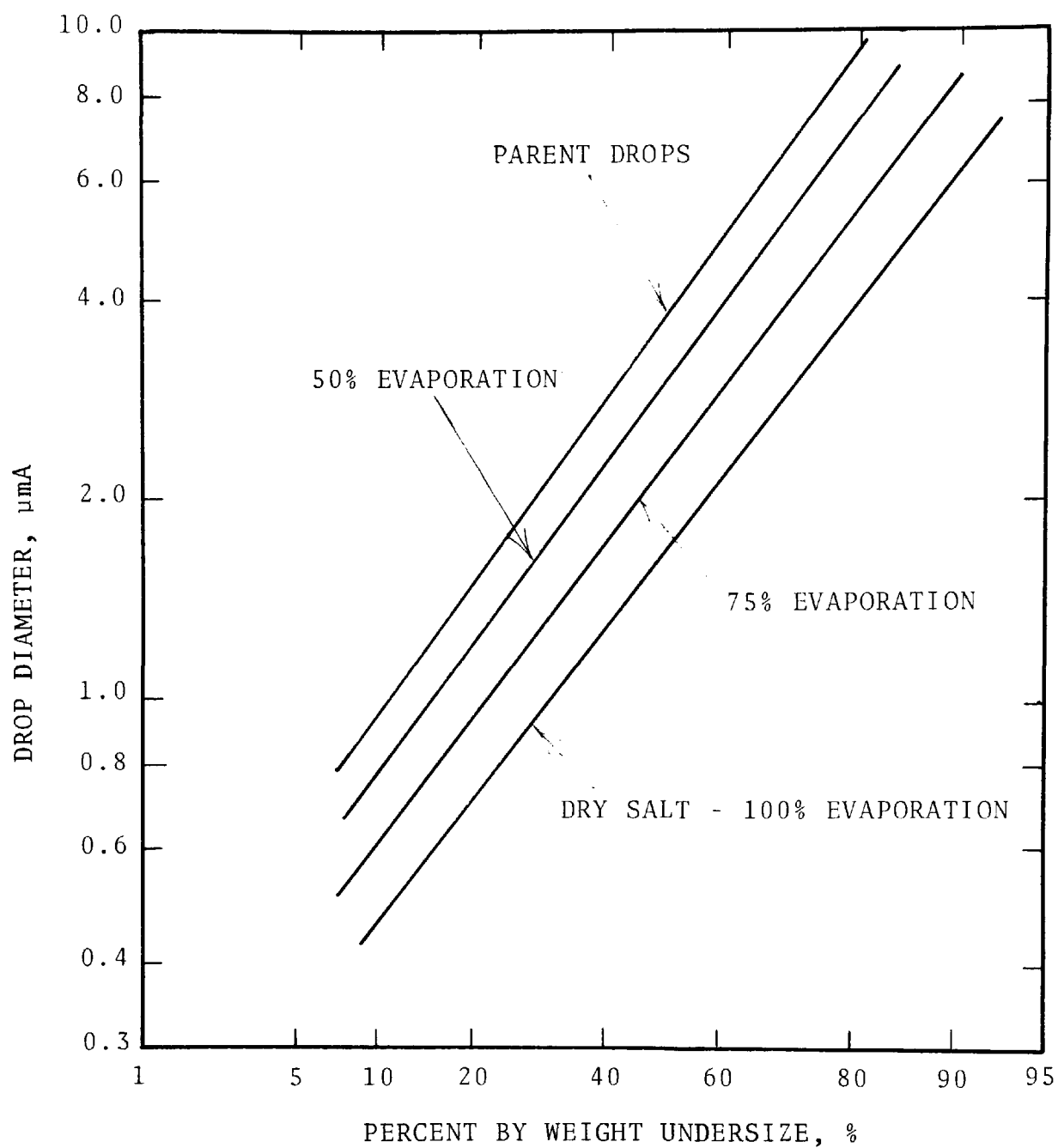


Figure 7. Predicted drop size distribution as a function of water evaporated.

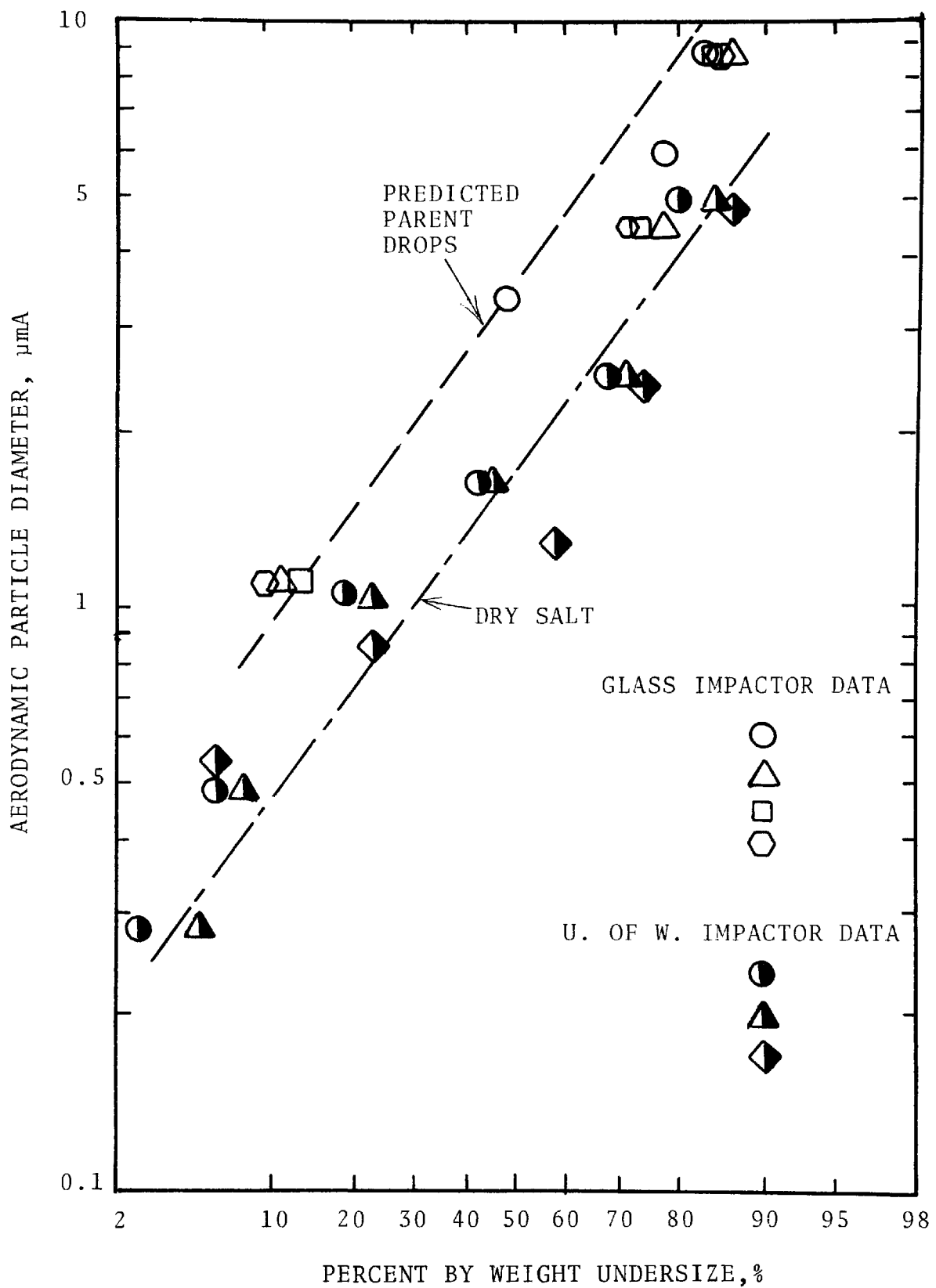


Figure 8. Measured wet size distributions, U. of W. impactor and series glass impactor.

be deduced that evaporation occurred within the cascade impactor. The reason for evaporation might be due to the pressure drop across the jet plate and the negative pressure existing in the cascade impactor.

To verify that evaporation did not occur before the cascade impactor, a second series of experiments were conducted using a series of glass impactors which allowed observation of the jet and impaction plate. Figure 9 shows the experimental setup. Each glass impactor consisted of one jet. By properly selecting the jet diameter, the pressure drop across each stage could be kept at a minimum.

A solution of 5% by weight salt was atomized and dried by mixing it with heated dilution air. The dry salt size distribution confirmed the previously obtained dry size distribution from the University of Washington cascade impactor.

Several runs were then run without dilution air. The results are shown in Figure 10 along with the predicted wet particle size distribution. As can be seen, there is a reasonably good fit between the glass impactor data and the predicted wet particle size for diameters below 3  $\mu\text{m}$ . There is slight deviation for drops larger than 3  $\mu\text{m}$  in diameter. The parent drop size distribution was calculated from the dried salt distribution measured with the University of Washington cascade impactor. It is possible that the drying was incomplete in the first part of the experiment, causing the predicted parent drop size to be larger than it should be.

The wet size distribution measured with the University of Washington impactor differs from that of the glass impactors for particles smaller than 3  $\mu\text{m}$  in diameter. The agreement between the two for larger particle sizes is fairly good. Apparently, significant evaporation from the small particles occurred within the University of Washington impactor. The results shown in Figure 8 show that particles of 1  $\mu\text{m}$  in diameter have their diameters reduced to 0.6-0.7  $\mu\text{m}$  by evaporation.

These experiments confirmed that evaporation from the particles is due to the pressure reduction in the cascade

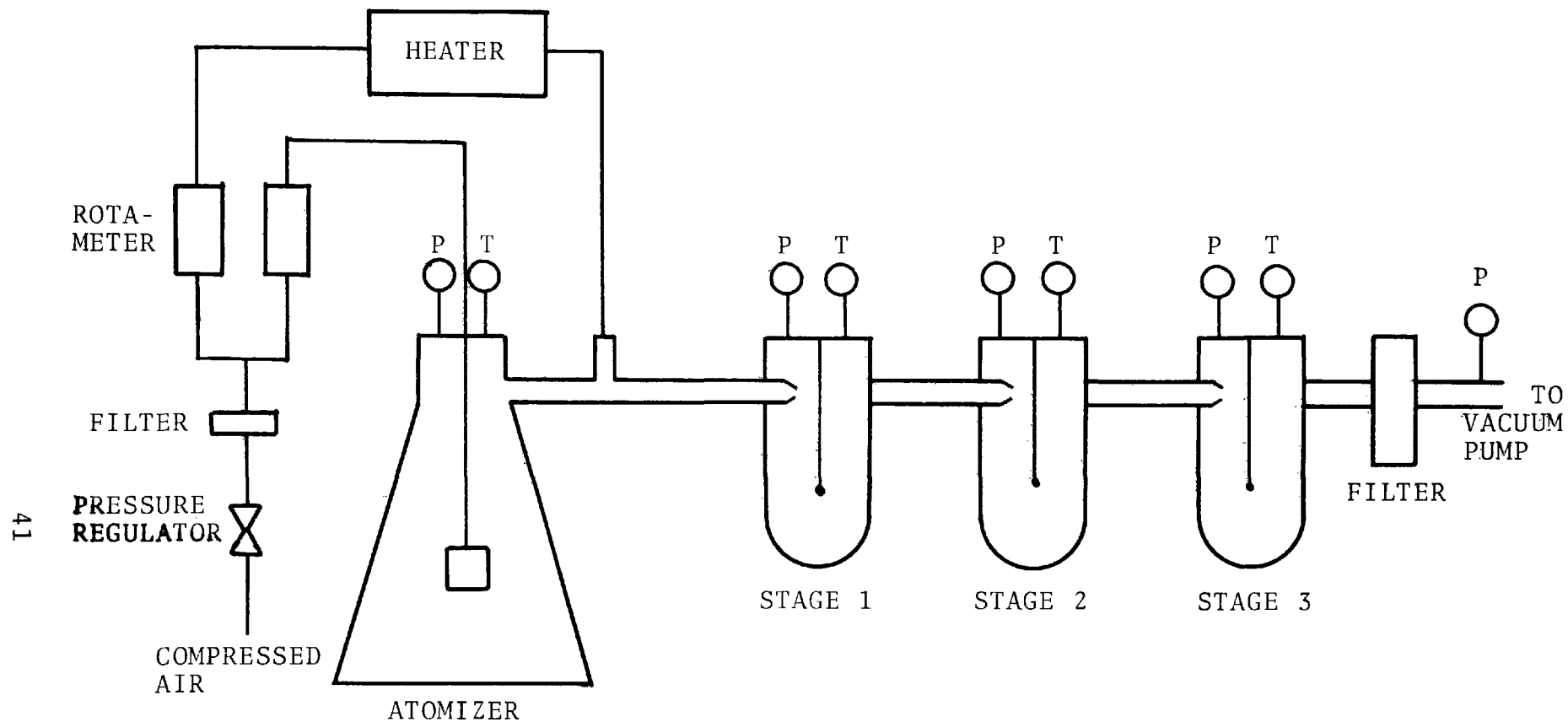


Figure 9. Experimental setup for glass impactors.

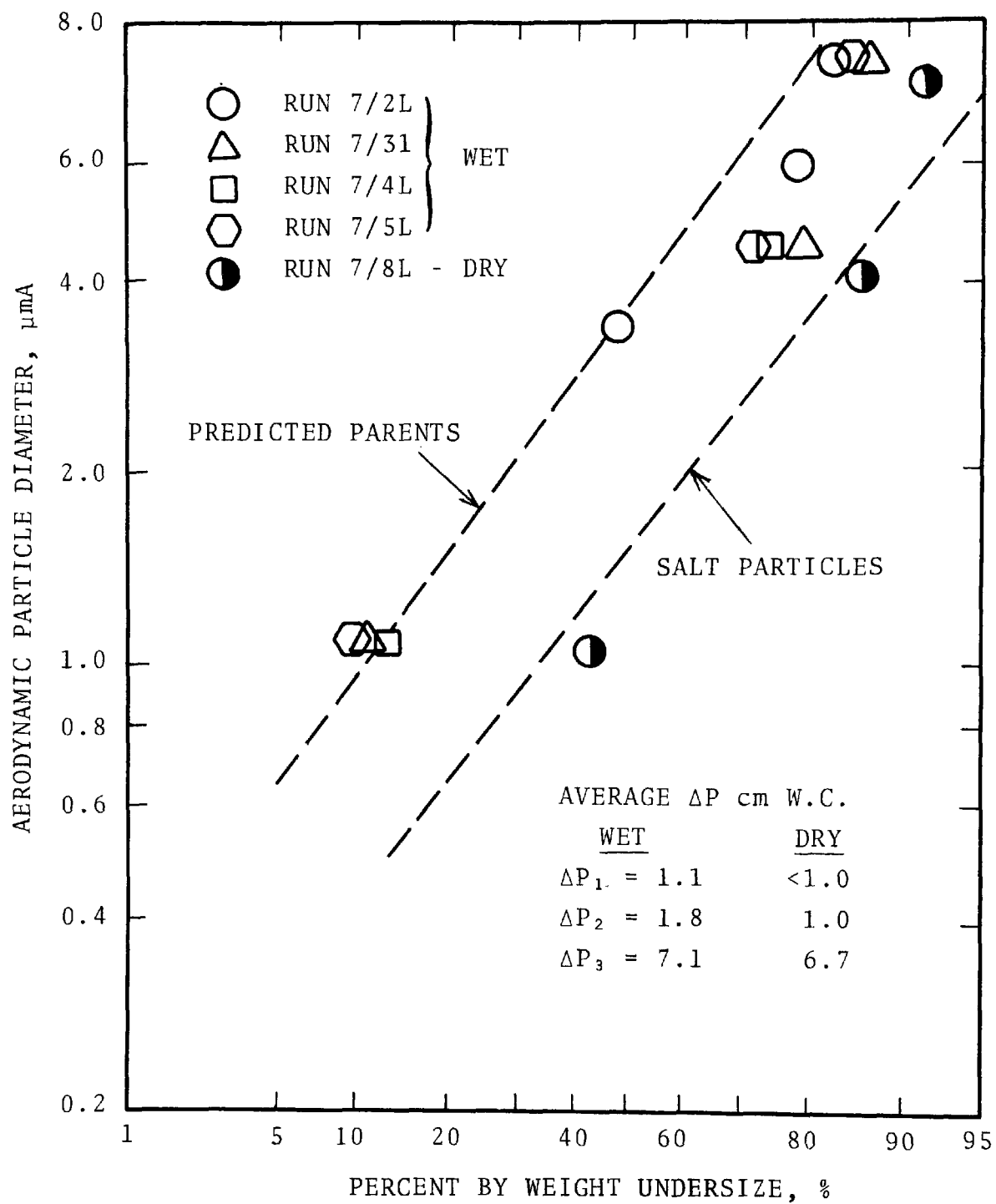


Figure 10. Wet size distribution obtained with glass impactors.

impactor. The pressure drop across the glass impactor was relatively low. Therefore, little or no evaporation from particles occurs and the measured wet particle size distribution is close to predictions.

#### Entrainment Data Corrections -

By assuming evaporation from drops of 10% by weight of sodium chloride was the same as that for 5% by weight, corrections were made to the impactor data. The results are plotted in Figure 11. As can be seen, there are still large discrepancies between the two measurement methods. The remaining discrepancies may be caused by the inability of the drop counter to detect drops smaller than 1  $\mu\text{m}$  in diameter.

These auxiliary experiments explained the differences between the drop counter data and the cascade impactor data for drops smaller than 10  $\mu\text{m}$  in diameter. They did not answer the question of why the overall entrainment loading measured with the drop counter is much lower than that reported by Calvert et al. (1977) and that based on the pre-cutter catch of the present study. It was discovered later that salt residues coated the platinum wire used for drop detection after the drops had been vaporized. The salt coating may reduce the sensitivity of the platinum hot wire.

The scrubber liquid was subsequently changed to clean water and a few entrainment measurements were carried out with the drop counter. When using clean water, the total number concentration of entrainment increased even though scrubber operation was the same. For a superficial gas velocity of 2.9 m/s and  $Q_L/Q_G$  of 6.9  $\ell/\text{m}^3$ , entrainment volume increased to 0.057  $\text{ml}/\text{Nm}^3$  from 0.025  $\text{ml}/\text{Nm}^3$ . Even though the entrainment loading detected was more than double that for salt solution, it was still about 25 times less than that of pre-cutter catch and about 200 times less than that reported by Calvert et al. (1977).

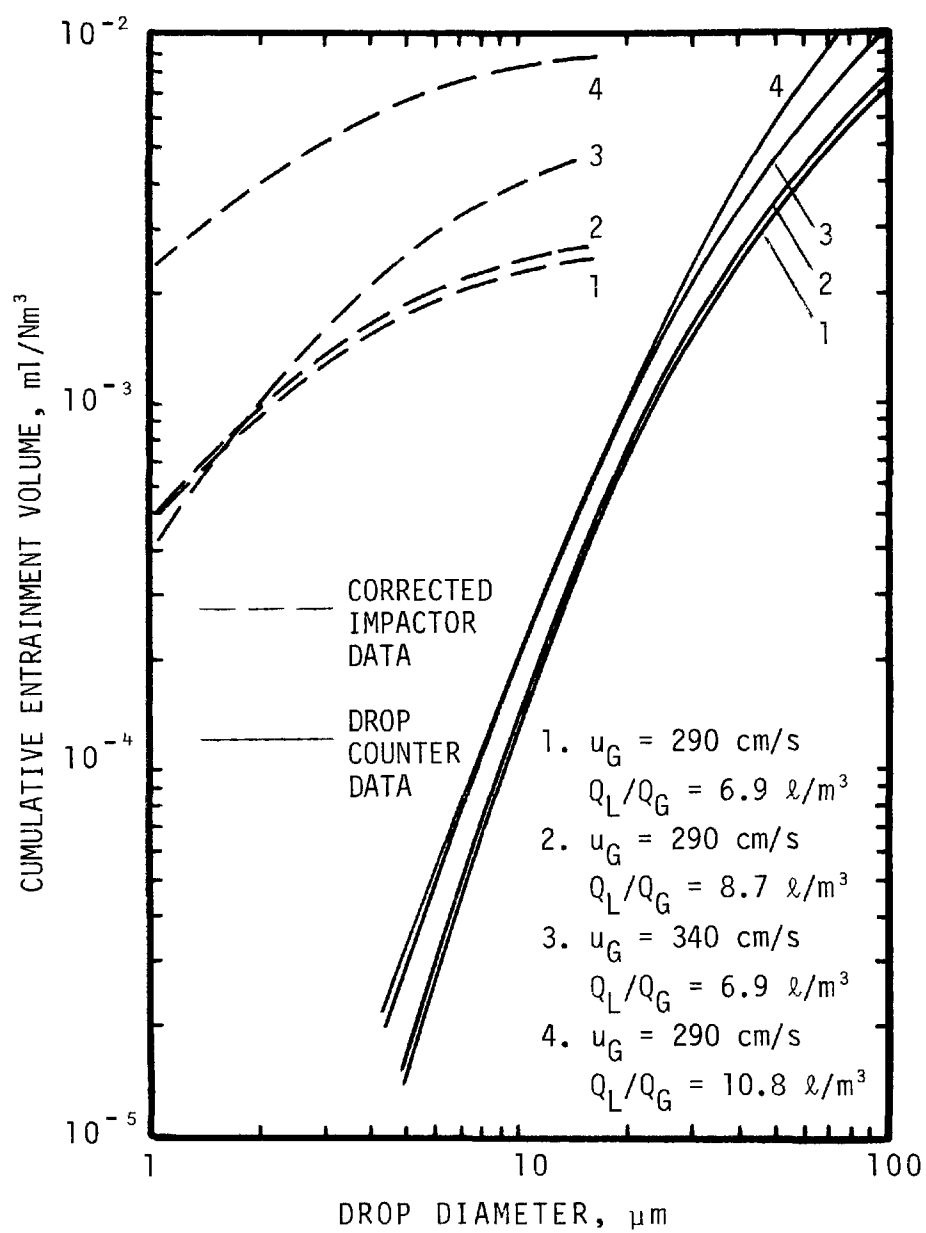


Figure 11. Comparison between cascade impactor and DC-1 drop counter data.



The drop counter also did not detect any drops larger than 245  $\mu\text{m}$  diameter in the mobile bed despite their being visible. During drop measurements with the DC-1 drop counter, it was noticed that some drops shattered upon impaction on the hot wire. Therefore, the drop counter detected less drops than existed. This might be the reason the drop counter gave a lower entrainment loading.

Goldschmidt and Householder (1969) have studied the measurement of liquid drops with the hot wire anemometer. They gave the following equation to estimate the largest drop size to hit the wire without shattering.

$$d_{d \text{ max}} = \frac{12 \sigma_L \rho_L}{u_G^2} \quad (17)$$

where  $d_{d \text{ max}}$  = maximum drop diameter without shattering  
upon impaction, cm

$u_G$  = gas velocity, cm/s

$\sigma_L$  = surface tension of liquid, dyne/cm

$\rho_L$  = liquid density, g/cm<sup>3</sup>

For clean water, equation (17) becomes

$$d_{d \text{ max}} = \frac{864}{u_G^2} \quad (18)$$

This equation reveals that for a gas velocity of 2.9 m/s, drops below 103  $\mu\text{m}$  in diameter will never shatter upon impaction. When gas velocity is increased to 3.8 m/s, the smallest drop to shatter upon impact on wire is 60  $\mu\text{m}$  in diameter.

#### Drop Counter Mobile Bed Entrainment Data

Since we are only interested in small drops, entrainment from the mobile bed was measured with the counter for three levels of gas velocity and five levels of clean water flow rate. Raw data are given in Appendix A. Table 5 lists mobile bed operating conditions for all runs.

TABLE 5. DC-1 DROP COUNTER ENTRAINMENT DATA  
AND SCRUBBER OPERATING CONDITIONS

Run No	Scrubber Operating Conditions					Liquid Entrainment		
	Superficial Gas Velocity (m/s)	Gas Flow Rate (m <sup>3</sup> /min)	Liquid Flow Rate (ℓ/min)	Pressure Drop (cm W.C.)	Bed Expansion (%)	Entrainment Flow Rate (ml/m <sup>2</sup> -min)	Mass Median Drop Dia. (μm)	Geometric Standard Deviation
DC1	3.5	44.2	250	5.1	140	35.5	330	3.2
DC2	3.5	44.2	250	5.1	140	-	198	3.0
DC3	3.5	44.2	318	5.3	160	-	176	3.0
DC4	3.5	44.2	318	5.3	160	42	209	3.0
DC5	3.5	44.2	356	5.8	180	55	156	2.9
DC6	3.5	44.2	356	5.8	180	-	174	2.9
DC7	3.5	44.2	386	6.1	190	-	217	3.0
DC8	3.5	44.2	386	6.1	190	45.8	141	2.9
DC9	3.4	42.5	454	6.4	220	-	298	3.1
DC10	3.4	42.5	454	6.4	220	82.6	160	2.9
DC11	2.9	36.3	454	6.1	170	83.5	382	3.2
DC12	2.9	36.3	454	6.1	170	-	174	2.9
DC13	2.9	36.3	390	5.6	140	-	105	2.6
DC14	2.9	36.3	390	5.3	140	23.5	127	2.8
DC15	2.9	36.3	318	5.3	105	13.9	100	2.7
DC16	2.9	36.3	318	5.3	100	-	137	2.8
DC17	2.9	36.3	265	5.1	90	-	224	3.0
DC18	2.9	36.3	265	5.1	90	9.6	93	2.7
DC19	2.4	29.7	265	5.1	50	4.6	54	2.4

TABLE 5. DC-1 DROP COUNTER ENTRAINMENT DATA  
AND SCRUBBER OPERATING CONDITIONS  
(continued)

Run No	Scrubber Operating Conditions					Liquid Entrainment		
	Superficial Gas Velocity (m/s)	Gas Flow Rate (m <sup>3</sup> /min)	Liquid Flow Rate (ℓ/min)	Pressure Drop (cm W.C.)	Bed Expansion (%)	Entrainment Flow Rate (ml/m <sup>2</sup> -min)	Mass Median Drop Dia. (μm)	Geometric Standard Deviation
DC20	2.4	29.7	265	5.1	60	-	198	2.9
DC21	2.4	29.7	318	5.1	70	-	161	3.0
DC22	2.4	29.7	318	5.1	60	8.1	149	3.0
DC23	2.4	29.7	356	5.3	80	12.5	114	2.7
DC24	2.4	29.7	356	5.1	80	-	135	2.7
DC25	2.4	29.7	390	5.8	90	-	168	2.9
DC26	2.4	29.7	390	5.8	90	10.5	106	2.7
DC27	2.4	29.7	454	6.1	120	11.2	80	2.6
DC28	2.4	29.7	454	6.1	120	-	162	2.9

The size distribution measured by the drop counter is an approximately log-normal number distribution. For practical usage, it is more convenient to express the size distribution based on mass instead of number. Since for a log-normal distribution the number and mass distributions have the same geometric standard deviation, the following equation is used to convert number median to mass median diameter (see Orr, 1966):

$$\ln \frac{d_{dM}}{d_{dN}} = 3 \ln^2 \sigma_g \quad (19)$$

where  $d_{dM}$  = mass median drop diameter,  $\mu\text{m}$  or  $\text{cm}$   
 $d_{dN}$  = number median drop diameter,  $\mu\text{m}$  or  $\text{cm}$   
 $\sigma_g$  = geometric standard deviation, dimensionless

The calculated mass median drop diameter and geometric standard deviation are tabulated in Table 5. Figure 12 is a plot of mass median drop diameter versus liquid/gas ratio, with superficial gas velocity as a parameter. It can be seen that under normal industrial scrubber operating conditions, the liquid entrainment has a mass median drop diameter of approximately  $170 \mu\text{m}$ , which is smaller than that reported by Calvert et al. (1977). Calvert et al. (1977) used chemically treated filter papers to determine the drop size distribution. The mass median drop diameter reported by them is approximately  $400 \mu\text{m}$ .

The geometric standard deviation for all drop counter test runs averages about 2.9.

Figures 13 through 15 are cumulative entrainment volume plots for the three gas velocities studied. These plots can be useful for designing and specifying entrainment separators. The dashed lines in the figures are the calculated maximum drop size without being shattered upon impaction on the hot wire.

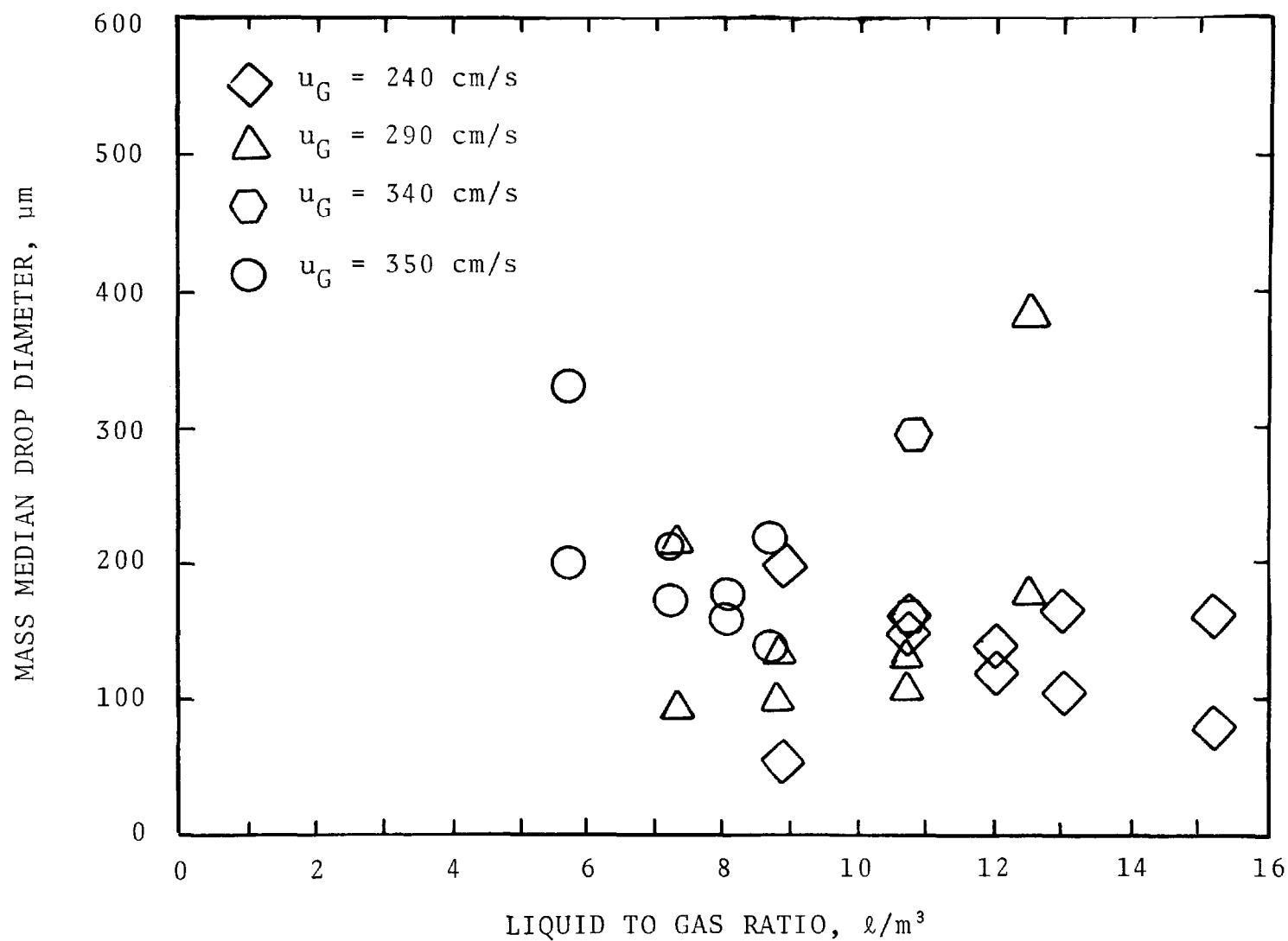


Figure 12. Mass median drop diameter of entrainment from mobile bed scrubber (Drop counter data).

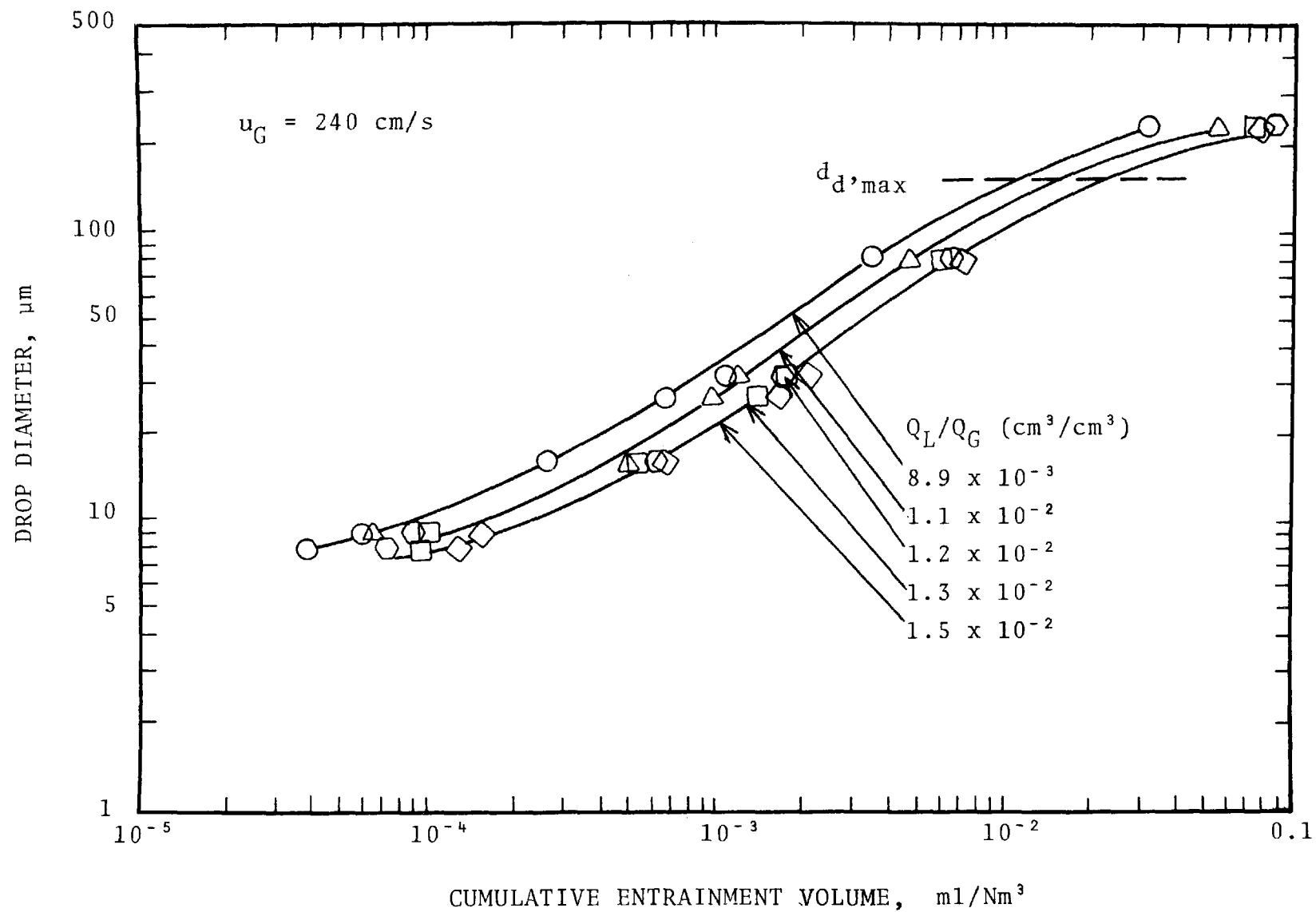


Figure 13. Cumulative entrainment loading (Drop counter data).

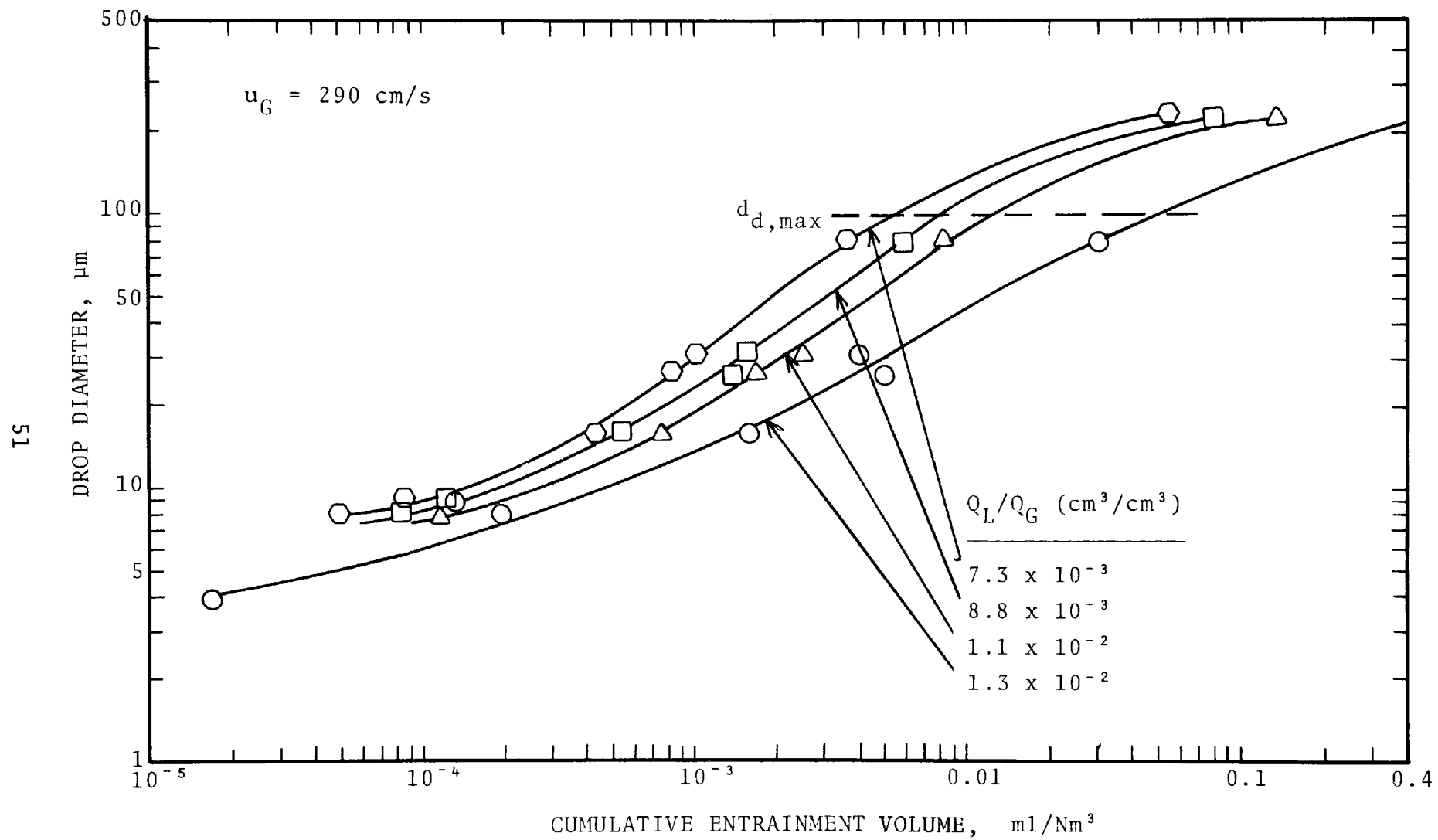


Figure 14. Cumulative entrainment loading (Drop counter data).

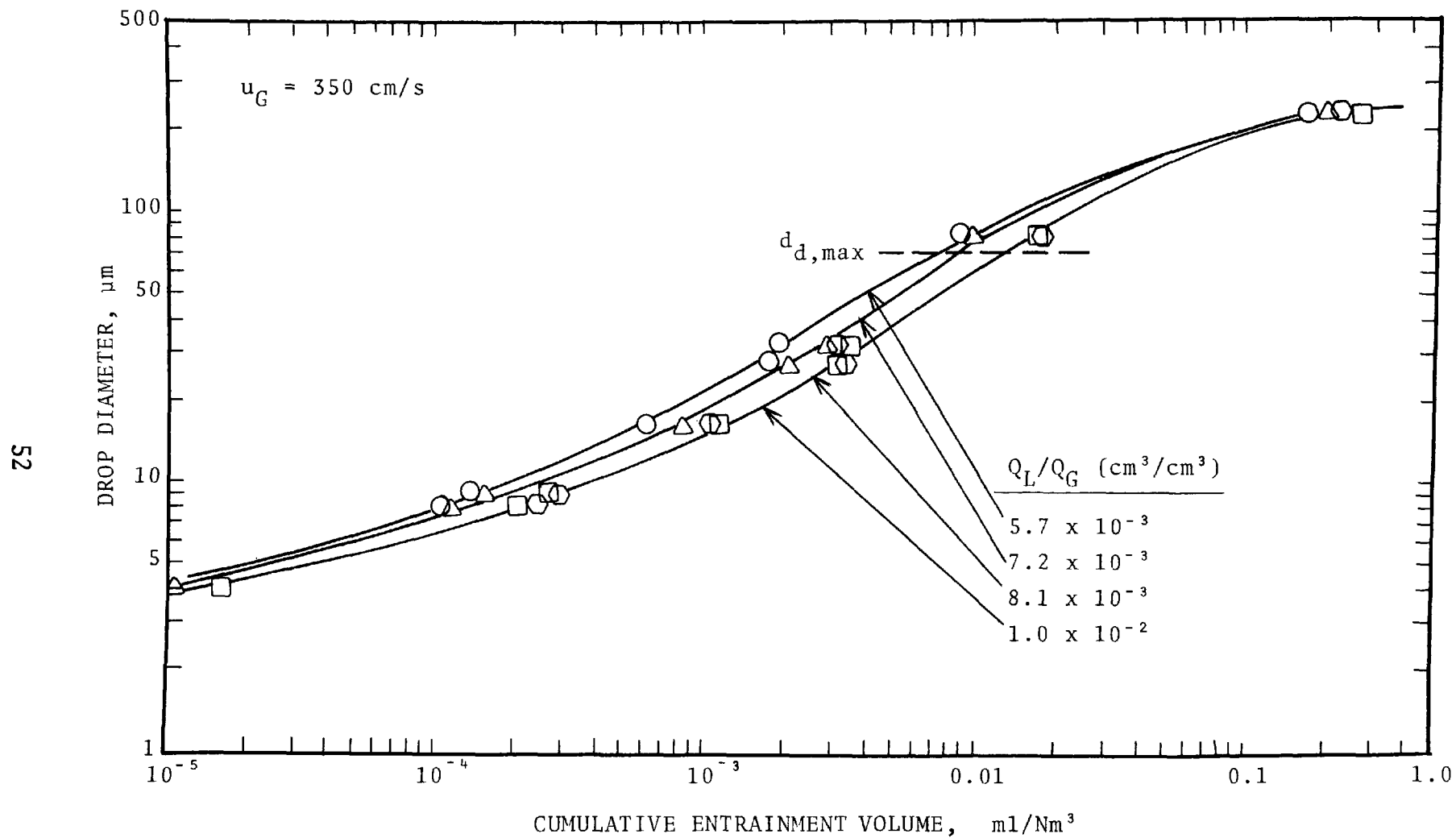


Figure 15. Cumulative entrainment loading (Drop counter data).



Figure 16 is a plot of total entrainment flow rates versus liquid/gas ratio with superficial gas velocity as parameter. It can be seen that entrainment flow rate is both a function of gas flow rate and liquid flow rate. The entrainment flow rate may be low due to shattering of drops. Calvert et al. (1977) gave a similar plot which has much higher entrainment loadings.

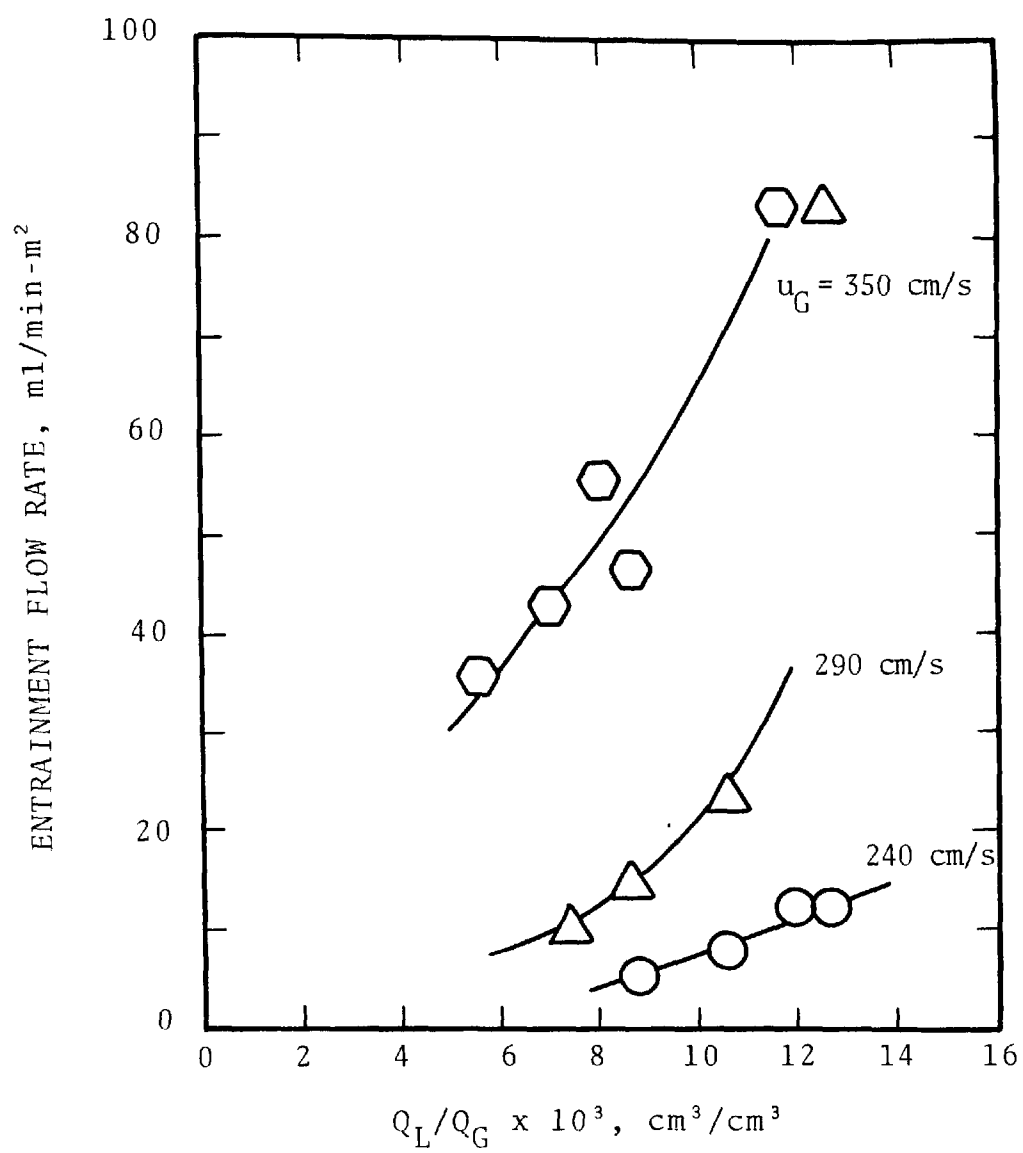


Figure 16. Entrainment flow rate (Drop counter data).

## SECTION 4

### MOBILE BED F/C SCRUBBER PILOT PLANT

#### MOBILE BED F/C SCRUBBER PILOT PLANT

The schematic flow diagram of the mobile bed F/C scrubber system is shown in Figure 17. Components of the scrubber system are listed in Table 6. Table 7 describes the flow rates in the lines shown in Figure 17 when the inlet gas stream to the scrubber is  $28 \text{ Am}^3/\text{min}$  (1,000 ACFM) and saturated with water vapor at  $60^\circ\text{C}$ .

Figures 18 through 22 are detailed design and layout of the mobile bed F/C scrubber pilot plant. A brief description of the pilot plant components are given below.

#### Mobile Bed Scrubber

The mobile bed scrubber shell was made from fiberglass reinforced plastic duct with an inside diameter of 0.51 m (20 in.). The overall height of the scrubber was 6.1 m (20 ft) of which 2.75 m (9 ft) was reserved for mobile beds. A maximum of three stages can be housed in this space. There was an empty space of 0.92 m (3 ft) above the top retaining grid. This space was provided for the settling out of large entrainment drops. Figure 23 is a schematic diagram of the mobile bed scrubber.

#### Mobile Bed Packing -

The mobile bed packings were hollow polypropylene spheres. Three sphere sizes -- 2.5 cm, 3.8 cm, and 5.1 cm diameter -- were studied. The average weight for each sphere was 1.5 g, 4.5 g, and 8.0 g for 2.5 cm, 3.8 cm, and 5.1 cm diameter balls, respectively.

#### Retaining and Supporting grids -

Two types of bed supporting and retaining grids were used in the mobile bed scrubber. They were hardware screens and

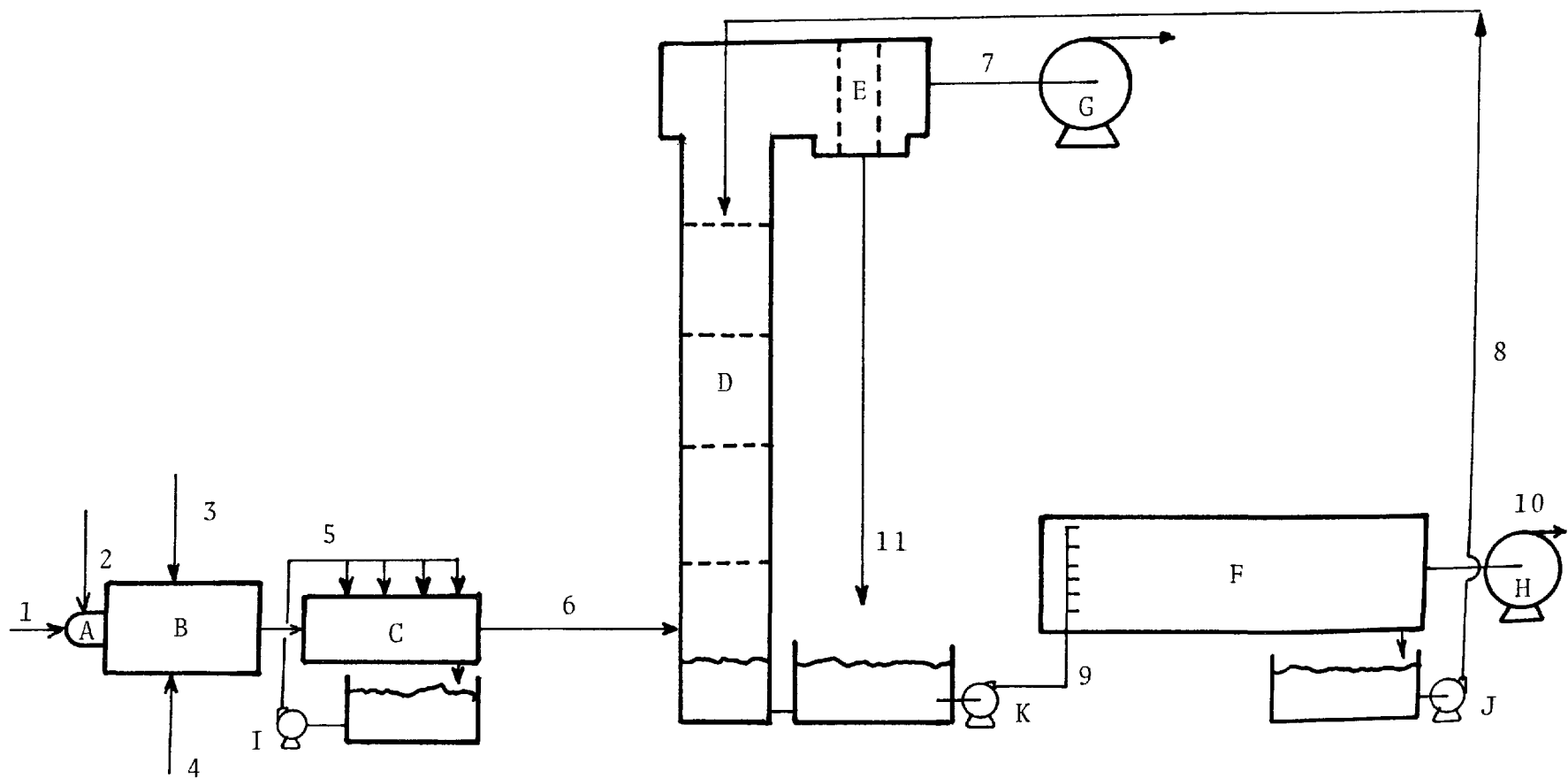


Figure 17. Process flow diagram of mobile bed F/C scrubber system.

TABLE 6. LIST OF PILOT PLANT COMPONENTS

EQUIPMENT

A. Gas Burner

Nozzle mix type, natural gas open flame gas burner with a capacity of  $3.52 \times 10^5$  J/s (1,200,000 Btu/hr).

B. Furnace

Insulating fire-brick lined, rectangular box with provision for dilution air and aerosol inlet.

C. Quencher

0.76 m in diameter and 2.44 m long horizontal vessel with fine water spray.

D. FF/C Scrubber

Three stage mobile bed.

E. Entrainment Separator

Staggered tube bank type demister.

F. Water Cooling Tower

A horizontal spray type. Cooling range  $17^\circ\text{C}$  ( $30^\circ\text{F}$ ) at 340  $\ell/\text{min}$  (90 GPM).

G. Blower

Centrifugal fan with capacity of  $1.23 \text{ m}^3/\text{sec}$  (2,610 CFM) and static head of 5.2 kPa (53 cm W.C.)

H. Cooling Tower Fan

$9.4 \text{ m}^3/\text{s}$  and 0.5 kPa (5 cm W.C.) head.

I. Pump

75  $\ell/\text{min}$  and 350 kPa pressure (20 GPM and 120 ft head).

J. Pump

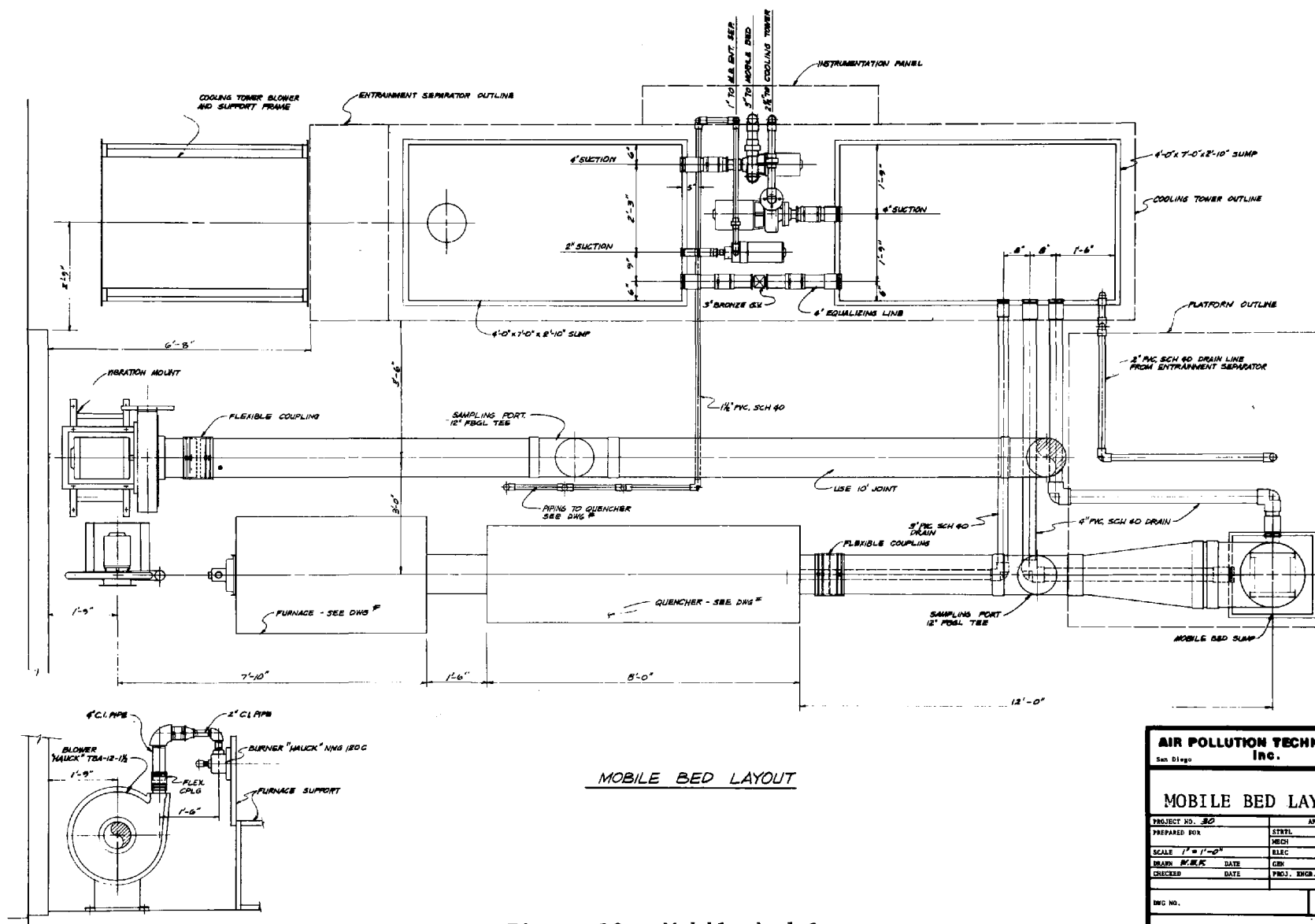
680  $\ell/\text{min}$  and 118 kPa pressure (180 GPM and 40 ft head).

K. Pump

610  $\ell/\text{min}$  and 350 kPa pressure (160 GPM and 120 ft head).

TABLE 7. FLOW RATES AND CONDITIONS FOR MOBILE  
BED F/C SCRUBBER PILOT PLANT

Stream No.	Composition	Temp. °C	Gauge Press. cm W.C.	Volume m <sup>3</sup> /s	Flow ℓ/s
1	Natural Gas	20	+17.8	0.0063	
2	Room air containing 0.007 g H <sub>2</sub> O/g dry air	29	--	0.069	
3	Room air containing 0.007 g H <sub>2</sub> O/g dry air	29	--	0.28	
4	Test aerosol dust	--	--	--	--
5	Water	32	305		1.25
6	Aerosol - air mixture containing 0.15 g H <sub>2</sub> O/g dry air	60	-17	0.47	
7	Air mixture contain- ing 0.043 g H <sub>2</sub> O/g dry air	38	-36	0.44	
8	Water	32	--		3.5
9	Water	49	305		3.5
10	Humid air	30	+ 5	708	
11	Water	49	--	--	--



MOBILE BED LAYOUT

Figure 18. Mobile bed layout.

<b>AIR POLLUTION TECHNOLOGY, Inc.</b>			
San Diego		California	
<b>MOBILE BED LAYOUT</b>			
PROJECT NO. 30	APPROVALS		
PREPARED FOR	STRYL		
SCALE 1" = 1'-0"	MECH		
DRAWN BY R.R.R.	DATE	CEN	
CHECKED	DATE	PROJ. ENGR.	DATE
DWG NO.		REVISION	

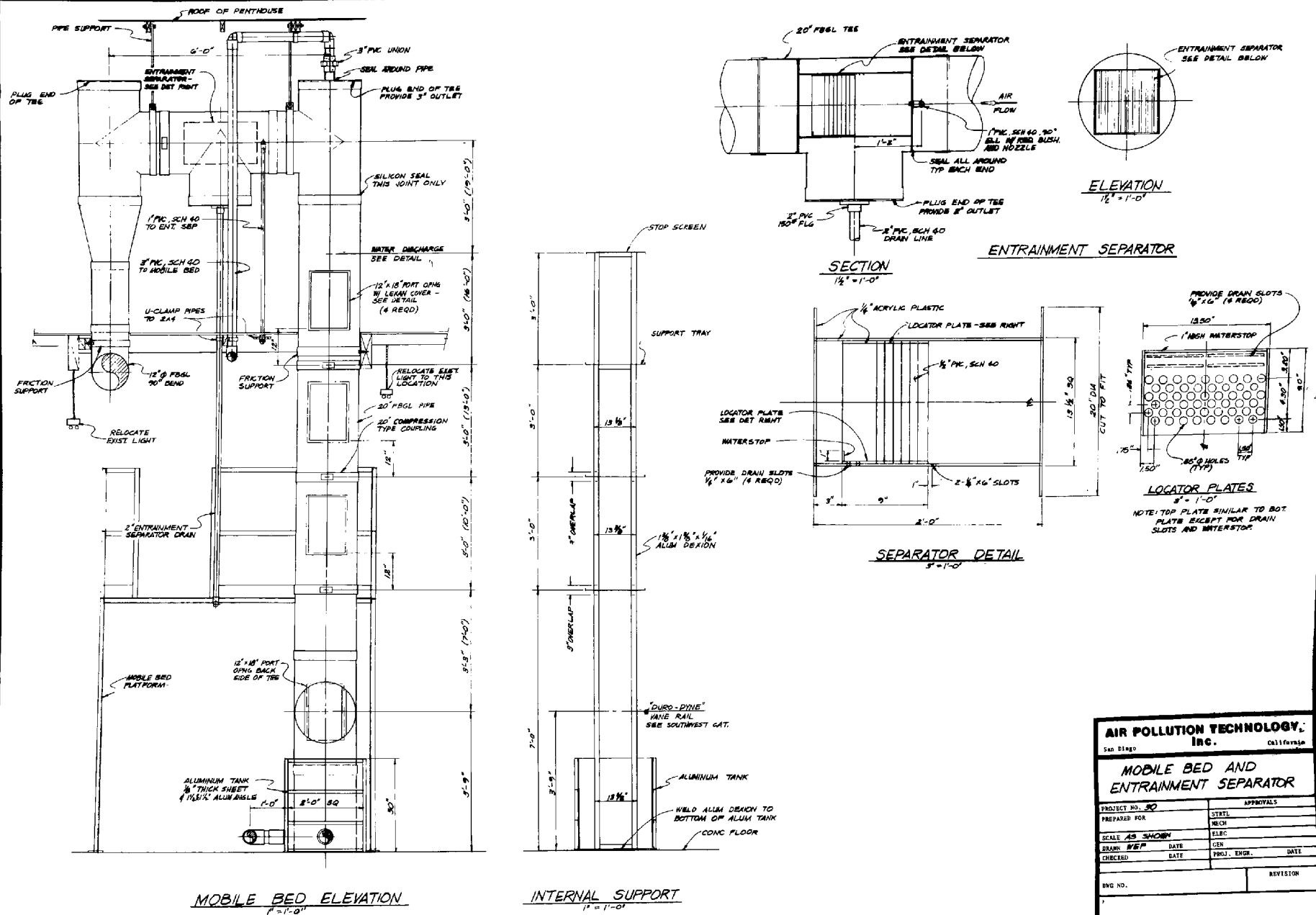


Figure 19. Mobile bed and entrainment separator.

<b>AIR POLLUTION TECHNOLOGY, Inc.</b>			
San Diego		California	
<b>MOBILE BED AND ENTRAINMENT SEPARATOR</b>			
PROJECT NO. 30		APPROVALS	
PREPARED FOR	DATE	STRTL	MECH
SCALE AS SHOWN	DATE	ELEC	
DRAWN BY	DATE	CEN	
CHECKED	DATE	PROJ. ENGR.	DATE
BVD NO.		REVISION	



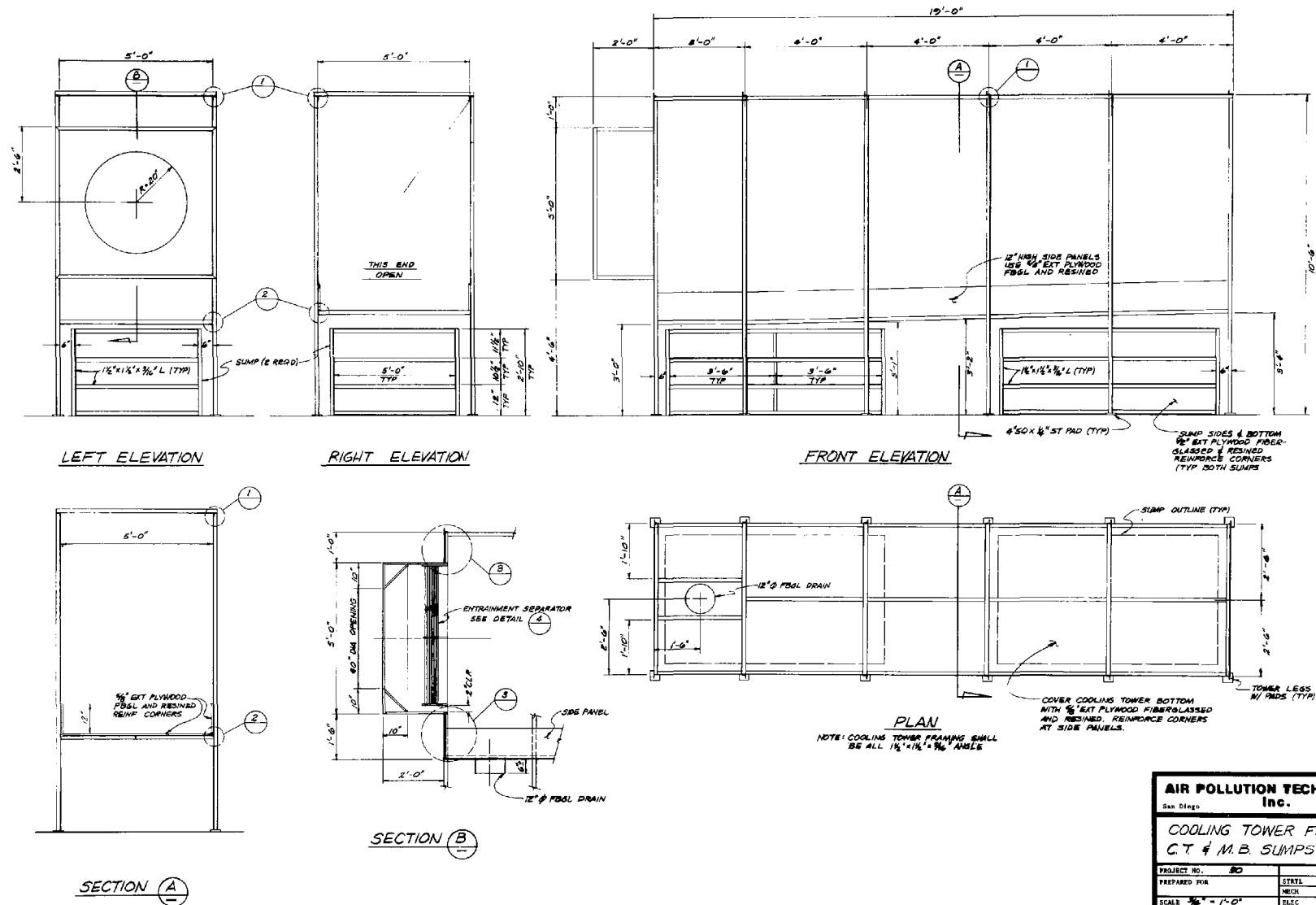


Figure 20. Cooling tower framing and mobile bed sumps.

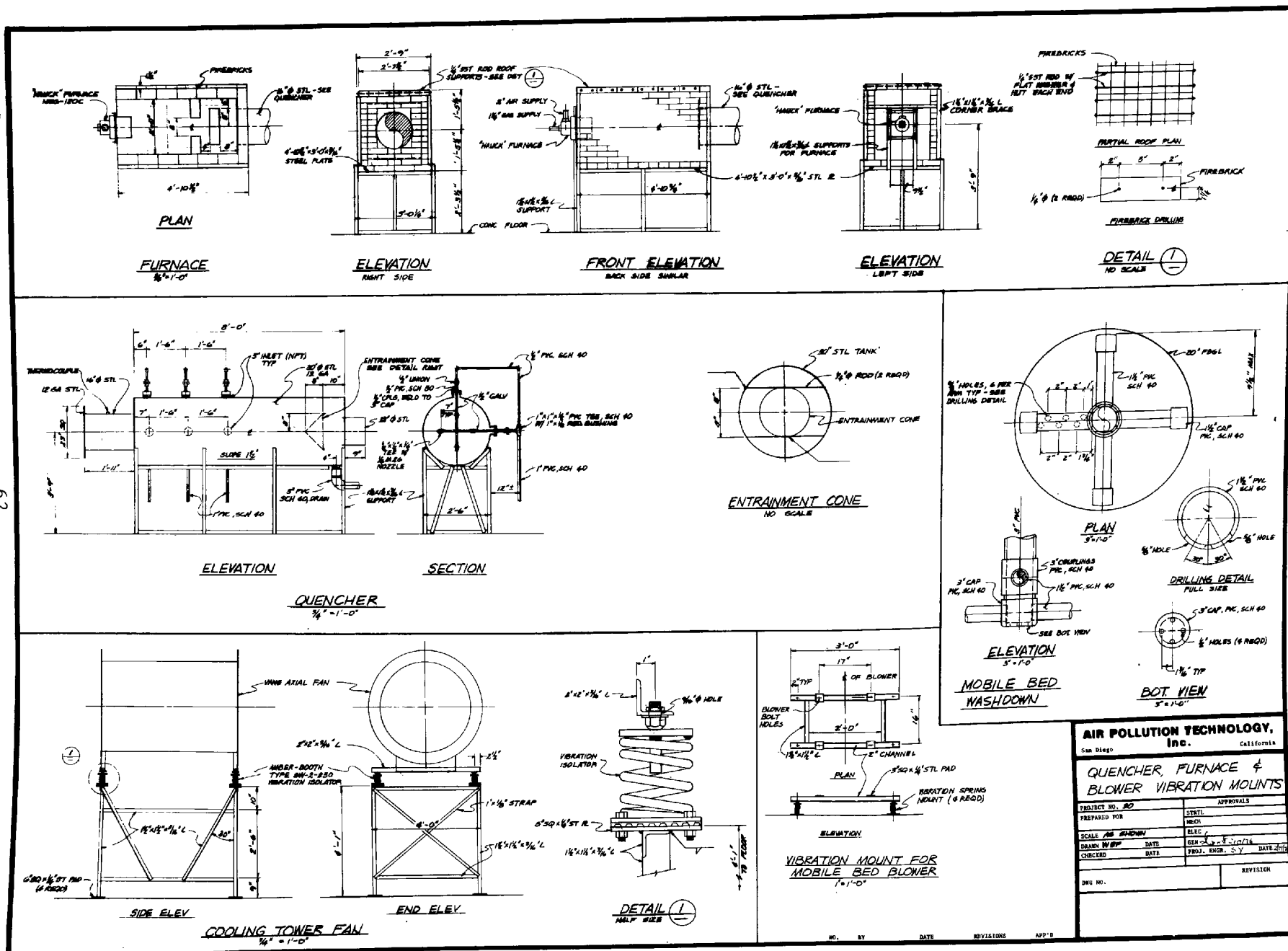
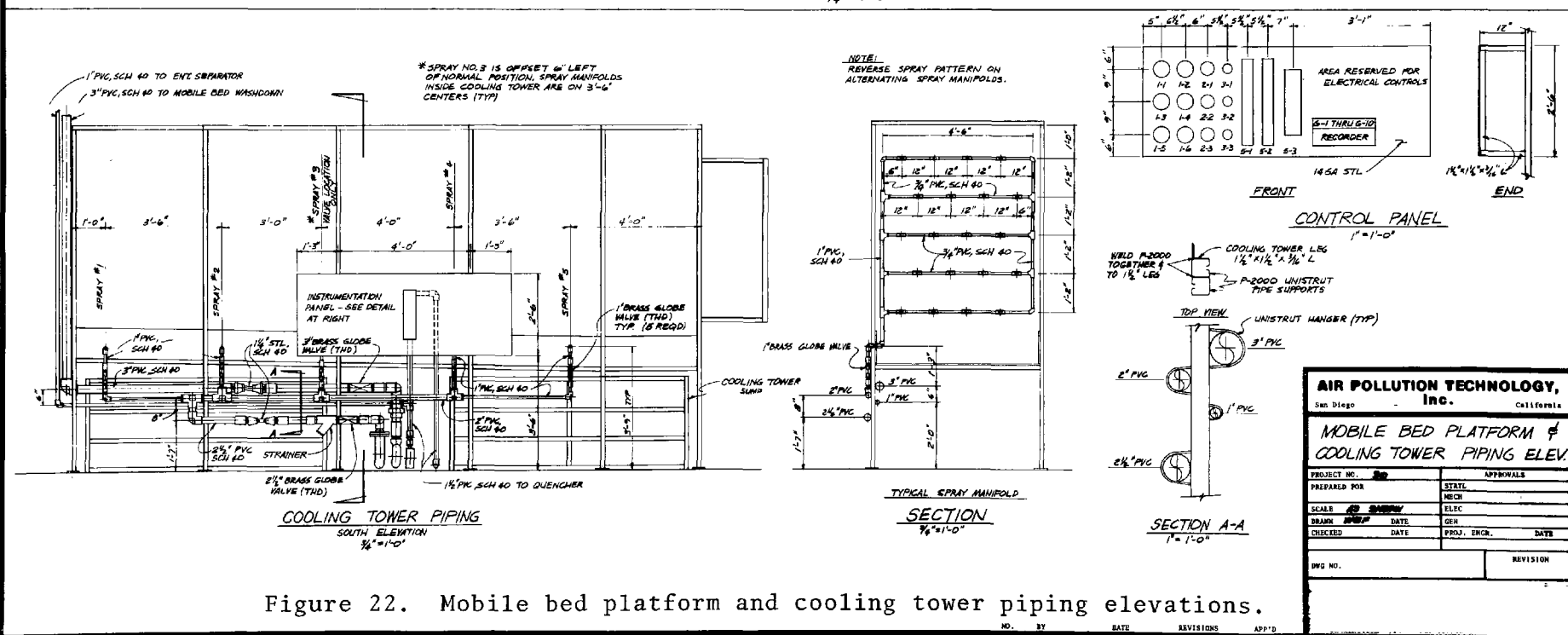


Figure 21. Quencher, furnace and blower vibration mounts.



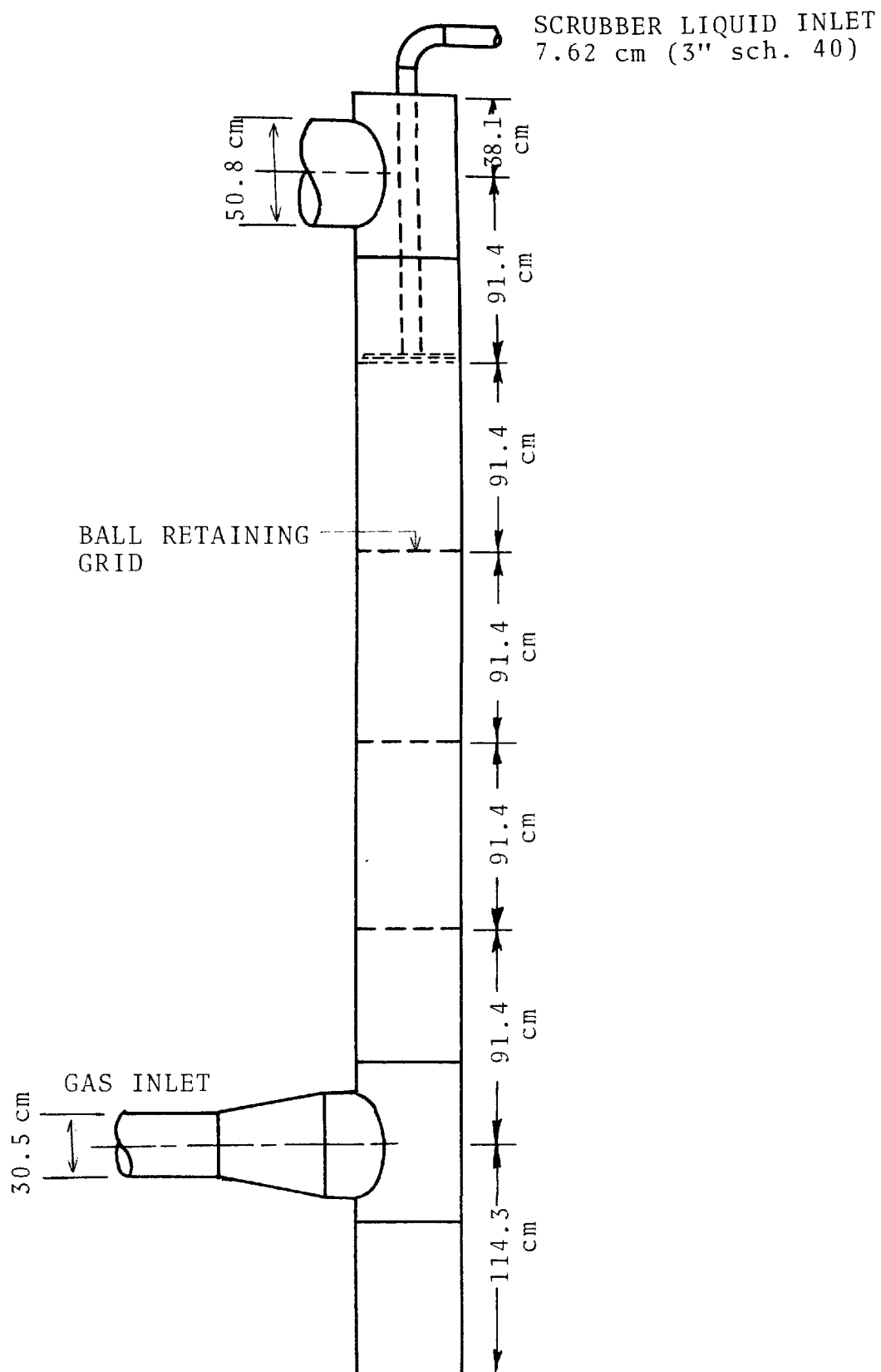


Figure 23. Mobile bed scrubber.

plastic nets. The wire diameter of the hardware screen was 0.16 cm (1/16 in.) and the openings were 1.1 cm x 2.4 cm (7/16 in. x 15/16 in.). The open area was about 82%. The plastic net was made of polypropylene ribbons which were 0.40 cm (5/32 in.) wide. The openings were 0.6 cm x 0.75 cm (15/64 in. x 19/64 in.) and the open area was about 40%. The grids were rested on square frames made of 2.5 cm aluminum angles 33 cm on a side. The effective open areas of the hardware screen support and the plastic net support were 68% and 34%, respectively.

#### Liquid Distribution -

Scrubber liquid was distributed evenly to the mobile bed just above the third stage top retaining grid through four PVC pipes (1-1/2" sch 40) drilled with 1.27 cm (0.5 in.) holes. The inlet header pipe was 3" sch 40.

#### Entrainment Separator

The entrainment separator consisted of six rows of staggered PVC pipe banks. The external diameter of the pipe was 2.13 cm (1/2" sch 40). The spacing between pipes within a row was 3.4 cm center to center. The cross section of the entrainment separator was 34.3 cm square.

#### Cooling Tower

The cooling tower was a horizontal cocurrent spray chamber. The cross section was 1.53 m x 2.14 m (5 ft x 7 ft) and the length of the spray section was 5.8 m (19 ft).

There were two entrainment separators at the outlet of the spray section. The first entrainment separator was zigzag baffles which were made of corrugated fiberglass. The second entrainment separator was pipe banks of the same design as that for the mobile bed scrubber. The baffles were used to remove large drops and to reduce the entrainment loadings reaching the pipe bank entrainment separator.

There were five spray banks, each with twenty spray nozzles. The liquid flow rate was 75  $\ell$ /min per spray bank at a pressure of 370 kPa (40 psig).

Ambient air was induced through the cooling tower by a vane-axial fan (Chicago Blower vane-axial fan size 40-1/4) with a capacity of 9.4  $\text{m}^3/\text{s}$  (20,000 CFM) at a pressure of 0.5 kPa (5 cm W.C.) and a 15 hp motor.

### Quencher

The quencher was a horizontal vessel with fine water spray. The spraying rate was about 75  $\ell$ /min (20 GPM). The vessel was 0.76 m (2.5 ft) in diameter and 2.44 m (8 ft) in length.

### Furnace

The furnace was a rectangular box lined with insulating fire brick. The dimensions of the furnace were 0.92 m wide, 0.92 m tall, and 1.53 m long (3' x 3' x 5'). There were fire brick baffles in the furnace to induce turbulence and to give better mixing of combustion flue gas and air.

The gas burner was a nozzle mix type natural gas burner (Hauck NMG-130). The capacity of the burner was  $3.52 \times 10^5$  J/s ( $1.2 \times 10^6$  BTU/hr). Some safety devices were installed to ensure the proper operation of the burner. The devices included a UV scanner (Fireye scanner UV-1) to sense the pilot flame, a temperature controller at the quencher outlet to guard against malfunction of the quencher, a pressure switch in the combustion air line to ensure a consistent air supply to the gas burner, high and low pressure switches in the natural gas pipe line to guard against abrupt changes in natural gas pressure, and two normally closed solenoid valves in the main and pilot gas line. A control system (Fireye chasis UVM-2A) was installed to coordinate the functionings of the scanner, pressure switches, temperature controller, and to regulate the solenoid valve.

## Gas and Liquid Mover

Air and water were used for studies. Air was induced through the mobile bed by means of a centrifugal fan (Chicago Blower Turbo-Pressure blower 2T-15-12) with a capacity of  $1.23 \text{ m}^3/\text{s}$  (2,610 CFM) and a static pressure of 5.2 kPa (53 cm W.C.)

Two rectangular tanks with dimensions of 84 x 120 x 210 cm were used to store and supply the scrubber liquid. One 55 gallon barrel was used to serve as the scrubber sump and water seal. Scrubber liquid was pumped to the top of the mobile bed by means of a centrifugal pump (Allis Chalmers C-1). The capacity of the pump was 680  $\ell/\text{min}$  at a pressure of 118 kPa (180 GPM at 40 ft head).

The cooling tower pump was a centrifugal pump manufactured by Allis Chalmers with a capacity of 610  $\ell/\text{min}$  at a pressure of 350 kPa (160 GPM at 120 ft head). The quencher pump was a small centrifugal pump with a capacity of 75  $\ell/\text{min}$  at a pressure of 350 kPa (20 GPM at 120 ft head).

## INSTRUMENTATION AND CALIBRATION

The gas flow rate through the mobile bed scrubber was monitored by a venturi meter located in the scrubber outlet duct. It was calibrated against flow rates measured by standard pitot tube traverses.

Liquid flow rates were also measured by venturi meters. They were calibrated by measuring the volume of liquid flowing through the pipes in a given time.

Temperatures in the scrubber system were measured by copper-constantan (type T) thermocouples. The thermoelectric voltages were recorded on a strip chart recorder equipped with a potentiometric amplifier. The thermocouples were calibrated against a standard mercury bulb thermometer using constant temperature baths. In the latter part of the experiment, type K thermocouples and a digital temperature readout (Omega Engineering model 175-KF1) were used.

The scrubber gas line pressures were measured by "Magne-helic" pressure gauges. Pressure differences in the liquid venturi meters were measured with well-type mercury manometers. Pressure difference in the gas venturi meter was monitored with an inclined manometer.

Moisture contents in the inlet and outlet gas streams of the scrubber were measured by wet and dry bulb thermometers.

#### PARTICLE GENERATOR

The schematic diagram of the particle generator is shown in Figure 24. The aerosol was generated by redispersing the powder with a jet of compressed air which was ionized by passing through a Polonium 210 ionizing air nozzle (3M Company, model 906).

In the beginning of a test run, aerosol powder was loaded into the vibrating hopper and was fed by a screw feeder arrangement into the compressed air jet. The feed rate of the powder was controlled by regulating the screw turning speed through a variable speed motor. The air jet dispersed the powder into airborne particles. The dispersed aerosol next entered the cyclone pre-cutter to remove coarse particles from the dispersed aerosols. The aerosol then passed through a parallel plate electrostatic precipitator to remove any charged particles before entering the scrubber inlet duct.

The electrostatic precipitator consisted of 19 alternatively charged flat plates. The plates were 30.5 x 91.5 cm 20 gauge aluminum plates. Plate spacing was 1.5 cm. The maximum applied voltage was 10 kV.

#### PARTICULATE SAMPLING SYSTEM

Two identical, modified EPA Method 5 particle sampling trains with in-stack University of Washington Mark III cascade impactors were used to measure the particulate loadings and size distributions in the scrubber gas inlet and outlet streams simultaneously. Isokinetic sampling technique was used in the entire experimental program. The impactors in the inlet and outlet



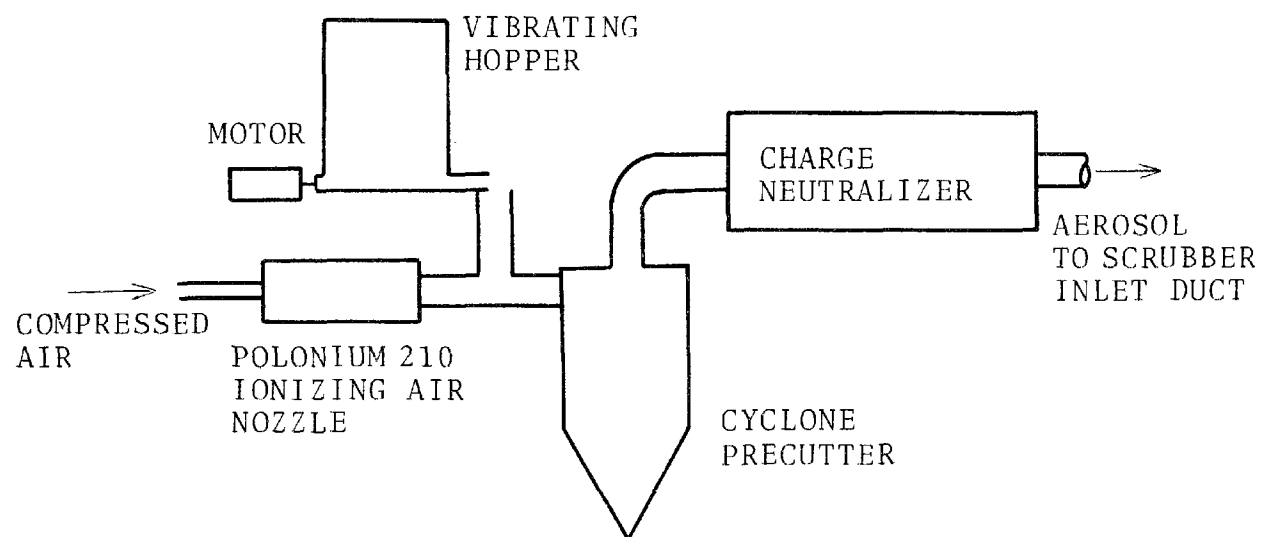


Figure 24. Powder redispersion particle generator.

were allowed to heat up to gas temperature before samples were taken.

The particle number concentration was measured using a batch dilution system and two particle counters - a Gardner Condensation Nuclei Counter (CNC) and an Electrical Mobility Analyzer (EMA) by Thermal Systems.

## DATA REDUCTION METHODS

### Particle Size Distribution

The particle size distributions were measured gravimetrically using the cascade impactor data.

The particle diameter measured by an impactor is called "aerodynamic diameter" and it has the units of "aerodynamic microns,  $\mu\text{mA}$ ." This is the effective diameter for particle separation by inertial impaction and it takes into account the effects of particle density and particle slip between gas molecules. Aerodynamic diameter is related to geometric diameter (actual size) by the following relationship:

$$d_{pa} = d_p (C' \rho_p)^{0.5} \quad (20)$$

where  $d_{pa}$  = aerodynamic diameter,  $\mu\text{mA} \equiv \mu\text{m} \sqrt{\text{g}/\text{cm}^3}$   
 $d_p$  = actual diameter,  $\mu\text{m}$   
 $C'$  = Cunningham slip factor, dimensionless  
 $\rho_p$  = particle density,  $\text{g}/\text{cm}^3$

The Cunningham slip factor is a complex function of the mean free path of the gas and the particle diameter. It increases as temperature increases and as pressure decreases. For air at standard temperature and pressure it is given approximately by:

$$C' = 1 + \frac{0.165}{d_p} \quad (21)$$

Cumulative mass of particles collected on a stage and all the stages below, including the absolute filter, were calculated as a percentage of the total weight gain. The cut diameters for the impactor stages were determined from the sampling flow rate and impactor calibration.

The particles were assumed to have a log-normal distribution. The cascade impactor stage cut diameters were plotted against the percent by weight of particles smaller than the cut diameters on a log-probability paper. A straight line was fitted to the data points. The 50% value of " $d_{pa}$ " is the geometric mass median diameter, " $d_{pg}$ " and the 84.1% value of " $d_{pa}$ " divided by the mass median diameter is equal to the geometric standard deviation, " $\sigma_g$ ".

#### Particle Loadings and Overall Penetrations

The total loadings in the inlet and outlet ducts were calculated in the following manner:

1. The sample flow rate was converted to the standard conditions of 0°C and 76 cm of mercury pressure.
2. Total weight gain on the sampling elements was measured with an analytical balance, Sartorius Model 244,  $\pm 0.05$  mg precision.
3. The particle mass loading,  $c_p$  (g/DNm<sup>3</sup>), was calculated from:

$$c_p = \frac{(\text{Total weight gain, g})}{(\text{Sampling rate, DNm}^3/\text{min}) \times (\text{Sampling time, min})}$$

4. The overall penetration was calculated from:

$$\overline{pt} = \frac{c_{po}}{c_{pi}} \quad (22)$$

where " $c_{po}$ " and " $c_{pi}$ " were the outlet and inlet particle loadings measured simultaneously for the run.

## Fractional Penetrations

The computation of penetration as a function of particle aerodynamic diameter, or the grade penetration through the scrubber, was done by a stepwise graphical procedure. The procedure is based on the following equations:

Overall penetration can be defined as:

$$\overline{Pt} = \frac{1}{c_{pt}} \int_0^c Pt_d dc_p \quad (23)$$

where " $c_{pt}$ " is the total particle loading and " $Pt_d$ " is the penetration for particle diameter " $d_{pa}$ " and it is given by:

$$Pt_d = \frac{f(d_{pa})_o}{f(d_{pa})_i} = \frac{\left[ \frac{dc_p}{d(d_{pa})} \right]_o}{\left[ \frac{dc_p}{d(d_{pa})} \right]_i} \quad (24)$$

where  $\left[ \frac{dc_p}{d(d_{pa})} \right]$  is the slope of cumulative mass loading less than " $d_{pa}$ " versus the aerodynamic particle diameter curve at " $d_{pa}$ ", and equals " $f(d_{pa})$ ".

Thus, to determine the fractional penetration, the following procedure was followed:

1. Cumulative mass loading for all the stages and the filter, below the stage with a cut diameter of " $d_{pa}$ ", was plotted against " $d_{pa}$ " from the inlet and outlet cascade impactor samples.
2. Slopes of the inlet and outlet plots above were determined for several " $d_{pa}$ " values in the range of 0.4 to 10  $\mu m$ . The fractional penetrations were then determined from the ratio of the slopes, as described above.

3. The fractional penetrations were plotted against particle diameters. The curve is termed grade penetration curve. The diameter whose penetration is 0.5 is the performance cut diameter of the scrubber.

#### Particle Number Concentration

Particle number concentration is an important parameter for F/C scrubbing. In the present study, particle number concentration was measured by means of a Gardner Condensation Nuclei Counter (C.N.C.) and a Thermal Systems Electrical Mobility Analyzer (E.M.A.).

Particle number can also be calculated from cascade impactor data if the size distribution is log-normal. The procedures are as follows:

1. Convert the impactor stage aerodynamic cut diameter into physical size diameter (equation 20).
2. Plot the physical cut diameter against the percent by weight of particles smaller than the cut diameter on a log-probability paper.
3. Obtain the physical geometric mean diameter,  $d'_{pg}$ , and geometric standard deviation,  $\sigma'_g$ , from the plot.
4. Calculate the mass mean diameter by the following equation:

$$\ln d_m = \ln d'_{pg} - 1.5 \ln^2 \sigma'_g \quad (25)$$

where  $d_m$  = mass mean diameter,  $\mu m$   
 $d'_{pg}$  = physical geometric mass median diameter,  $\mu m$   
 $\sigma'_g$  = physical size geometric standard deviation,  
dimensionless

5. Number concentration is calculated from

$$n_p = \frac{N}{V_s} = \frac{6m}{\pi \rho_p d_m^3} \frac{1}{V_s} \times 10^{12} \quad (26)$$

where  $n_p$  = particle number concentration,  $\#/cm^3$   
 $N$  = total number of particles, #  
 $V_s$  = volume of gas sampled,  $cm^3$   
 $m$  = total mass of particles, g  
 $\rho_p$  = particle density,  $g/cm^3$

## SECTION 5

### EXPERIMENTS

#### EXPERIMENTAL CONDITIONS STUDIED

The mobile bed scrubber performance was evaluated for three different scrubber operation modes. They were: 1) cold, 2) slurry scrubbing, and 3) F/C scrubbing.

##### Cold Runs

A cold run is defined as the condition in which both the gas and liquid going to and from the scrubber are at ambient temperatures. No preconditioning is applied to either one. This operation mode was designed to isolate the collection mechanisms which are responsible for particle collection in a mobile bed.

Air and water were used for this operation mode. Variables studied included: superficial gas velocity, liquid flow rate, packing diameter, static bed height, types of supporting grid, types of aerosol, and number of mobile bed stages.

The ranges of the variables studied were:

1. Superficial gas velocities ranged from 200 cm to 500 cm.
2. Liquid flow rates ranged from 136  $\ell$ /min to 410  $\ell$ /min.
3. Packing diameters. Three types of packing were studied. They were 2.5, 3.8, and 5.1 cm diameter polypropylene spheres. The average weight for each sphere was 1.5 g, 4.5 g, and 8.0 g for 2.5 cm, 3.8 cm, and 5.1 cm diameter balls, respectively. Since the 3.8 cm diameter balls are commonly used in industrial mobile beds, most of the experiments were conducted with this size packing.

4. Static bed height of the packing. Three bed depths were studied. They were 15, 23, and 30 cm.
5. Number of mobile bed stages. One, two, and three stage mobile beds were studied.
6. Supporting grids. Two types of supporting and retaining grids were studied. They were hardware screen and plastic nets. The characteristics of the supporting grids were presented in the last section.
7. Aerosol. Four types of aerosol dust were used. They were titanium dioxide, red iron oxide, power plant fly ash, and gray-iron cupola dust.

### Slurry Scrubbing

Experience with the  $\text{SO}_x$  scrubber systems at many power plants and experimental facilities has shown that the entrainment of scrubber liquid is a significant source of particulate effluent. The main objectives of the slurry test were:

1. Characterize the effect of scrubber slurry on emissions due to entrainment.
2. Evaluate any influence on the particle collection mechanism due to the slurry properties.

The experimental system for the slurry study was the same as the setup for the cold operation mode experiment, except for the addition of  $\text{CaCO}_3$  powder to the scrubbing liquor. No other chemical was added to modify the slurry. The slurry pH value and density were determined by an Electro-Mark pH Analyzer and by weight-volume measurement, respectively. The conditions studied were as follows:

1. Mobile bed scrubber  
A three stage mobile bed, each packed with 3.8 cm diameter spheres to a depth of 23 cm, was studied.
2.  $\text{CaCO}_3$  concentration (by weight)  
5% (pH value = 8.00, density =  $1.07 \text{ g/cm}^3$ ) and 10% (pH value = 8.2, density =  $1.18 \text{ g/cm}^3$ )



3. Superficial gas velocity  
250 and 320 cm/s of air velocity were tested.
4. Liquid flow rate  
227 l/min and 318 l/min were studied.
5. Aerosol powder  
Gray iron cupola dust was used as the aerosol powder.

### F/C Scrubbing

F/C (flux force/condensation) scrubbing is a particle collection mechanism which combines the collection phenomena of diffusiophoresis, thermophoresis, and particle growth by condensing water vapor on the particles. Depending on the condensation ratio, F/C scrubbing can be very efficient in removing submicron particles.

The benefit of condensation scrubbing was studied under this operation mode. The study was focused on the effect of condensation ratio and the particle collection efficiency.

The following conditions were studied:

1. Packing - 3.8 cm diameter hollow polypropylene spheres.
2. Bed height - 23 cm static bed height.
3. Gas velocity - 210 and 340 cm/s
4. Liquid flow rate - 273 l/min.
5. Condensation ratio - 0 to 0.25 gram of water condensed per gram of dry gas scrubbed.
6. Aerosol - gray iron cupola dust.
7. Supporting grids - hardware screen and plastic net.

## EXPERIMENTAL PROCEDURES

### Cold Runs

The mobile bed scrubber was the only equipment in operation for this operation mode. The cooling tower, burner, and the quencher were idle. Air and water at ambient conditions were used for study.

In starting the experiment, air and water flow rates were adjusted to and maintained at the desired levels. After steady conditions were reached, gas and liquid temperatures and the pressure drop were recorded. Aerosols were injected into the system at a location either before or after the quencher. Particle size distribution and loading were measured simultaneously at the scrubber inlet and outlet ducts by means of in-stack cascade impactors. Performance of the scrubber was calculated from the impactor data.

### Slurry Scrubbing

The experimental procedures were the same as that for cold runs except slurry was used as the scrubber liquid.

### F/C Scrubbing

Clean water and air were used for study in this mode of operation. In starting a run, the following procedures were followed:

1. Start the scrubber liquid pump and adjust the flow rate to desired level.
2. Start the quencher and adjust the flow rate.
3. Start the cooling tower and adjust spraying rate.
4. Turn on the mobile bed blower and adjust the flow rate.
5. Turn on the burner, monitor the gas temperature at the furnace outlet, and adjust the burner to obtain the desired gas temperature.
6. Readjust the flow rate through the mobile bed.
7. After steady state condition is reached, record the gas temperatures, liquid temperatures and pressure drops.
8. Inject aerosols into the furnace and start the sampling equipment.

## EXPERIMENTAL RESULTS

Experimental and sampling procedures, and the methods of data analyses and calculation of results are described in the preceding sections. During the experimental study, scrubber performance was determined as fractional penetration of particles (with respect to the aerodynamic particle diameter) and the overall particle penetration through the scrubbers. Since the scrubber inlet particle characteristics (size distribution and number concentration) were different for each run, the fractional penetrations provide a common base for comparing scrubber performances for different conditions.

The scrubber operating conditions and performance are tabulated in Appendix B. The fractional penetration plots for all cascade impactor runs are given in Appendices "C" through "E".

## DISCUSSIONS

### Cold Runs

#### Pressure Drop -

A typical diagram of the pressure drop across a mobile bed is shown in Figure 25 (Tichy and Douglas, 1973). If the liquid velocity is kept constant while the gas velocity is increased from zero, the following sequence of phenomena can be observed. At first, the packing spheres remain motionless in a static condition. The pressure drop in this region increases sharply with an increase in gas velocity. The condition continues until the gas velocity reaches the minimum fluidization velocity; i.e., the gas velocity at which the pressure drop is equal to the weight of packing plus weight of liquid holdup.

Increasing the gas velocity beyond the minimum fluidization velocity results in expansion and fluidization of the bed. The bed behaves like an aggregated fluidization bed and is called a mobile bed. For a mobile bed operating in the mode of

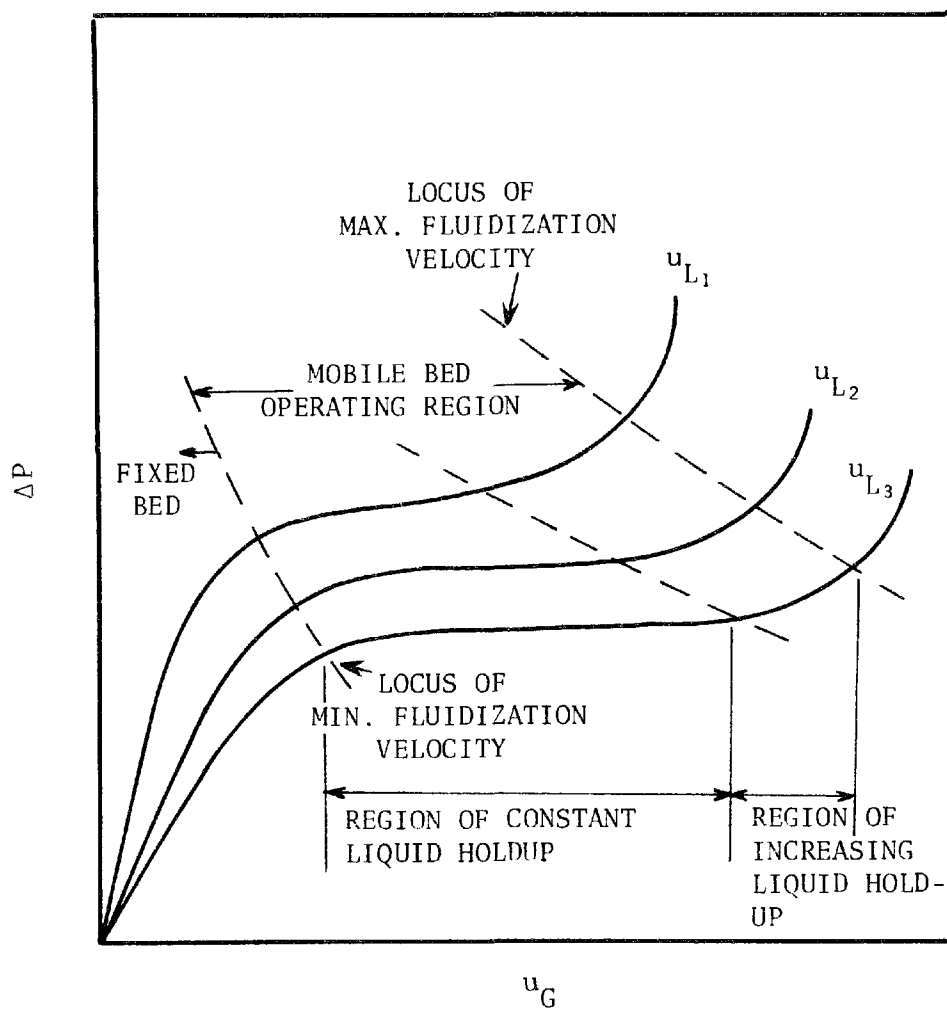


Figure 25. Pressure drop across one stage of a mobile bed versus gas velocity with liquid velocity as parameter.

fluidization without flooding (see next section for definition), liquid holdup at a fixed liquid rate remains approximately constant for different gas rates. The pressure drop across the bed levels off to a constant value as shown in Figure 25.

As the gas velocity increases further, approaching the terminal settling velocity of the wetted packing spheres, liquid holdup gradually increases. The pressure drop across the bed increases accordingly.

When the gas velocity reaches the terminal settling velocity of the wetted packing, the packing is pushed up underneath the upper retaining grids. When this happens, the mobile bed becomes a packed bed and pressure drop again increases sharply with gas flow rate.

The above sequence was confirmed in the present study. The experimental pressure drop curve for a mobile bed with hardware screen support (Figure 26) is similar to Figure 25.

For a fully developed mobile bed, the pressure drop is made up of the sum of the pressure drops due to the dry retaining grids, the weight of dry packing, the liquid layer retained on the supporting grid, the liquid retained in the bed, atomization of liquid drops and the wall friction (Blyakher et al., 1967; Kito et al., 1976); i.e.

$$\Delta P_w = \Delta P_b + \Delta P_{Lh} + \Delta P_L + \Delta P_a + \Delta P_c + \Delta P_f \quad (27)$$

where:  $\Delta P_w$  = overall pressure drop for one stage of the mobile bed, cm W.C.

$\Delta P_b$  = pressure drop due to weight of dry packing, cm W.C.

$\Delta P_{Lh}$  = pressure drop due to liquid holdup, cm W.C.

$\Delta P_L$  = pressure drop due to liquid head retained on supporting grid, cm W.C.

$\Delta P_a$  = pressure drop due to drop atomization, cm W.C.

$\Delta P_c$  = pressure drop due to wall friction, cm W.C.

$\Delta P_f$  = pressure drop due to friction of supporting grid, cm W.C.

If there is no liquid retained on the supporting grids and the losses due to wall friction, supporting grid friction, and drop

atomization are small, the pressure drop across the mobile bed can be considered equal to the sum of the weight of the packing and the liquid holdup in the bed (Tichy and Douglas, 1973; Kito et al., 1976), i.e.

$$\begin{aligned}
 \Delta P_w &= \Delta P_b + \Delta P_{Lh} \\
 &= (h_L \rho_L + h_b \rho_b) g H_d \\
 &= (h_{Lo} \rho_L + h_{bo} \rho_b) g H_s
 \end{aligned}
 \tag{28}$$

where  $\Delta P_w$  = overall pressure drop per stage of bed, cm W.C.

$\Delta P_b$  = pressure drop due to the weight of dry packing, cm W.C.

$\Delta P_{Lh}$  = pressure drop due to the weight of liquid holdup, cm W.C.

$h_L$  = liquid holdup in bed,  $\text{cm}^3/\text{cm}^3$

$\rho_L$  = density of liquid,  $\text{g}/\text{cm}^3$

$h_b$  = packing holdup,  $\text{cm}^3/\text{cm}^3$

$\rho_b$  = packing density,  $\text{cm}^3/\text{cm}^3$

$g$  = gravitational acceleration,  $\text{cm}/\text{s}^2$

$H_d$  = dynamic bed height, cm

$h_{Lo}$  = liquid holdup related to fixed bed,  $\text{cm}^3/\text{cm}^3$

$h_{bo}$  = packing holdup related to fixed bed  
 $= 1 - \epsilon$ ,  $\text{cm}^3/\text{cm}^3$

$H_s$  = static bed height, cm

$\epsilon$  = static bed porosity, fraction

Chen and Douglas (1968), Woźniak (1975), and Kito et al. (1976) experimentally measured the liquid holdup in a mobile bed. They found that the liquid holdup per unit of fixed bed volume is approximately independent of gas flow rate (Chen and Douglas's correlation and Kito et al.'s correlation for liquid holdup in a mobile bed are given in a later section). Since the weight of dry packing is also independent of gas flow rate, the pressure drop across a fully developed mobile bed is expected to be independent of gas flow rate.

Figure 26 is the pressure drop data for the three stage hardware screen supported mobile bed scrubber. The pressure drop of the scrubber without packing is small (0.4 cm W.C. at

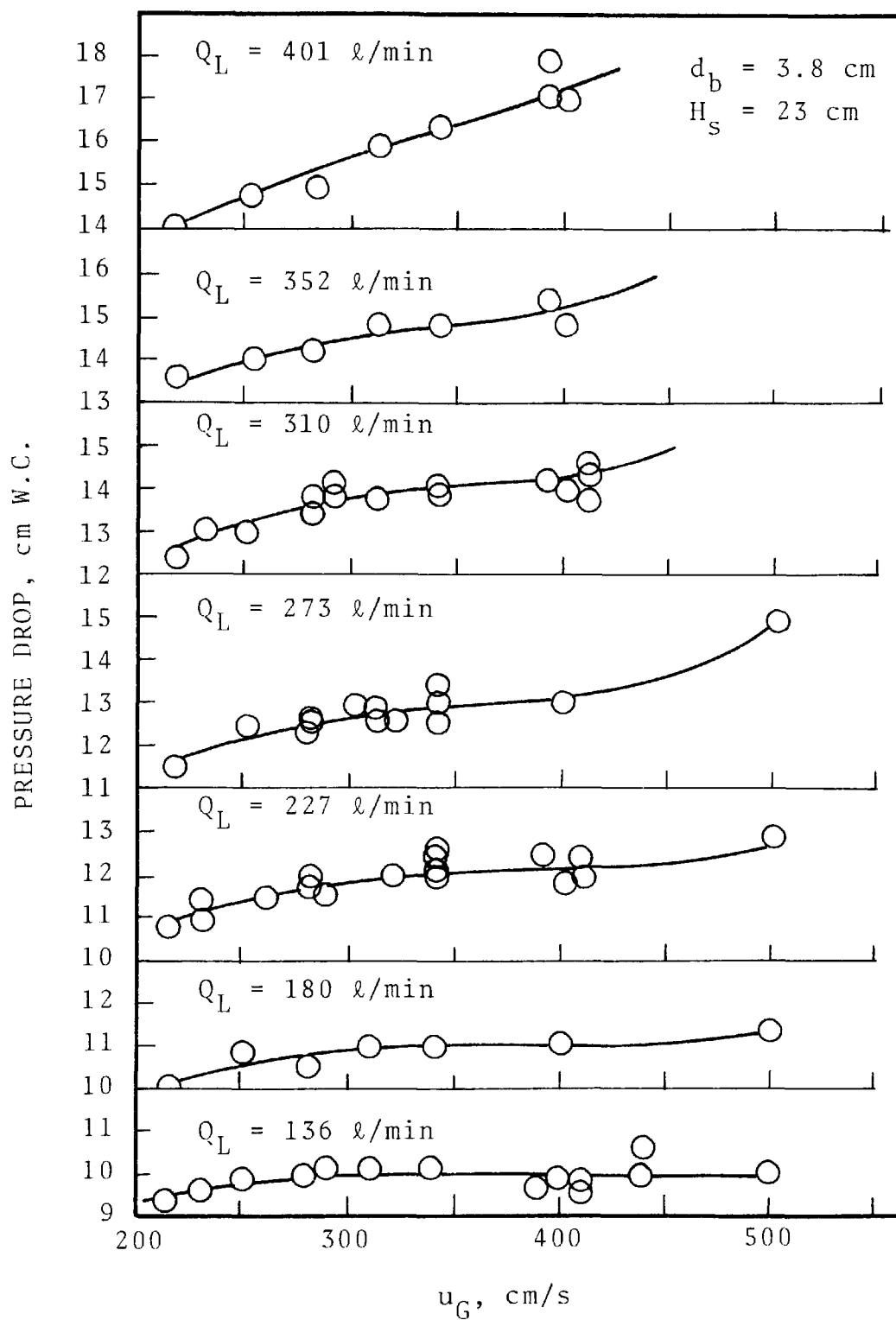


Figure 26. Experimental pressure drop of a 3-stage mobile bed with hardware screen support.

$u_G = 500 \text{ cm/s}$ ) and can be neglected. The measured pressure drop across the mobile bed is almost independent of gas flow rate when the liquid rate is low. At higher liquid rate, the pressure drop is slightly dependent on gas flowrates. These findings are consistent with Wóznia (1975), Blyakher, et al., (1967), Barile and Meyer (1973), and Epstein, et al.,'s results. Wóznia has found that the pressure drops increase proportionally to the linear gas velocity to the 0.2 power.

Figure 27 is a plot of the pressure drop versus liquid-to-gas ratio with superficial gas velocity as parameter. The mobile bed is 23 cm deep of 3.8 cm diameter spheres. The bed support and retaining grids were hardware screens. As can be seen, the pressure drop varies linearly with liquid-to-gas ratio. The slope of the straight lines depends on the gas velocity.

Figure 28 shows the effects of static bed depth and number of stages on pressure drop. The pressure drop is approximately proportional to the number of mobile bed stages but not to the static bed depth. The pressure drops increase proportionally to the static bed depth to the 0.84 power.

Figure 29 shows the effect of packing sphere diameter on pressure drop. As can be seen, pressure drop is higher for a smaller ball diameter. This is expected since smaller packing not only has a higher packing density, it also has higher liquid holdup. Both of these contribute to higher pressure drop.

Plastic Net - Figure 30 shows the pressure drop data of the plastic net supported mobile bed. Under the same operating conditions, the plastic net support has a higher pressure drop than the hardware screen support. The increase in pressure drop is not solely due to the high friction loss of the plastic net support.

Two possible factors cause the pressure drop to rise with the plastic net support. The first one is that liquid holdup in the bed may be higher than with other support. In Chen and Douglas' experiment, they only used one type of supporting grid, parallel rods. Therefore, in their correlation the effects of the supporting grid geometry on liquid holdup was not accounted for.



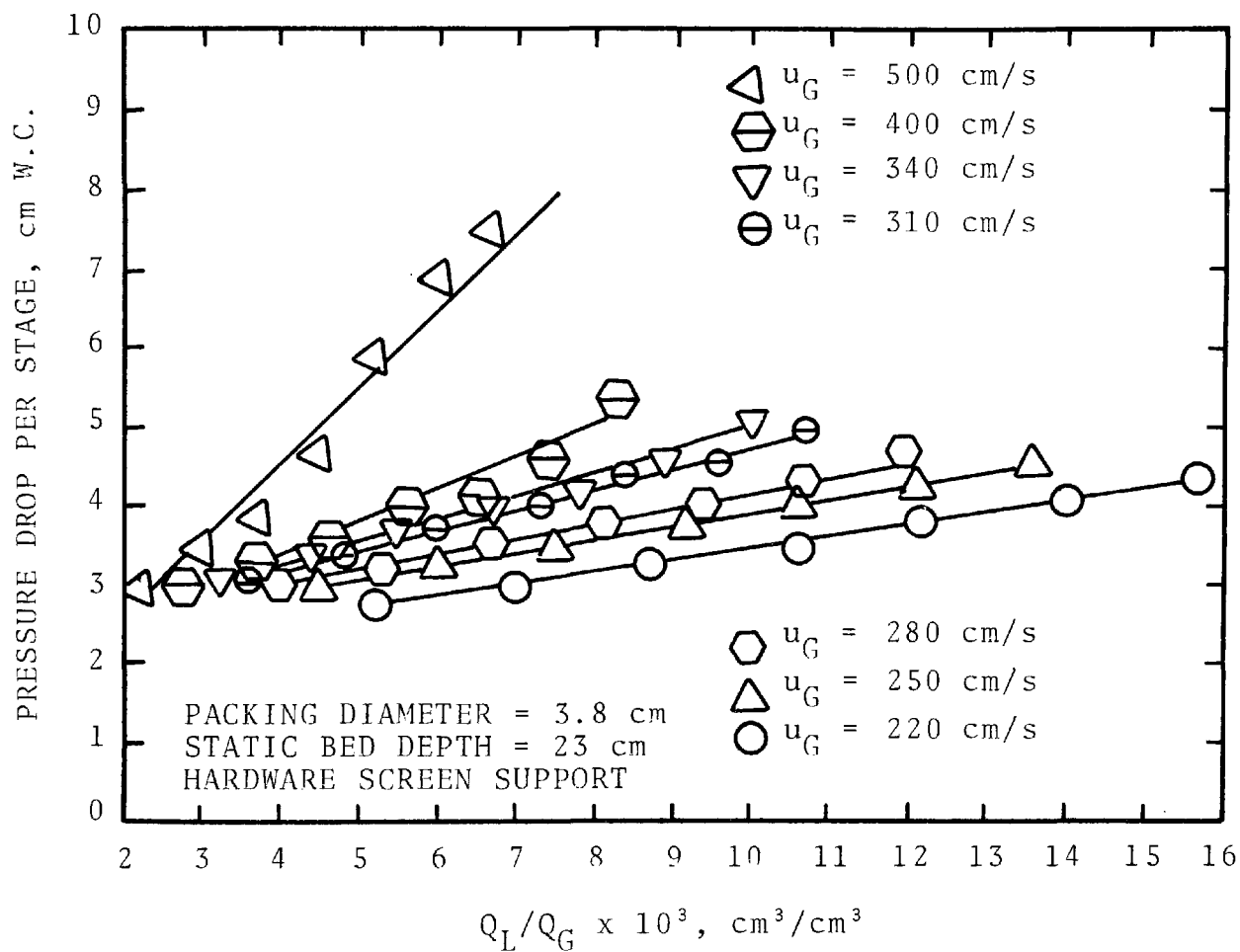


Figure 27. The variation of pressure drop with liquid-to-gas ratio and air velocity.

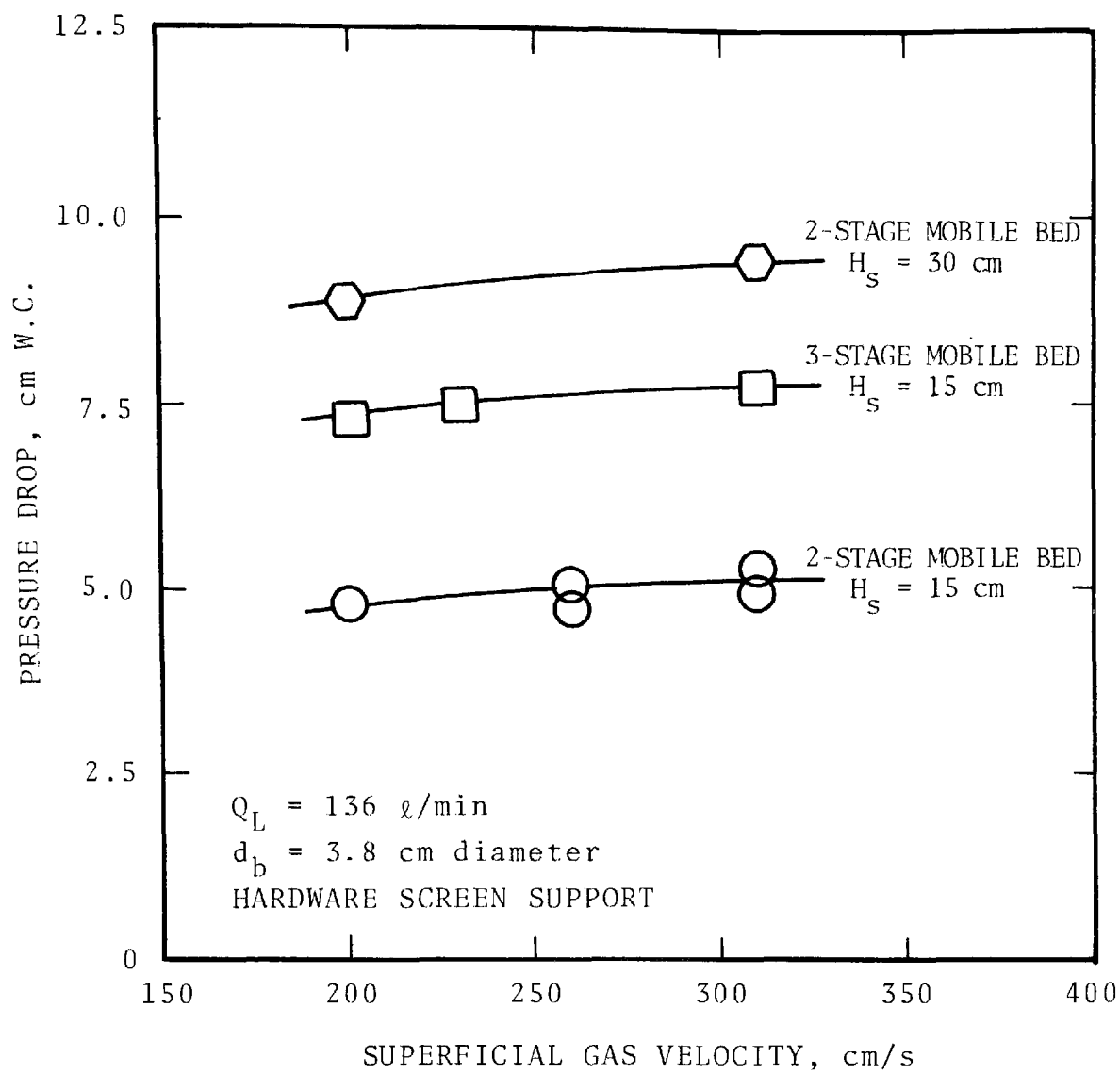


Figure 28. Effects of bed depth and number of stages on pressure drop.

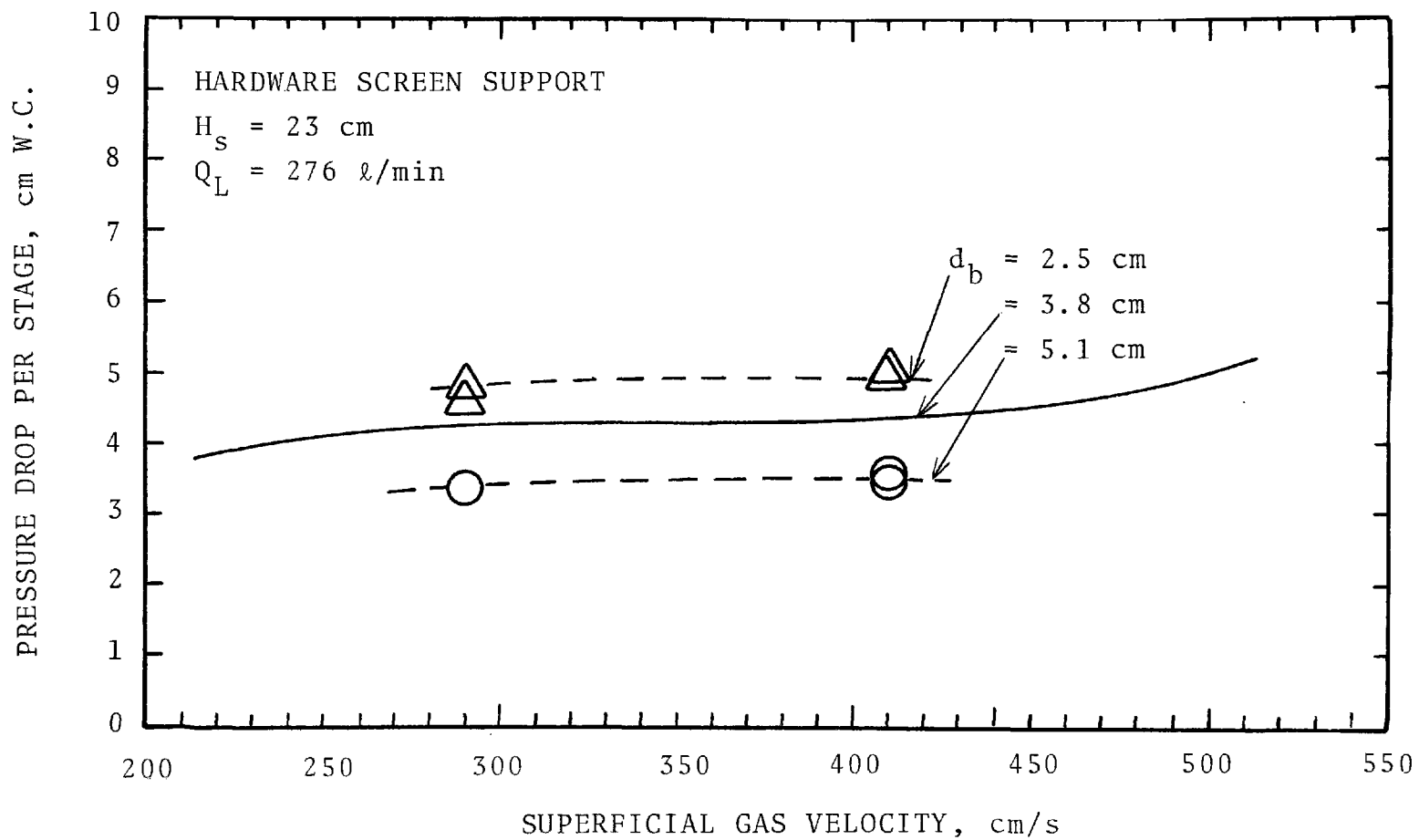


Figure 29. Effect of packing diameter on pressure drop.

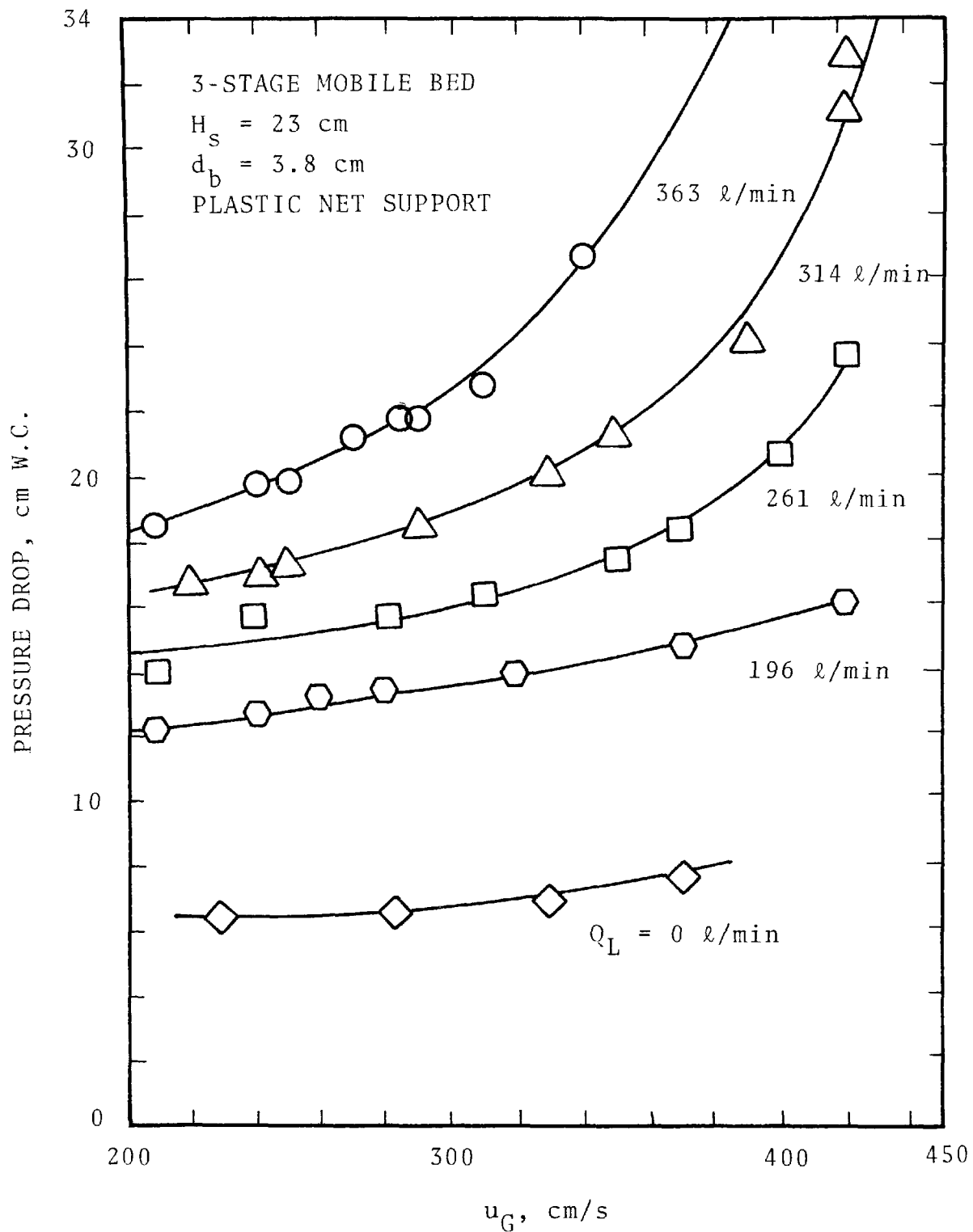


Figure 30. Pressure drop vs. superficial gas velocity for 3-stage mobile bed with plastic net support.

Kito, et al. (1976c) used three different grids (8 mesh, 5 mesh, and metal screen with 1.2 cm openings and 84% opening ratio) in their experiments. They found that the geometry of the supports has great effect on the amount of liquid holdup. Grids with smaller openings give higher liquid holdup which in turn causes the pressure drop to rise.

A second possibility is that liquid froth may be retained on the plastic net. Russian researchers (Blyakher et al., 1967) have observed that a liquid froth was retained on the grids which had small openings. It is possible that grids with small openings and small fractional open area act as sieve plates.

Figure 31 is the pressure drop across the three stage plastic net supports; i.e., three stage mobile bed with packings removed. This pressure drop is due to liquid retention on the grids.

Figure 32 is a plot of the difference in pressure drop with and without packing for the plastic net supported mobile bed. The difference is equal to the pressure drops due to the weights of packings and liquid holdup. As can be seen from Figure 32, the pressure drop due to the weight of packing and liquid holdup is independent of gas flow rate up to the flooding velocity. The calculated  $\Delta P_b + \Delta P_{Lh}$  for the plastic net support is lower than that for the hardware screen support. It is possible that Figure 31 is not a true representation of the liquid head on the grid. When there are packings, some of the liquid froth will enter the fluidized bed. Therefore, liquid holdup in the bed increases and the retention on the grid decreases by the same amount.

#### Particle Collection -

Particle collection data have been reduced into plots of particle penetration versus particle diameter for all experimental runs. Figures 33 through 35 are examples of the results.

As revealed by comparing the grade penetration curves, the scrubber performance depends only on the overall pressure drop across the scrubber. The grade penetration curves of two mobile bed scrubbers, which have different bed geometries and operating conditions, would be the same if they have the same overall pressure

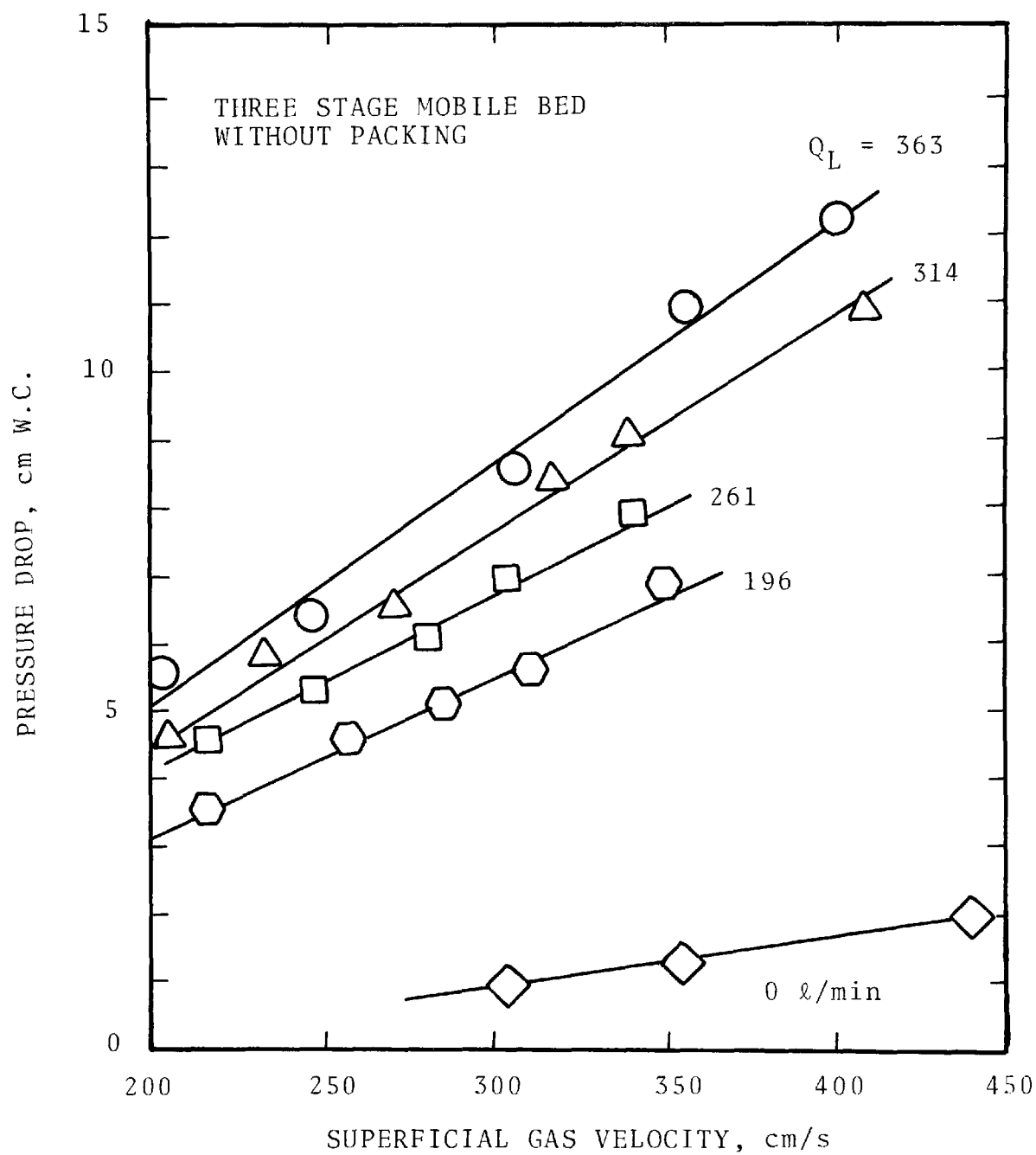


Figure 31. Pressure drop across four plastic net supports.

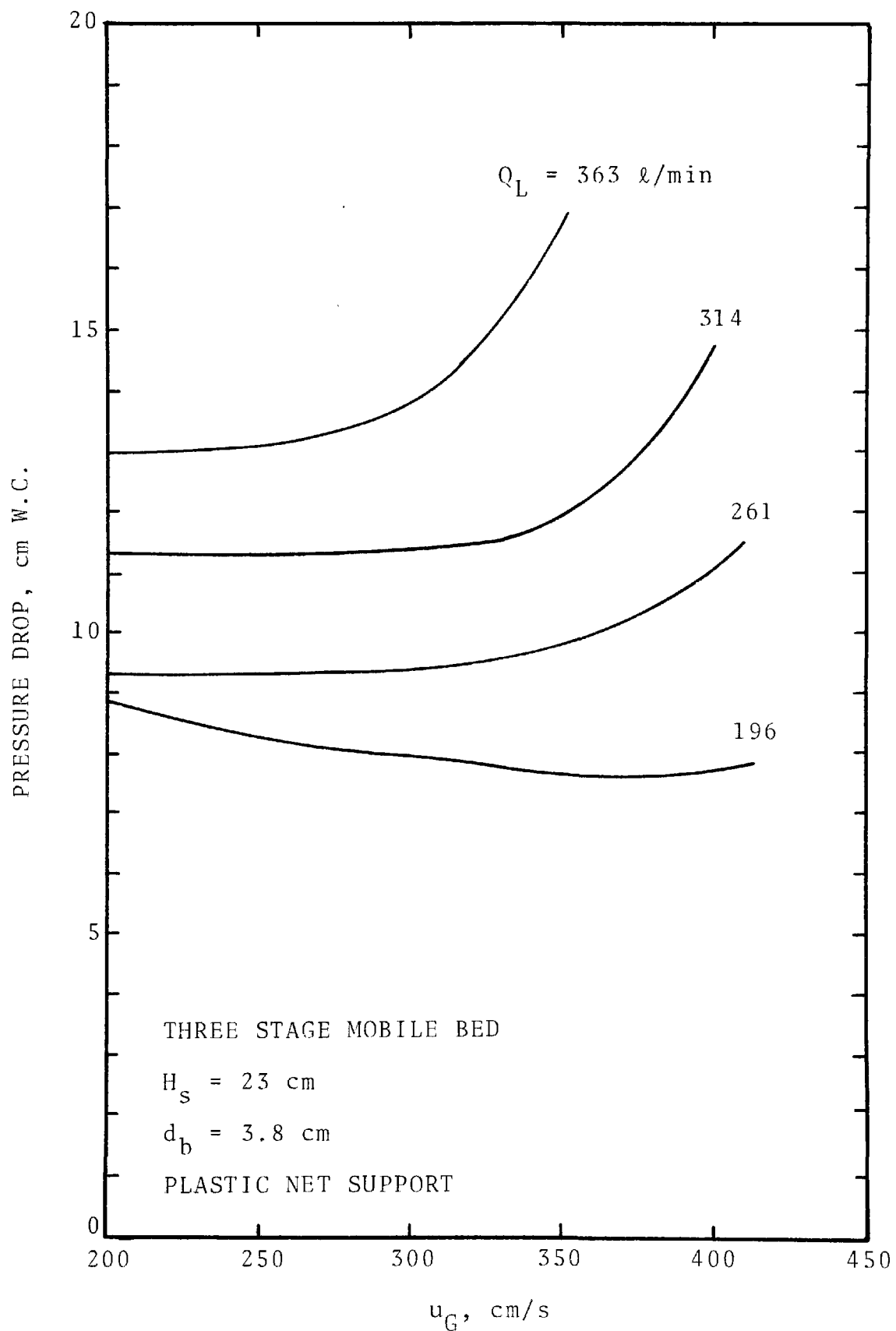


Figure 32. Pressure drop due to liquid holdup and weight of packing.

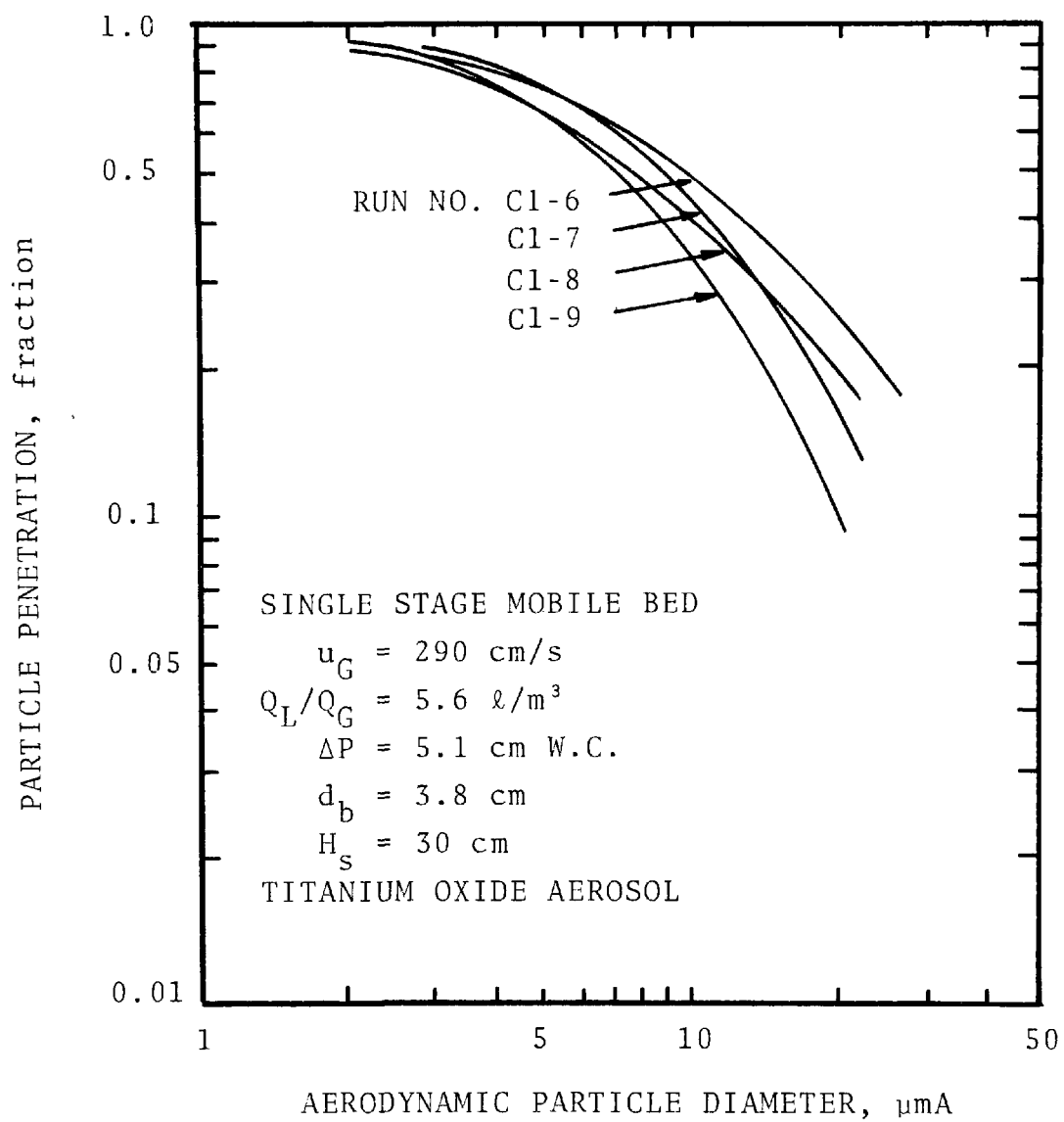


Figure 33. Experimental grade penetration curves.



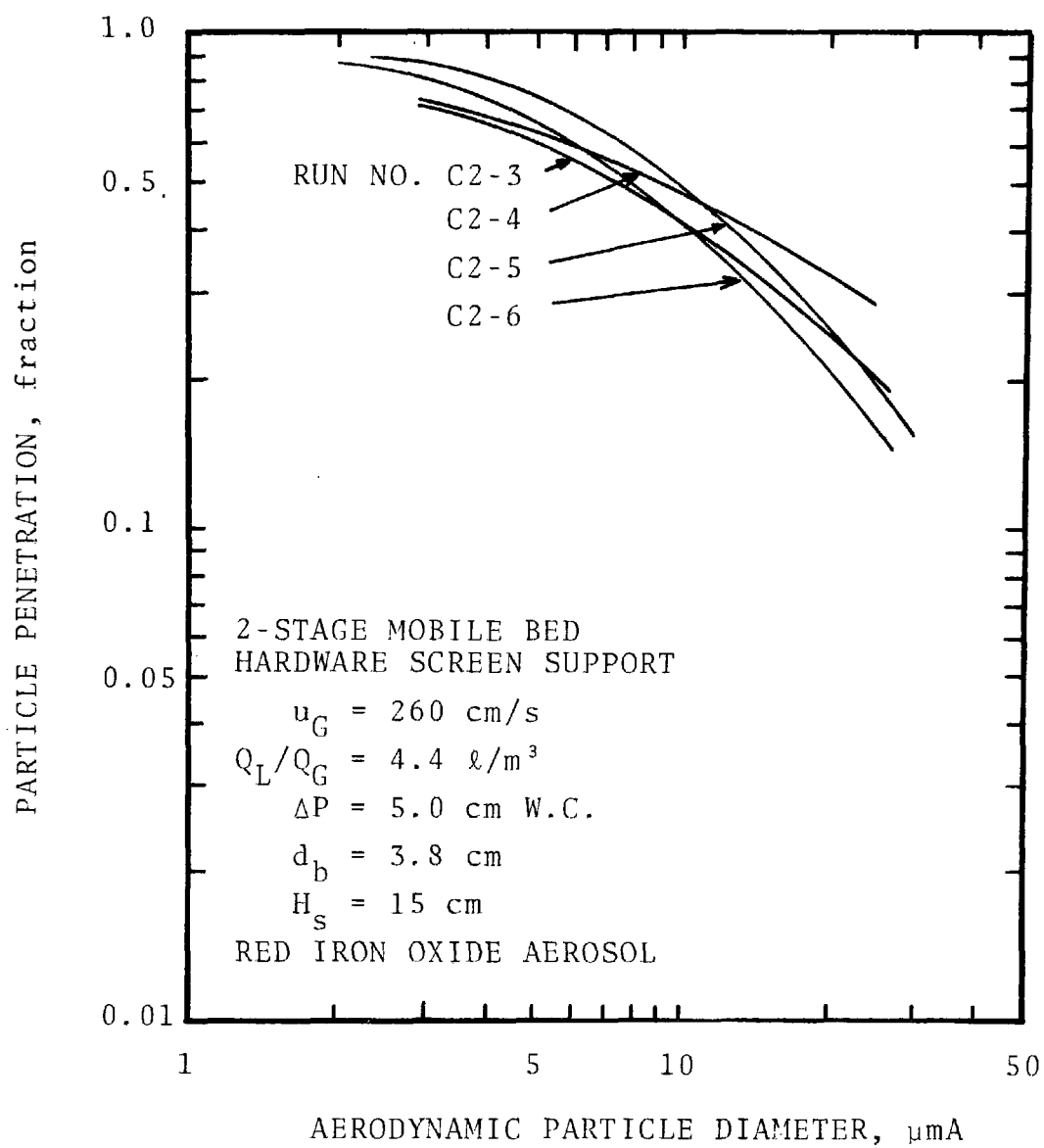


Figure 34. Experimental grade penetration curves.

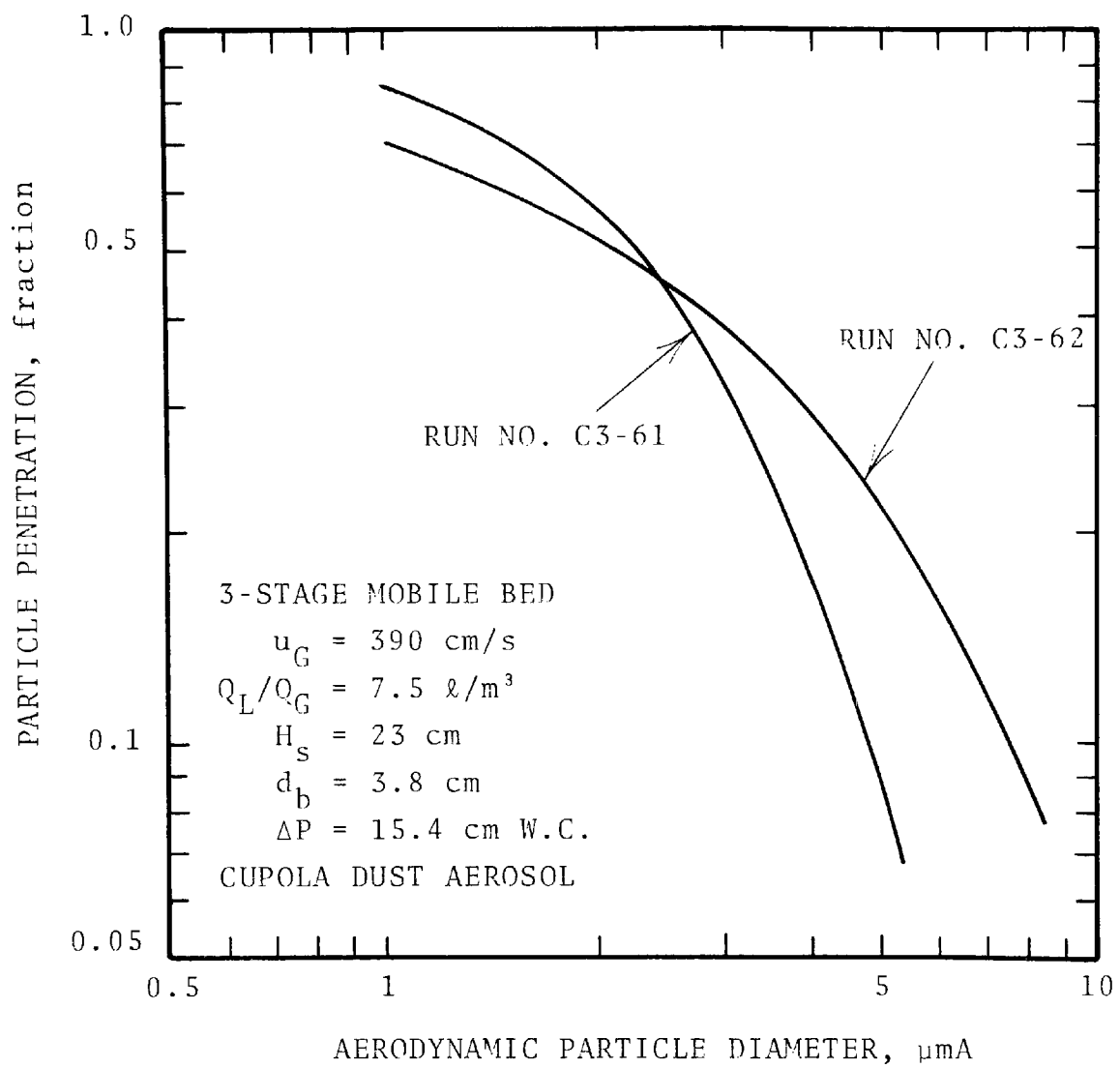


Figure 35. Experimental grade penetration curves.

drop. This characteristic is in line with mass transfer in mobile bed scrubbers. After analyzing the  $\text{SO}_2$  absorption data reported by EPA (Borgwardt, 1972, 1974a, 1974b, and 1975) and Epstein (1976), McMichael et al. (1976) and Wen and Chang (1978) concluded that the efficiency for absorption of  $\text{SO}_2$  in lime and limestone slurry depends only on the pressure drop across the mobile bed scrubber.

Since the scrubber performance depends only on the scrubber pressure drop, any parameter that leads to a higher pressure drop will increase the collection efficiency accordingly. Pressure drop may be increased by using higher liquid flow rate, heavier packings, deeper bed, and supports with smaller openings or open area.

The particle collection of a 3-stage mobile bed scrubber cannot be projected from the collection of a 1-stage scrubber; i.e.  $P_{t3} \neq P_{t1}^3$ . The projected penetration is slightly higher than that actually measured (Figure 36). The cause may be due to particle bypassing due to channeling. In a multiple stage scrubber, the stages are attached one on top of another. This arrangement provides both mixing and a damping action which reduce particle bypassing.

Some inter-stage samplings were conducted on the multi-stage scrubber. Results indicated that even though the particle collection of a multi-stage scrubber cannot be projected from the collection of a 1-stage scrubber, it can be projected from the collection of one of its stages (Figure 37).

Particle collection in a mobile bed scrubber stems from inertial impaction on the atomized liquid drops and on the packing elements. For scrubbers which rely on inertial impaction for particle collection, the performance depends on the gas-phase pressure drop or the power input to the scrubber.

Different mobile bed scrubber geometries and operating conditions result in different scrubber performances and pressure drops. It is very difficult to evaluate and compare the scrubber capability based only on the grade penetration curves. A mobile bed scrubber with plastic net supports has a higher collection efficiency than a hardware screen supported mobile bed with the same bed geometry and operated under the same parameters. It is not true that plastic net is better than hardware screen since the pressure drop is higher with plastic net.

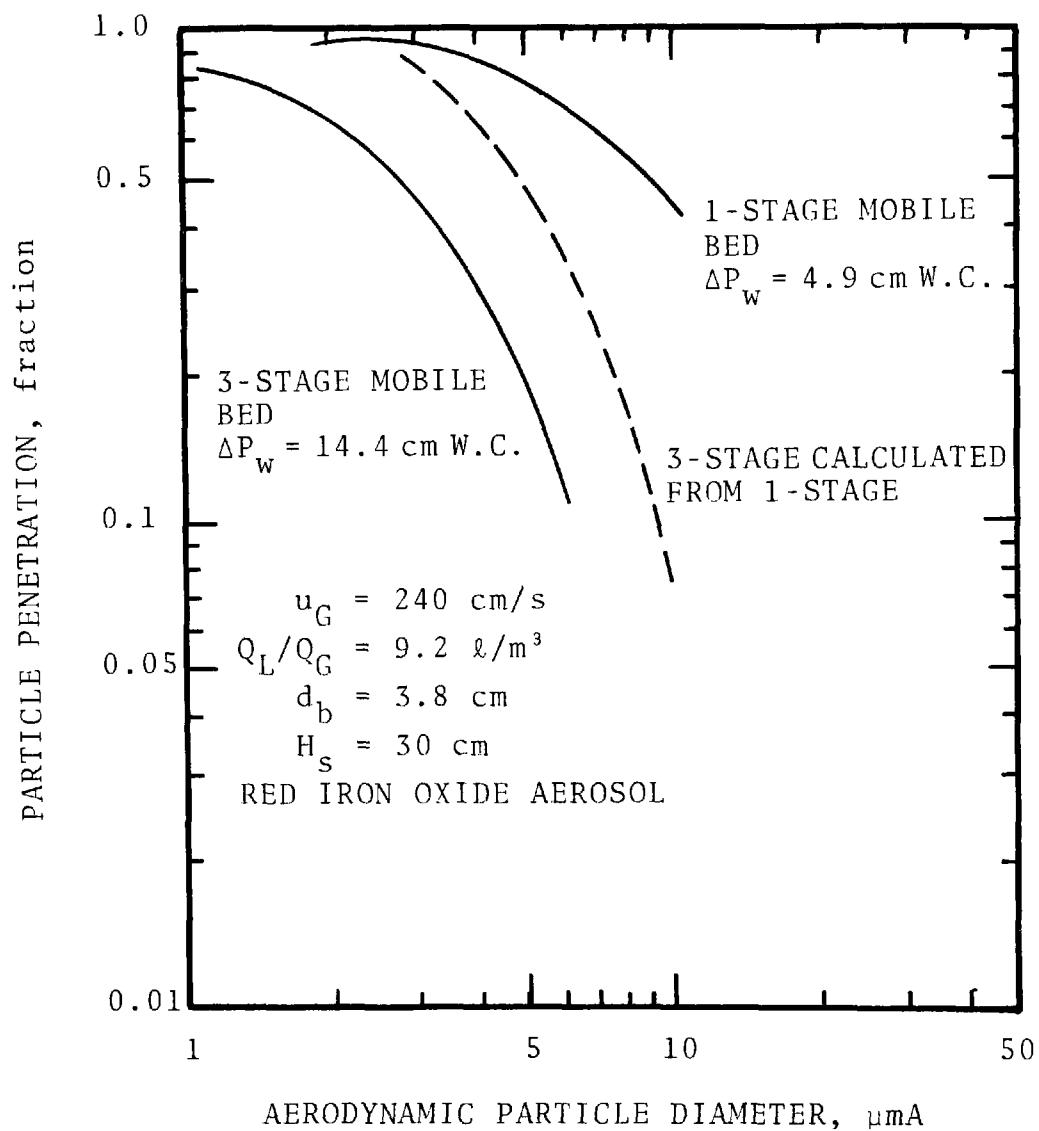


Figure 36. 1-stage and 3-stage mobile bed scrubber performance.

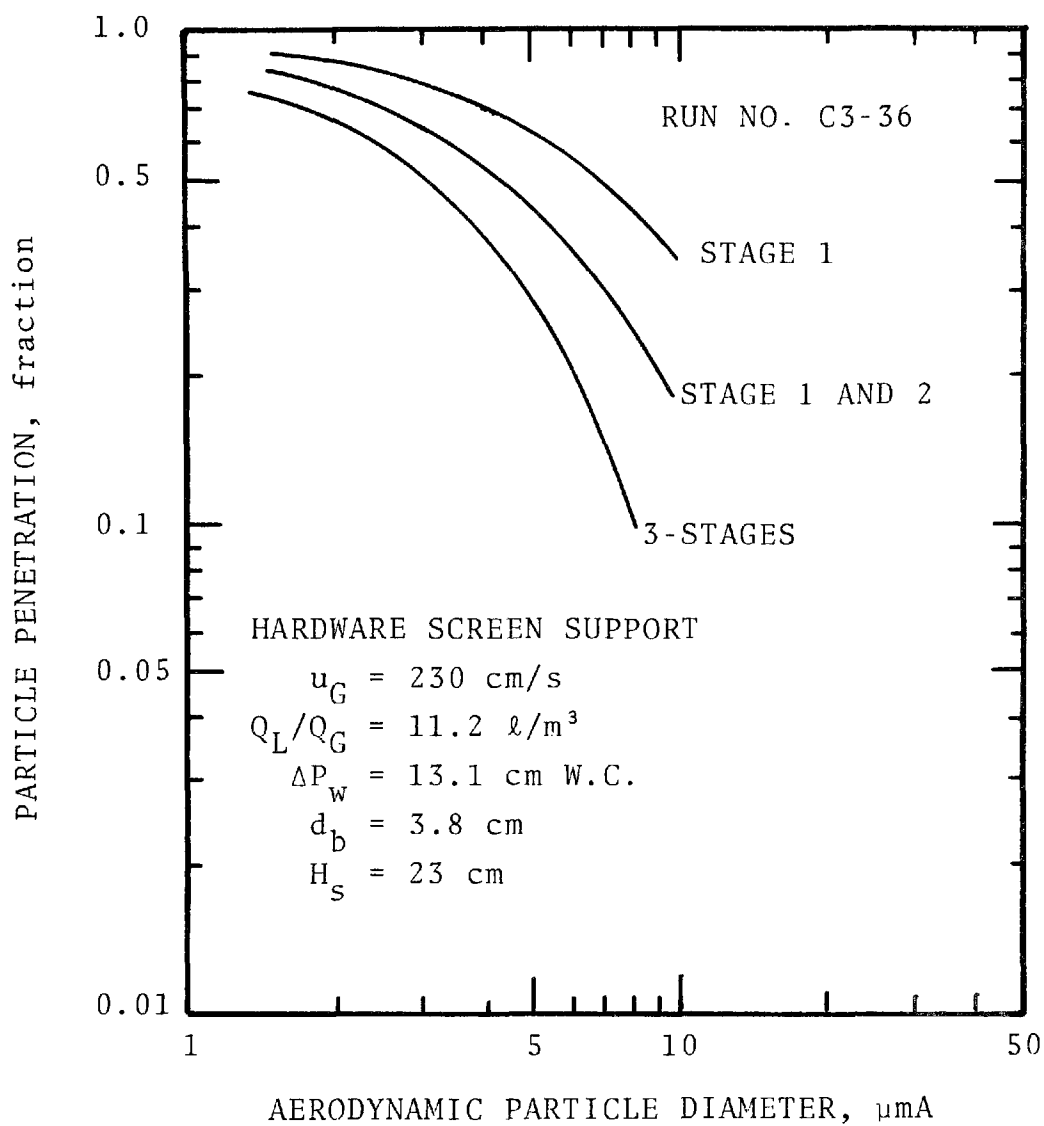


Figure 37. Penetration curves from interstage sampling.

A useful correlation called the cut/power relationship has been developed by Calvert (1974) for scrubber evaluation purposes. Calvert has shown that the scrubber performance cut diameter is a very convenient parameter for describing the performance and capability of a particle scrubber. Cut diameter is the particle diameter whose collection efficiency is 50% and it can be obtained from the experimental grade penetration curve. The cut/power relationship is a plot of the cut diameter given by the scrubber against pressure drop or power input.

Figure 38 is a plot of the measured performance cut diameter of the mobile bed scrubber versus measured pressure drop for various scrubber configurations and operating conditions. The data fall on a straight line on log-log paper. The equation describing the straight line is

$$d_{pc} = 60.2 (\Delta P_w)^{1.23} \quad (29)$$

where  $d_{pc}$  = scrubber performance cut diameter,  $\mu\text{m}$   
 $\Delta P_w$  = pressure drop, cm W.C.

The equation was obtained by linear regression and the correlation coefficient is -0.94.

Comparison of data with other researchers' data - Figure 39 compares the published mobile bed performance data with that of present study. As can be seen, data reported by Epstein et al. (1975), Johnson et al. (1976), and Rhudy and Head (1977) agree with that of present study. Data of Ensor et al. (1976) show slightly higher efficiency.

Ensor et al. (1976) conducted a performance test on a mobile bed scrubber which was installed in a coal burning power plant. The scrubber was installed to supplement the particulate control by the electrostatic precipitator. The flue gas from the precipitator (17,000  $\text{Am}^3/\text{min}$  at  $137^\circ\text{C}$ , 610,000 ACFM at  $280^\circ\text{F}$ ) enters a presaturator to reduce the gas temperature to approximately  $52^\circ\text{C}$  ( $125^\circ\text{F}$ ). From the presaturator, the gas enters the scrubber. At the scrubber outlet, the gas first

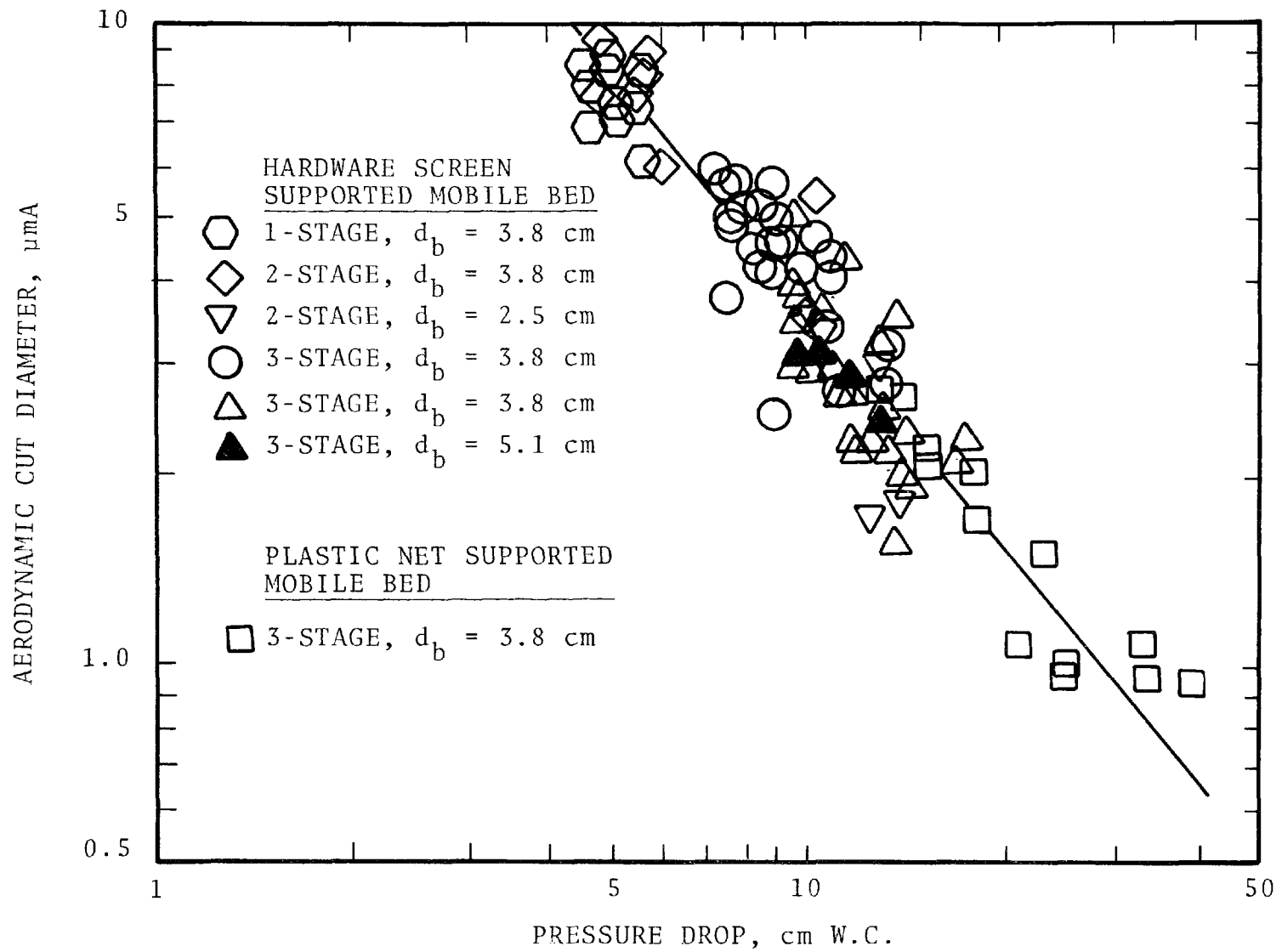
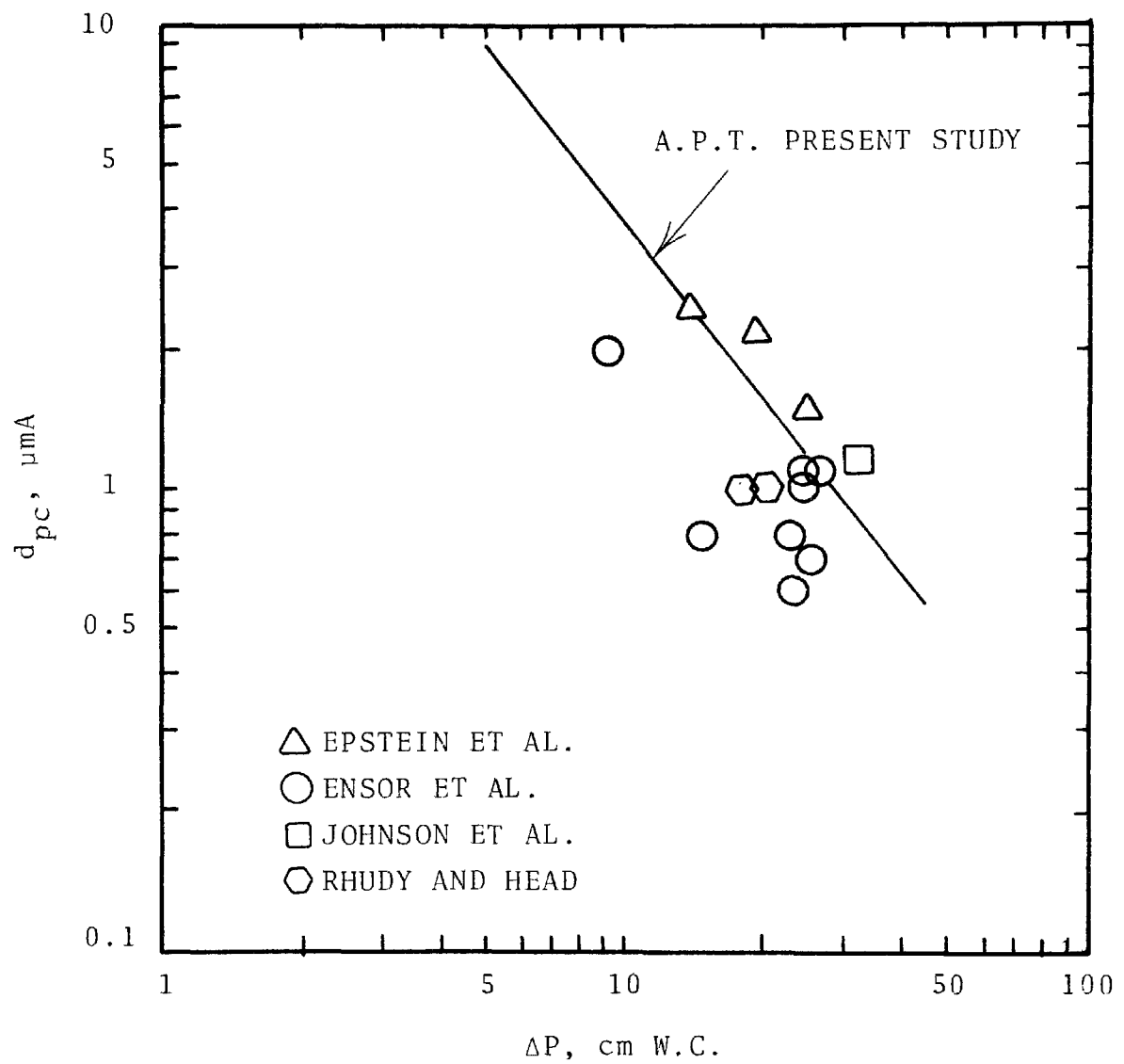


Figure 38. Experimental cut/power relationship for mobile bed scrubber.





passes through a chevron-type mist eliminator then is heated by steam coil to 85°C (185°F) before entering the stack. Particle samples were taken before the presaturator and after the reheater. Thus, Ensor et al.'s particle sample might not be a representative sample of what actually existed in the scrubber especially since there was a presaturator in between. Particle growth might occur in the presaturator.

#### Bed Expansion -

When the gas velocity in a mobile bed scrubber is maintained above the minimum fluidization velocity, the bed expands. Therefore, the retaining grids should be far enough apart to allow this expansion. The operating bed heights were measured in this study by observation. Since the operating bed height fluctuates during a run, an average based on the judgement of the observer was recorded. The data obtained by this method might not be accurate. However, they provide information on the general trends.

Figures 40 and 41 show the bed expansion as a function of the liquid-to-gas ratio with gas velocity as a parameter for the 15 and 23 cm static bed depths; respectively. Figure 42 shows the effect of packing size on bed expansion. Bed expansion is defined as:

$$\text{Bed expansion (\%)} = \frac{H_d - H_s}{H_s} \times 100\% \quad (30)$$

where  $H_d$  = dynamic or operating bed height, cm

$H_s$  = static bed height, cm

The results show that the bed expands linearly with increasing liquid-to-gas ratio. The rate of expansion depends on gas flow rate. The rate increases with increasing superficial gas velocity. Under the same operating conditions, the 23 cm deep bed expands less than the 15 cm deep bed. 5.1 cm diameter packings result in a smaller expansion than the 3.8 cm diameter packing. These phenomena are expected since the weight of the bed is higher with the deeper bed and smaller packings.

#### Minimum Fluidization Velocity -

Chen and Douglas (1968) defined the minimum fluidization velocity of a mobile bed as the maximum gas flowrate that will

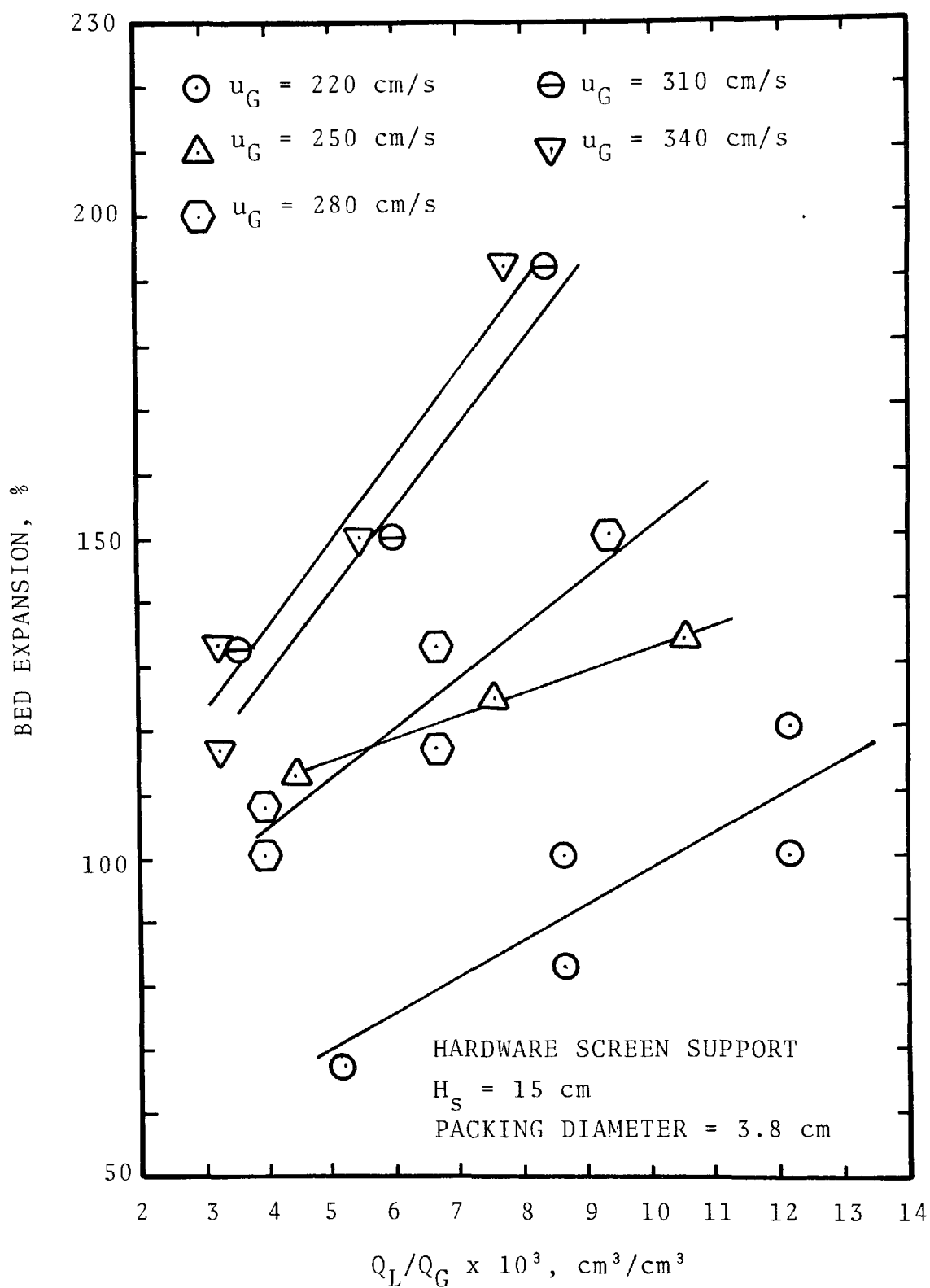


Figure 40. The variation of bed expansion with liquid-to-gas ratio.

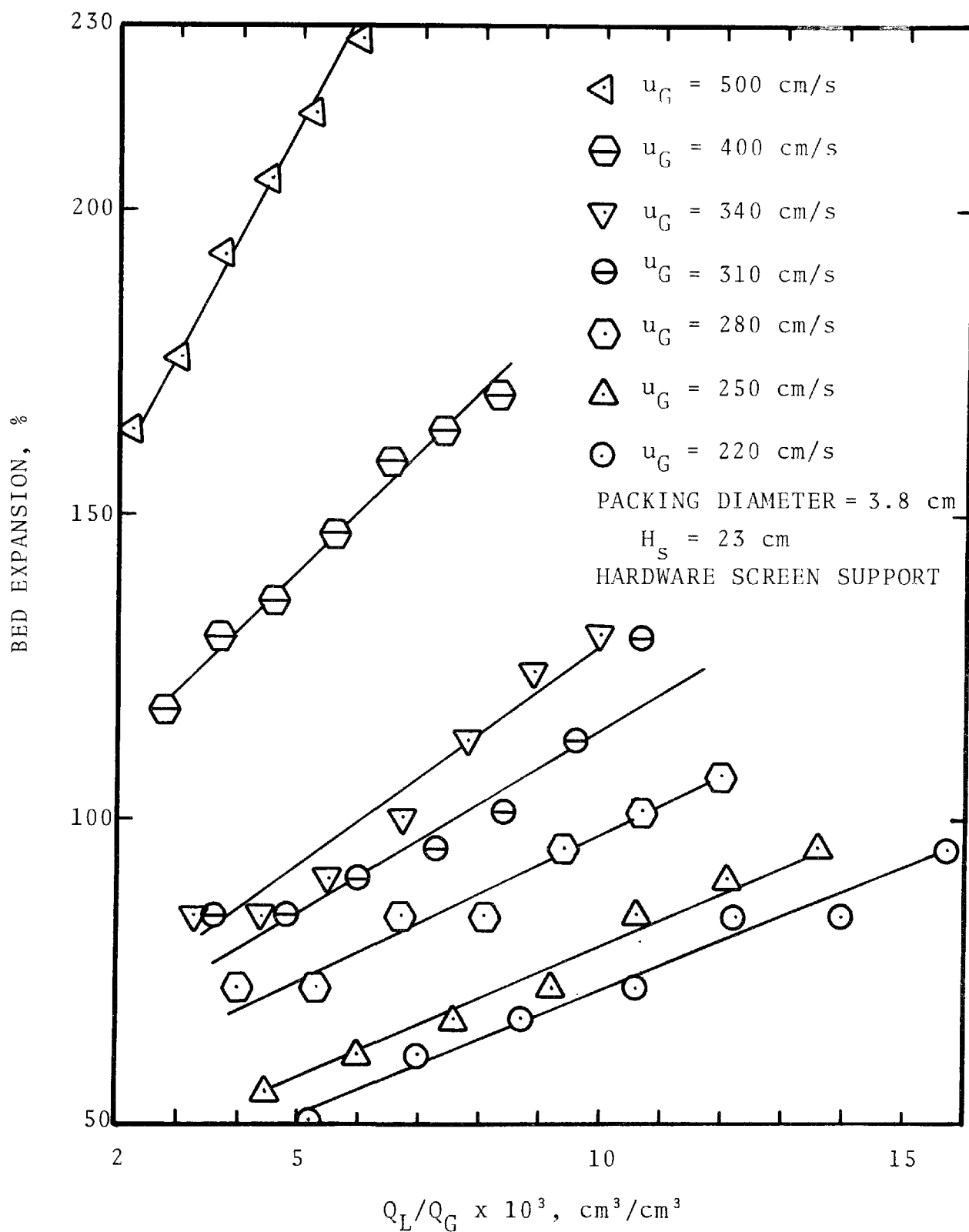


Figure 41. The variation of bed expansion with liquid-to-gas ratio.

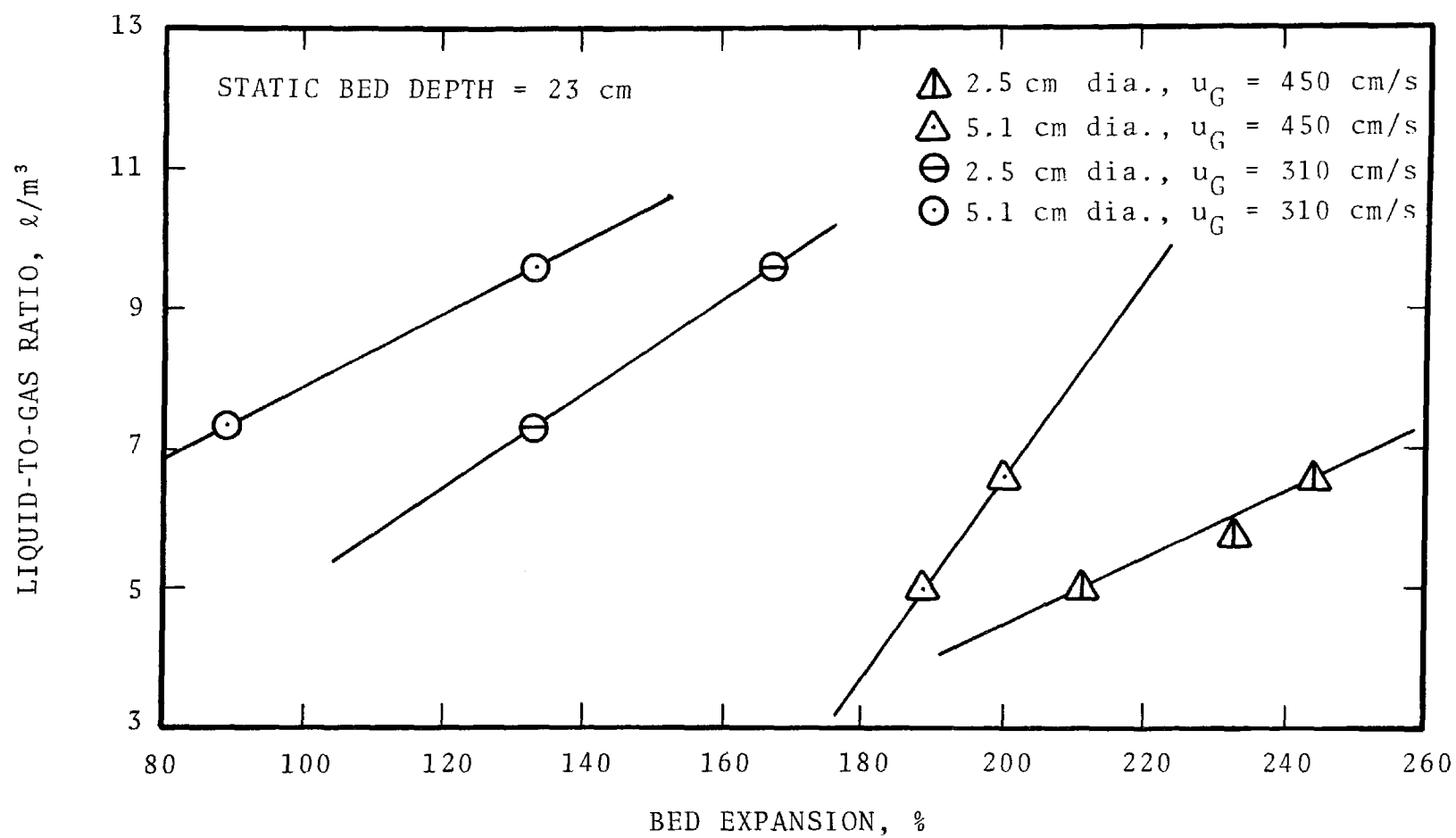


Figure 42. Effect of packing diameter on bed expansion.

maintain the static packed bed height. They found that the minimum fluidization velocity increases with increasing packing diameter and decreases with increasing liquid rate. Their findings are confirmed in this study as illustrated in Figures 43 and 44. The minimum fluidization velocity was obtained by extrapolating the bed expansion curves in Figures 40 and 41 to zero bed expansion.

### Slurry Scrubbing

#### Pressure Drop -

The overall pressure drop of a 3-stage mobile bed scrubber with a limestone slurry as the scrubbing liquid are plotted in Figure 45 along with cold run data. The addition of  $\text{CaCO}_3$  to the scrubber liquid has no effect on the scrubber pressure drop.

#### Particle Collection -

Runs #S3-1 through S3-9 of slurry scrubbing were planned to investigate the effect of the slurry characteristics on the scrubber particle collection mechanisms. The scrubber performance cut diameters are listed in Table B-10. Figure 46 is a plot of the scrubber performance cut diameter versus pressure drop along with the cut/power relationship determined in the cold operation mode. Since the data for the slurry tests fall on the line of the cold run cut/power, it appears that the calcium carbonate particles suspended in the scrubber liquid do not affect the particle collection mechanisms and efficiency of the mobile bed scrubber.

Runs #S3-10 through S3-17 were intended to determine the contribution of entrainment to particle emission. For these runs, no aerosol was fed into the scrubber system. The particle loading was determined with cascade impactors in the scrubber outlet duct. As can be seen from Table B-10, the particle loading due to entrainment is very low. The tube bank entrainment separator in the mobile bed performed satisfactorily.

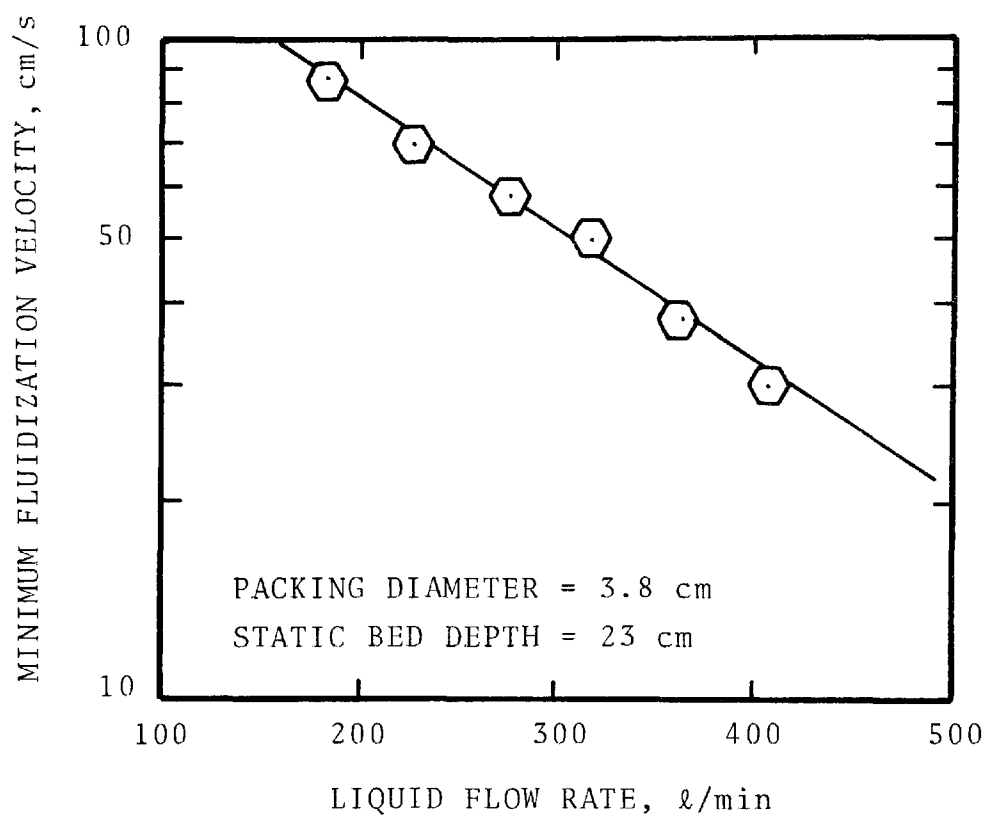


Figure 43. The variation of minimum fluidization velocity with liquid flow rate.

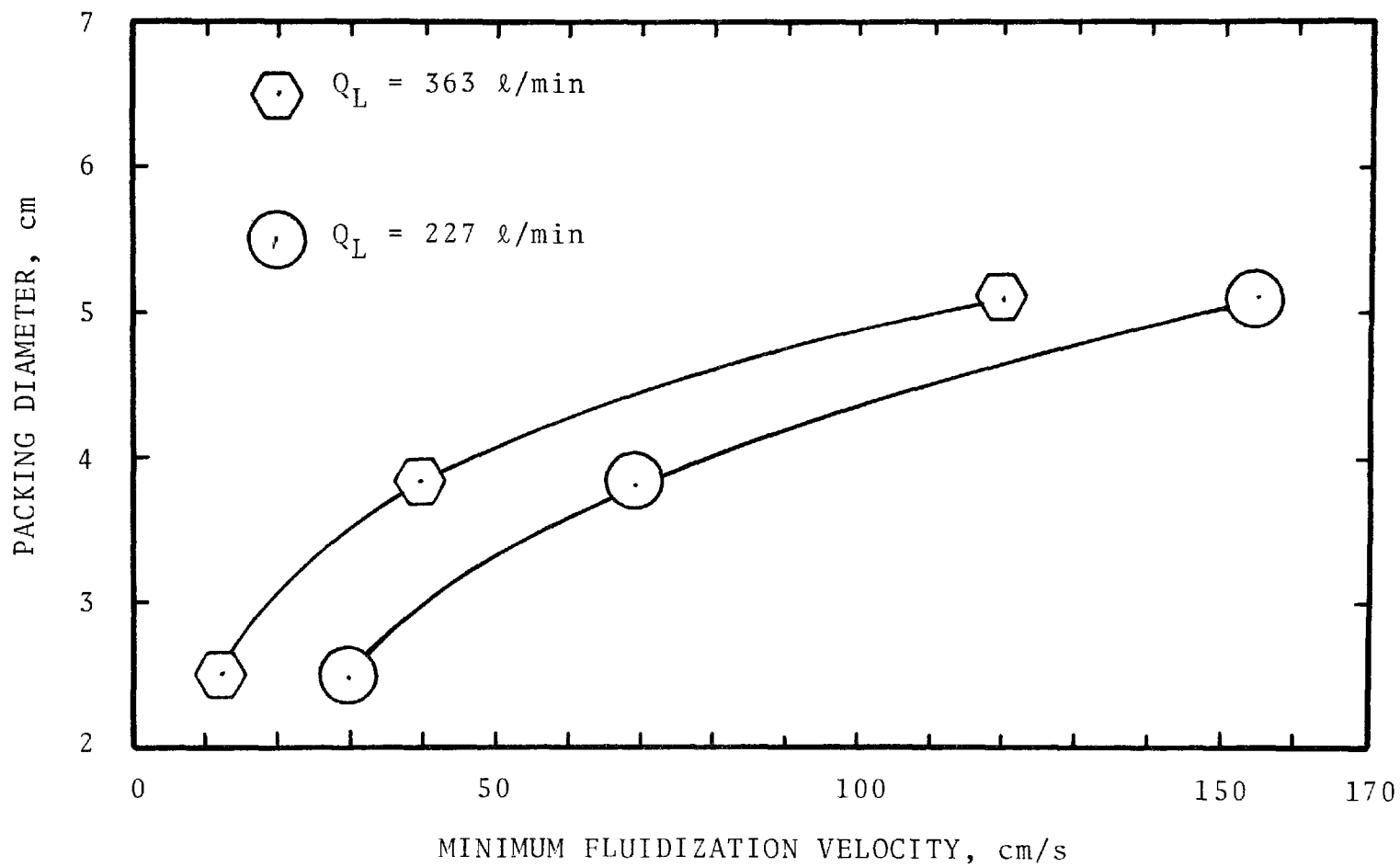


Figure 44. The variation of minimum fluidization velocity with packing sphere diameter.

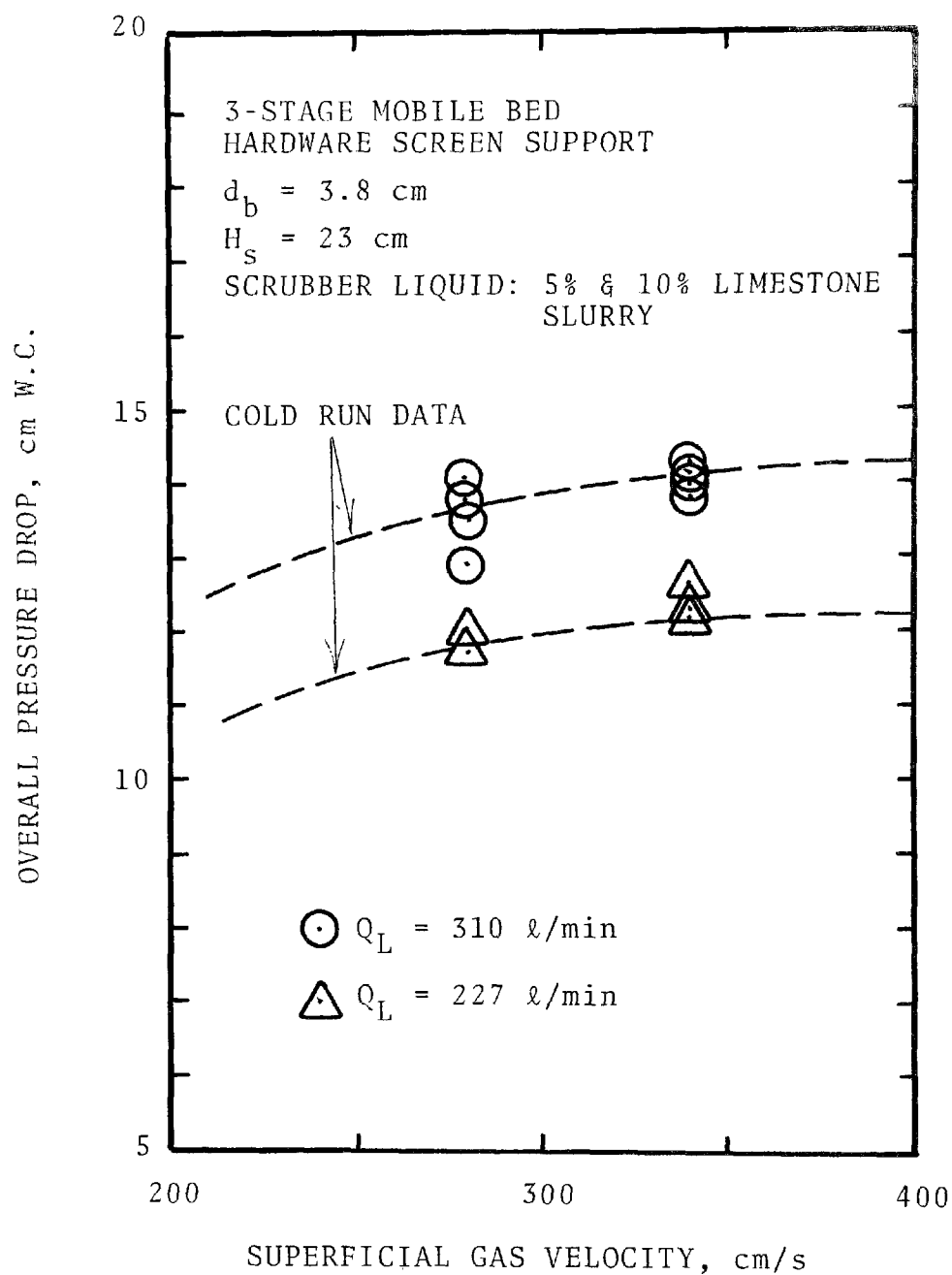


Figure 45. Effects of slurry on pressure drop.



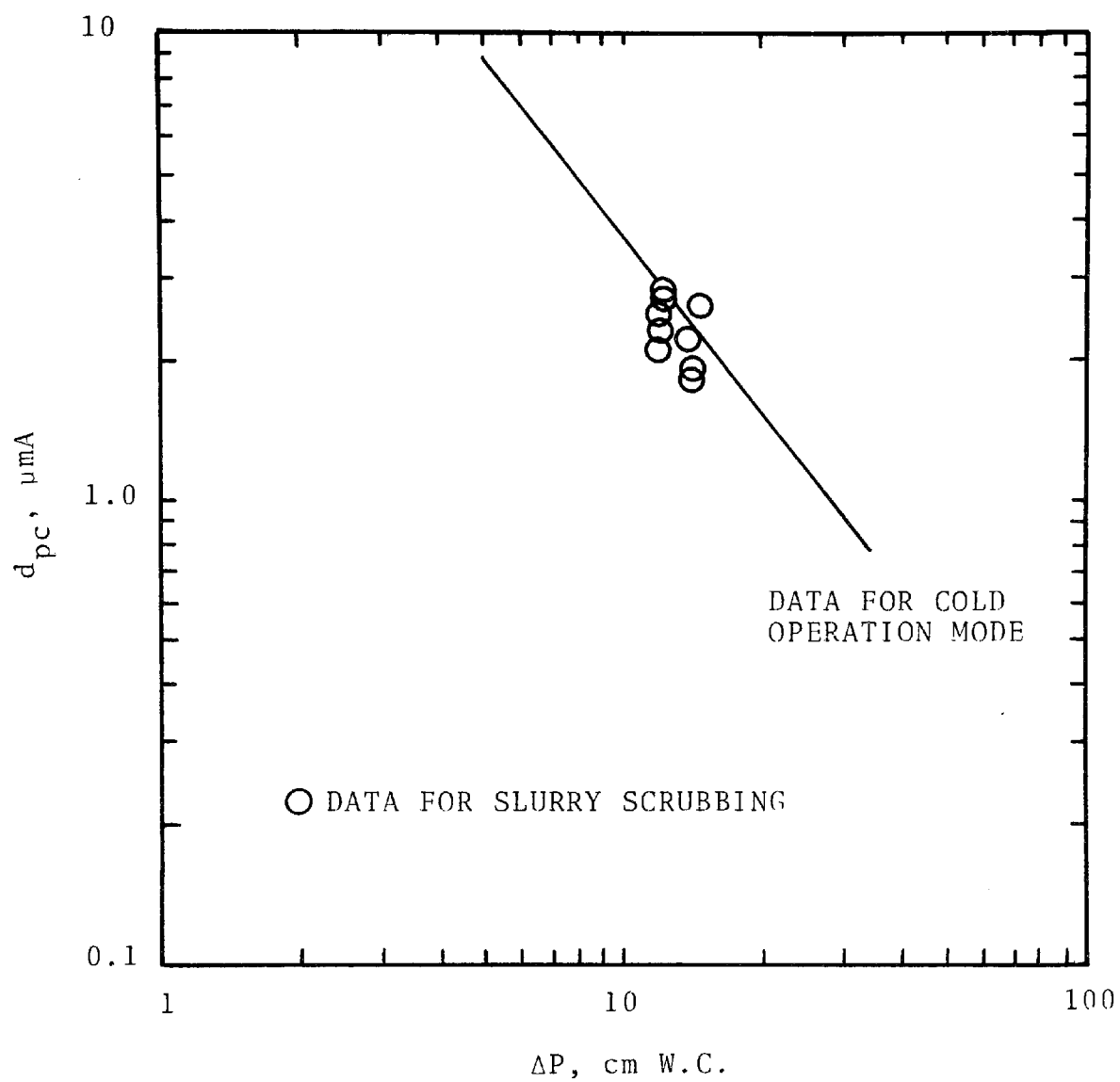


Figure 46. Slurry scrubbing test data.

## F/C Scrubbing

### Pressure Drop -

The pressure drop data for F/C scrubbing are plotted in Figure 47 along with data from cold operating mode. As can be seen, F/C scrubbing will not increase the scrubber pressure drop.

### Particle Collection -

The F/C runs were designed to study the feasibility of using the mobile bed scrubber as a flux force/condensation scrubber. A total of 27 runs were made with a three stage scrubber. Each stage was packed with 3.8 cm diameter balls to a depth of 23 cm. Twenty-two of the runs were using the hardware screen support; the remaining five runs used the plastic net support. The scrubber water flow rate was maintained at 273  $\ell/\text{min}$ . The overall scrubber pressure drop ranged from 12.6 cm W.C. to 15.0 cm W.C. The average pressure drop for all runs was about 13 cm W.C. The experimental conditions are listed in Table B-11 and B-12. The experimental grade penetration curves are presented in Appendix E.

Figure 48 is a plot of performance cut diameter versus condensation ratio. The condensation ratio is defined as grams of water vapor condensed per gram of dry air in the scrubber. It describes the maximum amount of water vapor per gram of air that can be contributed to particle growth.

As can be seen from the figure, the cut diameter decreases as the condensation ratio increases. The performance cut diameter is reduced from 2.7  $\mu\text{m}$  with no F/C effect to about 0.7  $\mu\text{m}$  for a condensation ratio of 0.25 g/g dry air, under approximately the same scrubber operating pressure drop. This is a significant improvement in performance per unit of power. To achieve a cut diameter of 0.7  $\mu\text{m}$ , the required pressure drop for a mobile bed scrubber without F/C effect is about 37 cm W.C. instead of 13 cm W.C. with F/C.

Figure 49 shows the effect of condensation ratio on the penetration of 1.0  $\mu\text{m}$  particles. The penetration decreased from

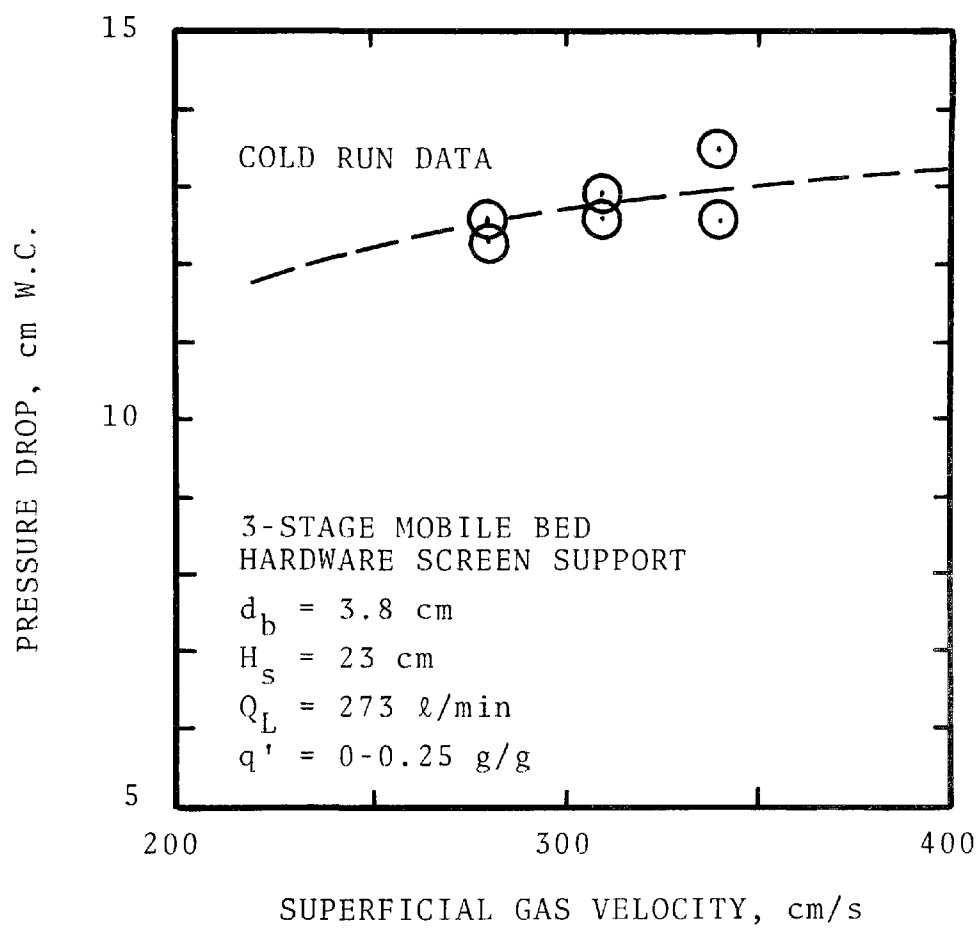


Figure 47. F/C scrubbing pressure drop.

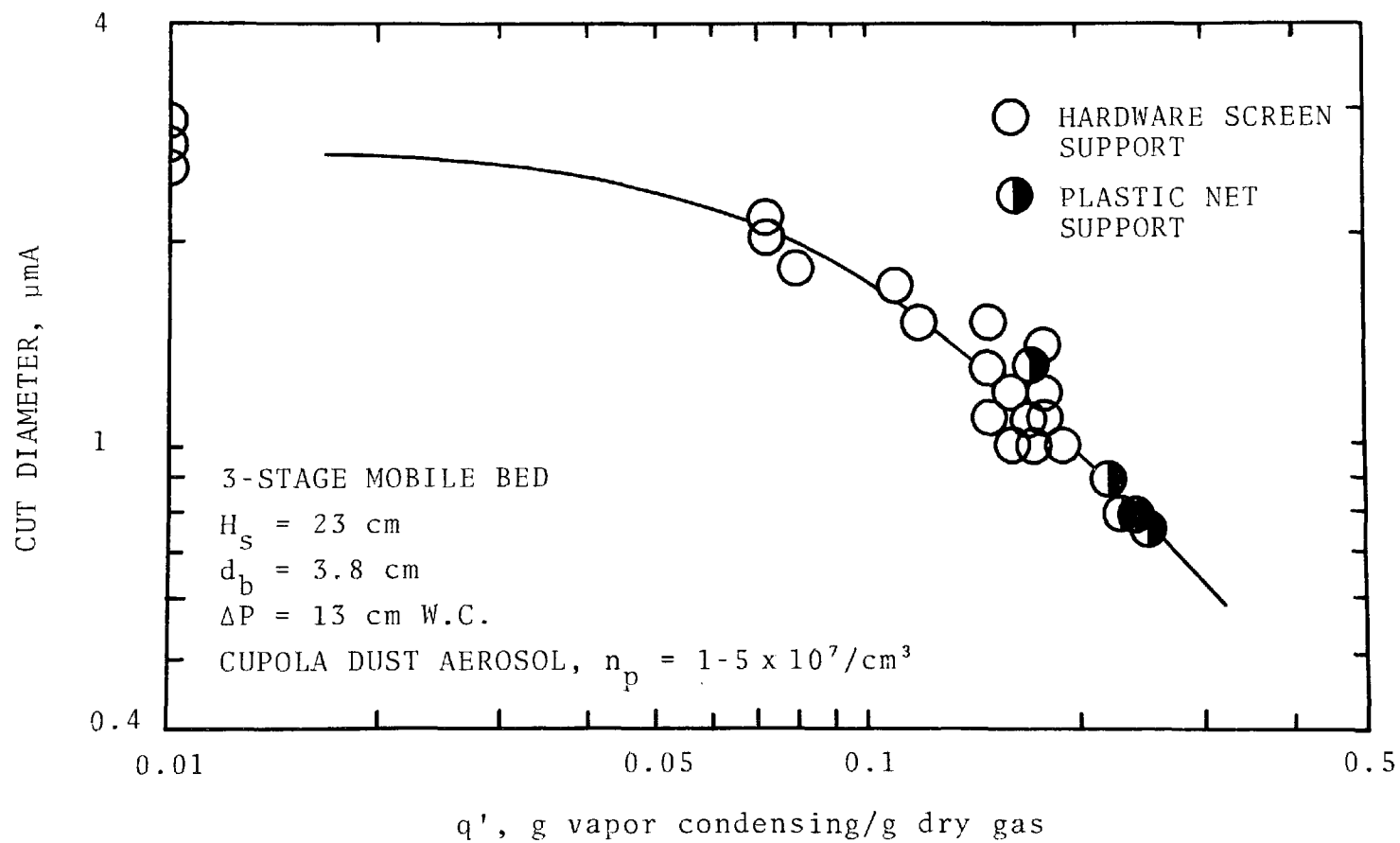


Figure 48. The variation of cut diameter with condensation ratio.

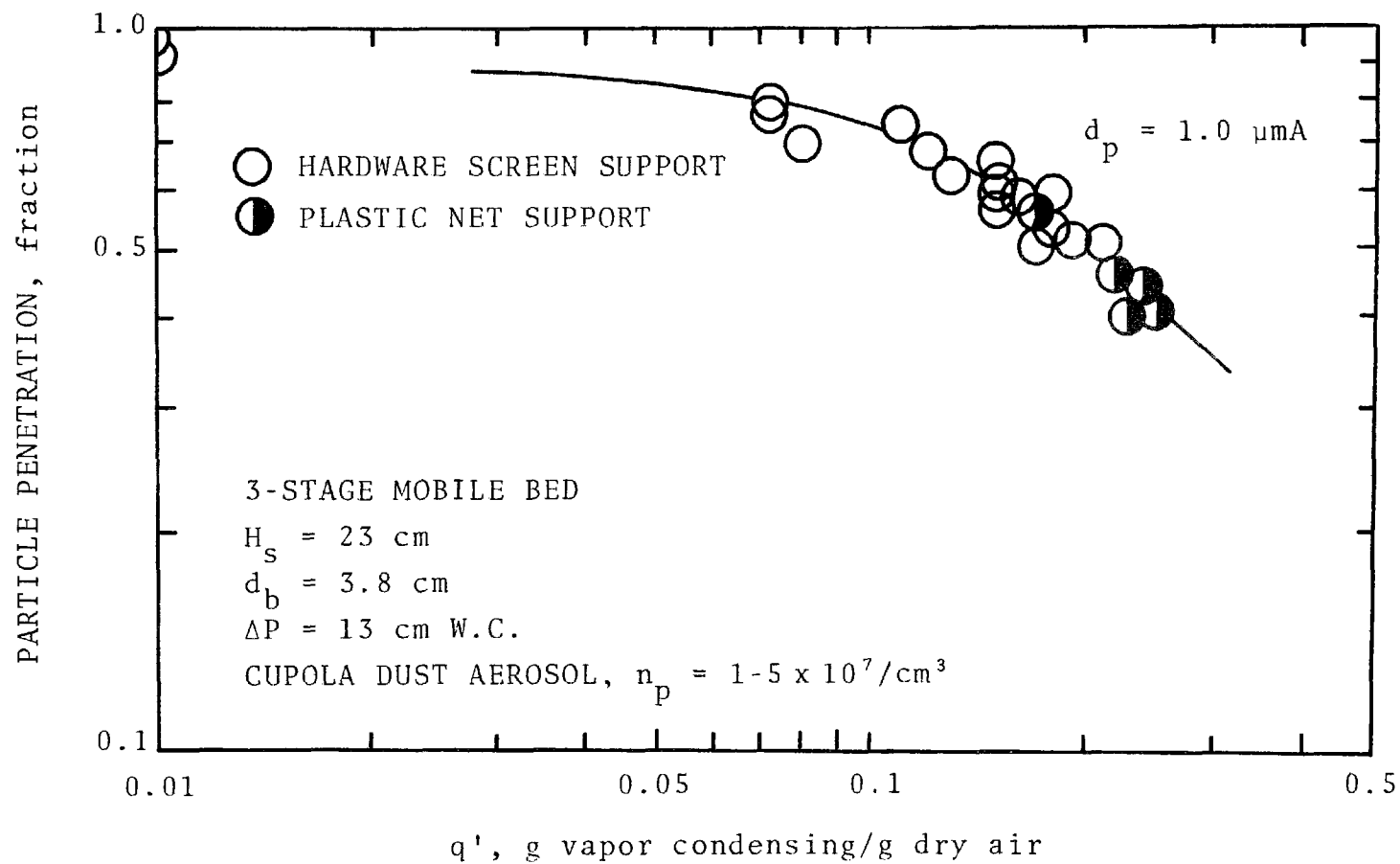


Figure 49. Penetration for  $1.0 \mu\text{m}$  diameter particle versus condensation ratio.

about 98% to about 40% when the condensation ratio increased from 0 to 0.25 g/g dry air.

#### Particle Number Concentration Measurements -

The improvement in collection efficiency of a F/C scrubber is due to particle growth and due to the addition of other particle collection mechanisms, diffusiophoresis and thermophoresis. Diffusiophoretic deposition is caused by the condensation of water vapor from the gas onto a cold liquid surface which exerts a force "sweeping" particles to the surface. Calvert et al. (1973) have shown that the condensation ratio is sufficient to define the particle deposition rate if there is no condensation on the particles. Whitmore (1976) concluded that the fraction of particles removed from the gas by diffusiophoresis is equal to either the mass fraction or the mole fraction condensing, depending on what theory is used for deposition velocity.

"Particle growth" means the enlargement of particle mass by condensing a water film around the particle. The enlarged particle is more susceptible to collection by inertial impaction. Particle growth is dependent on how well the particles can compete with the cold surface for the condensing water and the particle number concentration.

The particle number concentration was measured by using a batch dilution system and two counters - a Gardner Condensation Nuclei Counter (C.N.C.) and a Thermal Systems Electrical Mobility Analyzer (E.M.A.) in the present study. The results of the count experiments are shown in Table 8. The average inlet concentration was found to be  $5 \times 10^7/\text{cm}^3$  using the C.N.C. The E.M.A. data were obtained using all but the lowest size channel due to electrical instability with this channel. In all but Run 1, the E.M.A. count was lower than that of the C.N.C. in this test. The outlet particle concentration was found to be  $1.9 \times 10^7/\text{cm}^3$  with the C.N.C. for this run. The particulate loadings for these series of runs are also given in Table 8.

The aerosol used for these experiments was redispersed cupola dust which had a mass mean particle diameter of  $1.6 \mu\text{m}$ .

TABLE 8. PARTICLE COUNT RESULTS

<u>Run</u>	<u>Location</u>	<u>C.N.C.</u>	<u>E.M.A.</u>
0	Ambient	$2.7 \times 10^5$	$8.7 \times 10^4$
1	Inlet	$2.6 \times 10^7$	$3.3 \times 10^7$
2	Inlet	$7.6 \times 10^7$	$1.1 \times 10^7$
3	Inlet	$4.5 \times 10^7$	$2.1 \times 10^7$
4	Inlet	$5.2 \times 10^7$	$3.2 \times 10^7$
5	Outlet	$1.8 \times 10^7$	$4.2 \times 10^6$
6	Outlet	$2.0 \times 10^7$	$1.4 \times 10^7$

## Notes

1. E.M.A. data obtained with channels 2-10
2. Inlet loading during runs  $225 \text{ mg/DNm}^3$   
Outlet loading  $110 \text{ mg/DNm}^3$

In contrast to the particulate existing at the foundry, the redispersed dust is reasonably log normal and has a larger size distribution. The large amount of submicron condensation type aerosol is absent when redispersed.

The loading of the redispersed aerosol has varied significantly during the F/C experiments from about 30 mg/DNm<sup>3</sup> to 250 mg/DNm<sup>3</sup>. The size distribution does not change significantly with loading hence the assumption was made that the particulate number concentration varies in direct proportion to particulate loading.

#### Grown Particle Size Measurement -

The grown particle size is a function of particle number concentration and the effective condensation ratio. The effective condensation ratio is defined as the total condensation ratio,  $q'$ , multiplied by a factor,  $f_p$ , which indicates the fraction of the water vapor which condenses on the particles. Calvert and Gandhi (1977) have predicted that the fraction of condensing vapor condensed on the particle could range from about 0.1 to 0.4 for sieve plates and each individual particle obtained approximately the same amount of condensate.

If the particle number concentration is known, the grown particle size can be calculated by assuming that each individual particle obtains the same amount of condensing water.

$$d_{p_2} = \left\{ \frac{6 f_p q'}{772 n_p \rho_{p_2} \pi} + \frac{\rho_{p_1}}{\rho_{p_2}} (d_{p_1} \times 10^{-4})^3 \right\}^{1/3} \times 10^4 \quad (31a)$$

$$\text{where } \rho_{p_2} = \frac{f_p q' + 3.78 \times 10^{-10} n_p d_{p_1}^3 \rho_{p_1}^2}{f_p q' + 3.78 \times 10^{-10} n_p d_{p_1}^3 \rho_{p_1}} \quad (31b)$$



$d_{p1}$  = initial particle diameter,  $\mu\text{m}$   
 $d_{p2}$  = final particle diameter,  $\mu\text{m}$   
 $n_p$  = particle number concentration,  $\#/\text{cm}^3$   
 $f_p$  = fraction of water vapor condensed on the particles, g water/g gas  
 $q'$  = condensation ratio, g water/g gas  
 $\rho_{p1}$  = initial particle density,  $\text{g}/\text{cm}^3$   
 $\rho_{p2}$  = density of grown particle,  $\text{g}/\text{cm}^3$

There is no published information on the effective condensation ratio in a mobile bed scrubber. Several particle growth experiments were conducted to determine the extent of particle growth and " $f_p$ " for mobile bed scrubbers. This was accomplished by measuring the particle size distribution simultaneously at the scrubber inlet and at the top of the scrubber second stage. A University of Washington cascade impactor was used for inlet size distribution measurement. A special device designed by A.P.T. was used at the top of the second stage.

The device consisted of a one-stage impactor followed by a total filter and a regular sampling train for flow measurement and control. The one-stage impactor was a modified Greenburg-Smith impinger with a 0.16 cm diameter nozzle attached to the inner glass tube. The impinger was filled with 100 ml of distilled water.

The sampling probe was a side port probe. To prevent entrained water from entering the sampling device, an automatic drainer was built into the probe. The experimental setup is shown in Figure 50.

For each run, amounts of particles caught by the filter and the one-stage impactor were determined. The fraction of the total caught on the filter is the fraction of particles which has diameters less than the cut-diameter of the one-stage impactor.

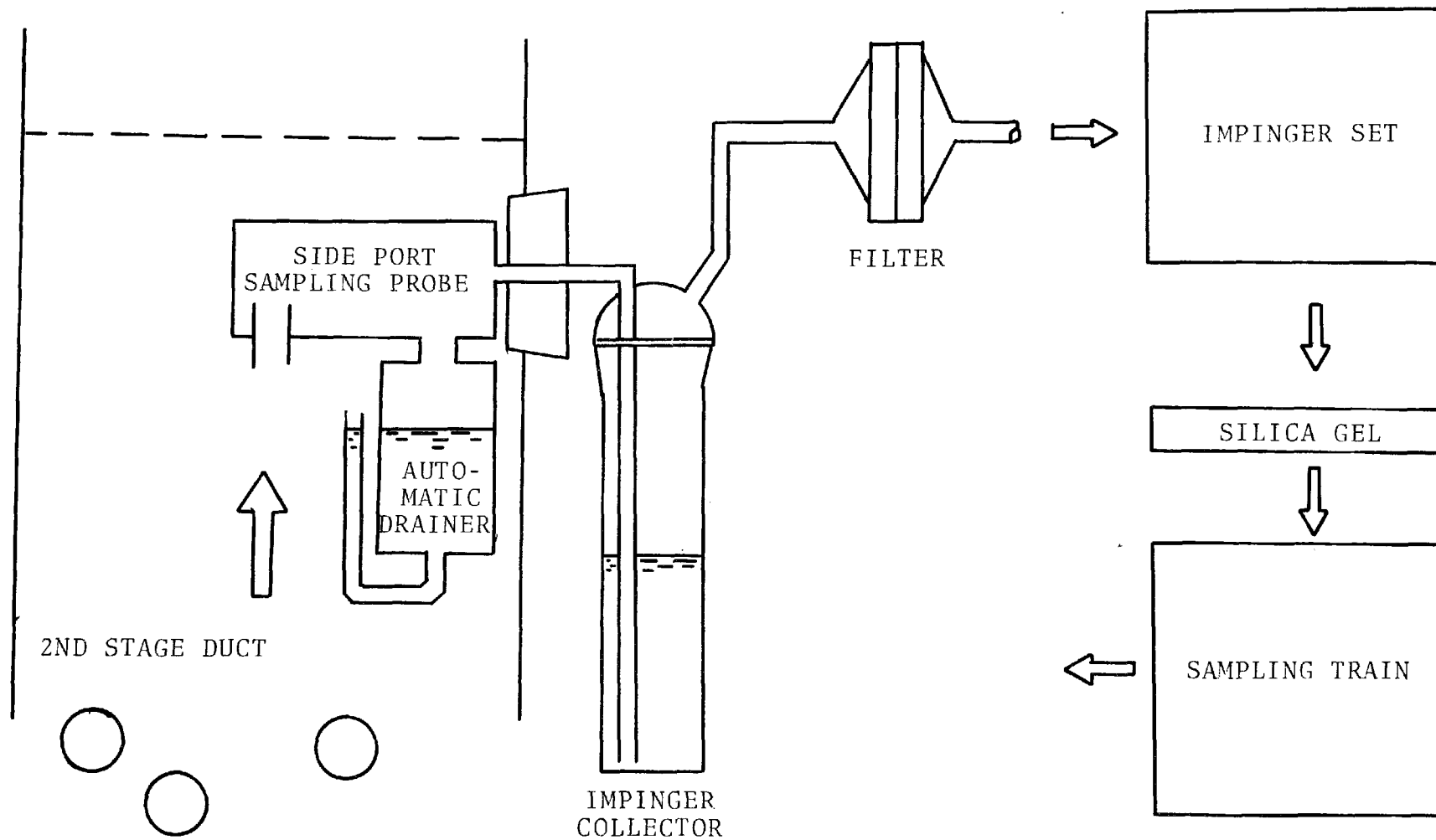


Figure 50. The grown particle experimental set-up.

Three runs were made, and the results are shown in Table 9 and plotted in Figure 51. The solid line in Figure 51 is the predicted dry particle size distribution at the top of the second stage. It was predicted from the measured inlet particle size distribution and the combined grade penetration curve of stages 1 and 2.

By assuming a " $f_p$ ", the growth particle size distribution can be predicted from equation (31) and the dry particle size distribution. The growth particle size distribution was predicted for several " $f_p$ 's". When compared with data, it was found that the predicted size distribution for  $f_p = 0.15$  agreed with data, as shown in Figure 51. Therefore, the fraction of condensate which condenses on the particles appears to be 0.15 for a mobile bed scrubber operated in the range of these experiments.

TABLE 9. PARTICLE GROWTH DATA

Run	q'	Impinger Cut Point $d_{pc}, \mu mA$	Impinger Collection mg	Filter Collection mg	% Caught on Filter*
1	.24	1.1	12.4	4.1	25
2	.22	1.6	5.4	2.8	34
3	.25	1.6	2.6	2.0	43

\* Fraction caught on filter has particle size less than the cut diameter of modified impinger.

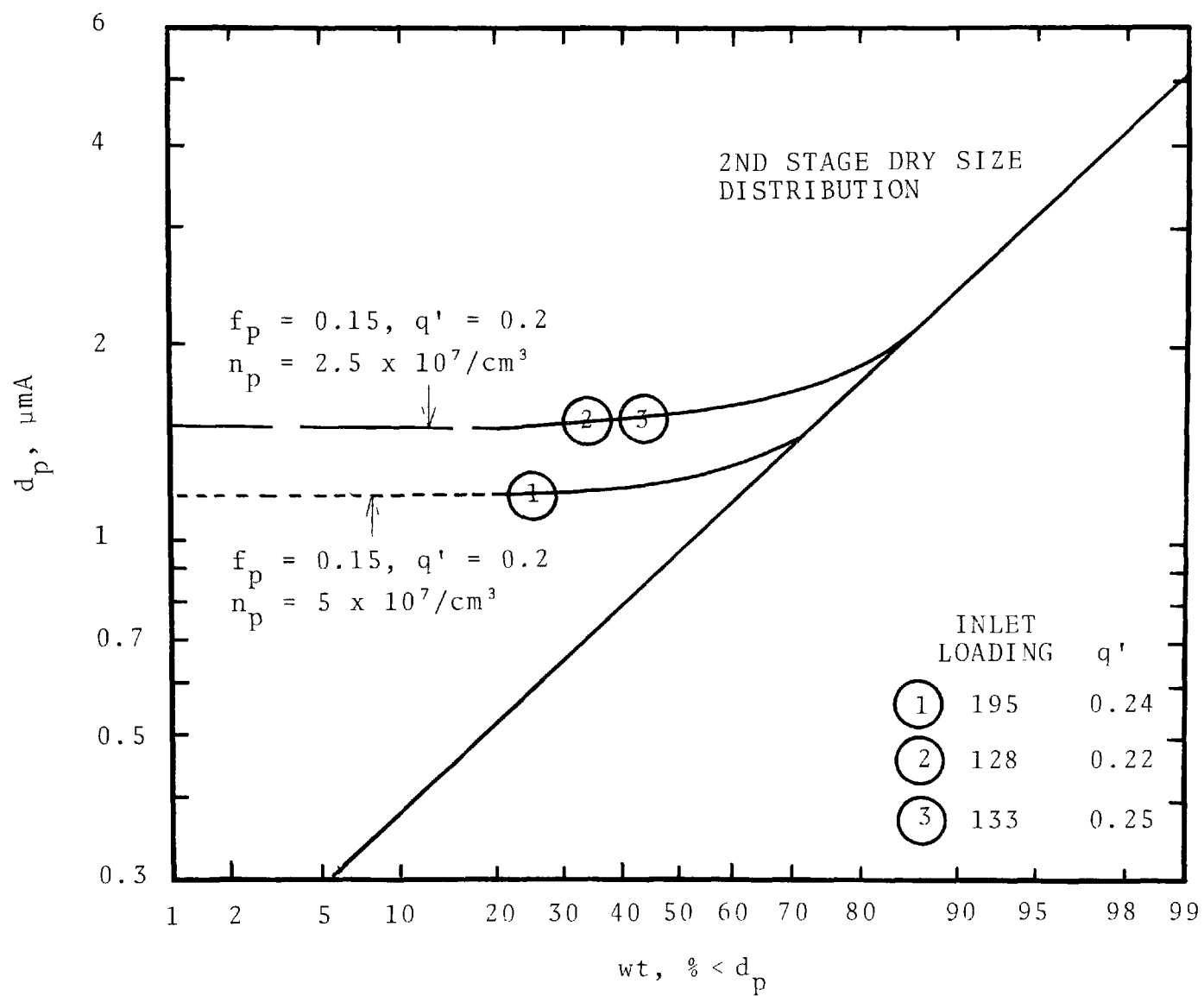


Figure 51. The predicted and measured particle grown size distribution.

## SECTION 6

### MATHEMATICAL MODELING

#### LITERATURE SEARCH

A bed of low density spheres fluidized by upward flowing gas and irrigated by downward flowing liquid may be used as a gas-liquid contacting operation. The spheres may typically be hollow plastic spheres of from 1 to 5 cm diameter and of density considerably below that of water.

The operation may be used for gas absorption in general and should be expected to have favorable heat and mass transfer characteristics because of the turbulent motion of the spheres. It has also been used for scrubbing of industrial gases containing solid particles.

Fundamental studies on the mechanics of mobile beds such as hydrodynamics, pressure drop, liquid holdup, minimum fluidization velocity and axial liquid mixing have been conducted by a number of investigators. The following is a brief review of the literature.

#### Hydrodynamics

The mobile bed scrubber consists of several packed beds stacked inside a vessel shell. It is in many ways similar to conventional packed towers. For a packed bed, if the pressure drop across the bed is less than the sum of the weights of liquid holdup and packing, the bed will remain stationary. However, if the pressure drop is greater than the weight of packing plus liquid holdup, the bed will expand and fluidization occurs; i.e., it becomes a mobile bed.

O'Neill et al. (1972) have studied the hydrodynamics of mobile bed scrubbers. They indicated that the mobile bed scrubber can be operated in either of two modes, namely fluidization without flooding and fluidization due to incipient flooding. For mass transfer applications, operation in the incipient flooding mode is desirable since it results in a higher gas-liquid interfacial activity.

The different modes of operation of a mobile bed can be inferred from the traditional loading flooding curve of a packed bed. The flow characteristics of a packed tower are usually presented graphically as a series of curves similar to those shown in Figure 52. Here, the pressure drop in the tower is expressed as a function of the gas flow, with liquid flow as parameter. The curves are traditionally drawn with two distinct changes in slope, and the break points "B" and "C" are known as the loading and the flooding points, respectively.

Fluidization which occurred at flowrates below the flooding point of a packed bed which has the same geometry as the expanded fluidized bed is termed fluidization without incipient flooding. Fluidization which occurred after the flooding point is termed fluidization due to incipient flooding.

For the operation mode of fluidization without incipient flooding, the minimum fluidization velocity is expected to increase with packing density. If the fluidization occurred below the loading point, the liquid holdup at a fixed liquid flowrate is expected to remain approximately constant for different gas rate. Slight dependence of holdup on gas flow rates is expected if the fluidization occurs between the loading point and the flooding point.

For fluidization due to incipient flooding, the liquid holdup will increase with increasing gas flow rate and with increasing density of the packing material. The minimum fluidization velocity is independent of the density of the packing material.

The mode of operation depends largely on the density of the packing material and to a lesser extent on packing size, liquid

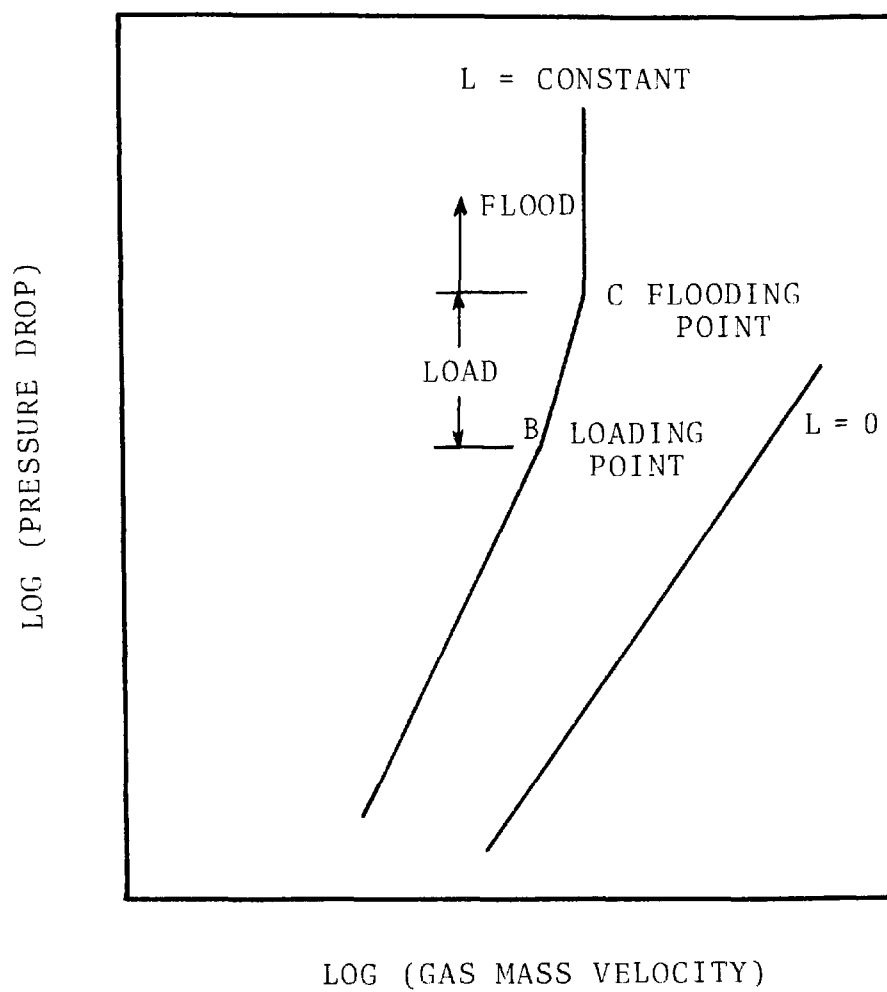


Figure 52. Typical pressure drop - flow characteristics in conventional packed towers.



flow rate and physical properties of the liquid. Figure 53 given by O'Neill, et al. shows the regime of the two operational modes. It was derived from the assumption of a constant pressure gradient at flooding of a static packed bed (20.8 cm W.C./m of packing, 2.5 in. W.C./ft) and from the application of Chen and Douglas' correlation for liquid holdup. This figure will be useful in predicting the mode of operation of the mobile bed scrubber.

The mechanics of the mobile bed are extremely complex. Little theoretical work on the predictions of minimum fluidization, liquid holdup, and bed expansion has been published. However, a large number of papers on experimental measurements on mobile beds have been published. Numerous empirical correlations are presently available to predict pressure drop, liquid holdup, minimum fluidization velocity, interfacial area, and heat and mass transfer coefficients. In using these empirical correlations, care should be given to the scrubber operation mode and the ranges of the variables which the researchers had used in their experiments. The following is a summary of the empirical correlations.

#### Minimum Fluidization Velocity -

The minimum fluidization velocities of mobile beds have been investigated by Chen and Douglas (1968), Balabekov, et al. (1969, 1971), and Kito, et al. (1976c).

Chen and Douglas defined the minimum fluidization velocity of a mobile bed as the maximum gas flow rate that will maintain the static bed height. They measured the dynamic bed height, " $H_d$ " for various gas and liquid flow rates. They then plotted the ratio of dynamic bed height and static bed height versus gas flow rate for a constant liquid flow rate. A straight line was obtained. They extrapolated the line to the ratio equal to 1 to obtain the minimum fluidization velocity. The empirical correlation given by them for predicting the minimum fluidization velocity is:

$$G_{mf} = 0.106 d_b^{1.15} 10^{0.36 L} \quad (32)$$

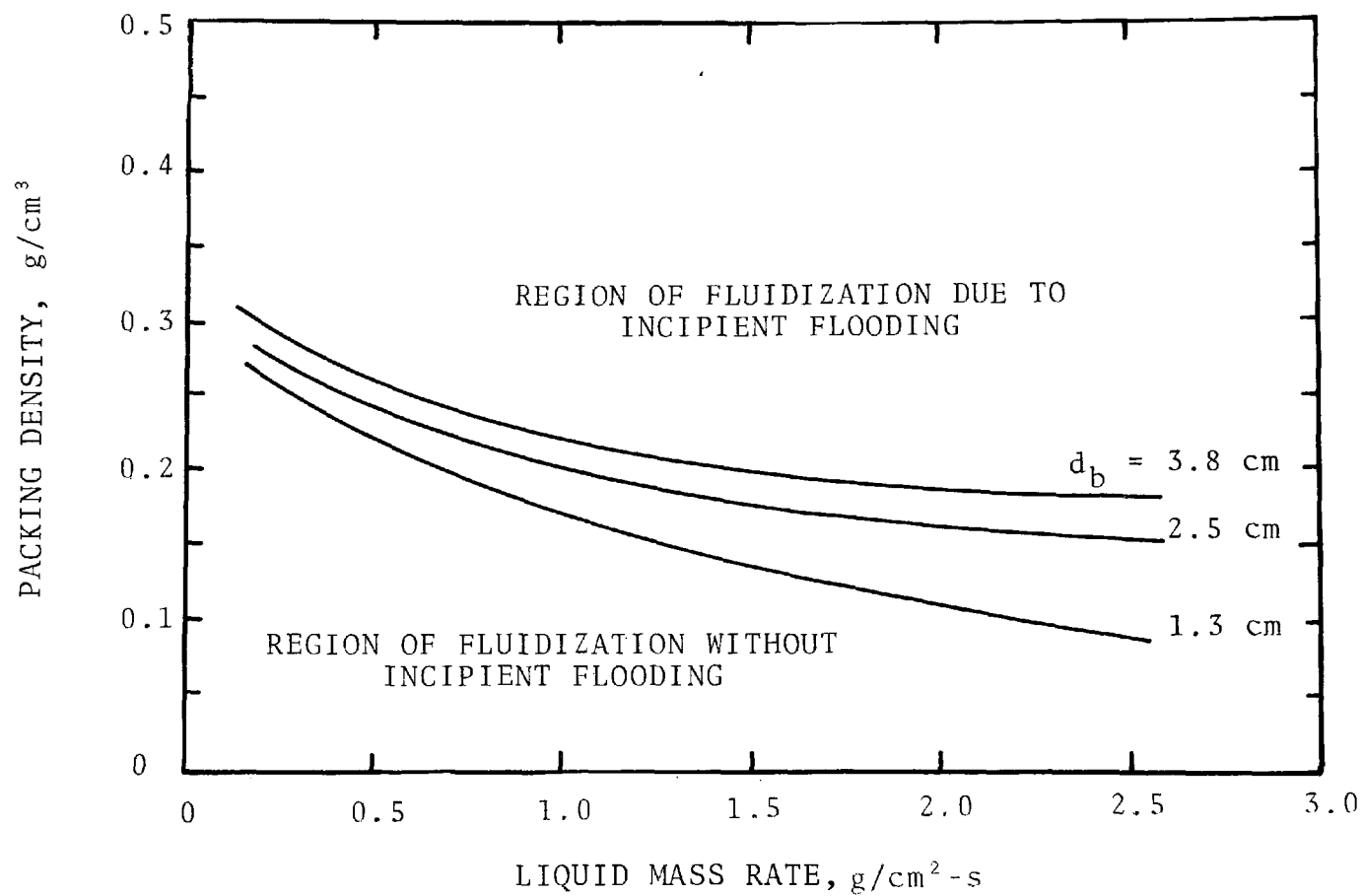


Figure 53. Region of mobile bed operation mode.

where:

- $G_{mf}$  = minimum fluidization gas mass velocity, g/cm<sup>2</sup>-s  
 $d_b$  = ball diameter, cm  
 $L$  = Liquid mass velocity, g/cm<sup>2</sup>-s

The packings used by Chen and Douglas were 1.26 cm, 2.54 cm, and 3.8 cm diameter polystyrene spheres. The densities were 0.16 g/cm<sup>3</sup>, 0.17 g/cm<sup>3</sup>, and 0.16 g/cm<sup>3</sup> for 1.26 cm, 2.54 cm, and 3.8 cm diameter spheres, respectively. The ranges of gas and liquid mass velocities studied were:

$$0 \leq G \leq 0.38 \text{ g/cm}^2\text{-s}$$

$$0 \leq L \leq 1.5 \text{ g/cm}^2\text{-s}$$

Therefore, Chen and Douglas operated their mobile bed in the nonflooding mode.

Balabekov, et al. (1969,1971) determined the minimum fluidization velocity from pressure losses just as in conventional fluidized beds, and followed the effects of liquid flow rate packing size, and packing density on this minimum fluidization velocity. Their correlation is:

$$\frac{u_{Gmf}^2}{g} \frac{a}{\rho_L} \frac{\rho_G}{\rho_L} = 8 f_s^{1.5} \left( \frac{\rho_w}{\rho_L} \right)^{0.64} \exp \left[ -4 \left( \frac{L}{G} \right)^{0.25} \left( \frac{\rho_G}{\rho_L} \right)^{0.125} \right] \quad (33)$$

where:

- $u_{Gmf}$  = minimum fluidization gas velocity, cm/s  
 $a$  = interfacial area of packing, cm<sup>2</sup>/cm<sup>3</sup>  
 $g$  = gravitational acceleration, cm/s<sup>2</sup>  
 $\rho_G$  = gas density, g/cm<sup>3</sup>  
 $\rho_L$  = liquid density, g/cm<sup>3</sup>  
 $\rho_w$  = density of water, g/cm<sup>3</sup>  
 $f_s$  = fractional open area of supporting grid, fraction  
 $L$  = liquid mass velocity, g/cm<sup>2</sup>-s  
 $G$  = gas mass velocity, g/cm<sup>2</sup>-s

Kito, et al. (1977c) used the same approach as Balabekov, et al. and included the effects of liquid holdup and the geometry of the supporting grid on the minimum fluidization velocity. They correlated the minimum fluidization velocity by using the fluidization velocity for dry spheres. The correlation is expressed as:

$$\frac{u_{Gmf}}{u_{Gmfd}} = 3.14 f_s^{0.24} \left( \frac{d_e}{D_c} \right)^{0.48} u_L^{-0.36}, f_s \left( \frac{d_e}{D_c} \right) \leq 0.05 \quad (34)$$

$$\frac{u_{Gmf}}{u_{Gmfd}} = 0.78 u_L^{-0.36}, f_s \left( \frac{d_e}{D_c} \right) > 0.05 \quad (35)$$

where:

$u_{Gmf}$  = minimum fluidization gas velocity, cm/s

$u_{Gmfd}$  = minimum fluidization velocity of dry packing, cm/s

$u_L$  = superficial liquid velocity, cm/s

$d_e$  = equivalent diameter of the pore on the supporting grid, cm

$D_c$  = column diameter, cm

$f_s$  = fractional opening area of the supporting grid, fraction

" $u_{Gmfd}$ ", the minimum fluidization velocity for a packed bed without liquid flow is that calculated from Wen and Yu's (1966) correlation.

$$1.75 \left[ \frac{(1-\epsilon_{mf})}{\epsilon_{mf}^3} \frac{\rho_G u_{Gmfd}^2}{d_b} \right] + 150 \left[ \frac{(1-\epsilon_{mf})^2}{\epsilon_{mf}^3} \frac{\mu_G u_{Gmfd}^2}{d_b^2} \right] - (\rho_b - \rho_G)(1-\epsilon_{mf}) g = 0 \quad (36)$$

where:

- $u_{Gmf}$  = minimum fluidization velocity for dry spheres, cm/s
- $\epsilon_{mf}$  = voidage of bed at minimum fluidization velocity, fraction
- $d_b$  = ball diameter, cm
- $\rho_b$  = packing density, g/cm<sup>3</sup>
- $\rho_G$  = gas density, g/cm<sup>3</sup>
- $\mu_G$  = gas viscosity, g/cm-s
- $g$  = gravitational acceleration, cm/s<sup>2</sup>

The packings used by Kito et al. (1976c) have the following properties:

$d_b$ , cm	1.16	1.95	1.95	1.95	2.85	2.85
$\rho_b$ , g/cm <sup>3</sup>	0.76	0.17	0.54	1.16	0.29	0.59

The characteristics of the supporting grids were:

	$f_s$	$d_e$ , cm
Grid 1	0.712	0.22
Grid 2	0.705	0.39
Grid 3	0.84	1.2

The superficial liquid flow rates in their experiments ranged from 0 to 3.5 cm/s.

Strumillo, et al. (1974) observed that there is a distinct effect of the column diameter and liquid flow rate on the minimum fluidization velocity. They presented an empirical equation for the calculation of the minimum fluidization velocity. The equation was based on limited data and a small column diameter. Therefore, it is applicable only to their system.

Tichy and Douglas (1972) measured the expanded bed heights in a mobile bed for polystyrene spherical packings of two sizes, 1.25 cm and 1.9 cm in diameter, packing densities from 0.153 to

0.458 g/cm<sup>3</sup>, and fixed bed heights from 14 to 35 cm. The supporting grid was 0.24 cm diameter rods spaced at 1.25 cm apart. The free area of the grid was 78%. They derived an empirical equation for predicting the bed height. The minimum fluidization velocity can be obtained by letting  $H_d/H_s = 1$ ; i.e., by using Chen and Douglas' (1967) definition of minimum fluidization velocity.

$$G_{mf} = 3.16 (0.115 + 18.33 d_b - 0.5852L^{0.6} d_b^{0.5}) \quad (37)$$

where:

$G_{mf}$  = minimum fluidization gas mass velocity, g/cm<sup>2</sup>-s  
 $d_b$  = ball diameter, cm  
 $L$  = liquid mass velocity, g/cm<sup>2</sup>-s

Blyakher, et al. (1967) gave the following equation for predicting the minimum fluidization velocity.

$$u_{Gmf} = u_{Gmfd} + \frac{6.7 \times 10^{-3} u_{Gmfd} u_L^{0.9}}{1 + 0.67 u_L^{0.9}} \quad (38)$$

where:

$u_{Gmf}$  = minimum fluidization velocity, cm/s  
 $u_{Gmfd}$  = minimum fluidization velocity of dry packing, cm/s  
 $u_L$  = liquid velocity, cm/s

The minimum fluidization velocity of dry packing in equation (38) was derived from Ergun's equation for packed bed pressure drop. The gas velocity at which the pressure across the packed bed equals the weight of the dry packing is " $u_{Gmfd}$ ".

$$u_{Gmfd} = \frac{0.80 d_b^{0.715} (\rho_b - \rho_G)^{0.572}}{\mu_G^{0.143} \rho_G^{0.429}} \quad (39)$$

where:

$d_b$  = ball diameter, cm  
 $\rho_b$  = packing density, g/cm<sup>3</sup>

$\rho_G$  = gas density, g/cm<sup>3</sup>

$\mu_G$  = gas viscosity, g/cm-s

The packings employed by Blyakher, et al. (1967) were 3.8 cm diameter hollow polyethylene spheres (packing density = 0.17 g/cm<sup>3</sup>) and 3.8 cm cellulose acetate spheres (packing density = 0.090 g/cm<sup>3</sup>). Supporting grids with 19, 30, 41 and 90% open area were studied. The grid which had an open area of 90% was a network of steel rods with diameters of 0.2 cm and with a spacing of 2.5 cm between them. The remaining grids had holes with diameters varying from 1.4 to 2.4 cm.

#### Liquid Holdup -

Chen and Douglas (1968) determined the liquid holdup in a mobile bed scrubber from the dynamic response curve for tracer injection. They found that the liquid holdup related to the fixed bed column is approximately independent of the gas flow rate. It is a function of liquid flow rate and the packing diameter. Their empirical correlation for liquid holdup in a mobile bed is:

$$h_{Lo} = 9.44 \times 10^{-2} d_b^{-0.5} L^{0.6} + 0.02 \quad (40)$$

where:

$h_{Lo}$  = liquid holdup based on fixed bed volume, cm<sup>3</sup>/cm<sup>3</sup>

$L$  = liquid mass velocity, g/cm<sup>2</sup>-s

$d_b$  = ball diameter, cm

The apparatus used by Chen and Douglas is the same as that presented earlier. Therefore, this correlation is limited to mobile beds which are operated in the nonflooding mode.

Kito et al. (1976d), using the same setup presented in the last section, also found that the liquid holdup is indepen-

dent of gas flow rate. In addition to liquid flow rate and packing diameter, they found that the geometry of the retaining grid also affects the amount of liquid holdup in the bed. Their empirical equation is:

$$h_{Lo} = 0.06 + 0.0316 f_s^{-0.42} \left( \frac{d_e}{D_c} \right)^{-0.84} (d_b)^{-0.84} (\rho_b)^{0.18} (H_s)^{-0.4} u_L \quad (41)$$

where:

- $h_{Lo}$  = liquid holdup related to fixed bed volume,  $\text{cm}^3/\text{cm}^3$
- $f_s$  = fractional open area of the supporting grid, fraction
- $d_e$  = equivalent diameter of grid opening, cm
- $D_c$  = column diameter, cm
- $d_b$  = ball diameter, cm
- $\rho_b$  = packing density,  $\text{g}/\text{cm}^3$
- $H_s$  = static bed height, cm
- $u_L$  = superficial liquid velocity,  $\text{cm}/\text{s}$

The liquid holdup predicted by Kito, et al.'s correlation is about three times higher than that predicted by Chen and Douglas' correlation. The main reasons are probably that Kito et al. used grids with smaller openings and packings with high packing density. The supporting grid used by Chen and Douglas was 0.24 cm diameter rods spaced at 1.25 cm apart. Therefore, in Chen and Douglas' setup, no water was retained on the grid. In Kito et al.'s setup, the supporting grids had much smaller openings. As revealed in the experiments conducted in the present study on the plastic net support, water was retained on the grid even though there was no packing.

#### Bed Expansion -

Tichy and Douglas (1972), Balabekov, et al. (1972), Blyakher, et al. (1967), and Kito, et al. (1976d) derived empirical equations to predict the expanded bed height of mobile bed scrubbers. Their equations are:



Tichy and Douglas (1972):

$$\frac{H_d}{H_s} = 0.8849 + 3.166 G - 0.1833 d_b + 0.233 L^{0.6} d_b^{0.5} \quad (42)$$

Balabekov, et al. (1971):

$$H_d = \frac{(1-\epsilon) H_s + H_L}{1 - h_G} \quad (43)$$

Blyakher, et al. (1967):

$$\frac{H_d}{H_s} = 1.17 + (6.5 \times 10^{-3} + 7.8 \times 10^{-3} u_L^{0.75}) (u_G - u_{Gmf}) \quad (44)$$

Kito, et al. (1976d):

$$\frac{H_s}{H_d} = \frac{1 + h_{Lo} - \epsilon}{1 - 0.151 u_G^{0.44}} \quad (45)$$

where:

- $u_G$  = superficial gas velocity, cm/s
- $H_d$  = dynamic or expanded bed height, cm
- $H_s$  = static bed height, cm
- $G$  = gas mass velocity, g/cm<sup>2</sup>-s
- $L$  = liquid mass velocity, g/cm<sup>2</sup>-s
- $d_b$  = ball diameter, cm
- $u_L$  = superficial liquid velocity, cm/s
- $u_{Gmf}$  = minimum fluidization velocity, cm/s
- $h_{Lo}$  = liquid holdup, cm<sup>3</sup>/cm<sup>3</sup>
- $\epsilon$  = void fraction of dry static bed, fraction
- $h_G$  = gas holdup, cm<sup>3</sup>/cm<sup>3</sup>
- $H_L$  = height of liquid column retained on the supporting grid, cm

The packing diameters, packing densities, and supporting grid configurations used by these investigators were given in earlier sections.

#### Gas Holdup -

Kito, et al. (1976a) investigated the effects of operating parameters on gas holdup in mobile beds. They found that only the gas flow rate and the liquid surface tension influenced the holdup.

$$\frac{h_G}{\left[ h_G (1 - h_G)^2 \right]^{0.44}} = 0.5 N_{We}^{0.11} N_{Fr}^{0.22} \quad (46)$$

$$N_{We} = \text{Weber Number} = \frac{D_c u_G^2 \rho_L}{\sigma_L} \quad (47)$$

$$N_{Fr} = \text{Froude Number} = \frac{u_G}{(g D_c)^{0.5}} \quad (48)$$

where:

- $h_G$  = gas holdup,  $\text{cm}^3/\text{cm}^3$
- $D_c$  = mobile bed column diameter, cm
- $u_G$  = superficial gas velocity, cm/s
- $\rho_L$  = liquid density,  $\text{g}/\text{cm}^3$
- $\sigma_L$  = surface tension of liquid, dyne/cm
- $g$  = acceleration of gravity,  $\text{cm}/\text{s}^2$

The above equation can be approximated by:

$$h_G = 0.055 u_G^{0.44} \quad (49)$$

#### Flooding Velocity -

Balabekov, et al. (1971) presented the following equation for the determination of flooding velocity of mobile beds:

$$u_{Gf} = u_G \left[ \frac{H - (1-\epsilon) H_s - H_L}{1.16 \epsilon H_L} \right]^5 \quad (50)$$

where:

$u_{Gf}$  = flooding velocity, cm/s

$u_G'$  = original entrainment velocity in wetted packing, cm/s

$H$  = packed column height or the distance between retaining grids, cm

$H_L$  = height of clear liquid column retained on retaining grid, cm

$\epsilon$  = void fraction of dry packed bed, fraction

$H_s$  = static bed height, cm

Uchida, et al. (1977) defined that the flooding point of a mobile bed is reached when the terminal settling velocity of the wetted packing is equal to the gas velocity. Since the diameter of the packings in the mobile bed is large, the relation between the flooding velocity and the minimum fluidization velocity can be approximated by the following equation:

$$\frac{u_{Gf}}{u_{Gmf}} = 8.72 \quad (51)$$

where:

$u_{Gf}$  = flooding velocity, cm/s

$u_{Gmf}$  = minimum fluidization velocity, cm/s

#### Liquid-Gas Interfacial Area -

Woźniak and Ostergaard (1973) and Woźniak (1977) derived an empirical equation for the calculation of liquid-gas interfacial area of mobile beds. The mobile bed scrubber was a two-stage mobile bed, each packed with 1.96 cm diameter polypropylene spheres (packing density 0.266 g/cm<sup>3</sup>). The supporting grids were wire mesh with approximately 60% open area. The diameter of the scrubber was 20 cm.

From the data of absorption of CO<sub>2</sub> by NaOH solution, they back calculated the interfacial mass transfer area. The effective interfacial area, pressure drop, amount of gas and liquid holdup are correlated by the following equation:

$$\frac{a}{a_b} = 9.2 \times 10^{-4} \left( \frac{h_G}{1-h_G} \right)^{0.8022} \left( \frac{H_d (\Delta P_w)}{u_G \mu_G} \right)^{0.9337} \quad (52)$$

where:

- $a$  = effective interfacial area per unit volume of static packing,  $\text{cm}^2/\text{cm}^3$
- $a_b$  = geometrical surface area of static bed per unit volume of static packing,  $\text{cm}^2/\text{cm}^3$
- $h_G$  = gas holdup,  $\text{cm}^3/\text{cm}^3$
- $H_d$  = dynamic bed height, cm
- $\Delta P_w$  = pressure drop across bed, cm W.C.
- $u_G$  = superficial gas velocity, cm/s
- $\mu_G$  = viscosity of gas, g/cm-s

Kito, et al. (1976b) used the same technique to determine the liquid-gas interfacial area. They found that the interfacial area, on a tower volume basis, increases proportionately to the gas flow rate up to 200 cm/s, and to gas holdup to 0.6, and is not affected by the geometry of the supporting grid, the static bed height, and the packing density. The interfacial area decreases with an increasing gas flow rate over 200 cm/s and gas holdup over 0.6. No equation was given by them for the prediction of interfacial area.

#### Pressure Drop

For a fully fluidized mobile bed, the pressure drop is made up of the sum of pressure drops due to weight of dry packing, weight of liquid holdup in the bed, the friction loss of the retaining grids and column, liquid head retained on the supporting grid, and drop atomization (Blyakher, et al., 1967; Kito, et al., 1976); i.e.:

$$\Delta P_w = \Delta P_b + \Delta P_{Lh} + \Delta P_L + \Delta P_a + \Delta P_c + \Delta P_f \quad (53)$$

where:

- $\Delta P_w$  = overall pressure drop per stage of bed, cm W.C.
- $\Delta P_b$  = pressure drop due to weight of dry packing, cm W.C.
- $\Delta P_{Lh}$  = pressure drop due to liquid holdup, cm W.C.
- $\Delta P_L$  = pressure drop due to liquid head retained on supporting grid, cm W.C.
- $\Delta P_a$  = pressure drop due to drop atomization, cm W.C.
- $\Delta P_c$  = pressure drop due to wall friction, cm W.C.
- $\Delta P_f$  = friction loss of supporting grid, cm W.C.

#### Pressure Drop Due to Weight of Dry Packing -

The pressure drop due to the weight of dry packing can be expressed as:

$$\Delta P_b = (\rho_b - \rho_G)(1-\epsilon) H_s \quad (54)$$

where:

- $\rho_b$  = packing density, g/cm<sup>3</sup>
- $\rho_G$  = gas density, g/cm<sup>3</sup>
- $\epsilon$  = static bed porosity, fraction
- $H_s$  = static bed height, cm

#### Pressure Drop Due to Liquid Holdup -

The pressure drop due to the weight of liquid holdup in the bed is:

$$\Delta P_{Lh} = \rho_L h_L H_d = \rho_L h_{Lo} H_s \quad (55)$$

where:

- $\rho_L$  = liquid density, g/cm<sup>3</sup>
- $h_L$  = liquid holdup, cm<sup>3</sup>/cm<sup>3</sup>
- $H_d$  = dynamic bed height, cm
- $h_{Lo}$  = liquid holdup related to static bed, cm<sup>3</sup>/cm<sup>3</sup>
- $H_s$  = static bed height, cm

Chen and Douglas (1968) and Kito, et al. (1976) determined the liquid holdup in a mobile bed. Their empirical correlations are given in an earlier section. Chen and Douglas (1968) and Kito, et al. (1976) both found that the liquid holdup is independent of gas velocity. Therefore, by using their correlation in equation (55), the pressure drop due to liquid holdup should be independent of the gas flow rate.

Uchida, et al. (1977) modified Kito, et al.'s liquid holdup correlation to include the experimental data obtained from a large scale mobile bed scrubber. Their correlation for pressure drop due to liquid holdup is:

$$\Delta P_{Lh} = 795.6 \mu_L^{2.3} f_s^{-0.42} \left( \frac{d_e}{D_c} \right)^{-0.84} d_b^{-0.84} \rho_b^{0.18} H_s u_L \quad (56)$$

where:

- $\mu_L$  = viscosity of liquid, g/cm-s
- $f_s$  = fractional opening area of the supporting grid, fraction
- $d_e$  = equivalent diameter of grid opening, cm
- $D_c$  = column diameter, cm
- $d_b$  = ball diameter, cm
- $\rho_b$  = packing density, g/cm<sup>3</sup>
- $H_s$  = static bed height, cm
- $u_L$  = superficial liquid velocity, cm/s

Woźniak (1977) performed a dimensional analysis and conducted experiments to determine the coefficients. His correlation for pressure drop due to liquid holdup is:

$$\Delta P_{Lh} = 476.6 \rho_G u_G^2 \left( \frac{H_s}{d_b} \right)^{0.4515} \left( \frac{d_b u_G \rho_G}{\mu_G} \right)^{1.798} \left( \frac{d_b u_L \rho_L}{\mu_L} \right)^{0.8261} \quad (57)$$

where:

- $\Delta P_{Lh}$  = pressure drop due to liquid holdup, cm W.C.
- $\rho_G$  = gas density, g/cm<sup>3</sup>
- $u_G$  = superficial gas velocity, cm/s

$H_s$  = static bed height, cm  
 $d_b$  = ball diameter, cm  
 $\mu_G$  = gas viscosity, g/cm-s  
 $\mu_L$  = liquid viscosity, g/cm-s  
 $u_L$  = superficial liquid velocity, cm/s  
 $\rho_L$  = liquid density, g/cm<sup>3</sup>

Blyakher, et al. (1967) and Balabekov, et al. (1971) proposed other equations for calculating the pressure drop due to liquid holdup. Their equations contain empirical coefficients which need to be determined experimentally.

Pressure Drop Due to Liquid Froth Retained on Supporting Grid -

" $\Delta P_L$ ", the pressure drop due to liquid froth retained on the supporting grid is given by the following equation (Blyakher, et al. 1967):

$$\Delta P_L = \xi_f u_G^{1.75} u_L^{0.5} \quad (58)$$

where:

$u_G$  = superficial gas velocity, cm/s  
 $u_L$  = superficial liquid velocity, cm/s  
 $\xi_f$  = coefficient dependent upon the geometric characteristics of the grid, dimensionless

Supporting Grid and Column Friction Loss -

The friction losses of the supporting grid and the column can both be expressed by the following equation (Perry, 1973):

$$\Delta P_f \text{ or } \Delta P_c = f \frac{\rho_G u_G^2}{2g} \quad (59)$$

where:

$f$  = hydraulic resistance coefficient, dimensionless

Pressure Drop Due to Drop Atomization -

The pressure drop due to drop atomization is (Calvert, 1968):

$$\Delta P_a = k \frac{u_G^2}{2g} \left( \frac{Q_L}{Q_G} \right) \quad (60)$$

where:

$Q_L$  = liquid volumetric flowrate,  $\text{cm}^3/\text{s}$

$Q_G$  = volumetric gas flowrate,  $\text{cm}^3/\text{s}$

$k$  = constant characterizing the fraction of liquid being atomized, fraction

### Heat and Mass Transfer Coefficient

The heat and mass transfer capabilities of mobile bed scrubbers were studied by Douglas (1964) and Gel'perin, et al. (1973). Douglas (1964) conducted two series of experiments. The first was the absorption of ammonia by boric acid solutions. The results were given in terms of height of transfer unit and as mass transfer coefficients. Both of these performance values were calculated using the overall gas logarithmic mean driving force and were based on the static bed height. He found that the height of transfer unit decreased with increasing liquid mass velocity and increased with increasing gas mass velocity.

The second series of experiments were designed to obtain the rate of simultaneous heat and mass transfer. The technique used was the dehumidification and cooling of hot saturated gas. He found that the effect of gas velocity on the height of transfer unit was the same as that observed for the absorption of ammonia. However, the effect of liquid mass velocity was different for the two cases. The height of transfer unit, instead of decreasing with liquid rate, increased with liquid rate for the dehumidification tests.

Douglas (1964) presented experimental data but no mathematical correlations. Gel'perin et al. (1973) studied the process of adiabatic evaporation of water during its contact with hot gas in a mobile bed scrubber. The heat and mass transfer coefficients referred to the unit volume of the expanded bed were given by Gel'perin, et al. as follows:



$$k_G = 1.07 \times 10^{-9} u_G^{1.3} u_L^{0.3} H_S^{0.4} \quad (61)$$

$$h_G = 3.9 \times 10^{-13} u_G^{1.3} u_L^{0.3} H_S^{0.4} \quad (62)$$

where:

$$k_G = \text{mass transfer coefficient, } \frac{g}{\text{cm}^3 \cdot \text{s} \cdot \text{atm}}$$

$$h_G = \text{heat transfer coefficient, kcal/cm}^3 \cdot \text{s} \cdot ^\circ\text{C}$$

$$u_G = \text{superficial gas velocity, cm/s}$$

$$u_L = \text{superficial liquid velocity, cm/s}$$

$$H_S = \text{static bed height, cm}$$

The ratio of heat transfer coefficient to mass transfer coefficient is  $3.65 \times 10^{-4} \text{ kcal-atm/g} \cdot ^\circ\text{C}$ . According to Gel'perin et al., the dynamic height of the mobile bed depends on the same parameters as the coefficients of heat and mass transfer and the mass transfer coefficient based on unit expanded bed volume is independent on the liquid rate.

#### Particle Collection

The only model available for particle collection in a mobile bed is the semi-empirical relationship presented by Bechtel Corporation in a June 1971 report on the Shawnee project for the EPA and was cited by Calvert et al. (1972). This correlation is based on the premise that collection efficiency is due to inertial impaction on the balls.

$$Pt_d = \exp \left[ - 9.5 \times 10^6 \left( \frac{Q_L}{Q_G} \right)^{3.3} (u_G \rho_G)^{3.66} K_p \frac{n H_S}{d_b} \right] \quad (63)$$

$$K_p = \frac{d_{pa}^2 u_{Gi}}{9 \mu_G d_b} \times 10^{-8}$$

where:

- $Pt_d$  = particle penetration for particles with diameter  $d_{pa}$ ,  
fraction
- $Q_L$  = volumetric liquid flowrate,  $cm^3/s$
- $Q_G$  = volumetric gas flowrate,  $cm^3/s$
- $u_G$  = superficial gas velocity,  $cm/s$
- $\rho_G$  = gas density,  $cm/s$
- $n$  = number of mobile bed stages, dimensionless
- $H_s$  = static bed height,  $cm$
- $d_b$  = ball diameter,  $cm$
- $K_p$  = inertial impaction parameter, dimensionless
- $d_{pa}$  = aerodynamic particle diameter,  $\mu m$
- $u_{Gi}$  = gas velocity in bed,  $cm/s$
- $\mu_G$  = gas viscosity,  $g/cm-s$

## COMPARISON OF EXPERIMENTAL DATA WITH PREDICTIONS

### Pressure Drop

Pressure drop predictions by correlations of Chen and Douglas (1969), Woźniak (1977), Kito et al. (1976d), and Uchida et al. (1977) were compared with the experimental data obtained in this study in Figures 54 through 57. The experimental data have been corrected for friction losses.

The comparison revealed that predictions by Uchida et al.'s correlation are much higher than that measured. Predictions by Kito et al.'s correlation are better than Uchida et al.'s correlation; but it still is higher than that measured. Woźniak's equation overestimated the pressure drops of the mobile bed with hardware screen support and underestimated the pressure drops of the mobile bed with plastic net support. The predictions by Chen and Douglas agree only with the data for the hardware screen supported mobile bed. However, the correlation by Chen and Douglas did not predict the correct dependence of pressure drop on liquid flow rate (Figure 58). Compared to the pressure drop data on the plastic net supported mobile bed, the correlation by Chen and Douglas is much lower than that measured.

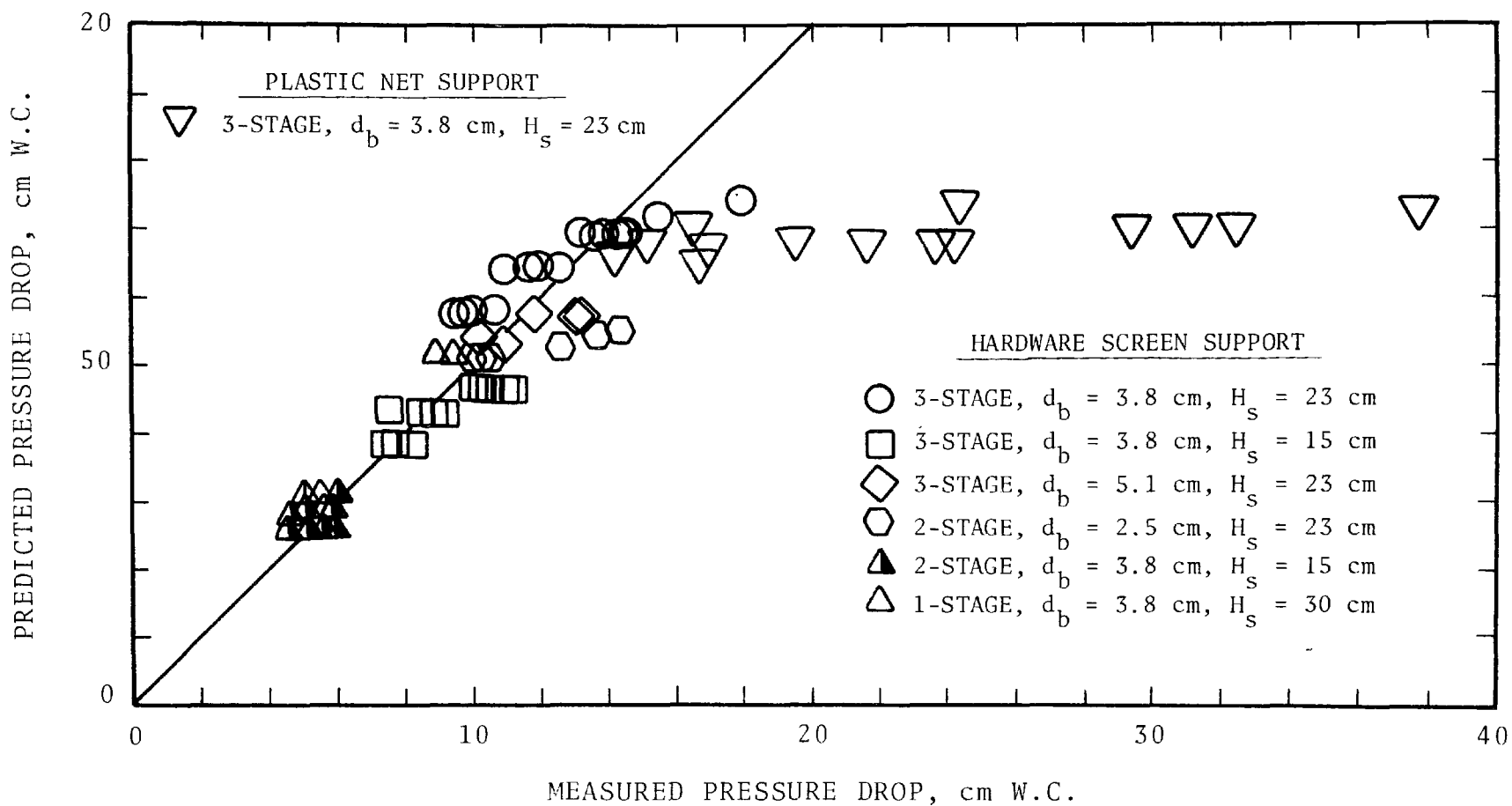


Figure 54. Predicted and measured pressure drop (Chen and Douglas's correlation).

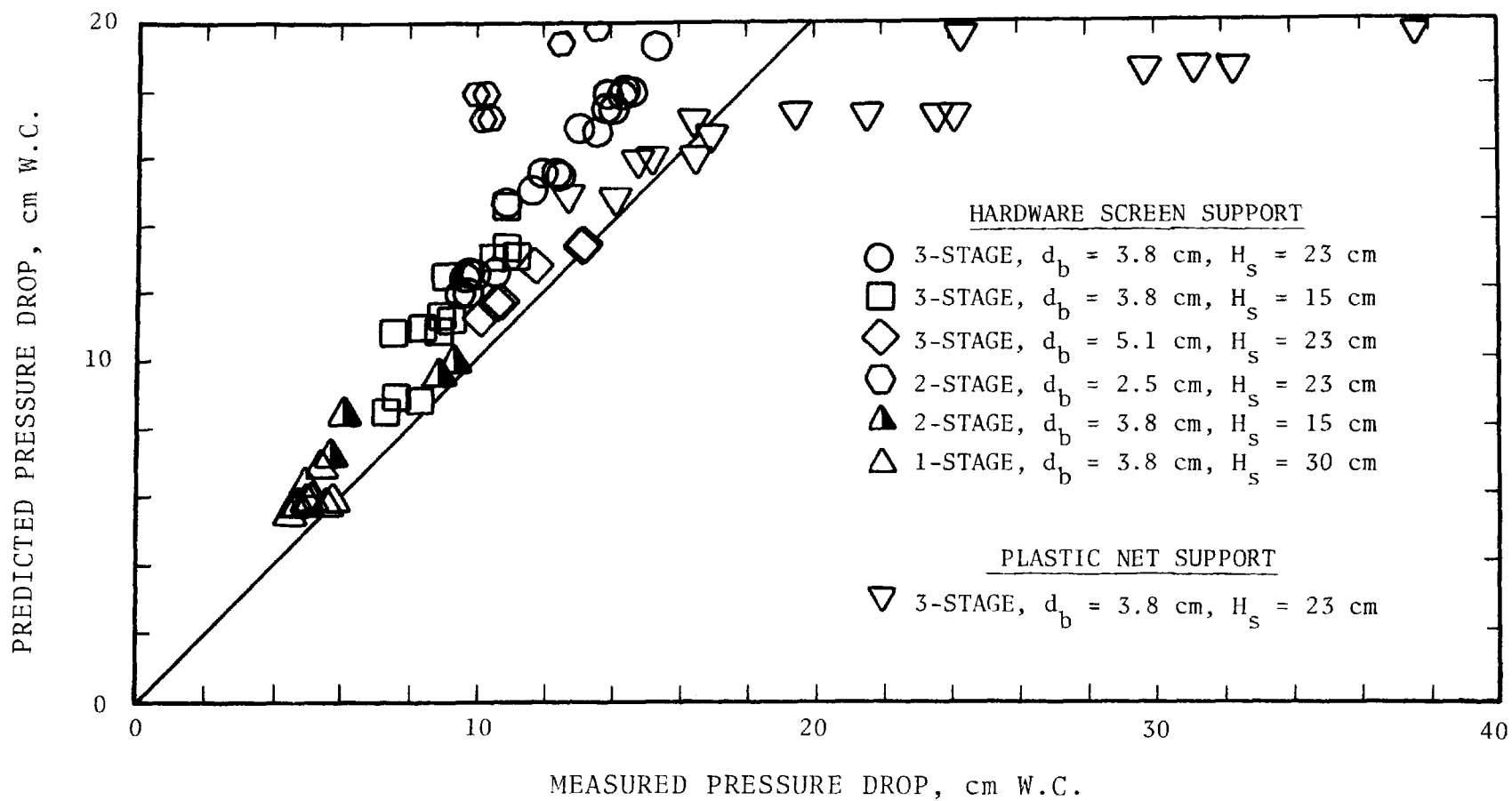


Figure 55. Predicted and measured pressure drop (Woźniak's correlation).

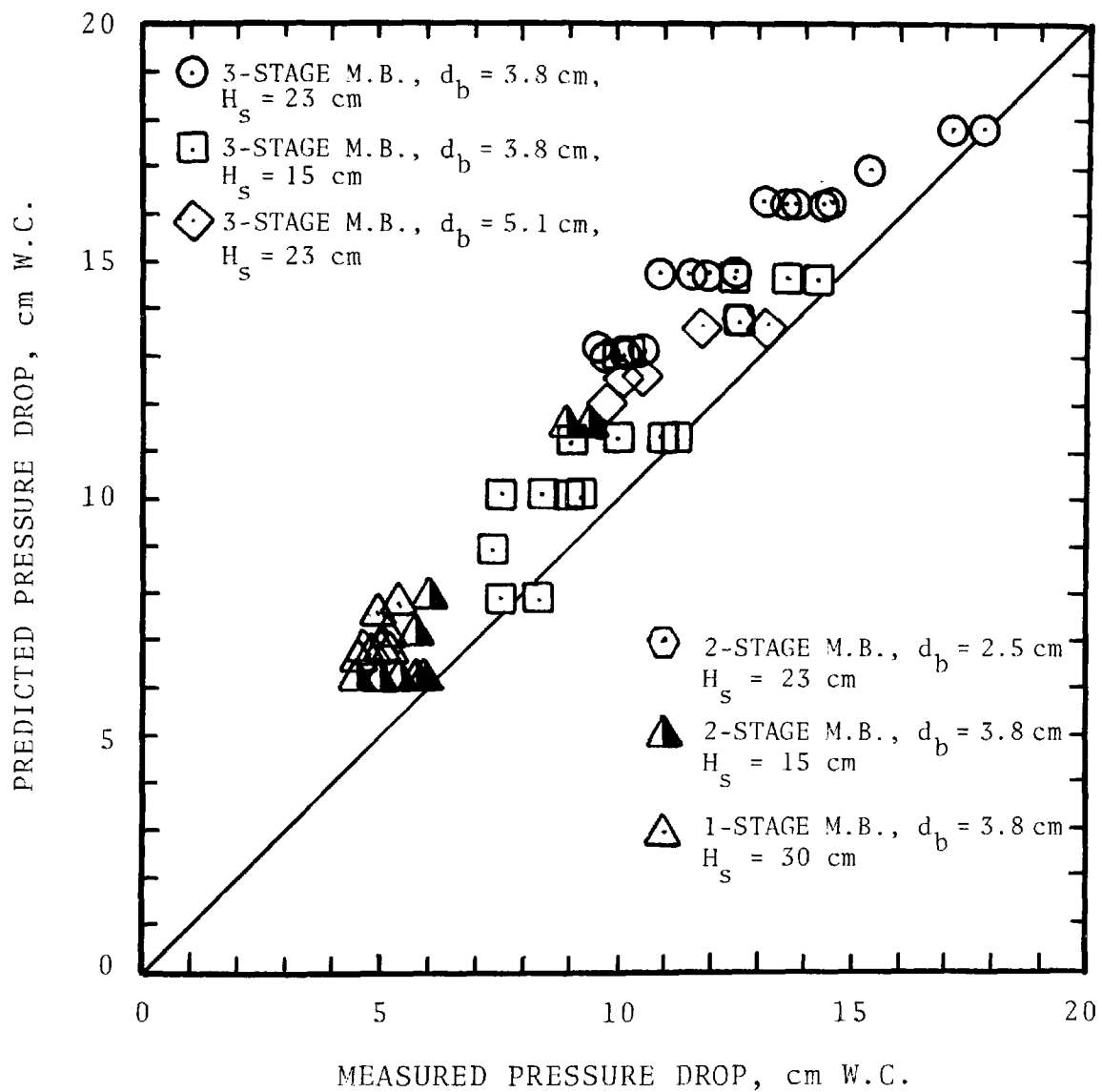


Figure 56. Predicted and measured pressure drop (Kito et al.'s correlation).

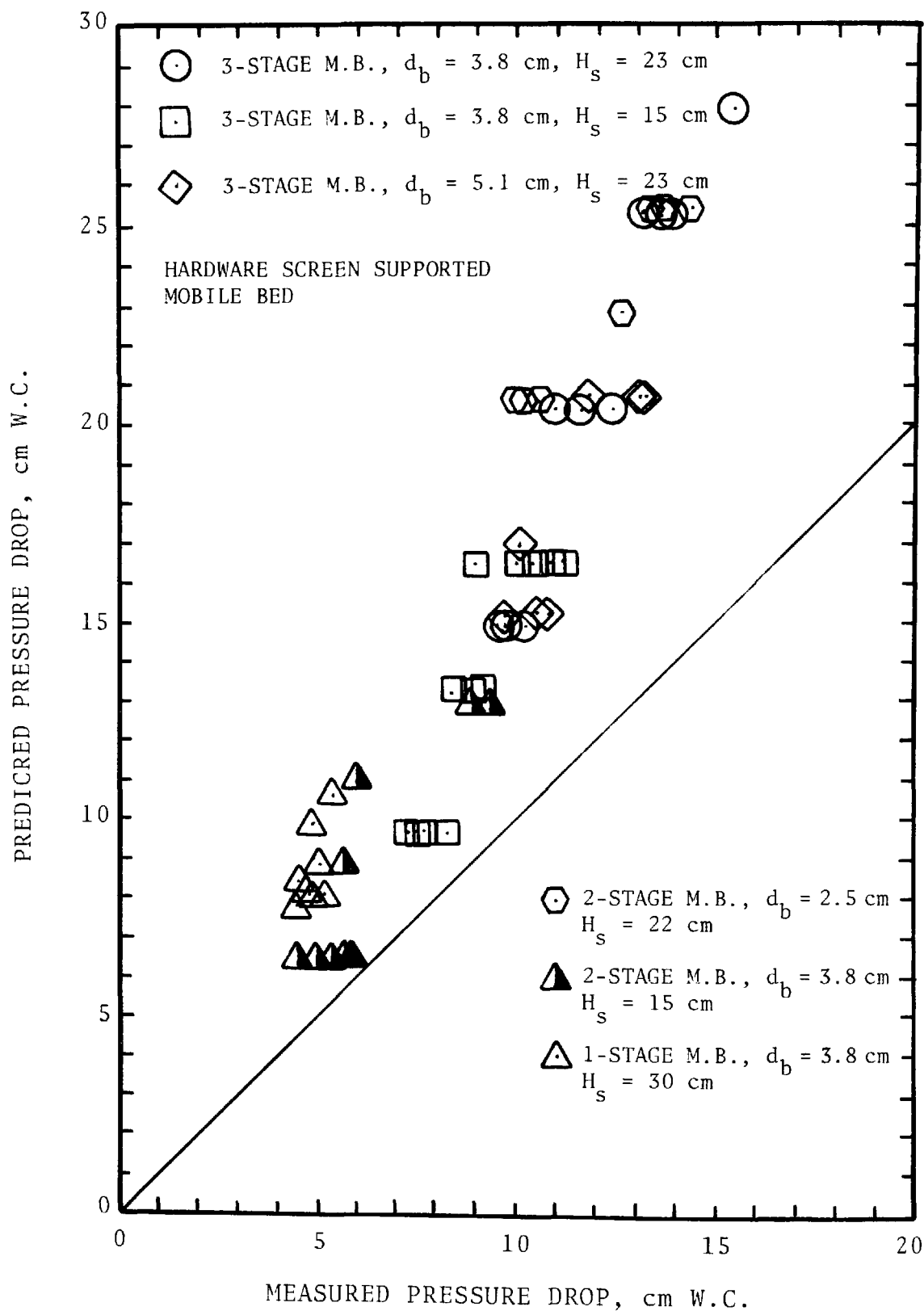


Figure 57. Predicted and measured pressure drop (Uchida et al.'s correlation).

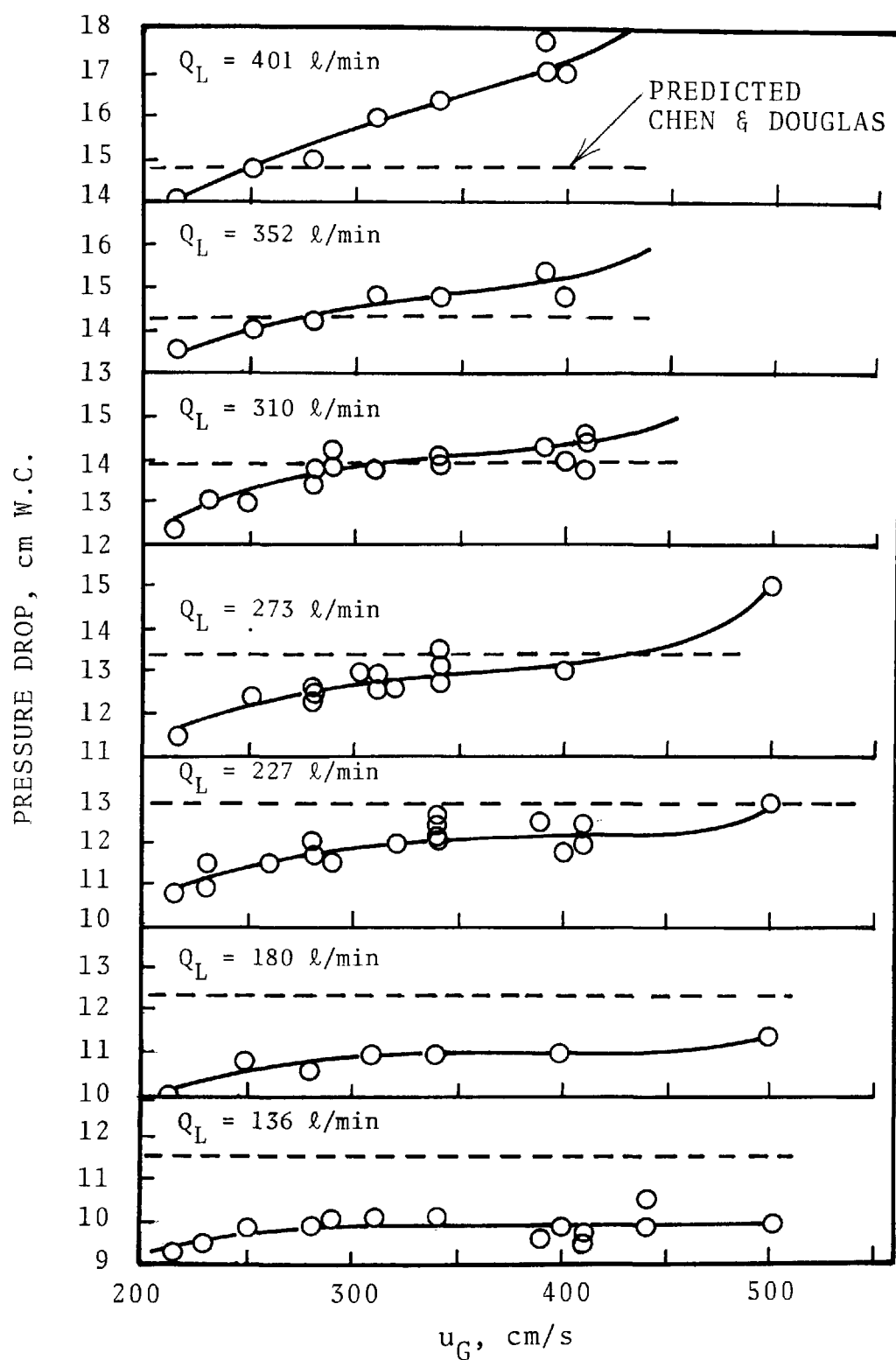


Figure 58. Measured and predicted pressure drop for a three-stage mobile bed scrubber with hardware screen support, and each stage packed with 3.8 cm dia. spheres to a depth of 23 cm.

## Particle Collection

The predicted particle collection in the mobile bed scrubber by equation (63) did not agree with the experimental data obtained in this study. The predictions were lower than that measured.

Bechtel Corporation's correlation; i.e., equation (63) was derived based on the premise that particle collection is due to inertial impaction on balls. We may note that the impaction parameter has a value of about  $5 \times 10^{-4}$  for a gas velocity of 305 cm/s (10 ft/s), ball diameter of 3.8 cm, and aerodynamic particle diameter of 1.0  $\mu$ m. The collection efficiency for a sphere is 0% for values of the impaction parameter smaller than about 0.1; consequently, it is impossible to attribute collection efficiency to this mechanism.

Another drawback of equation (63) is that it did not include the effect of supporting grids on particle collection. As mentioned earlier, the efficiency of a plastic net supported mobile bed is higher than that of a hardware screen supported mobile bed with the same bed geometry and liquid and gas flow rates.

## MATHEMATICAL MODELING

### Pressure Drop

An empirical correlation was derived in this study for the prediction of pressure drop due to liquid holdup. The correlation was derived by dimensional analysis. The correlation is:

$$P_{Lh} = 83.0 \rho_G u_G^2 \left( \frac{H_s}{d_b} \right)^{0.8} \left( \frac{d_b \rho_G u_G}{\mu_G} \right)^{-1.75} \left( \frac{d_b \rho_L u_L}{\mu_L} \right)^{0.96} \left( \frac{\rho_b}{\rho_L} \right)^{0.4} \quad (64)$$

where  $P_{Lh}$  = pressure drop due to liquid holdup in bed, cm W.C.  
 $\rho_G$  = gas density, g/cm<sup>3</sup>  
 $\rho_L$  = liquid density, g/cm<sup>3</sup>  
 $\rho_b$  = packing density, g/cm<sup>3</sup>  
 $H_s$  = static bed height, cm  
 $d_b$  = packing diameter, cm  
 $u_G$  = superficial gas velocity, cm/s



$u_L$  = superficial liquid velocity, cm/s  
 $\mu_G$  = gas viscosity, g/cm-s  
 $\mu_L$  = liquid viscosity, g/cm-s

An empirical correlation was also derived in this study for the prediction of pressure drop due to the liquid froth retained on the grid.

$$\Delta P_L = 9.2 \times 10^{-9} \left( \frac{D_c}{f_s d_e} \right)^{2.6} u_G^{0.5} u_L^{2.0} \quad (65)$$

If the friction losses are neglected, the pressure drop across one stage of the mobile bed is:

$$\Delta P = (1-\epsilon)\rho_b H_s + \Delta P_{Lh} + \Delta P_L \quad (66)$$

For a multi-stage mobile bed scrubber, the overall pressure drop will be:

$$\Delta P_w = n \Delta P + \Delta P_f + \Delta P_c \quad (67)$$

where  $\Delta P_w$  = Overall pressure drop, cm W.C.

$\Delta P_f$  = friction loss of retaining grids, cm W.C.

$\Delta P_c$  = wall friction loss, cm W.C.

The predictions by the above equation are compared with data reported by Epstein et al. (1974), Barile and Meyer (1971), Kito et al. (1976), Blyakher et al. (1967), Tichy et al. (1973), and Douglas et al. (1963) in Figures 59 and 60. The data reported by Epstein et al. were obtained on a full scale mobile bed which was installed in a power plant. They used two types of support, mesh and bar-grid. The bars were 0.95 cm (3/8") diameter stainless steel and spaced at 3.2 (1-1/4") on centers. The wire diameter of the wire mesh grid was 0.38 cm (0.148"). The spacing between the wire was not reported. In the pressure drop predictions, the wire mesh was assumed to have the same geometry as the bar grid; i.e., same " $f_s$ " and " $d_e$ ". As can be seen from Figures 59 and 60, the agreement between predictions and data is good.

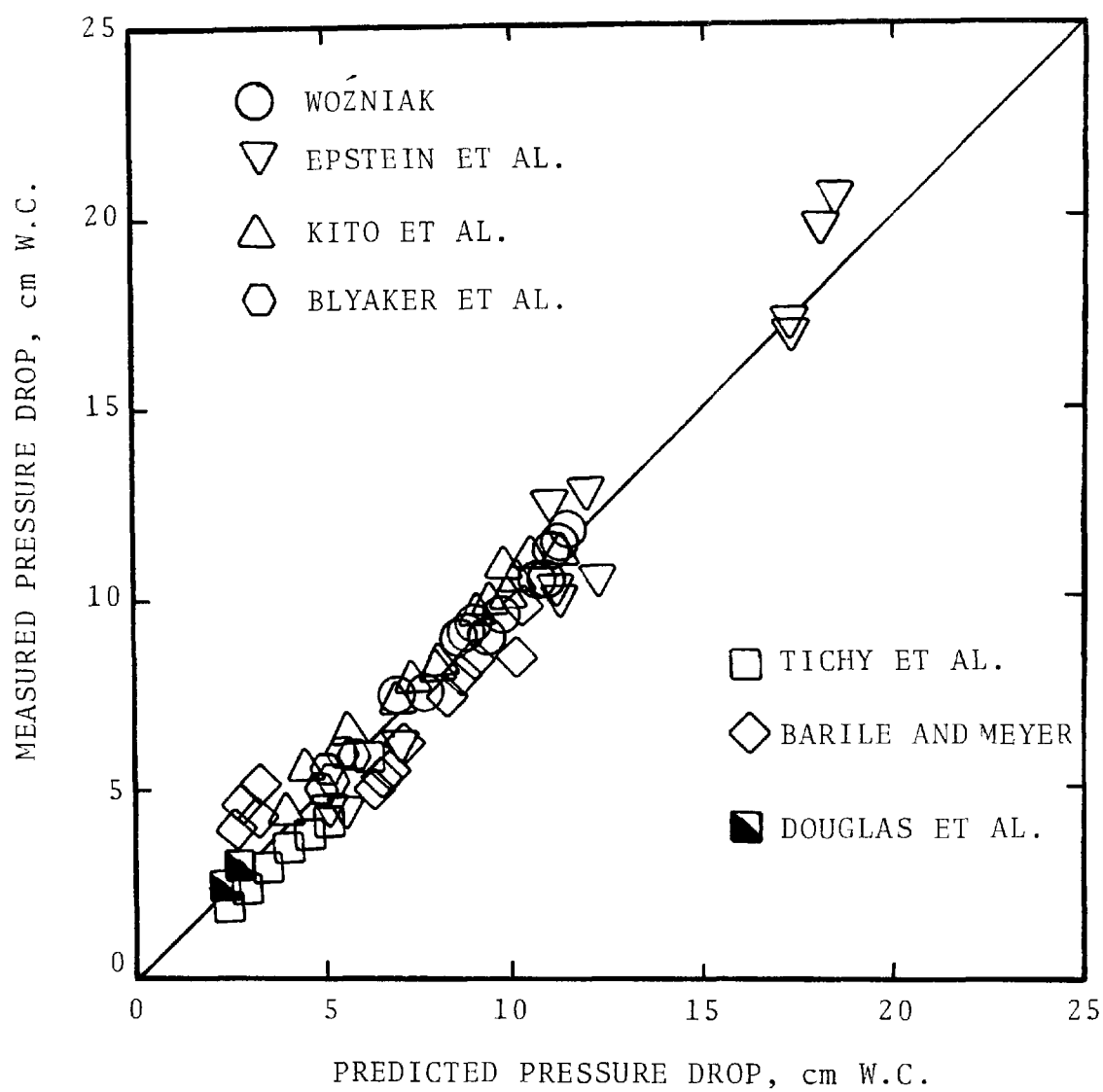


Figure 59. Comparison between measured and predicted mobile bed pressure drop.

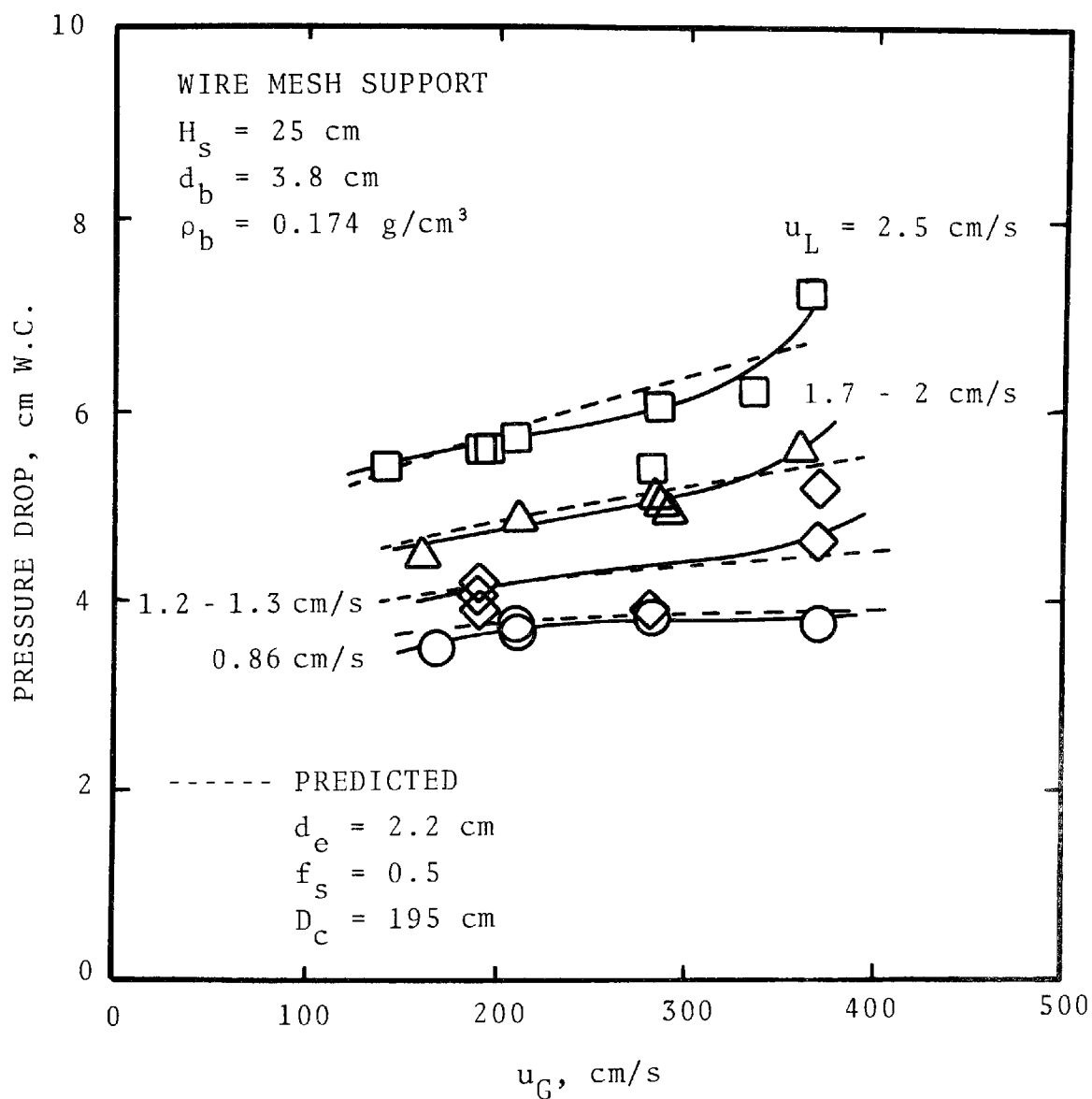


Figure 60. Pressure drop through a single stage of a mobile bed obtained at EPA/TVA Shawnee plant.

## Particle Collection

Particle collection in a mobile bed scrubber may be due to inertial impaction on the atomized liquid drops. Thus, particle collection can be predicted if the atomized drop diameter and amount of liquid in drop form can be calculated. However, the hydrodynamics of a three-phase fluidized bed are extremely complex. It is impossible to derive the theoretical equations for drop size and quantity of drops. Empirical approximations based on pressure drop relationships for gas atomized scrubbers were used to predict collection efficiency without success. An empirical equation was developed for particle collection in a mobile bed scrubber. The empirical equation is:

$$Pt_d = \exp[-9.84 \times 10^{-4} (\Delta P_w)^{1.96} d_{pa}^{1.6}] \quad (68)$$

where  $Pt_d$  = penetration for particle diameter " $d_{pa}$ ", percent or fraction

$\Delta P_w$  = overall pressure drop across the mobile bed scrubber, cm W.C.

$d_{pa}$  = aerodynamic particle diameter,  $\mu m$

## F/C SCRUBBING

When a hot and saturated gas is in contact with cold water or a cold solid surface, condensation of water vapor occurs. Part of the vapor will be condensed on the particles which serve as condensation nuclei. Thus, the particles will have grown in mass due to the layer of water they carry and will be more susceptible to collection by inertial impaction. While condensation occurs, there will be diffusio-phoretic and thermophoretic deposition on the cold surfaces as well as some inertial impaction. The particle growth by condensation in combination with diffusio-phoresis and thermophoresis is referred to as "flux force/condensation" (F/C) scrubbing.

Several phenomena are simultaneously involved in a F/C scrubber and the mathematical model is complex and cumbersome. Calvert and Gandhi (1977), through a series of studies, concluded that the flux force effects and condensation effect can be treated separately. Based on this conclusion, they developed a simplified performance prediction and design method. Their method is summarized in the following paragraphs.

### Basic Concepts

Before proceeding to the details of the mathematical model, the basic concepts and outline of the approach will be discussed. If we consider a typical F/C scrubbing system, it might have the features shown in Figure 61. The gas leaving the source is hot and has a water vapor content which depends on the source process. The first step is to saturate the gas by quenching it with water. This will cause no condensation if the particles are insoluble, but will if they are soluble. There will be a diffusiophoretic force directed away from the liquid surface.

Condensation is required in order to have diffusiophoretic deposition, any growth on insoluble particles, and extensive growth on soluble particles. Contacting with cold water or a cold surface is employed to cause condensation. While condensation occurs there will be diffusiophoretic and thermophoretic deposition as well as some inertial impaction (and, perhaps, Brownian diffusion). The particles in the gas leaving the condenser will have grown in mass due to the layer of water they carry.

Subsequent scrubbing of the gas will result in more particle collection by inertial impaction. This will be more efficient than impaction before particle growth because of the greater inertia of the particles. There may be additional condensation, depending on water and gas temperatures, and its effects can be accounted for as discussed above.

One can apply this general outline of F/C scrubbing to a variety of scrubber types. The condenser may be a separate

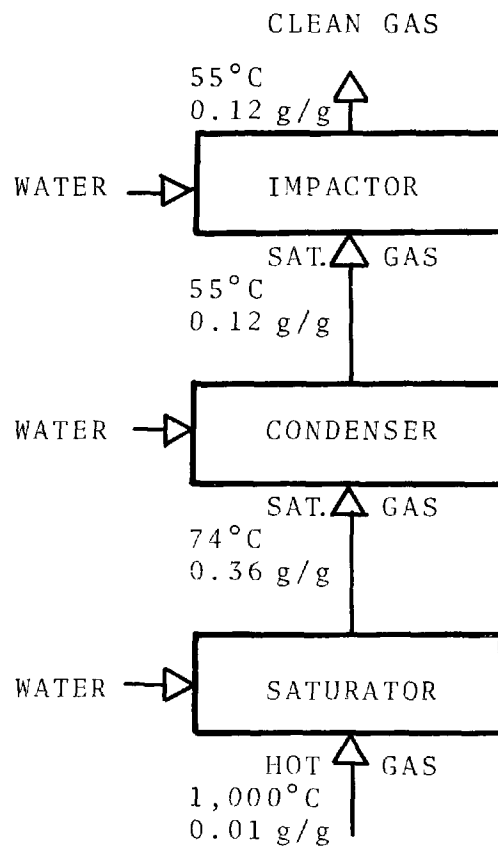


Figure 61. Generalized F/C scrubber system.

unit or can be part of the scrubber as in the pilot plant of the present study.

The efficiency of heat and mass transfer is high for mobile bed scrubbers; most of the condensation occurs in the first stage. In subsequent stages, the gas is scrubbed by inertial impaction and there will be a minor amount of additional condensation.

#### Diffusiophoretic Deposition

Particle deposition by diffusiophoresis was described by the following equation (Calvert et al. 1973, 1975, 1976):

$$u_{pD} = \frac{\sqrt{M_1} D_G}{\left[ y \sqrt{M_1} + (1-y) \sqrt{M_2} \right] (1-y)} \left( \frac{dy}{dr} \right), \text{ cm/s} \quad (69)$$

or,

$$u_{pD} = C_1 D_G \left( \frac{1}{1-y} \right) \frac{dy}{dr} \quad (70)$$

where  $D_G$  = diffusivity of water vapor in carrier gas,  $\text{cm}^2/\text{s}$   
 $M_1$  = molecular weight of water,  $\text{g/mol}$   
 $M_2$  = molecular weight of nontransferring gas,  $\text{g/mol}$   
 $y$  = mole fraction water vapor, dimensionless  
 $r$  = distance in the direction of diffusion,  $\text{cm}$

The molecular weight and composition function represented by " $C_1$ " described the effect of molecular weight gradient on the deposition velocity corresponding to the net motion of the gas due to diffusion (the "sweep velocity"). For water mole fraction in air ranging from 0.1 to 0.5, " $C_1$ " varies from 0.8 to 0.88. Calvert and Gandhi (1977) used a rough average of 0.85 for " $C_1$ " for computing " $u_{pD}$ " and consequent particle collection efficiency by integrating over the period of condensation.

Whitmore (1976) concludes that the fraction of particles removed from the gas by diffusiophoresis is equal to either the mass fraction or the mole fraction condensing, depending on what theory is used for deposition velocity. In other words, it is not necessary to follow the detailed course of the condensation process, computing instantaneous values of deposition velocity, and integrating over the entire time to compute the fraction of particles collected. One can simply observe that if some fraction of the gas is transferred to the liquid phase it will carry along its load of suspended particles.

Calvert and Gandhi (1977) have used Whitmore's general concept but with two modifications. First, one can see from equation (69) that Whitmore's theory would be comparable to assuming that the particles move with the same velocity as the gas phase. Calvert and Gandhi have chosen to retain the correction for molecular weight gradient, which means that they will compute the particle collection efficiency as 85% of the volume fraction of gas condensing on the cold surface.

The second modification concerns how to compute the proper value of the volume fraction of gas condensing. The problem is that not all of the condensate goes to the heat transfer surface; some of it goes to the suspended particles. The fraction of the condensate which causes particle growth depends on several factors and ranged from about 0.1 to 0.4 of the total condensate for the range of parameters they explored.

If one is concerned only with diffusiophoretic deposition, the particle collection efficiency would, therefore, be 60% to 90% of that computed without accounting for condensation on particles. In the case of a scrubber which also employs inertial impaction, the particles would be agglomerated to some extent by the diffusional sweep, so they would have higher mass and be easier to collect.



Rather than going into a detailed model of this phenomenon one could use either of two simplifying assumptions:

1. Assume that the condensation on particles causes no agglomeration.
2. Assume that the condensation on particles causes agglomeration and that the inertial impaction efficiency is sufficiently high enough that all of the particles swept to other particles will be collected by impaction.

The first assumption will lead to too low an efficiency and the second to too high an efficiency. However, the maximum difference between the two for a representative case of 25% of the volume condensing and 25% of that going to the particles would be 5.3% (i.e.,  $0.25 \times 0.85 \times 0.25 \times 100$ ). This is a relatively small effect compared to the other uncertainties.

#### Particle Growth

Particle growth is dependent on how well the particles can compete with the cold surface for the condensing water. There are several transport processes at work simultaneously in the condenser section of an F/C scrubber:

1. Heat transfer
  - a. from the gas to the cold surface
  - b. from the particles to the gas
2. Mass transfer
  - a. from the gas to the cold surface
  - b. from the gas to the particles

A mathematical model which accounted for these transport processes in addition to particle deposition has been described in EPA reports by Calvert et al. (1973, 1975, 1976). The portions of that model relating to particle deposition were deleted to provide a model which would describe particle growth in the absence of deposition. The basic relationships involved are as follows:

The rate of change of particle radius is given by a mass balance,

$$\frac{dr_p}{dt} = \frac{k'_{pG} (p_G - p_{pi})}{\rho_M}, \text{ cm/s} \quad (71)$$

where  $k'_{pG} = \frac{2 D_G P}{RT_G d_p p_{BM}}$  = particle to gas mass transfer coefficient, gmol/cm<sup>2</sup>-s-atm (72)

$p_G$  = water vapor partial pressure in bulk of gas, atm

$p_{BM}$  = mean partial pressure to nontransferring gas, atm

$r_p$  = particle radius, cm

$T_G$  = gas bulk temperature, °K

$\rho_M$  = molar density of water, gmol/cm<sup>3</sup>

$p_{pi}$  = water vapor partial pressure at vapor-liquid interface, atm

Particle temperature can be computed from an energy balance:

$$h_{pG} (T_{pi} - T_G) + \left( \frac{\rho_p C_{pp} r_p}{3} \right) \frac{dT_{pi}}{dt} = k'_{pG} L_M (p_G - p_{pi}) \quad (73)$$

where  $h_{pG} = \frac{2k}{d_p}$  = particle to gas heat transfer coefficient, cal/cm<sup>2</sup>-s-°K (74)

$T_G$  = gas bulk temperature, °K

$T_{pi}$  = gas particle interface temperature, °K

$C_{pp}$  = heat capacity of particle, cal/g-°K

$k$  = thermal conductivity of gas, cal/cm<sup>2</sup>-s-°K/cm

$L_M$  = latent heat of vaporization for water, cal/gmol

$t$  = time, s

$\rho_p$  = particle density, g/cm<sup>3</sup>

$r_p$  = particle radius

$k'_{pG}$  = particle to gas mass transfer coefficient, gmol/cm<sup>2</sup>-s-atm

$p_G$  = water vapor partial pressure in bulk of gas, atm

$p_{pi}$  = water vapor partial pressure at vapor-liquid interface, atm

The overall energy balance for the gas-liquid interface is given by:

$$k'_G a_t L_M (p_G - p_{Li}) A_p dz = h_L a_t (T_{Li} - T_L) A_p dz + h_G a_t (T_{Li} - T_G) A_p dz \quad (75)$$

where

$k'_G$  = mass transfer coefficient, gas to liquid,  
gmol/cm<sup>2</sup>-s-atm

$a_t$  = interfacial area for transfer volume of scrubber,  
cm<sup>2</sup>/cm<sup>3</sup>

$A_p$  = cross-sectional area of scrubber, cm<sup>2</sup>

$h_G$  = heat transfer coefficient, gas to liquid,  
cal/cm<sup>2</sup>-s-°K

$T_L$  = temperature of liquid bulk, °K

The equations given above can be used along with enthalpy and material balances for the total system of gas, liquid, and suspended particles to form a mathematical model for condensation and growth.

#### Prediction of Condensation

Calvert and Gandhi (1977) solved the equations through a finite difference method on an electronic computer for sieve plates under various situations to predict the fraction of the total condensate which goes to the particles (this fraction defined as " $f_p$ "). It was found that " $f_p$ " depends heavily on " $n_p$ " and liquid phase heat transfer coefficient. It decreases significantly with " $n_p$ " below about 10<sup>6</sup> particles/cm<sup>3</sup> and does not change much for particle number concentration greater than 10<sup>7</sup>/cm<sup>3</sup>.

" $f_p$ " varies between 0.1 and 0.4. Calvert and Gandhi (1977) used an average of 0.25 for the sieve plate scrubbers. The fraction of the total condensate which goes to the particles was experimentally measured to be about 0.15 for the mobile bed

scrubber at  $q' \approx 0.25$  and for water and air conditions used in the present work. This value can be used to compute the amount of particle growth that will result from a given condensation ratio. If the inlet particle size distribution is known, one can predict the overall penetration that will be achieved in the mobile bed scrubber.

#### Performance Prediction Method

Case 1. Condensation and particle growth occurred within the mobile bed scrubber.

The sequence of steps to be followed in predicting the performance of a mobile bed F/C scrubber system is as follows:

1. Determine the initial particle size distribution at the scrubber inlet.
2. Compute particle penetration due to inertial impaction in the first stage. Use the inlet particle size distribution and the penetration relationship for the mobile bed given in equation (68). In using this equation, " $\Delta P_w$ " should be the overall pressure drop of the scrubber, not the pressure drop for one stage. The penetration for stage 1 is

$$Pt_{d_1} = Pt_d^{1/n} \quad (76)$$

where  $Pt_{d_1}$  = particle penetration for particle diameter " $d_p$ " in stage 1, fraction  
 $Pt_d$  = overall penetration for particle diameter " $d_p$ ", fraction  
 $n$  = number of stages, -

3. Calculate the condensation ratio corresponding to the scrubber operating conditions, from this compute " $f_v$ ", the volume fraction of gas condensing,

and then calculate the penetration due to diffusio-phoresis ( $Pt_c$ ) according to equation (77) for a conservative estimate or equation (78) for an optimistic estimate:

$$1 - Pt_c = 0.85 (f_v) (1 - f_p) \quad (77)$$

$$1 - Pt_c = 0.85 f_v \quad (78)$$

where:

$$f_v = \frac{\text{moles H}_2\text{O condensed}}{\text{total moles originally in vapor}} = \frac{q'}{H_1 + \frac{18}{29}}$$

where:

$H_1$  = original humidity ratio, g/g

$q'$  = condensation ratio, g/g

The diffusio-phoretic penetration applies equally to all particle sizes so it will not change the size distribution but will decrease the particle concentration.

4. Determine the particle size distribution leaving the first stage from the values of " $q'$ " and " $f_p$ " (by equation 31).
5. Compute the particle penetration for the remaining stages of the scrubber. Use the grown particle size distribution leaving stage 1.

$$Pt_{2-n} = Pt_d^{n-1/n} \quad (79)$$

6. The total overall fractional penetration for the mobile bed F/C scrubber, " $Pt_d$ ", will be the product of the following:

- a) "Pt<sub>1</sub>"
- b) "Pt<sub>c</sub>"
- c) "Pt<sub>2-n</sub>"

i.e.  $Pt_d = Pt_1 \times Pt_c \times Pt_{2-n}$

The above steps can be combined to obtain the following equation:

$$Pt_d = \left[ 1 - \frac{0.85 q' (1 - f_p)}{0.62 + H_1} \right] \left[ \exp \left( -9.84 \times 10^{-4} \Delta P_w^{1.96} d_{pa}^{1.6} \right) \right]^{1/n} \left[ \exp \left( -9.84 \times 10^{-4} \Delta P_w^{1.96} d_{pa_2}^{1.6} \right) \right]^{(n-1)/n} \quad (80)$$

where:

$$d_{pa_2} = d_{p_2} \left[ \left( 1 + \frac{0.165}{d_{p_2}} \right) \rho_{p_2} \right]^{0.5} \quad (81)$$

$$d_{p_2} = \left[ (d_{p_1} \times 10^{-4})^3 \frac{\rho_{p_1}}{\rho_{p_2}} + \frac{6 f_p q'}{772 \pi n_p \rho_{p_2}} \right]^{1/3} \times 10^{-4} \quad (82a)$$

$$\rho_{p_2} = \frac{f_p q' + 3.78 \times 10^{-10} n_p d_{p_1}^3 \rho_{p_1}^2}{f_p q' + 3.78 \times 10^{-10} n_p d_{p_1}^3 \rho_{p_1}} \quad (82b)$$

$$d_{p_1} = \frac{0.165 + (0.0272 + f_p^4 d_{pa} / \rho_{p_1})^{0.5}}{2} \quad (82c)$$

$d_{pa2}$  = grown aerodynamic particle diameter,  $\mu\text{m}$   
 $d_{p2}$  = grown physical particle diameter,  $\mu\text{m}$   
 $d_{pa}$  = original aerodynamic particle diameter,  $\mu\text{m}$   
 $f_p$  = fraction of water vapor condensing on particles, fraction  
 $H_1$  = humidity in the saturated inlet gas, g/g  
 $n_p$  = particle number concentration,  $\#/\text{cm}^3$   
 $Pt_d$  = particle penetration for diameter  $d_{pa}$ , fraction  
 $q'$  = condensation ratio, g/g  
 $\Delta P_w$  = overall pressure drop across mobile bed scrubber, cm W.C.  
 $\rho_{p1}$  = particle density,  $\text{g}/\text{cm}^3$   
 $n$  = number of mobile bed stages, --  
 $d_{p1}$  = initial physical particle diameter,  $\mu\text{m}$   
 $\rho_{p2}$  = density of grown particle

Case 2. Condensation and particle growth occurred before the mobile bed scrubber.

The sequence of steps to be followed for this case is similar to case 1.

1. Determine the initial particle size distribution at the condenser inlet.
2. Calculate the condensation ratio corresponding to the condenser operating conditions.
3. Calculate the penetration due to diffusiophoresis according to equation (77). Collection by other mechanisms may be neglected.
4. Calculate the grown particle size distribution at the condenser outlet according to equations (81) and (82).
5. Compute the particle penetration for the mobile bed scrubber. Use the grown particle size distribution leaving the condenser.
6. Calculate the total overall fractional penetration for the mobile bed F/C scrubber system.

The preceding six steps are equivalent to the following equation:

$$Pt_d = \left[ 1 - \frac{0.85 q' (1 - f_p)}{0.62 + H_1} \right] \left[ \exp (-9.84 \times 10^{-4} \Delta P_w^{1.96} d_{pa_2}^{1.6}) \right] \quad (83)$$

where " $d_{pa_2}$ " is given by equation (81), and

$Pt_d$  = particle penetration for diameter  $d_{pa}$ , fraction

$q'$  = condensation ratio, g/g

$f_p$  = fraction of water vapor condensing on particles,

--

$H_1$  = humidity of the saturated gas at condenser inlet,  
g/g

$\Delta P_w$  = overall scrubber pressure drop, cm W.C.

### Overall Penetration

In order to determine the overall penetration of the system  $\overline{Pt}$ , the penetration curve has to be integrated over the entire range of the initial size distribution curve. This can be accomplished either mathematically on a programmable calculator or graphically by plotting penetration versus percent mass under-size over the initial size range. Then the area under the curve represents the total penetration,  $\overline{Pt}$ , of the system. The total efficiency of the system can then be determined as:

$$E = 1 - \overline{Pt}$$

### Sample Calculation

Prediction based on the model described above was made for case 1 and for the following conditions.

1. Three stage mobile bed with plastic net support. Packing diameter = 3.8 cm. Bed depth = 23 cm.
2.  $u_G = 2.1$  cm/s
3.  $Q_L/Q_G = 11.2$  l/m<sup>3</sup>



4. Particle size distribution at the scrubber inlet:  $d_{pg} = 1.6 \mu\text{m}$ ;  $\sigma_g = 3.3$
5.  $q' = 0.24 \text{ g/g}$
6.  $n_p = 5 \times 10^7 / \text{cm}^3$
7.  $T_G = 70^\circ\text{C}$  (i.e.  $H_1 = 0.278 \text{ g/g}$ )

Calculation Procedure -

Step 1: Particle size distribution at the scrubber inlet was given.

Step 2: From equation (66), the pressure drop across the scrubber is 15.3 cm W.C. Therefore, the particle penetration for stage 1 is

$$Pt_1 = [\exp(-0.207 d_{pa_1}^{1.6})]^{1/3} \quad (84)$$

The grade penetration curve calculated from equation (84) for the first stage is shown in Figure 62.

Step 3: The condensation ratio,  $q'$ , is 0.24 g/g. Then " $f_v$ ", the volume fraction of gas condensing is

$$f_v = \frac{q'}{H_1 + \frac{18}{29}} = \frac{0.24}{0.278 + \frac{18}{29}} = 0.267$$

According to equation (77), the penetration due to diffusiophoresis is

$$\begin{aligned} Pt_c &= 1 - 0.85(f_v)(1 - fp) \\ &= 0.81 \end{aligned}$$

Since " $Pt_c$ " is independent on particle size, the grade penetration will be a horizontal line as shown in Figure 62.

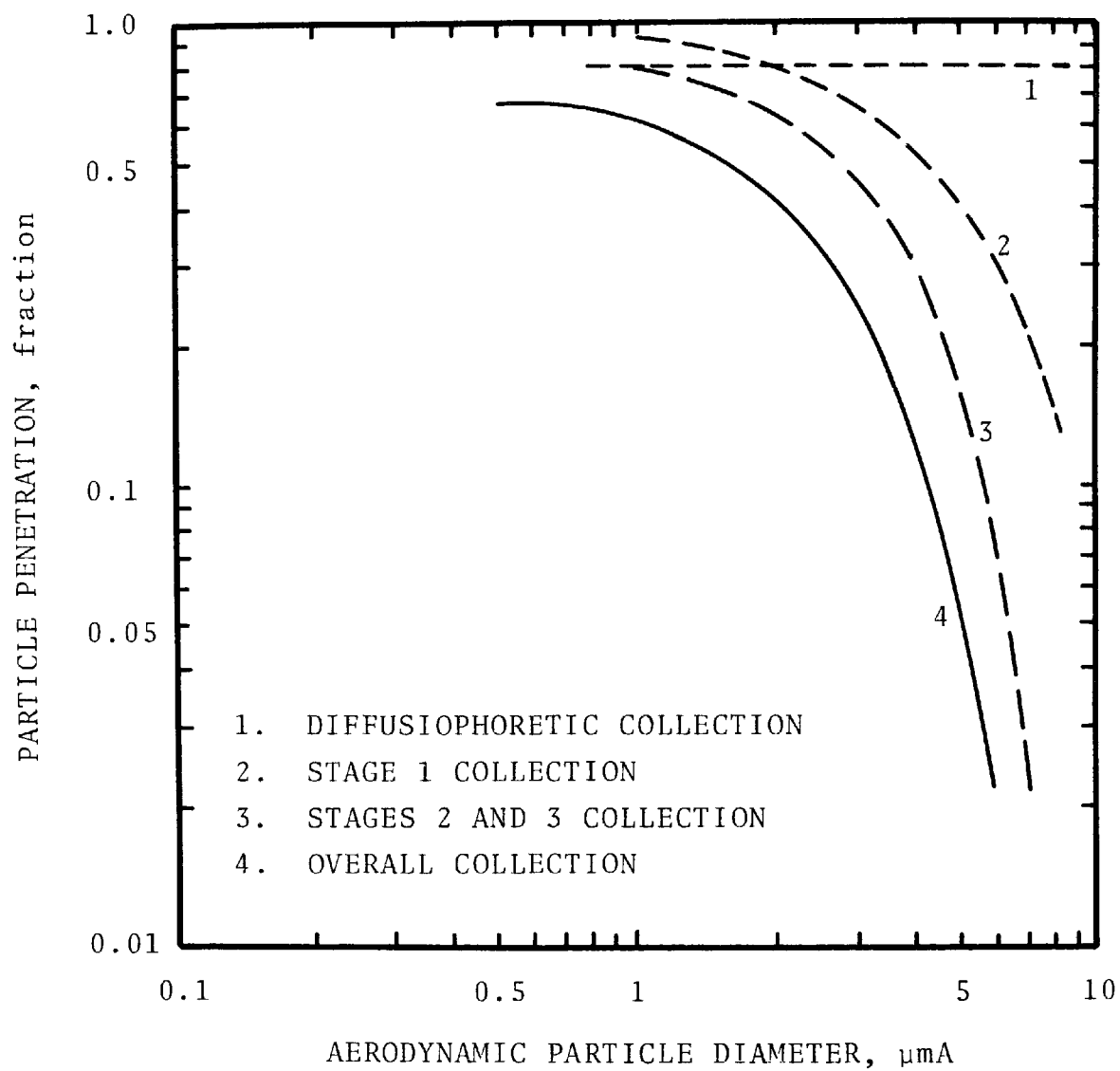


Figure 62. Scrubber penetration for different scrubber stages.

Step 4: The grown aerodynamic particle size is calculated by equations (81) and (82).

The initial and the calculated grown particle size distribution is shown in Figure 63.

Step 5: The combined particle penetration for stages 2 and 3 are calculated from the following equation:

$$Pt_{2-3} = [\exp(-0.207 d_{pa_2}^{1.6})]^{2/3}$$

The calculation result is shown in Figure 62.

Step 6: The overall fractional penetration for the mobile bed F/C scrubber is:

$$Pt_d = 0.81 Pt_1 Pt_{2-3}$$

The overall grade penetration curve for this example is shown in Figure 62.

#### Comparison of Experimental Data with Predictions

The predicted F/C mobile bed performance is compared with measurements in Figures 64 through 66. The agreement is fair. In general, the predicted grade penetration curve crossed the measured curve at around 1  $\mu$ m particle diameter. The model underestimated penetration for submicron particles and overestimated the penetration for particles larger than 1.0  $\mu$ m in diameter.

Figure 67 shows the predicted and measured particle penetration as a function of condensation ratio for a 1  $\mu$ m diameter particle. Figure 68 is a similar plot for the cut diameter. Since the predicted and measured grade penetration curves cross each other at 1.0  $\mu$ m, the prediction should agree with this measurement. This is confirmed by Figure 67. The mathematical model predicted a higher cut diameter than that actually measured.

In the theoretical calculations, " $f_p$ " is assumed to be 0.15 and  $n_p = 3 \times 10^7/\text{cm}^3$  for all runs. In reality, " $f_p$ " and " $n_p$ " vary from run to run. Better agreement would result if one could use more accurate values of " $f_p$ " and " $n_p$ ".

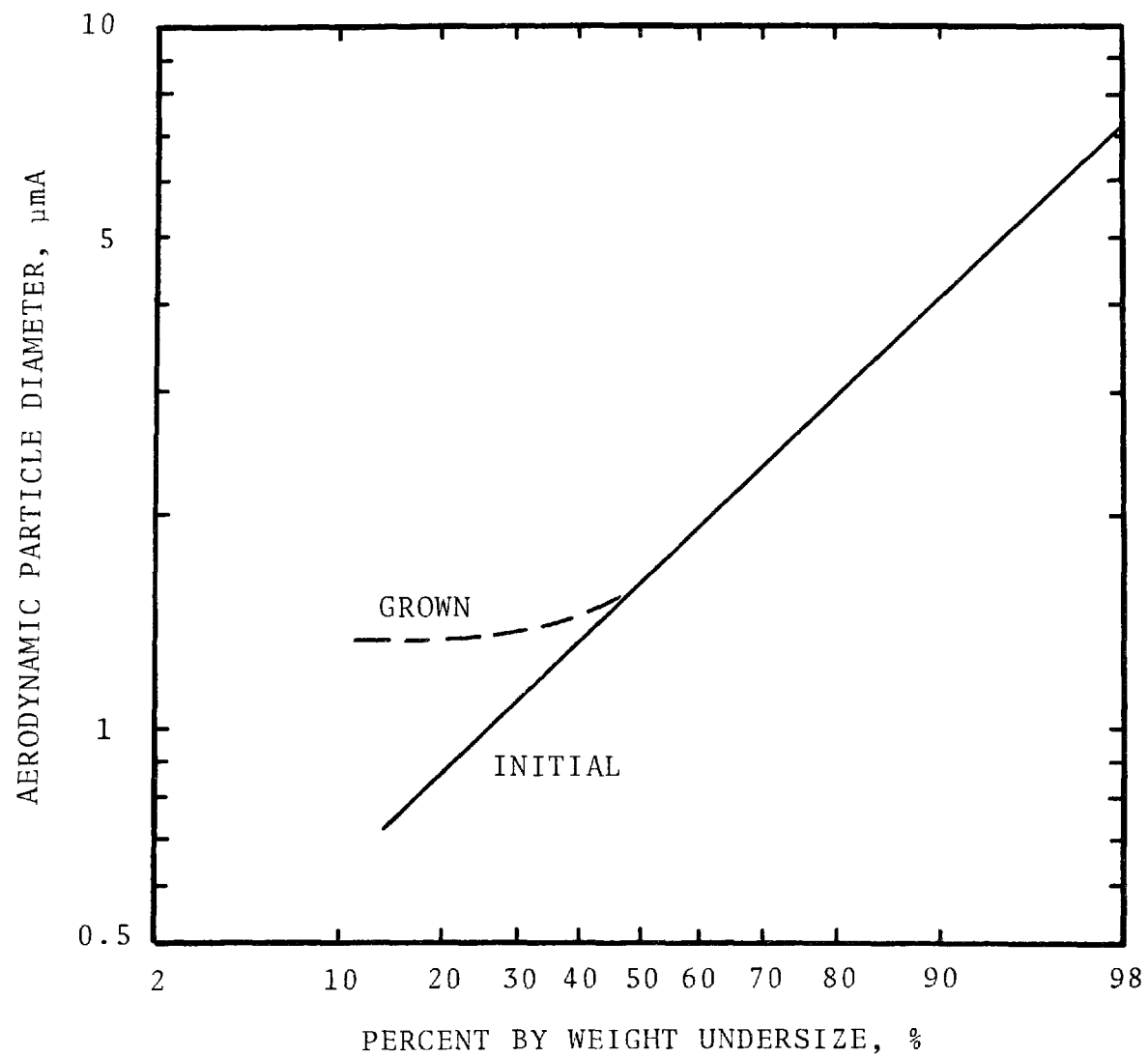


Figure 63. Initial and grown particle size distribution.

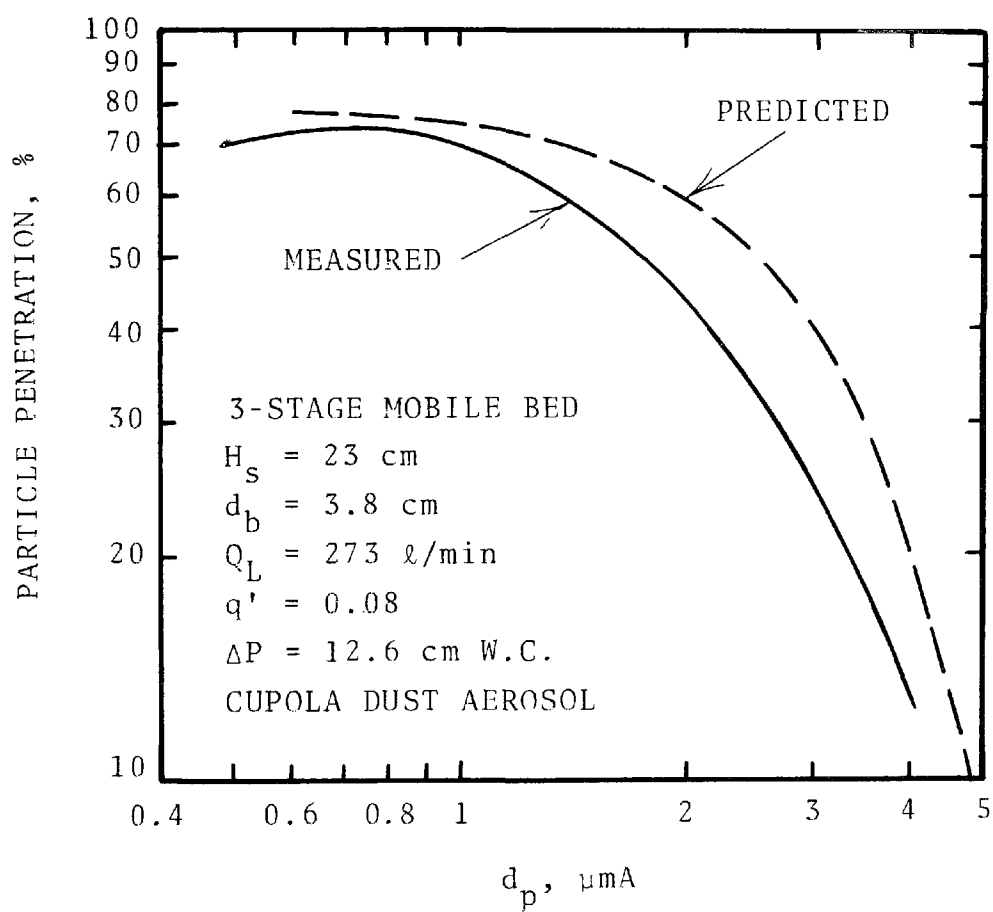


Figure 64. The penetration curve for Runs No. FC-7 and FC-8.

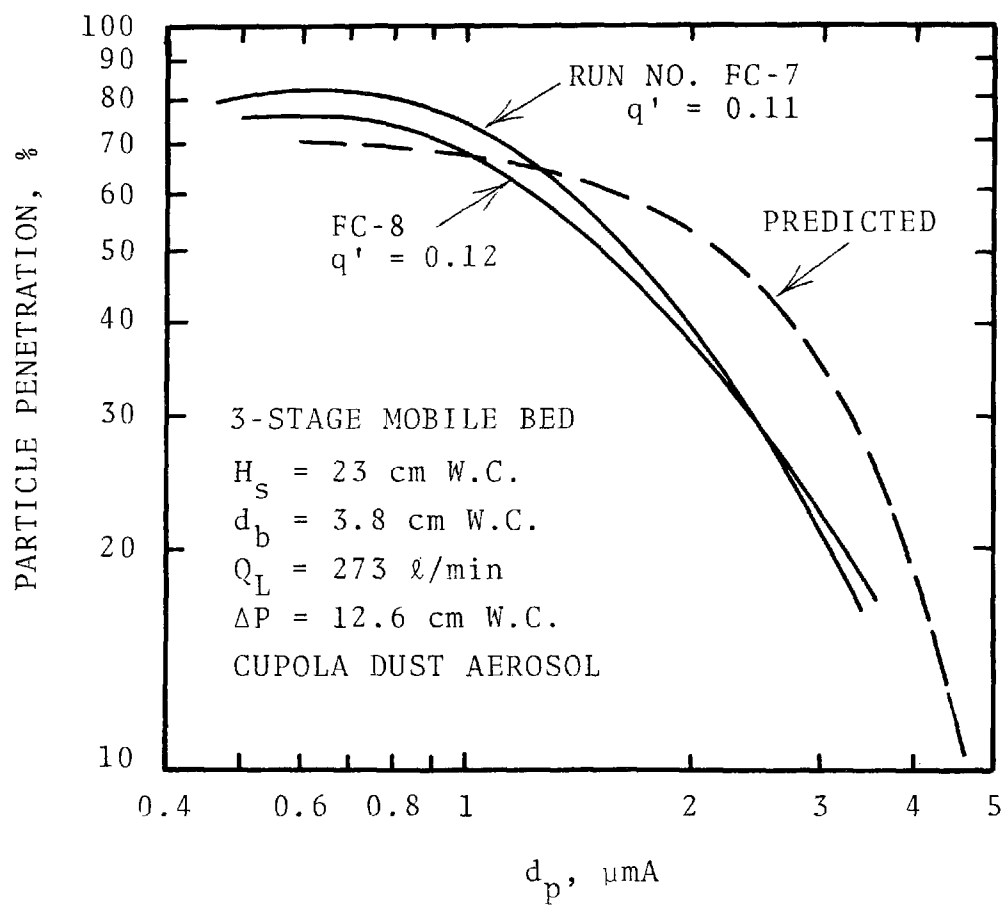


Figure 65. The penetration curve for Runs No. FC-7 and FC-8.

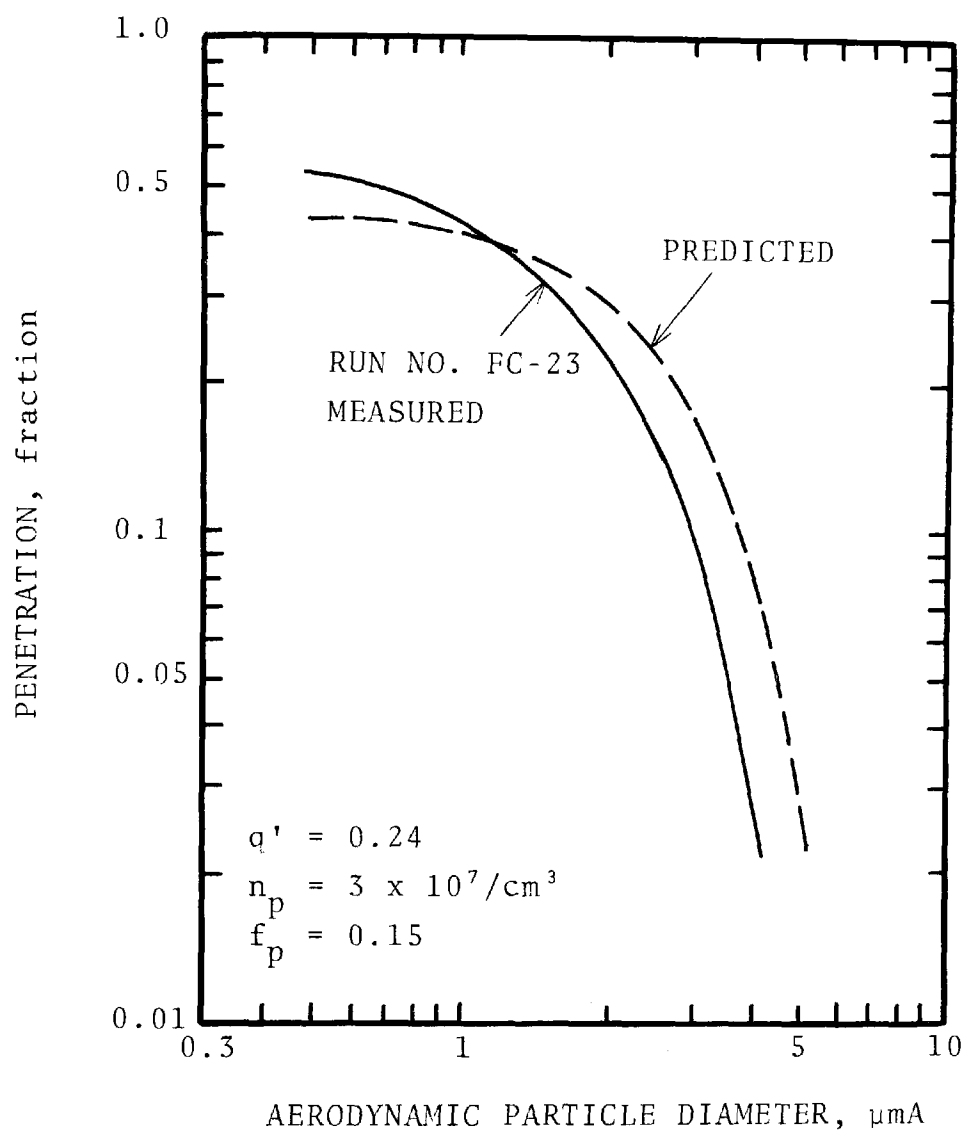


Figure 66. Predicted and measured particle penetration for Run No. FC-23.

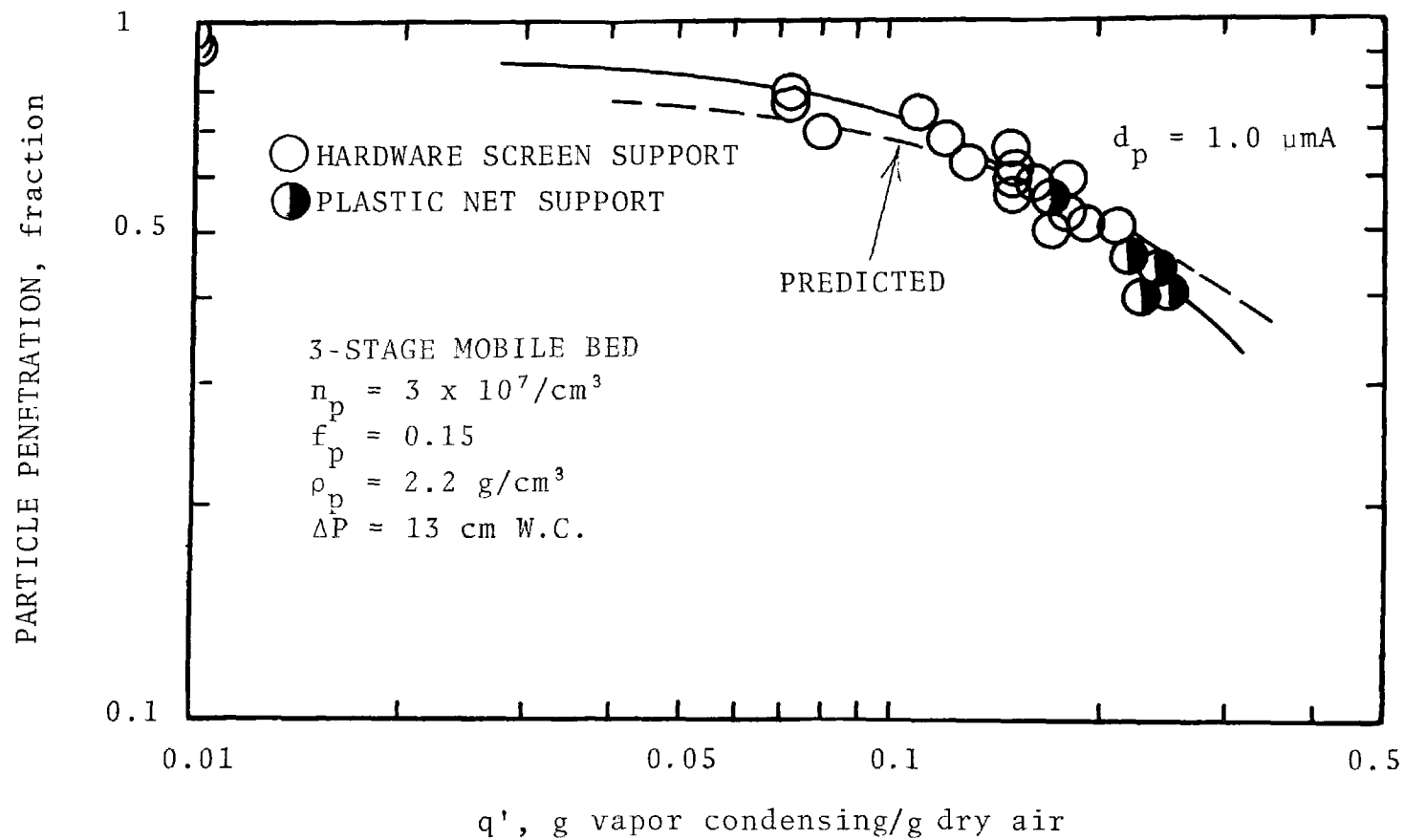


Figure 67. Predicted and measured penetration for  $1.0 \mu m$  diameter particle versus condensation ratio.



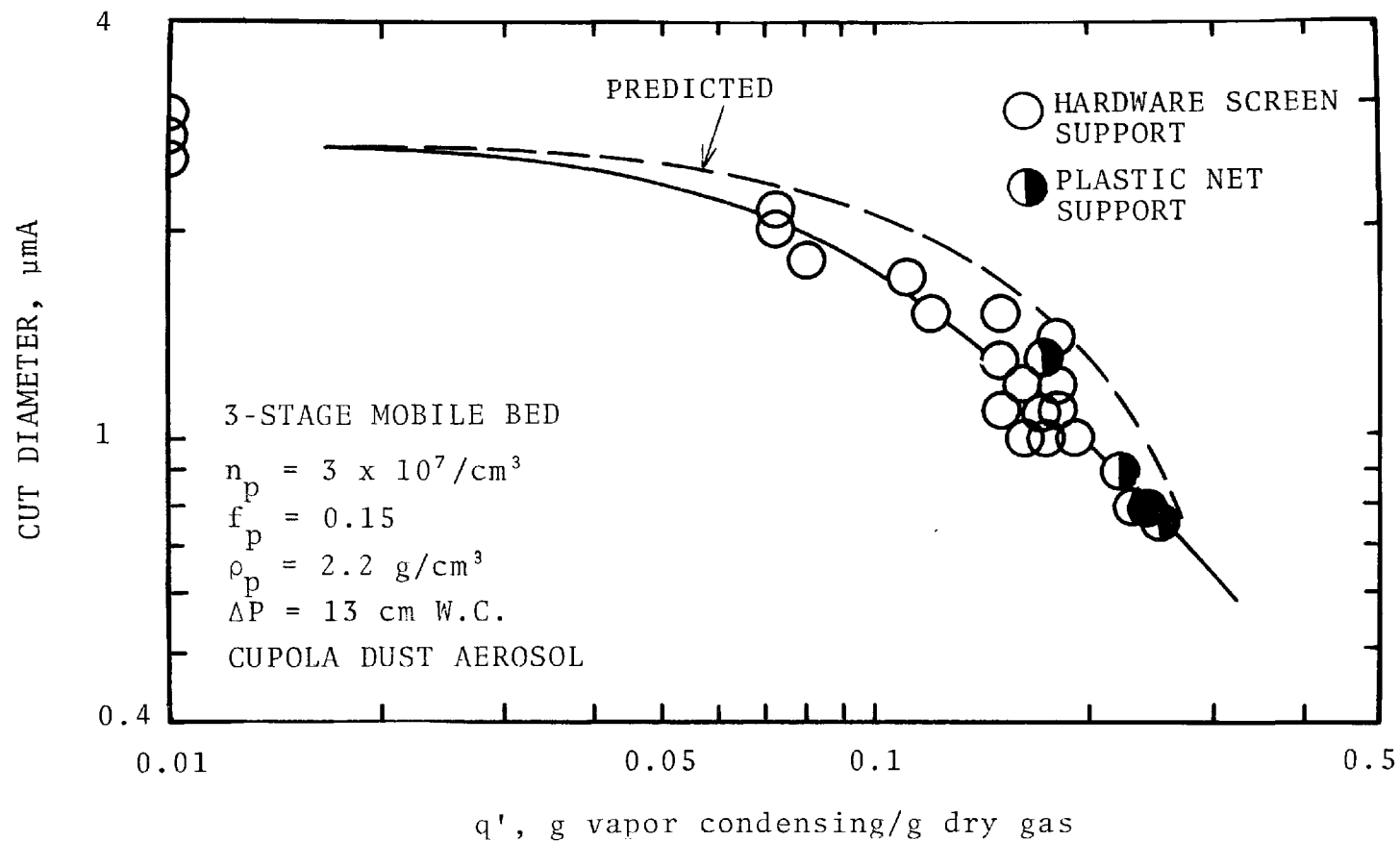


Figure 68. Predicted and measured variation of cut diameter with condensation ratio.

## SECTION 7

### EVALUATION OF MOBILE BED SCRUBBER

#### PARTICLE SCRUBBING

Each scrubber type has a typical cut/power relationship which describes the dependency of scrubber performance on pressure drop. The uniqueness of the cut/power relationship offers a simple method to evaluate the capabilities of different scrubber types. Figure 69 is a plot of the cut/power relationship for several scrubber types.

Of the four scrubber types: gas atomized spray, mobile bed, packed bed, and sieve plate, the gas atomized spray scrubber has the highest performance capability because it can attain the smallest cut diameter with the same pressure drop. At a pressure drop of 20 cm W.C., the gas atomized spray scrubber can achieve a performance cut diameter of  $0.75 \mu\text{m}$ . At the same pressure drop the performance cut diameters are  $1.6 \mu\text{m}$ ,  $1.7 \mu\text{m}$ , and  $1.2 \mu\text{m}$  for the mobile bed, packed bed, and sieve plate with 0.32 cm hole diameter, respectively. Industrial mobile beds usually operate at pressure drops around 30 cm W.C. The performance cut diameter is about  $0.9 \mu\text{m}$  which is better than packed beds and sieve plates but less efficient than venturi scrubbers.

One can observe that at low power input the mobile bed behaves like a sieve plate with very large holes. As power input increases the mobile bed tends toward gas-atomized spray performances. This is in keeping with the visual observation that more atomization occurs as power input increases.

Other than particle collection efficiency, mobile bed scrubbers also have lower gas handling capacity and require more liquid than venturi scrubbers. The superficial gas velocity in a mobile bed ranges from 230 to 400 cm/s. The gas velocity in

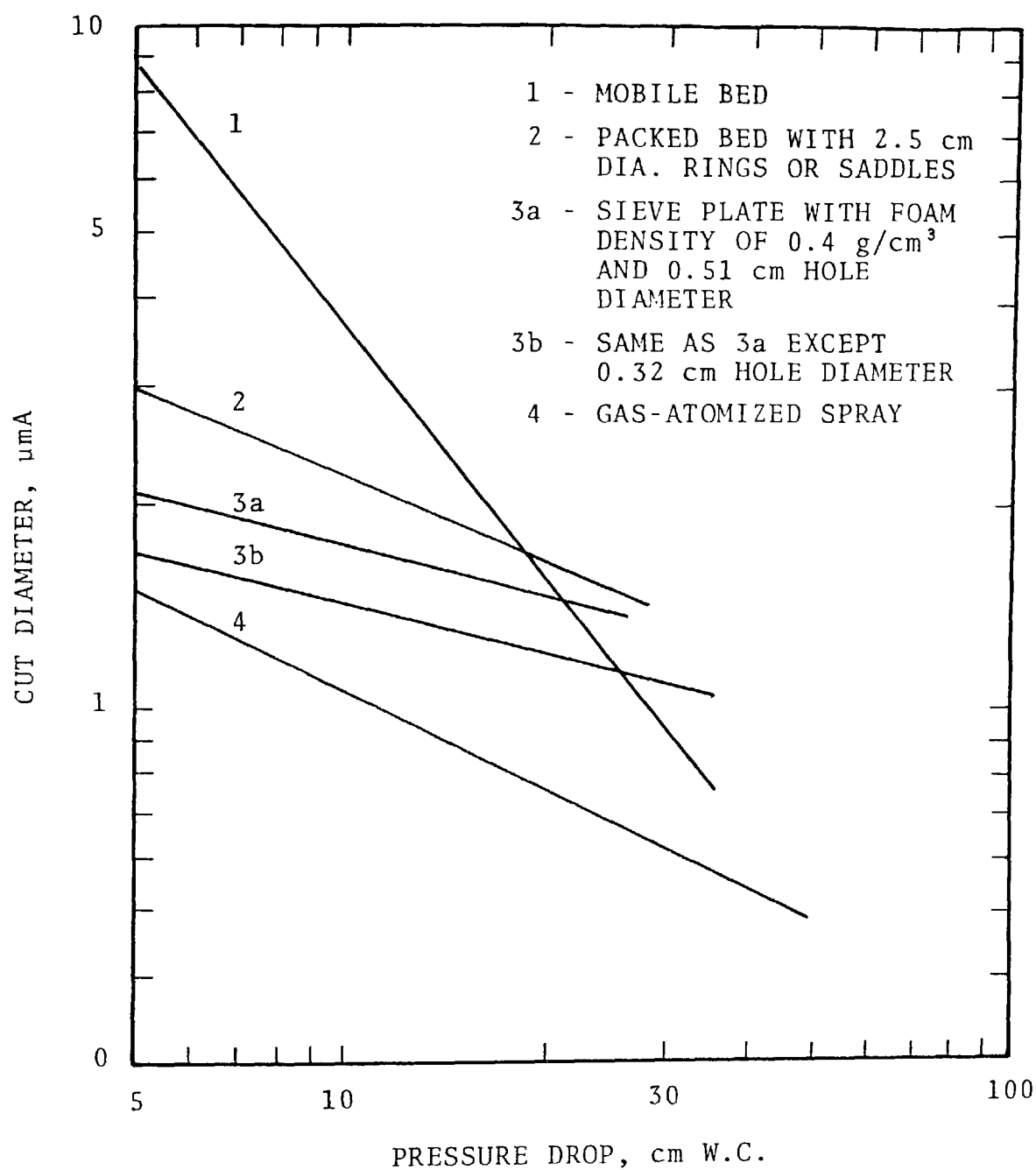


Figure 69. Cut/power relationship for scrubbers.

the venturi throat is usually above 5000 cm/s. Therefore, venturi scrubbers are more compact and the capital investments are lower, although they still need a large entrainment separator.

The liquid/gas ratio in a venturi scrubber is about  $2 \times 10^{-3} \text{ cm}^3/\text{cm}^3$  (15 gal/MCF) which is about three times lower than that in a mobile bed scrubber. This results in a higher cost in liquid handling and moving for mobile bed scrubbers.

A mobile bed scrubber also requires a higher degree of maintenance, especially the packing spheres. Epstein (1975) reported that due to erosion the life of the HDPE (high density polypropylene) spheres was approximately 2,000 hours. Thermoplastic rubber (TPR) spheres were a little better than HDPE spheres. After 500 hours of operation, TPR spheres had lost approximately 2.6% of their original weight and the HDPE spheres from 8-14%. After approximately 2,500 hours of operation, all TPR spheres were dimpled on one side, about 2.4% failed at the seam, and the weight loss average was about 6%. Epstein (1975) estimated that the life of the TPR spheres was about one year.

The mobile bed scrubber does have one advantage over the venturi scrubber. The mobile bed scrubber is capable of high mass transfer and can be used to remove particulate and gaseous pollutants simultaneously.

#### MOBILE BED AS A F/C SCRUBBER

Experimental results presented in the previous sections clearly show that the mobile scrubber can be used as a F/C scrubber. Calvert, et al. (1975) and Calvert and Gandhi (1977) have studied other F/C scrubber configurations - sieve plate scrubber and spray scrubber. The mobile bed F/C scrubber is critically evaluated and compared with the F/C sieve plate scrubber and the F/C spray scrubber in the following sections.

##### Performance Capability

##### Mobile Bed Versus Sieve Plate Scrubber -

As discussed in the last section and revealed by Figure 69, a non-F/C mobile bed scrubber has a higher performance capability

than a non-F/C sieve plate scrubber when the scrubber pressure drop is above 20 cm W.C. When operated in F/C mode, the condensation ratio for the mobile bed scrubber is roughly the same as that for the sieve plate scrubber. It is expected that the extent of particle growth will be about the same in the two scrubber systems. Therefore, as a F/C scrubber, the mobile bed scrubber should also have a higher performance capability than that of a sieve plate scrubber. This is confirmed when comparing the results of the present study with those reported by Calvert et al. (1975) and Calvert and Gandhi (1977).

Calvert et al. (1975) presented results of a laboratory pilot scale evaluation of a multiple plate sieve plate scrubber. They plotted particle penetration against condensation ratio for 0.6  $\mu\text{m}$  and 1.0  $\mu\text{m}$  diameter particles. The solid line in Figure 70 shows their results for the sieve plate scrubber with four plates. The particle number concentration was about  $2 \times 10^8/\text{cm}^3$  and the pressure drop across the four plates ranged from 32 cm W.C. to 39 cm W.C. (average = 35 cm W.C.).

In the present study, the mobile bed F/C scrubber was operated at a pressure drop around 13 cm W.C. Therefore, the results of the present study cannot be directly compared with the data by Calvert et al. In the last section it was shown that the mathematical model can reasonably predict the penetration of 1  $\mu\text{m}$  diameters in a mobile bed F/C scrubber. Predictions by the mathematical model are compared with data by Calvert et al. in Figure 70. As can be seen, a mobile bed F/C scrubber with a pressure drop of about 30 cm W.C. will have the same collection efficiency as a sieve plate F/C scrubber operating at a pressure drop of 35 cm W.C.

Calvert and Gandhi (1977) reported results of a pilot scale demonstration of F/C scrubbing for fine particle control carried out on a secondary metal recovery furnace. The scrubber was a 5-plate sieve plate scrubber. The scrubber performance was reported in terms of grade penetration curves. Figure 71 shows

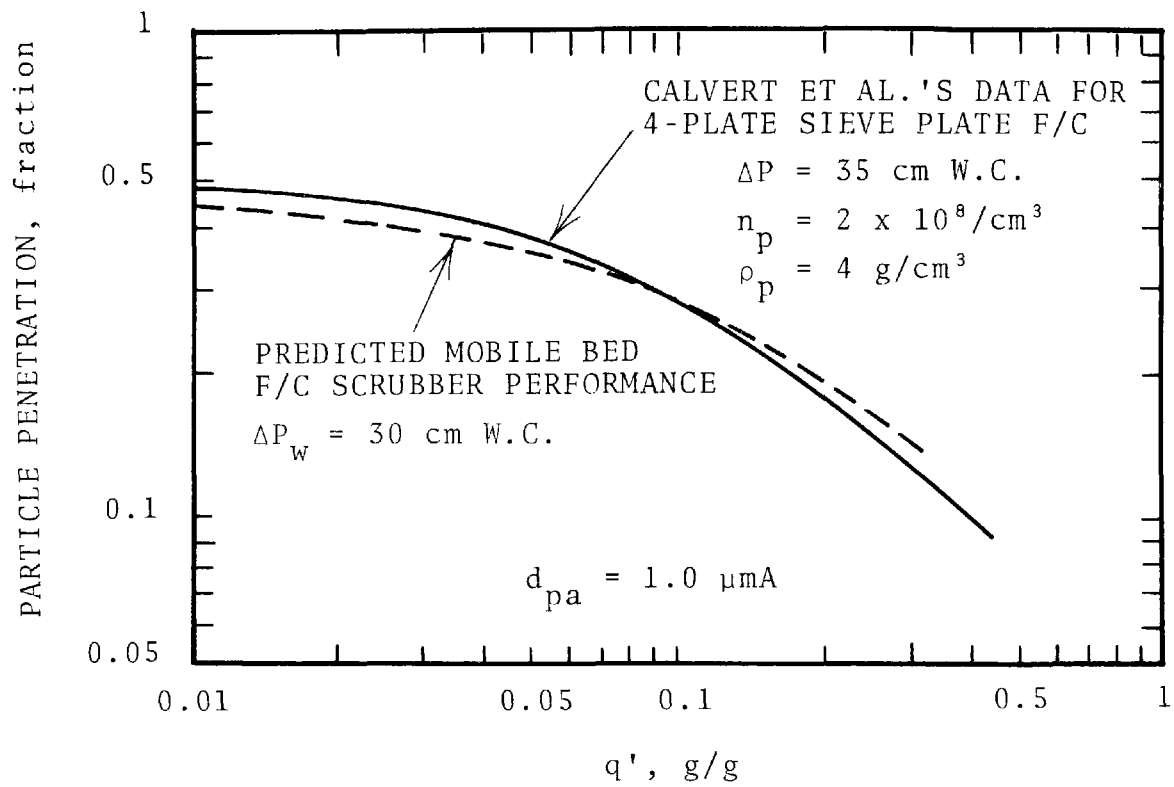


Figure 70. Comparison between mobile F/C and sieve plate F/C scrubber performance.

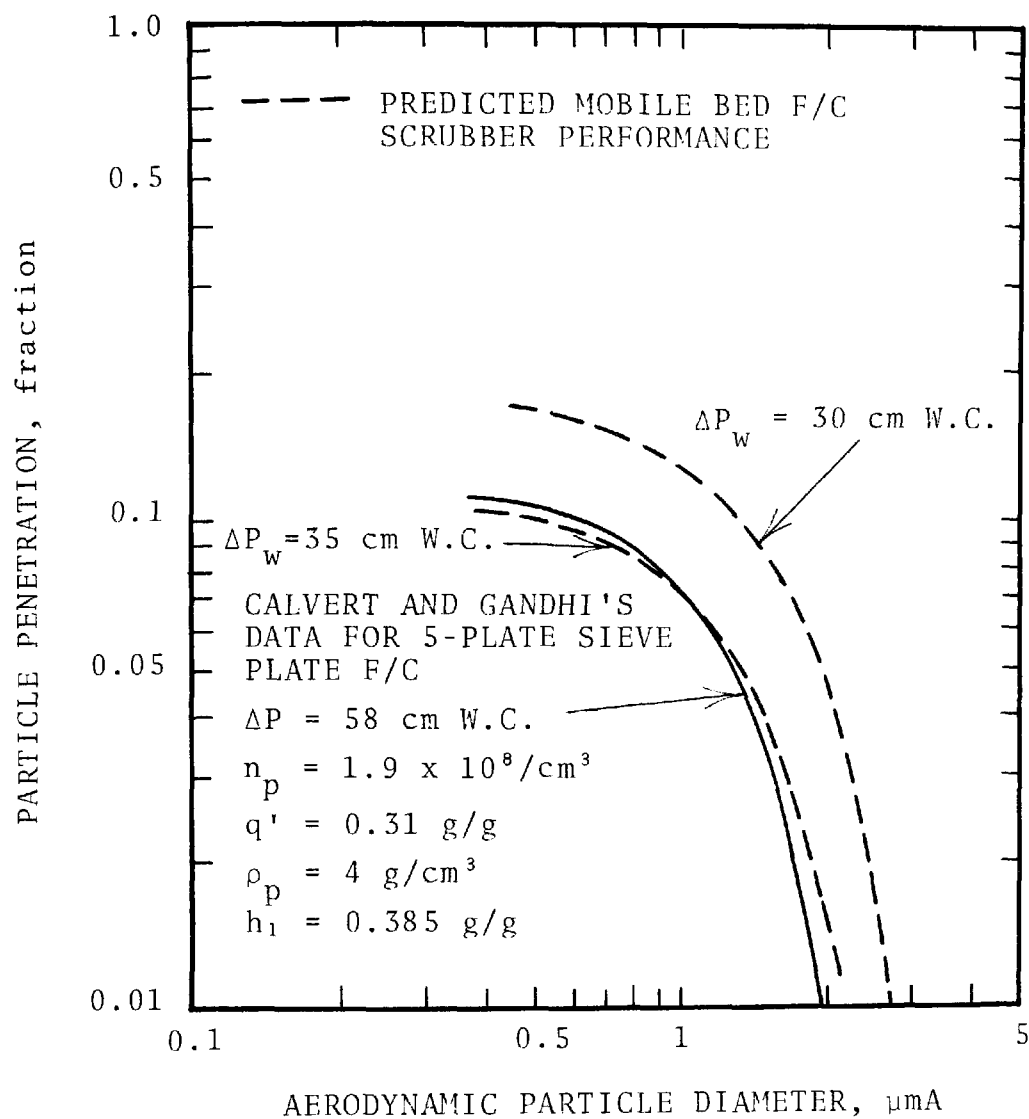


Figure 71. Comparison between mobile bed F/C and sieve plate F/C scrubber performance.

data for one of their runs along with the theoretical prediction for the mobile bed scrubber. As can be seen, the mobile bed F/C scrubber will have the same performance at a pressure drop saving of 23 cm W.C.

#### Mobile Bed Versus Spray Scrubber -

Calvert et al. (1975) also reported data obtained on a horizontal F/C spray scrubber. The water spraying rate was  $8 \text{ l/m}^3$  (60 gal/MCF) and the nozzle pressure was 276 kPa (40 psig). Thus, the energy input to the spray scrubber is equivalent to a gas phase pressure drop of 22.4 cm W.C.

Data by Calvert et al. for a three stage cocurrent spray are shown in Figure 72; a plot of particle penetration versus condensation ratio for  $1 \text{ }\mu\text{m}$  diameter particles. In their experiment, titanium dioxide was used as the test aerosol. The particle number concentration was quite low, approximately  $2 \times 10^6 - 6 \times 10^6/\text{cm}^3$ .

The predicted mobile bed F/C scrubber performance with a scrubber pressure drop of 22.4 cm W.C. and a particle number concentration of  $1 \times 10^7/\text{cm}^3$  and  $5 \times 10^6/\text{cm}^3$  is plotted in Figure 72. The predicted mobile bed performance is slightly better than the measured performance of the spray scrubber.

#### Cost Comparison -

Capital cost - The cost advantage of F/C scrubber systems over the conventional high energy scrubber systems has been demonstrated by Calvert et al. (1975) and Calvert and Gandhi (1977). This comparison will not be repeated here. In the following sections, the relative costs between a sieve plate F/C, a mobile bed F/C, and a spray F/C system are presented.

Although the details of the F/C scrubbing system design will be different for each source, the overall process design, illustrated in Figure 73, will be the same. The major components of the system includes a quencher, a F/C scrubber, and a cooling tower.



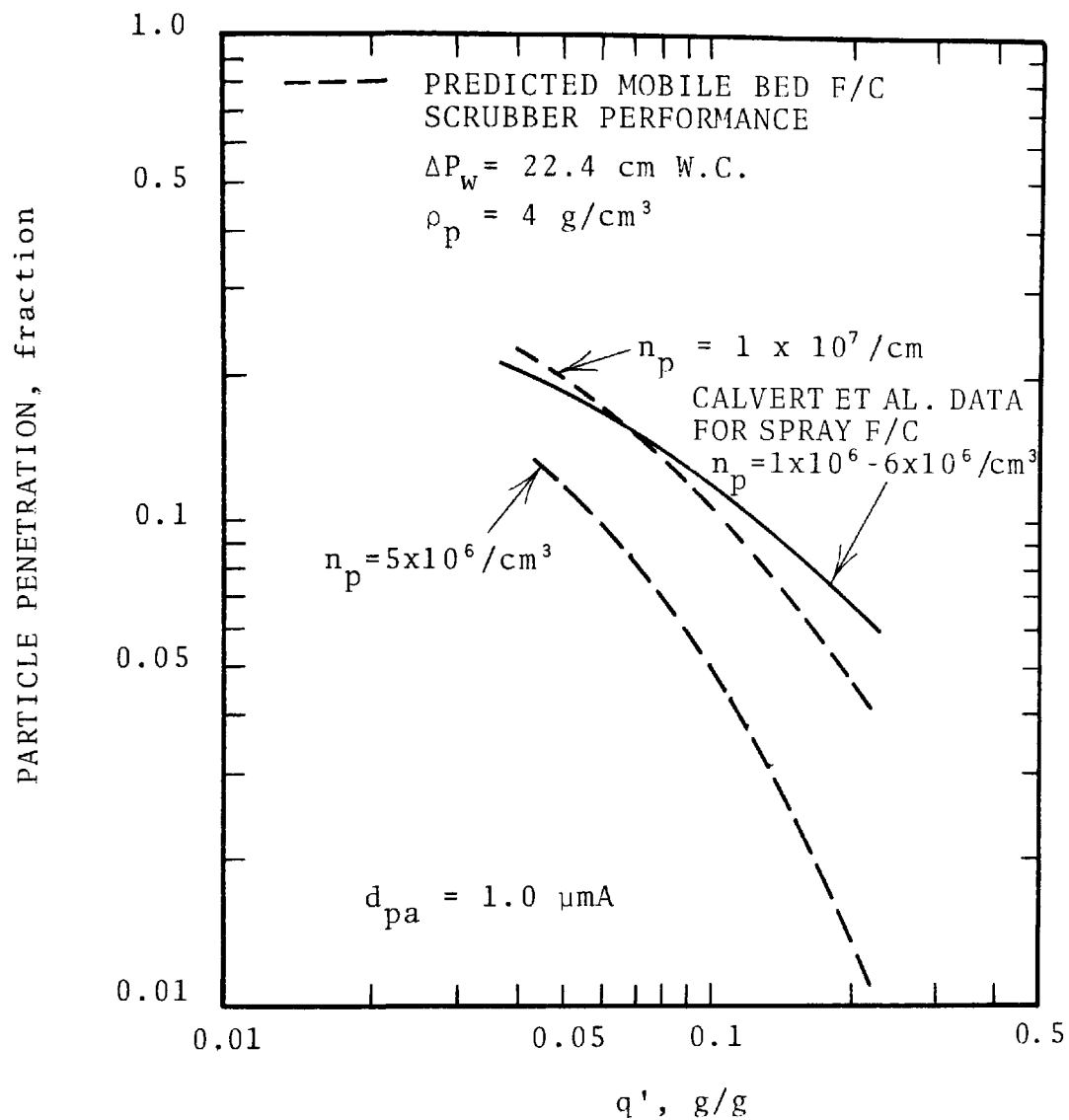


Figure 72. Comparison between mobile bed F/C and spray F/C scrubber performance.

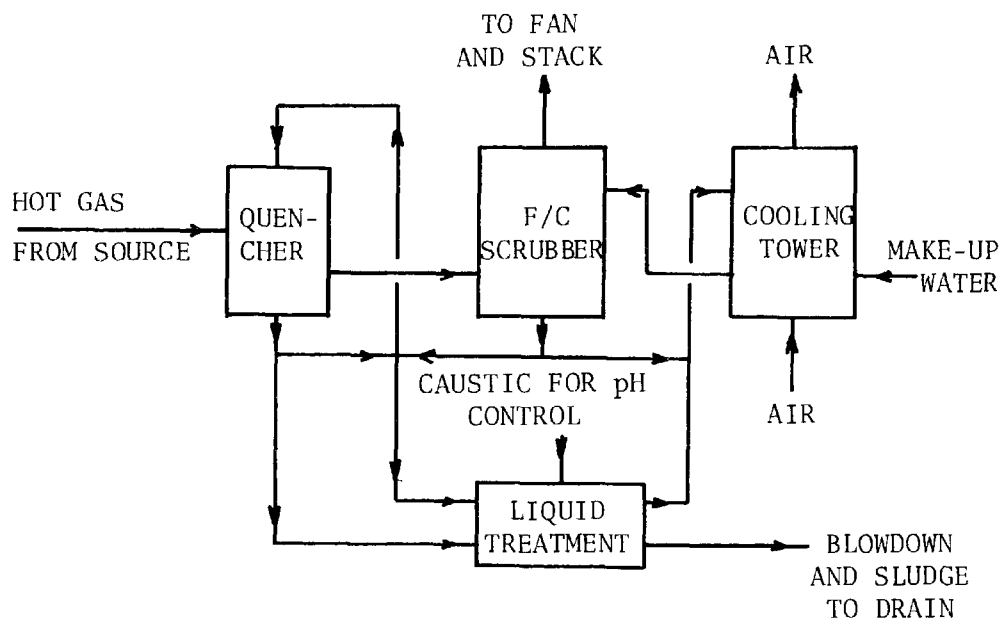


Figure 73. Typical process diagram of a F/C scrubber system.

The costs of the quencher, piping and ductwork, liquid treatment, instrumentation, and process control are roughly the same for the three F/C scrubber systems. The major cost differences between the three F/C scrubber systems are due to the costs of the scrubber itself and the cooling tower. This is because the mobile bed F/C scrubber system has a higher gas handling capacity than the sieve plate and spray scrubber. However, the mobile bed requires more liquid which results in a larger cooling tower.

To analyze the relative costs, the F/C scrubber system is assumed to be for cupola gas cleaning. The volumetric gas flow rate at the scrubber inlet is  $1,300 \text{ Am}^3/\text{min}$  (45,900 ACFM). Operating conditions for the three scrubber systems are as follows:

Sieve plate:	$u_G = 150 \text{ cm/s}$ (5 ft/sec) $Q_L/Q_G = 4 \text{ l/min}$ (30 gal/MCF) $\Delta P = 35 \text{ cm W.C.}$
Spray Scrubber:	$u_G = 110 \text{ cm/s}$ (3.6 ft/sec) $Q_L/Q_G = 8 \text{ l/m}^3$ (60 gal/MCF) $\Delta P = \text{negligible}$ Spray nozzle pressure = 276 kPa (40 psig)
Mobile bed:	$u_G = 340 \text{ cm/s}$ (11 ft/sec) $Q_L/Q_G = 8 \text{ l/min}$ (60 gal/MCF) $\Delta P = 25 \text{ cm W.C.}$

Based on these conditions, the estimated fabrication costs of the three scrubbers are \$25,000 (0.54/CFM), \$20,000 (0.44/CFM), and \$21,000 (0.46/CFM) for the sieve plate scrubber, mobile bed scrubber and the spray scrubber, respectively. The above costs only include material cost and fabrication labor cost.

Costs for design, administration, contingency, etc. are not included since those costs are about the same for the three scrubbers. Since the installed cost is about four times the fabrication cost, the cost of the sieve plate scrubber is approximately \$20,000 more than the mobile bed and spray scrubbers.

The price quotation for the cooling towers from the manufacturer is \$40,000 for the cooling towers in the mobile bed scrubber

system and in the spray scrubber system. It is \$20,000 for the cooling tower in the sieve plate system. The quoted price includes the costs of the cooling tower and fan, but it did not include the costs of the pump and the electrical connections.

Based on this analysis, it appears that the capital cost for the three F/C scrubber systems will be approximately the same.

Operating cost - If the scrubber and the cooling tower can be installed close together, the power requirement to operate the scrubber and cooling tower is 375 hp, 310 hp, and 295 hp for the mobile bed, sieve plate, and spray scrubber, respectively. A fan efficiency of 50% and a pump efficiency of 65% were assumed in the calculation. The mobile bed F/C system has the highest power requirement. The annual operating cost (not including annualized capital charges and depreciation) for the mobile bed F/C system is approximately \$19,000 higher than that of the sieve plate F/C system and approximately \$23,000 higher than the spray F/C scrubber system.

Maintenance - There will be no unusual maintenance problems with the mobile bed and sieve plate scrubber systems even though the mobile bed packing might have to be replaced every year. This is not the case with the spray scrubber. In order to obtain high collection efficiency for particles, the liquid drops should be small in diameter. In the experimental study reported by Calvert et al. (1975), drops as small as 400  $\mu\text{m}$  in diameter were used. Spray nozzles which can produce this drop size requires high pressure. The liquid flow rate per nozzle is small, less than 1 GPM. Therefore, a large quantity of spray nozzles are required. The manpower requirement to maintain the proper operation of the nozzles will be great.

#### POTENTIAL FOR POWER PLANT APPLICATION

Mobile bed scrubbers have been used in coal-fired power plants for the control of  $\text{SO}_x$  emissions as well as particulate

emissions. They are sometimes installed after the electrostatic precipitators as secondary collectors and this practice is expected to become more prevalent. At the precipitator outlet, flue gas temperature is about 138°C (280°F) and contains about 10% by volume of moisture. Typical fly ash size distribution at the ESP outlet is  $d_{pg} = 3.0 \mu m$  and  $\sigma_g = 3.0$  (Figure 74). Particle concentration is about 0.5 g/DNm<sup>3</sup> (0.2 gr/SCF).

A three-stage mobile bed scrubber without F/C effect and operated at a pressure drop of 30 cm W.C. would have a grade penetration curve as that shown in Figure 75. The predicted overall particle penetration will be 17% (overall collection efficiency = 83%) and the predicted outlet particle loading will be 0.085 g/DNm<sup>3</sup> (0.034 gr/SCF).

Assume the flue gas can be saturated by evaporation of water; it will saturate around 54°C (130°F) and the moisture content will be 0.11 g/g. By assuming that the particle number concentration is  $1 \times 10^8 / cm^3$  and the flue gas is cooled down to 43°C (110°F), a three-stage F/C mobile bed scrubber with a pressure drop of 30 cm W.C. will have a grade penetration curve like that shown by the dashed line in Figure 75. The predicted overall penetration will be 12% (88% overall collection efficiency) and the outlet particle loading will be 0.06 g/DNm<sup>3</sup> (0.024 gr/SCF).

For this application, the improvement in collection efficiency of the F/C mobile bed scrubber over the non-F/C mobile bed is small. The main reason is that the condensation ratio attainable in the power plant is too small (~0.056 g/g). If a large quantity of waste steam is available, the condensation ratio may be increased by injecting the steam into the gas. Steam injection causes an extremely high saturation ratio in the vicinity of the injection nozzle and this enhances the nucleation of condensation and particle growth. However, even though waste steam may be available, the mobile bed scrubber might not be a good choice for a F/C scrubber since the mobile bed is not an efficient particle scrubber. A better choice could be the combination of spray quencher and venturi scrubbers. The

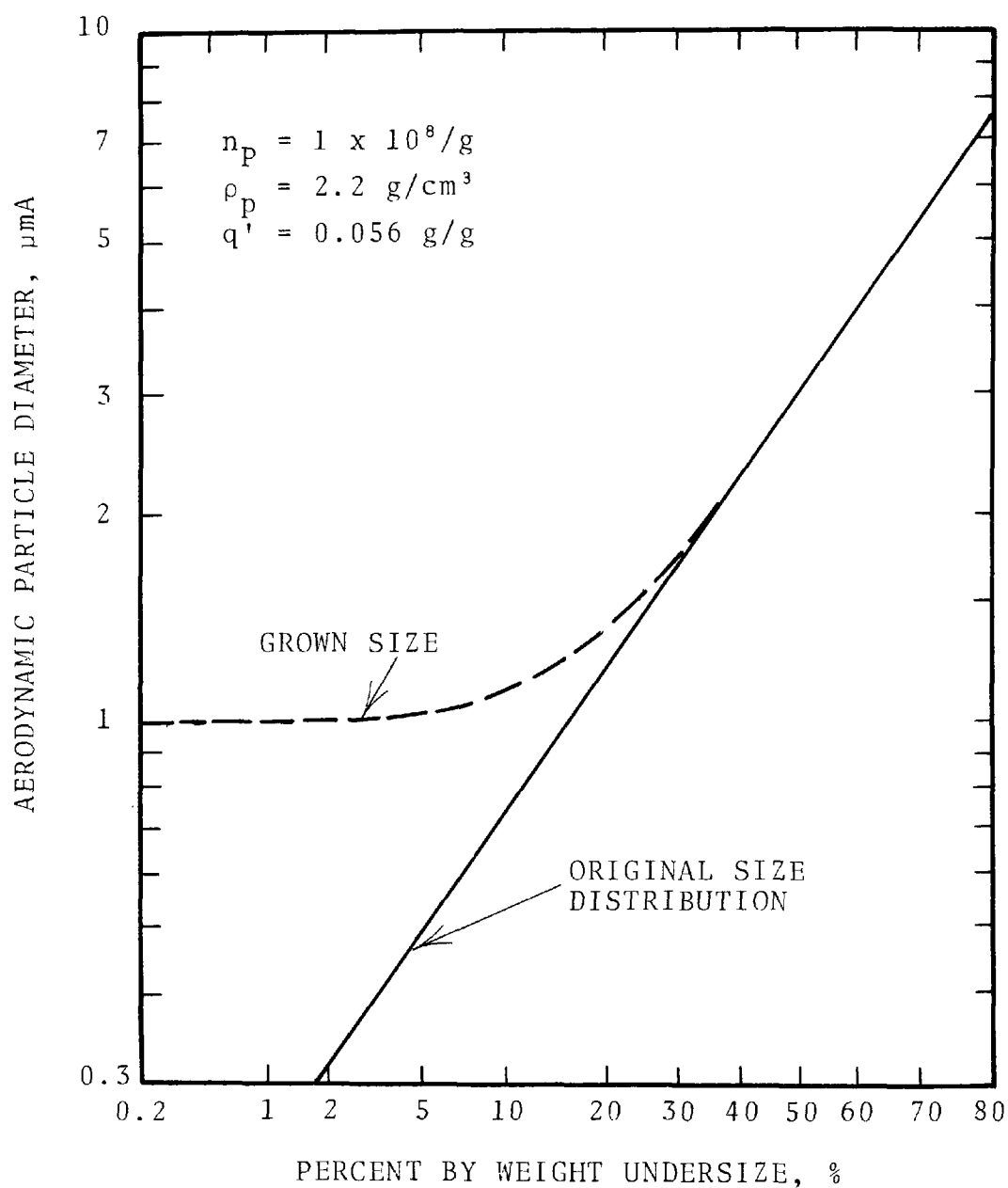


Figure 74. Typical fly ash distribution and grown size distribution.

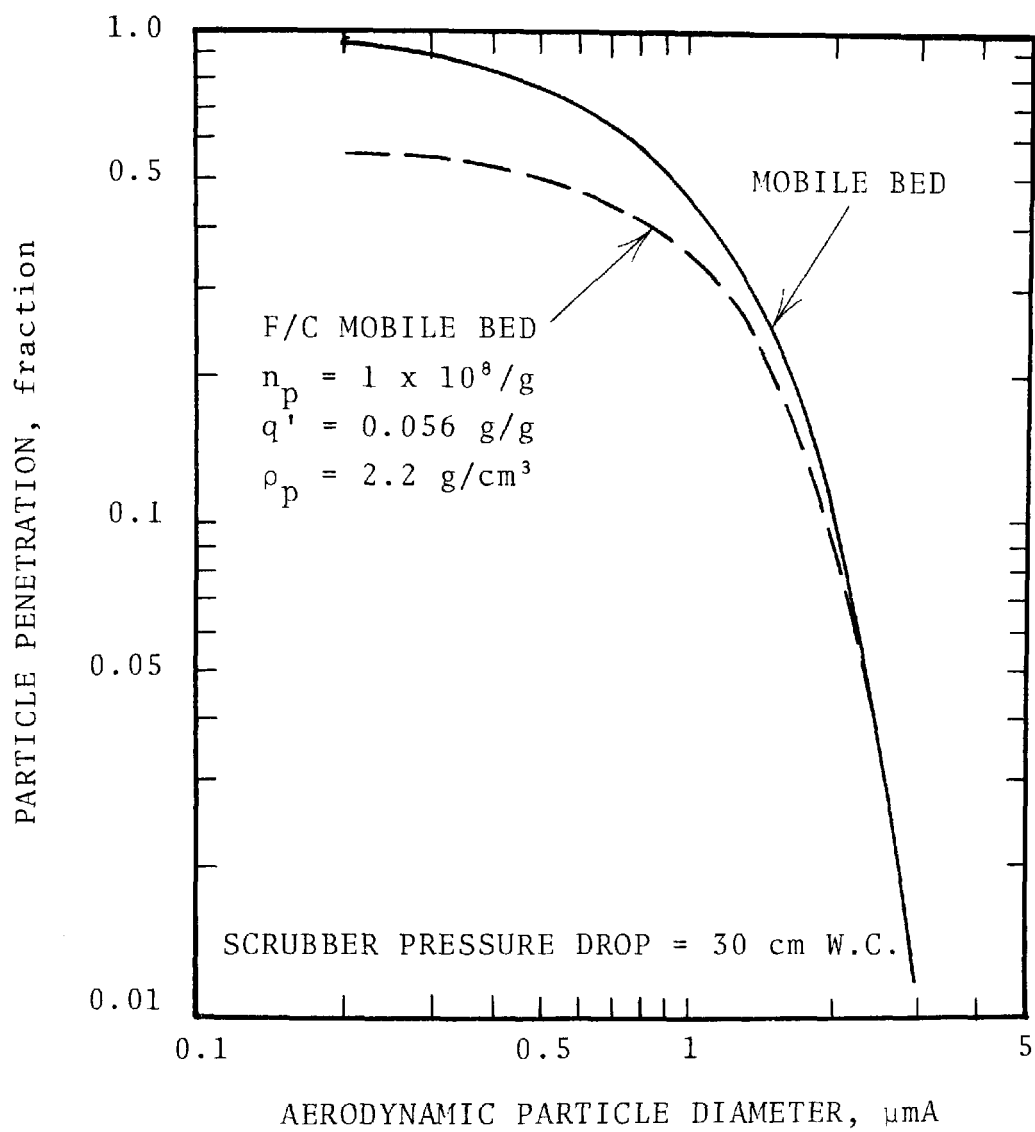


Figure 75. Predicted mobile bed and F/C mobile bed scrubber performance.

spray section is used for  $\text{SO}_x$  collection and for condensation and particle growth.

#### MOBILE BED SCRUBBER DESIGN RECOMMENDATIONS

The particle collection efficiency of a mobile bed scrubber depends only on the pressure drop across the bed. McMichael et al. (1976) and Wen and Chang (1978) have shown that the collection efficiency of a mobile bed scrubber for sulfur dioxide is also dependent only on the pressure drop. Therefore, if the pressure drop across the bed can be raised, the particle and  $\text{SO}_2$  collection efficiencies will increase.

As mentioned earlier, most of the mobile bed scrubber pressure drop is due to the weight of the packings, liquid holdup in the bed, and the liquid head retained on the supporting grids. An increase in any one of these will cause the scrubber pressure drop to increase.

The weight of packing in a mobile bed may be increased by increasing the static bed height by using heavier packings, and by using smaller packings. The packing spheres commonly used in industrial mobile bed scrubbers are hollow 3.8 cm diameter polypropylene balls. The average weight for each ball is about 4.5 g - 5 g (packing density = 0.137 - 0.175 g/cm<sup>3</sup>). Recently, the scrubber manufacturers have recommended using heavier balls. Balls as heavy as 7 g (packing density = 0.244 kg/cm<sup>3</sup>) were recommended.

Increasing the packing density has an added advantage: heat and mass transfer rates will be higher. According to O'Neill et al. (1972), the mobile bed can be operated either in the mode of fluidization without flooding or in the mode of fluidization due to incipient flooding. The operation mode of fluidization due to incipient flooding is the preferable mode. The flooding operation mode results in a higher liquid holdup in the bed and a higher gas-liquid interfacial activity which gives higher heat and mass transfer rate.



O'Neill et al. (1972) also say that the mode of operation depends largely on packing density and to a lesser extent on the packing size, liquid flow rate and physical properties of the liquid. Based on Chen and Douglas's empirical equation for liquid holdup, O'Neill et al. calculated that the transition of the non-flooding mode to the flooding mode occurred at a packing density of  $200 \text{ kg/m}^3$  for the 3.8 cm diameter packing. Thus, industrial mobile beds are operated in the nonflooding mode. The use of heavier 7 g spheres will shift the operation mode from nonflooding to flooding.

Smaller balls of the same wall thickness have a higher packing density. The use of smaller packing also causes liquid holdup in the bed to increase and causes the bed to be operated in the flooding mode sooner. The increase in weight and liquid holdup increases the pressure drop across the bed and improves the particle collection efficiency.

Liquid head retained on the supporting grids may be increased by using grids with smaller openings and a smaller percentage of open area. For a supporting grid with small openings and open area, it acts as a sieve tray operating in the weeping region. Liquid cannot freely flow downward through the openings and are partially retained on the tray. As in a sieve column, the liquid retained on the tray contributes to particle collection and pressure drop.

Another advantage of using supporting grids with small openings is that the bed motion is more uniform. The bed motion of the mobile bed with plastic net supports was observed to be more uniform than the bed with hardware screen supports. This observation conforms with others' findings. Numerous researchers have indicated that in the fluidization of solid by gas, the pressure drop across the gas distribution plate should be high enough to give uniform fluidization. The mobile bed is an irrigated fluidization of solid by gas. Thus to obtain uniform fluidization, the pressure drop across the

supporting grid should be high. One method to obtain high pressure drop across the grids is to use grids with less percentage of open area as well as smaller openings.

## SECTION 8

### FUTURE RESEARCH RECOMMENDATIONS

The objectives of studying the particle collection in a mobile bed scrubber and determining the feasibility of using it as a F/C scrubber have been achieved in this study through experimental and theoretical evaluation. It has been clearly shown that mobile beds are capable of being used as F/C scrubbers.

In order for the mobile bed scrubbers to be successfully used as F/C scrubbers, some fundamental research and development work are required. We recommend future research work in the following areas:

1. Theoretical and experimental study of condensation due to  $\text{SO}_x$  sorption on the fly ash.
2. Experimental and theoretical determination of the specific details of heat and mass transfer in mobile bed scrubbers.
3. Development of cooling devices suited for the cooling of scrubber liquid containing suspended and dissolved solids.
4. Experimental and theoretical evaluation of the effects of steam injection.
5. Experimental and theoretical study of particle growth due to condensation.

#### F/C Effects from $\text{SO}_x$ Sorption of Fly Ash

When fuel containing sulfur is burned, the hydrocarbons present are converted to sulfur dioxide. Part of the sulfur dioxide will oxidize further to sulfur trioxide at high temperature. Sulfur trioxide exists in dissociated form at high temperature. As the flue gas mixture is cooled, sulfur tri-

oxide associates with water vapor to form sulfuric acid vapor. Part of the acid vapor will be adsorbed by the fly ash.

As the gas cools down to below the dew point temperature, such as inside a scrubber, the remaining acid vapor will condense as acid mist. Due to the strong affinity of sulfuric acid towards water, the acid will absorb water. For those fly ash particles with acid adsorbed on their surfaces, the mass will increase. This phenomenon has the same effect as particle growth due to condensation of water vapor.

Mobile bed scrubbers are usually installed after the electrostatic precipitator as an additional particle scrubber. To decrease the fly ash resistivity, some ESP users use sulfur trioxide as the conditioning agent by injecting the  $\text{SO}_3$  gas into the flue gas. Therefore, it is possible to use  $\text{SO}_3$  as the conditioning agent for the electrostatic precipitator and as the F/C agent for the scrubber systems after the ESP. We recommend that this possibility be fully evaluated to determine its applicability. The following approach is recommended.

1. Survey literature on the adsorption of  $\text{SO}_3$  by fly ash, the nucleation of sulfuric acid, and the absorption of water by the sulfuric acid.
2. Conduct a bench scale study to obtain information on the conditions under which particle growth will occur and the rate of particle growth.
3. Determine the technical and economic feasibilities of using  $\text{SO}_3$  as the F/C agent.
4. Select promising scrubber systems and conduct a detailed experimental study as follows:
  - a) Laboratory pilot scale study with scrubber capacity of  $28 \text{ m}^3/\text{min}$  (1,000 CFM).
  - b) Pilot scale demonstration in a power plant with scrubber capacity around  $280 \text{ m}^3/\text{min}$  (10,000 CFM).
  - c) Full scale demonstration in a power plant.

## Heat and Mass Transfer in Mobile Bed Scrubbers

Information on the rates of heat and mass transfer and the gas-liquid contacting area are required for the proper design of mobile bed F/C scrubbers. The mass transfer rate and contacting area also determine the absorption efficiency of  $\text{SO}_2$  in lime and limestone slurry.

A few empirical correlations are available in the literature for the predictions of contacting area and heat and mass transfers; e.g., Woźniak (1975) on gas-liquid interfacial area, Gel'perin, et al. (1973) on heat and mass transfers, McMichael, et al. (1976) and Wen and Chang (1977) on absorption of  $\text{SO}_2$  in lime and limestone slurry. The application of these correlations are limited to scrubber geometries and conditions similar to those used by these investigators. The adequacy of these correlations for other situations has not been established. Therefore, it would be beneficial to study the specific details of heat and mass transfer in mobile bed scrubbers both theoretically and experimentally. The following approach is recommended:

1. Review and assess the published literature and available unpublished information pertaining to interfacial area and heat and mass transfer in mobile bed scrubbers.
2. Determine all factors which affect the interfacial area and heat and mass transfer rates and develop theory.
3. Conduct experiments to verify or improve the theory.

## Development of Liquid Cooling System

Due to the large requirement of cold scrubber liquor and the complications introduced by dissolved and suspended solids, the liquor cooling procedure has a significant effect on the economics of an F/C scrubber system. It represents the major cost difference between F/C and conventional scrubbing for many applications.

Concern over the possibility that solids deposition on cooling tower surfaces would lead to heavy buildup of adherent scale led to the choice of a spray-type cooler in the present study. The spray coolers have some drawbacks, such as low efficiency, high pressure nozzles required to produce small drops, and the plugging of spray nozzles. Therefore, the possibility of using packed or filled cooling towers should be investigated. The use of a standard commercial cooling tower would give the best combinations of cost, reliability, and proven design features. Purchase and installation of a standard cooling tower are also routine matters which can be accomplished through many vendors.

We recommend studies of solids deposition on surfaces of various materials which could be used for cooling tower construction. The solids deposition test involves the simple process of pumping a scrubber liquor over pieces of various packing materials to simulate their exposure in a cooling tower.

#### Steam Injection

Mobile bed scrubbers are currently used in power plants for removing particulates and  $\text{SO}_2$  from flue gas by utilizing lime and limestone slurries. The gas temperature and vapor content of the power plant are generally low ( $280^\circ\text{F}$ , 10% by volume moisture). Therefore, unless large quantities of spent steam are available, condensation effects and particle growth would be minimal.

The use of steam injection into saturated gas is an attractive but insufficiently explored ramification of F/C scrubbing. A bench-scale laboratory study could yield the information needed to determine the optimum balance between the quantity of steam to inject and the amount of condensation by cooling. Engineering design studies followed by pilot tests should be done to identify the best way of generating steam inexpensively.

Data from previous studies indicated that fine particle collection efficiency was greater when a given amount of steam was introduced into the gas than when an equivalent quantity was

condensed from the gas (see Calvert et al., 1975). The steam injection experiments were not made under the same conditions so the comparisons between them and F/C scrubbing with condensation only are not conclusive. However, the apparent benefit of steam injection is so large that further study is warranted.

The reason(s) for performance improvement by steam injection is (are) not known but can be hypothesized. If steam is mixed with saturated gas, only a small fraction will condense, depending on gas temperature. Thus, a given quantity of steam (say, 0.05 g/g dry gas) will give less condensate than 0.05 g/g, yet the particle collection efficiency is higher than for just condensation of 0.05 g/g. The most persuasive explanation is that steam injection causes an extremely high saturation ratio in the vicinity of the injection nozzle and this enhances the nucleation of condensation. This mechanism should be more significant for insoluble particles than for soluble ones.

If it is possible to obtain a substantial benefit from injection without subsequent cooling of the gas, there will be a reduction of the liquor cooling cost. On the other side, there will be some cost for steam generation. It would be valuable to know what benefits could be obtained by using various proportions of steam injection and condensation and what the costs would be.

An experimental program of determining particle growth under a range of parameters would provide the information needed to predict scrubber performance. The experiments could be done on bench scale with gas flow rates on the order of 0.1 to 0.5 m<sup>3</sup>/min. Soluble and insoluble particles should be studied at number concentrations ranging from 10<sup>6</sup>/cm<sup>3</sup> to 10<sup>9</sup>/cm<sup>3</sup>.

Costs for steam generation should be determined by engineering analysis and design studies. Conventional and nonconventional waste heat boilers should be evaluated. Cooling costs can be based on existing technology.

## Particle Growth

Laboratory research on particle growth is necessary to provide data which can be used in validating and/or revising the mathematical model. The experiments should be done with wettable and nonwettable particles in several types of bench-scale apparatus which incorporate contacting mechanisms typifying large scale equipment.

This experimental and analytical work is needed to clear up the present uncertainties about several interacting phenomena as represented in the mathematical model for particle growth. The points needing clarification are as follow:

1. The nucleation of condensation on the surface of insoluble particles may require some supersaturation of the gas, depending on the wettability of the surface. As presently set, the model accounts for condensation and growth when the saturation ratio is 1.0 or greater. It has been assumed that the supersaturation which occurs in the gas phase boundary layer close to the cold liquid surface when the bulk of the gas is just saturated (i.e.,  $s = 1.0$ ) might be sufficient to nucleate condensation on slightly wettable particles.

Because the degree and extent of the boundary layer supersaturation effect depends on the conditions of the gas and liquid, the geometry, and the hydrodynamics, there is no simple relationship defining the "effective" saturation ratio. As will be seen, it is also impossible to distinguish between the effects of the several phenomena which occur simultaneously during condensation scrubbing.

2. The rate of condensation from the gas depends on the temperature and vapor pressure differences between the phases and on the transfer coefficients. It also affects the fraction of total condensation which goes to the particles (i.e., " $f_p$ ") as predicted by the mathematical model.



3. The particle number concentration also influences " $f_p$ ", as computed from the model. The experimental data taken previously have not enabled very precise computation of number concentration, so the influence of this parameter has not been distinguishable from those of other parameters.

4. Soluble particles can cause condensation at saturation ratios less than 1.0 because the vapor pressure of water is lowered by the solute.

## REFERENCES

- Balabekov, V. S., P. G. Romankov, E. Ya. Tarat, and M. F. Mikhalev. J. Appl. Chem. USSR, 42:1454, 1969.
- Balabekov, V. S., E. Ya. Tarat, P. G. Romankov, and M. F. Mikhalev. J. Appl. Chem. USSR, 44:1061, 1971.
- Barile, R. G. and D. W. Meyer. Turbulent Bed Cooling Tower. Chem. Eng. Progr. Symposium Series 67, No. 119, 1971. pp. 134-143.
- Blyakher, I. G., L. Ya. Zhivaikin, and N. A. Yurovskaya. Investigation of Hydrodynamics and Mass Transfer in Equipment with Movable Packing. Int'l Chem. Engr., 7:485-490, 1967.
- Borgwardt, R. Limestone Scrubbing of SO<sub>2</sub> at EPA Pilot Plant. Report No. 1. August 1972.
- Borgwardt, R. Limestone Scrubbing of SO<sub>2</sub> at EPA Pilot Plant. Report No. 14. January 1974a
- Borgwardt, R. Limestone Scrubbing of SO<sub>2</sub> at EPA Pilot Plant. Report No. 16. June 1974b.
- Borgwardt, R. Limestone Scrubbing of SO<sub>2</sub> at EPA Pilot Plant. Report No. 21. June 1975.
- Calvert, S. Source Control by Liquid Scrubber. In: Air Pollution, Chapter 46, Arthur Stern, ed. Academic Press, New York, 1968.
- Calvert, S., J. Goldshmid, D. Leith, and D. Mehta. Wet Scrubber System Study, Volume 1, Scrubber Handbook. EPA-R2-72-118a, NTIS PB 213-016, August 1972.
- Calvert, S., J. Goldshmid, D. Leith, and N. Jhaveri. Feasibility of Flux Force/Condensation Scrubbing for Fine Particulate Collection. EPA 650/2-73-036, NTIS PB 227-307, 1973.
- Calvert, S. Engineering Design of Fine Particle Scrubbers. J. of A.P.C.A., 24:929-933, 1974.

emissions. They are sometimes installed after the electrostatic precipitators as secondary collectors and this practice is expected to become more prevalent. At the precipitator outlet, flue gas temperature is about 138°C (280°F) and contains about 10% by volume of moisture. Typical fly ash size distribution at the ESP outlet is  $d_{pg} = 3.0 \mu\text{m}$  and  $\sigma_g = 3.0$  (Figure 74). Particle concentration is about 0.5 g/DNm<sup>3</sup> (0.2 gr/SCF).

A three-stage mobile bed scrubber without F/C effect and operated at a pressure drop of 30 cm W.C. would have a grade penetration curve as that shown in Figure 75. The predicted overall particle penetration will be 17% (overall collection efficiency = 83%) and the predicted outlet particle loading will be 0.085 g/DNm<sup>3</sup> (0.034 gr/SCF).

Assume the flue gas can be saturated by evaporation of water; it will saturate around 54°C (130°F) and the moisture content will be 0.11 g/g. By assuming that the particle number concentration is  $1 \times 10^8/\text{cm}^3$  and the flue gas is cooled down to 43°C (110°F), a three-stage F/C mobile bed scrubber with a pressure drop of 30 cm W.C. will have a grade penetration curve like that shown by the dashed line in Figure 75. The predicted overall penetration will be 12% (88% overall collection efficiency) and the outlet particle loading will be 0.06 g/DNm<sup>3</sup> (0.024 gr/SCF).

For this application, the improvement in collection efficiency of the F/C mobile bed scrubber over the non-F/C mobile bed is small. The main reason is that the condensation ratio attainable in the power plant is too small (~0.056 g/g). If a large quantity of waste steam is available, the condensation ratio may be increased by injecting the steam into the gas. Steam injection causes an extremely high saturation ratio in the vicinity of the injection nozzle and this enhances the nucleation of condensation and particle growth. However, even though waste steam may be available, the mobile bed scrubber might not be a good choice for a F/C scrubber since the mobile bed is not an efficient particle scrubber. A better choice could be the combination of spray quencher and venturi scrubbers. The

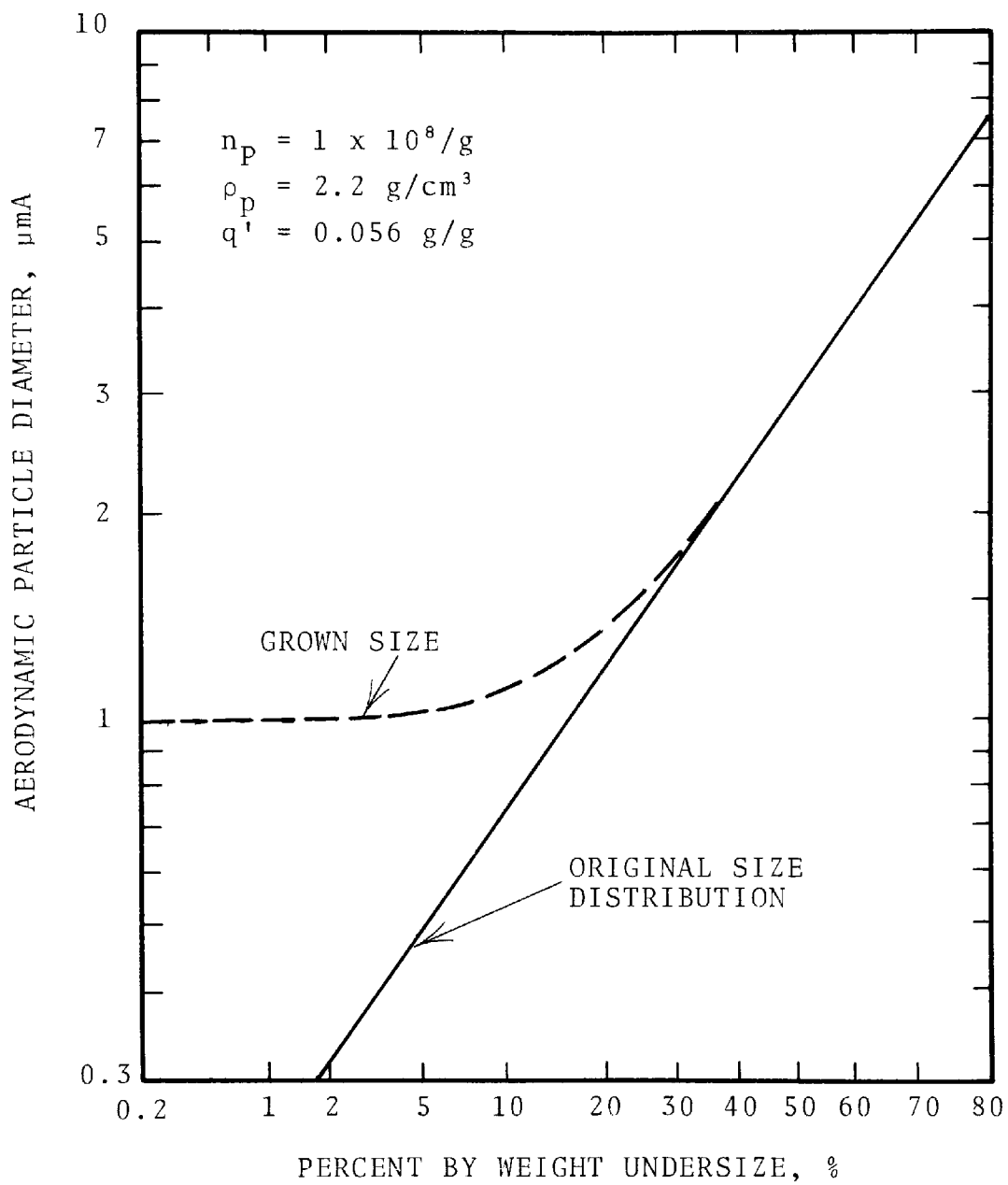


Figure 74. Typical fly ash distribution and grown size distribution.

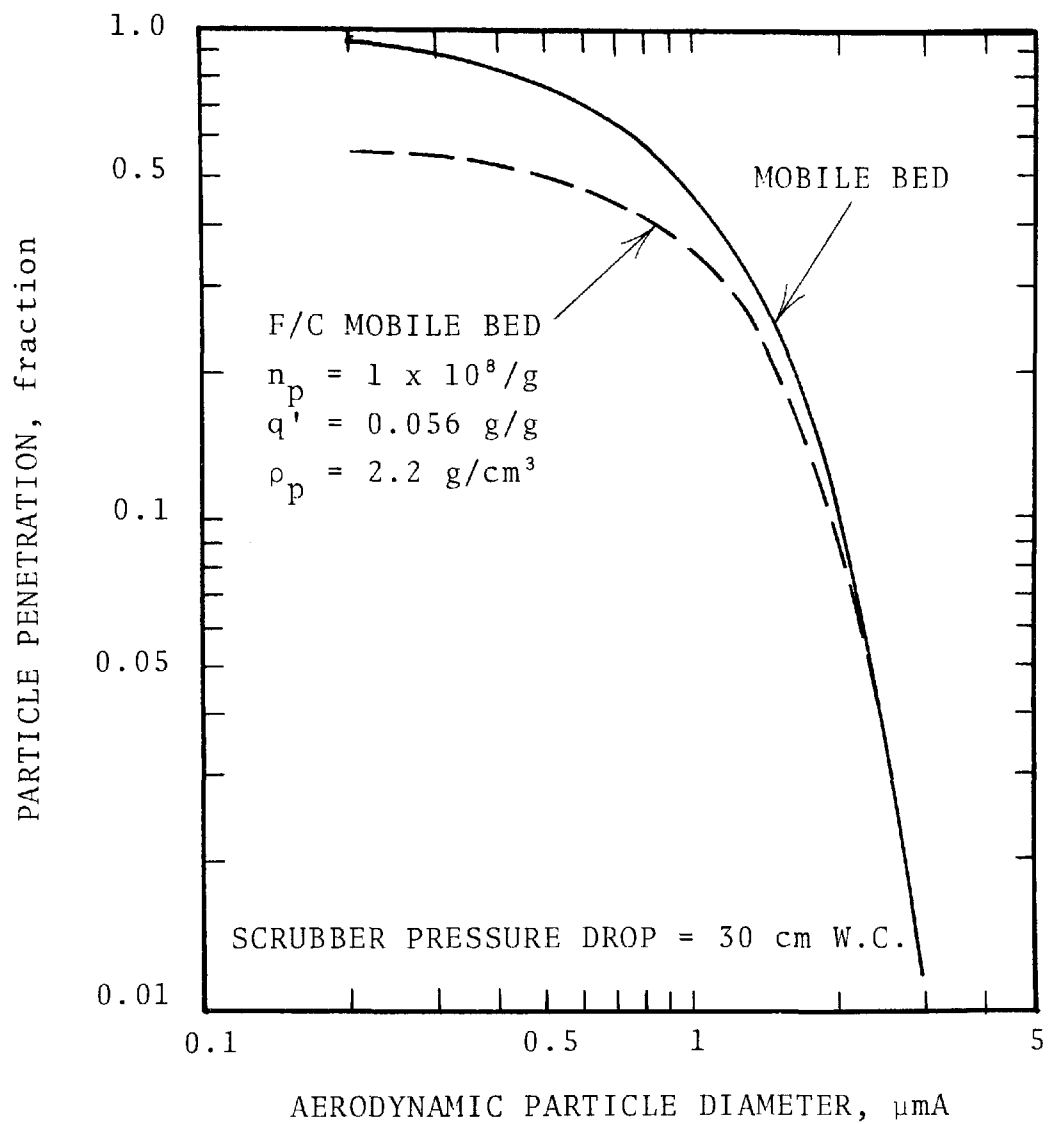


Figure 75. Predicted mobile bed and F/C mobile bed scrubber performance.

spray section is used for  $\text{SO}_x$  collection and for condensation and particle growth.

#### MOBILE BED SCRUBBER DESIGN RECOMMENDATIONS

The particle collection efficiency of a mobile bed scrubber depends only on the pressure drop across the bed. McMichael et al. (1976) and Wen and Chang (1978) have shown that the collection efficiency of a mobile bed scrubber for sulfur dioxide is also dependent only on the pressure drop. Therefore, if the pressure drop across the bed can be raised, the particle and  $\text{SO}_2$  collection efficiencies will increase.

As mentioned earlier, most of the mobile bed scrubber pressure drop is due to the weight of the packings, liquid holdup in the bed, and the liquid head retained on the supporting grids. An increase in any one of these will cause the scrubber pressure drop to increase.

The weight of packing in a mobile bed may be increased by increasing the static bed height by using heavier packings, and by using smaller packings. The packing spheres commonly used in industrial mobile bed scrubbers are hollow 3.8 cm diameter polypropylene balls. The average weight for each ball is about 4.5 g - 5 g (packing density =  $0.137 - 0.175 \text{ g/cm}^3$ ). Recently, the scrubber manufacturers have recommended using heavier balls. Balls as heavy as 7 g (packing density =  $0.244 \text{ kg/cm}^3$ ) were recommended.

Increasing the packing density has an added advantage: heat and mass transfer rates will be higher. According to O'Neill et al. (1972), the mobile bed can be operated either in the mode of fluidization without flooding or in the mode of fluidization due to incipient flooding. The operation mode of fluidization due to incipient flooding is the preferable mode. The flooding operation mode results in a higher liquid holdup in the bed and a higher gas-liquid interfacial activity which gives higher heat and mass transfer rate.

O'Neill et al. (1972) also say that the mode of operation depends largely on packing density and to a lesser extent on the packing size, liquid flow rate and physical properties of the liquid. Based on Chen and Douglas's empirical equation for liquid holdup, O'Neill et al. calculated that the transition of the non-flooding mode to the flooding mode occurred at a packing density of  $200 \text{ kg/m}^3$  for the 3.8 cm diameter packing. Thus, industrial mobile beds are operated in the nonflooding mode. The use of heavier 7 g spheres will shift the operation mode from nonflooding to flooding.

Smaller balls of the same wall thickness have a higher packing density. The use of smaller packing also causes liquid holdup in the bed to increase and causes the bed to be operated in the flooding mode sooner. The increase in weight and liquid holdup increases the pressure drop across the bed and improves the particle collection efficiency.

Liquid head retained on the supporting grids may be increased by using grids with smaller openings and a smaller percentage of open area. For a supporting grid with small openings and open area, it acts as a sieve tray operating in the weeping region. Liquid cannot freely flow downward through the openings and are partially retained on the tray. As in a sieve column, the liquid retained on the tray contributes to particle collection and pressure drop.

Another advantage of using supporting grids with small openings is that the bed motion is more uniform. The bed motion of the mobile bed with plastic net supports was observed to be more uniform than the bed with hardware screen supports. This observation conforms with others' findings. Numerous researchers have indicated that in the fluidization of solid by gas, the pressure drop across the gas distribution plate should be high enough to give uniform fluidization. The mobile bed is an irrigated fluidization of solid by gas. Thus to obtain uniform fluidization, the pressure drop across the

supporting grid should be high. One method to obtain high pressure drop across the grids is to use grids with less percentage of open area as well as smaller openings.



## SECTION 8

### FUTURE RESEARCH RECOMMENDATIONS

The objectives of studying the particle collection in a mobile bed scrubber and determining the feasibility of using it as a F/C scrubber have been achieved in this study through experimental and theoretical evaluation. It has been clearly shown that mobile beds are capable of being used as F/C scrubbers.

In order for the mobile bed scrubbers to be successfully used as F/C scrubbers, some fundamental research and development work are required. We recommend future research work in the following areas:

1. Theoretical and experimental study of condensation due to  $\text{SO}_x$  sorption on the fly ash.
2. Experimental and theoretical determination of the specific details of heat and mass transfer in mobile bed scrubbers.
3. Development of cooling devices suited for the cooling of scrubber liquid containing suspended and dissolved solids.
4. Experimental and theoretical evaluation of the effects of steam injection.
5. Experimental and theoretical study of particle growth due to condensation.

#### F/C Effects from $\text{SO}_x$ Sorption of Fly Ash

When fuel containing sulfur is burned, the hydrocarbons present are converted to sulfur dioxide. Part of the sulfur dioxide will oxidize further to sulfur trioxide at high temperature. Sulfur trioxide exists in dissociated form at high temperature. As the flue gas mixture is cooled, sulfur tri-

oxide associates with water vapor to form sulfuric acid vapor. Part of the acid vapor will be adsorbed by the fly ash.

As the gas cools down to below the dew point temperature, such as inside a scrubber, the remaining acid vapor will condense as acid mist. Due to the strong affinity of sulfuric acid towards water, the acid will absorb water. For those fly ash particles with acid adsorbed on their surfaces, the mass will increase. This phenomenon has the same effect as particle growth due to condensation of water vapor.

Mobile bed scrubbers are usually installed after the electrostatic precipitator as an additional particle scrubber. To decrease the fly ash resistivity, some ESP users use sulfur trioxide as the conditioning agent by injecting the  $\text{SO}_3$  gas into the flue gas. Therefore, it is possible to use  $\text{SO}_3$  as the conditioning agent for the electrostatic precipitator and as the F/C agent for the scrubber systems after the ESP. We recommend that this possibility be fully evaluated to determine its applicability. The following approach is recommended.

1. Survey literature on the adsorption of  $\text{SO}_3$  by fly ash, the nucleation of sulfuric acid, and the absorption of water by the sulfuric acid.
2. Conduct a bench scale study to obtain information on the conditions under which particle growth will occur and the rate of particle growth.
3. Determine the technical and economic feasibilities of using  $\text{SO}_3$  as the F/C agent.
4. Select promising scrubber systems and conduct a detailed experimental study as follows:
  - a) Laboratory pilot scale study with scrubber capacity of  $28 \text{ m}^3/\text{min}$  (1,000 CFM).
  - b) Pilot scale demonstration in a power plant with scrubber capacity around  $280 \text{ m}^3/\text{min}$  (10,000 CFM).
  - c) Full scale demonstration in a power plant.

## Heat and Mass Transfer in Mobile Bed Scrubbers

Information on the rates of heat and mass transfer and the gas-liquid contacting area are required for the proper design of mobile bed F/C scrubbers. The mass transfer rate and contacting area also determine the absorption efficiency of  $\text{SO}_2$  in lime and limestone slurry.

A few empirical correlations are available in the literature for the predictions of contacting area and heat and mass transfers; e.g., Woźniak (1975) on gas-liquid interfacial area, Gel'perin, et al. (1973) on heat and mass transfers, McMichael, et al. (1976) and Wen and Chang (1977) on absorption of  $\text{SO}_2$  in lime and limestone slurry. The application of these correlations are limited to scrubber geometries and conditions similar to those used by these investigators. The adequacy of these correlations for other situations has not been established. Therefore, it would be beneficial to study the specific details of heat and mass transfer in mobile bed scrubbers both theoretically and experimentally. The following approach is recommended:

1. Review and assess the published literature and available unpublished information pertaining to interfacial area and heat and mass transfer in mobile bed scrubbers.
2. Determine all factors which affect the interfacial area and heat and mass transfer rates and develop theory.
3. Conduct experiments to verify or improve the theory.

## Development of Liquid Cooling System

Due to the large requirement of cold scrubber liquor and the complications introduced by dissolved and suspended solids, the liquor cooling procedure has a significant effect on the economics of an F/C scrubber system. It represents the major cost difference between F/C and conventional scrubbing for many applications.

Concern over the possibility that solids deposition on cooling tower surfaces would lead to heavy buildup of adherent scale led to the choice of a spray-type cooler in the present study. The spray coolers have some drawbacks, such as low efficiency, high pressure nozzles required to produce small drops, and the plugging of spray nozzles. Therefore, the possibility of using packed or filled cooling towers should be investigated. The use of a standard commercial cooling tower would give the best combinations of cost, reliability, and proven design features. Purchase and installation of a standard cooling tower are also routine matters which can be accomplished through many vendors.

We recommend studies of solids deposition on surfaces of various materials which could be used for cooling tower construction. The solids deposition test involves the simple process of pumping a scrubber liquor over pieces of various packing materials to simulate their exposure in a cooling tower.

#### Steam Injection

Mobile bed scrubbers are currently used in power plants for removing particulates and  $\text{SO}_2$  from flue gas by utilizing lime and limestone slurries. The gas temperature and vapor content of the power plant are generally low ( $280^\circ\text{F}$ , 10% by volume moisture). Therefore, unless large quantities of spent steam are available, condensation effects and particle growth would be minimal.

The use of steam injection into saturated gas is an attractive but insufficiently explored ramification of F/C scrubbing. A bench-scale laboratory study could yield the information needed to determine the optimum balance between the quantity of steam to inject and the amount of condensation by cooling. Engineering design studies followed by pilot tests should be done to identify the best way of generating steam inexpensively.

Data from previous studies indicated that fine particle collection efficiency was greater when a given amount of steam was introduced into the gas than when an equivalent quantity was

condensed from the gas (see Calvert et al., 1975). The steam injection experiments were not made under the same conditions so the comparisons between them and F/C scrubbing with condensation only are not conclusive. However, the apparent benefit of steam injection is so large that further study is warranted.

The reason(s) for performance improvement by steam injection is (are) not known but can be hypothesized. If steam is mixed with saturated gas, only a small fraction will condense, depending on gas temperature. Thus, a given quantity of steam (say, 0.05 g/g dry gas) will give less condensate than 0.05 g/g, yet the particle collection efficiency is higher than for just condensation of 0.05 g/g. The most persuasive explanation is that steam injection causes an extremely high saturation ratio in the vicinity of the injection nozzle and this enhances the nucleation of condensation. This mechanism should be more significant for insoluble particles than for soluble ones.

If it is possible to obtain a substantial benefit from injection without subsequent cooling of the gas, there will be a reduction of the liquor cooling cost. On the other side, there will be some cost for steam generation. It would be valuable to know what benefits could be obtained by using various proportions of steam injection and condensation and what the costs would be.

An experimental program of determining particle growth under a range of parameters would provide the information needed to predict scrubber performance. The experiments could be done on bench scale with gas flow rates on the order of 0.1 to 0.5 m<sup>3</sup>/min. Soluble and insoluble particles should be studied at number concentrations ranging from 10<sup>6</sup>/cm<sup>3</sup> to 10<sup>9</sup>/cm<sup>3</sup>.

Costs for steam generation should be determined by engineering analysis and design studies. Conventional and nonconventional waste heat boilers should be evaluated. Cooling costs can be based on existing technology.

## Particle Growth

Laboratory research on particle growth is necessary to provide data which can be used in validating and/or revising the mathematical model. The experiments should be done with wettable and nonwettable particles in several types of bench-scale apparatus which incorporate contacting mechanisms typifying large scale equipment.

This experimental and analytical work is needed to clear up the present uncertainties about several interacting phenomena as represented in the mathematical model for particle growth. The points needing clarification are as follow:

1. The nucleation of condensation on the surface of insoluble particles may require some supersaturation of the gas, depending on the wettability of the surface. As presently set, the model accounts for condensation and growth when the saturation ratio is 1.0 or greater. It has been assumed that the supersaturation which occurs in the gas phase boundary layer close to the cold liquid surface when the bulk of the gas is just saturated (i.e.,  $s = 1.0$ ) might be sufficient to nucleate condensation on slightly wettable particles.

Because the degree and extent of the boundary layer supersaturation effect depends on the conditions of the gas and liquid, the geometry, and the hydrodynamics, there is no simple relationship defining the "effective" saturation ratio. As will be seen, it is also impossible to distinguish between the effects of the several phenomena which occur simultaneously during condensation scrubbing.

2. The rate of condensation from the gas depends on the temperature and vapor pressure differences between the phases and on the transfer coefficients. It also affects the fraction of total condensation which goes to the particles (i.e., " $f_p$ ") as predicted by the mathematical model.

3. The particle number concentration also influences " $f_p$ ", as computed from the model. The experimental data taken previously have not enabled very precise computation of number concentration, so the influence of this parameter has not been distinguishable from those of other parameters.

4. Soluble particles can cause condensation at saturation ratios less than 1.0 because the vapor pressure of water is lowered by the solute.

## REFERENCES

- Balabekov, V. S., P. G. Romankov, E. Ya. Tarat, and M. F. Mikhalev. J. Appl. Chem. USSR, 42:1454, 1969.
- Balabekov, V. S., E. Ya. Tarat, P. G. Romankov, and M. F. Mikhalev. J. Appl. Chem. USSR, 44:1061, 1971.
- Barile, R. G. and D. W. Meyer. Turbulent Bed Cooling Tower. Chem. Eng. Progr. Symposium Series 67, No. 119, 1971. pp. 134-143.
- Blyakher, I. G., L. Ya. Zhivaikin, and N. A. Yurovskaya. Investigation of Hydrodynamics and Mass Transfer in Equipment with Movable Packing. Int'l Chem. Engr., 7:485-490, 1967.
- Borgwardt, R. Limestone Scrubbing of SO<sub>2</sub> at EPA Pilot Plant. Report No. 1. August 1972.
- Borgwardt, R. Limestone Scrubbing of SO<sub>2</sub> at EPA Pilot Plant. Report No. 14. January 1974a
- Borgwardt, R. Limestone Scrubbing of SO<sub>2</sub> at EPA Pilot Plant. Report No. 16. June 1974b.
- Borgwardt, R. Limestone Scrubbing of SO<sub>2</sub> at EPA Pilot Plant. Report No. 21. June 1975.
- Calvert, S. Source Control by Liquid Scrubber. In: Air Pollution, Chapter 46, Arthur Stern, ed. Academic Press, New York, 1968.
- Calvert, S., J. Goldshmid, D. Leith, and D. Mehta. Wet Scrubber System Study, Volume 1, Scrubber Handbook. EPA-R2-72-118a, NTIS PB 213-016, August 1972.
- Calvert, S., J. Goldshmid, D. Leith, and N. Jhaveri. Feasibility of Flux Force/Condensation Scrubbing for Fine Particulate Collection. EPA 650/2-73-036, NTIS PB 227-307, 1973.
- Calvert, S. Engineering Design of Fine Particle Scrubbers. J. of A.P.C.A., 24:929-933, 1974.



- Calvert, S., N. Jhaveri, and T. Huiskong. Study of Flux Force/Condensation Scrubbing of Fine Particles. EPA 600/2-75-018, NTIS PB 249-297, 1975.
- Calvert, S. and S. Gandhi. Fine Particle Collection by a Flux Force/Condensation Scrubber: Pilot Demonstration. EPA 600/2-77-238, NTIS PB 227-075, 1977.
- Calvert, S., S. Yung, and L. E. Sparks. Liquid Entrainment from a Mobile Bed Scrubber. J. of A.P.C.A., 27:768-770, 1977.
- Chen, B. H. and W. J. M. Douglas. Axial Mixing of Liquid in a Turbulent-Bed Contactor. Can. J. Chem. Engr. 47:113-118, April 1969.
- Chen, B. H. and W. J. M. Douglas. Liquid Hold-up and Minimum Fluidization Velocity in a Turbulent Contactor. Can. J. Chem. Engr., 46:245-249, August 1968.
- Douglas, H. R., I. W. A. Snider, and G. Tomlinson. The Turbulent Contact Absorber. Chem. Engr. Prog., 59:85-89, December 1963.
- Douglas, W. J. M. Heat and Mass Transfer in a Turbulent Bed Contactor. Chem. Eng. Progr., 60:66-71, July 1964.
- Ensor, D. S., B. S. Jackson, S. Calvert, C. Lake, D. V. Wallon, R. E. Nilan, K. S. Campbell, T. A. Cahill, and R. G. Flocchini. Evaluation of a Particulate Scrubber on a Coal-Fired Utility Boiler. EPA 600/2-75-074, November 1975.
- Epstein, M. EPA Alkali Scrubbing Test Facility: Summary of Testing through October 1974. NTIS PB 244-901, June 1975.
- Epstein, M. EPA Alkali Scrubbing Test Facility: Advanced Program. Progress Report prepared by Bechtel for EPA, September 1976.
- Gel'perin, N. I., E. N. Bukharkin, V. Z. Grishko, and M. I. Tsysin. A Study of contact Heat and Mass Transfer in Equipment with Fluidized Spherical Packing. Int'l Chem. Engr., 13:615-618, 1973.
- Goldschmidt, V. W. and M. K. Householder. The Hot Wire Anemometer as an Aerosol Droplet Size Sampler. Atmos. Environ., 3:643-651, 1969.
- Johnson, J. M., D. G. Jones, A. Weir, W. C. Martin, and S. Calvert. Scrubber Experience at Mojave. Paper No. 11. EPA 600/7-76-016, October 1976.

- Kielback, A. W. The Development of Floating-Bed Scrubbers. Chem. Engr. Progr. Symposium Series, 57:51-54, 1961.
- Kito, M., M. Sawada, M. Shimada, M. Takata, T. Sakai, and S. Sugiyama. Gas Holdup in Mobile Beds with Stagnant Liquid Flow. Kagaku Kogaku Ronbunshu, 2:12-15, 1976; Int'l Chem. Engr., 16:701-704, 1976.
- Kito, M., M. Shimada, R. Iijima, T. Sakai, M. Takata, and S. Sugiyama. Liquid-Vapor Interfacial Area for a Liquid Batch-Type Mobile-Bed Contactor. Kagaku Kogaku Ronbunshu, 2:16-20, 1976b; Int'l Chem. Engr., 16:705-709, 1976.
- Kito, M., Y. Kayama, T. Sakai, and S. Sugiyama. Minimum Fluidization Velocity in a Mobile Bed. Kagaku Kogaku Ronbunshu, 2:21-24, 1976c; Int'l Chem. Engr., 16:710-713, 1976c.
- Kito, M., T. Monma, Y. Kayama, T. Sagai, and S. Sugiyama. Pressure Drop and Bed Expansion in a Mobile Bed. Kagaku Kogaku Ronbunshu, 2:476-479, 1976d.
- Levesh, I. P., N. I. Krainev, and M. I. Niyazov. Calculation of the Pressure Drop and Heights of Three-Phase Fluidized Beds. Int'l Chem. Engr., 8:311-312, 1968.
- Levesh, I. P., M. I. Niyazov, N. I. Krainev, and F. F. Ganikhanova. Mass Transfer in Absorbers with Fluidized Packed Beds. Int'l Chem. Engr., 8:379-380, 1968.
- McMichael, W. J., J. S. Fan, and C. Y. Wen. Analysis of Sulfur Dioxide Wet Limestone Scrubbing Data from Pilot Plant Spray and TCA Scrubbers. Ind. Eng. Chem., Process Des. Dev., 15:459-467, 1976.
- O'Neill, B. K., D. J. Nicklin, N. J. Morgan, and L. S. Leung. The Hydrodynamics of Gas-Liquid Contacting in Towers with Fluidized Packings. Can. J. Chem. Engr., 50:595-601, 1972.
- Orr, C. Particulate Technology. The MacMillan Company, New York, 1966.
- Perry, H. Chemical Engineers' Handbook. 5th Ed., McGraw-Hill Book Company, New York, 1973.
- Pollock, W. A., J. P. Tomany, and G. Frieling. Sulfur Dioxide and Fly Ash Removal from Coal Burning Power Plant. Air Engr., 24-28, September 1967.

- Rhudy, R. G. and H. N. Head. Results of Flue Gas Characterization Testing at the EPA Alkali Wet-Scrubbing Test Facility. Paper No. 13 in Second EPA Fine Particle Scrubber Symposium, R. Parker and S. Calvert, eds. EPA 600/2-77-193, September 1973.
- Strumillo, C., J. Adamiec, and T. Kudra. Packed Columns with Expanding Beds. *Int'l Chem. Engr.*, 14:652-657, 1974.
- Tichy, J., A. Wong, and W. J. M. Douglas. Pressure Drop in a Mobile-Bed Contactor. *Can. J. Chem. Engr.*, 50:215-220, 1972.
- Tichy, J. and W. J. M. Douglas. Bed Expansion in a Mobile-Bed Contactor. *Can. J. Chem. Engr.*, 50:702-707, 1972.
- Tichy, J. and W. J. M. Douglas. Certain Hydrodynamic Characteristics of Mobile-Bed Contactors. *Can. J. Chem. Engr.*, 51:618-620, 1973.
- Uchida, S., C. S. Chang, and C. Y. Wen. Mechanics of a Turbulent Contact Absorber. *Can. J. Chem. Engr.*, 55:392-396, 1977.
- Wen, C., and C. S. Chang. Absorption of SO<sub>2</sub> in Lime and Limestone Slurry: Pressure Drop Effect on Turbulent Contact Absorber Performance. *Environ. Sci. Tech.*, 12:703-707, 1978.
- Whitmore, P. J. Diffusiophoretic under Turbulent Conditions. Ph.D. Thesis, University of British Columbia, 1976.
- Woźniak, M. and K. Ostergaard. An Investigation of Mass Transfer in a Countercurrent Three-Phase Fluidized Bed. *Chem. Engr. Sci.*, 28:167-171, 1973.
- Woźniak, M. Pressure Drop and Effective Interfacial Area in a Column with a Mobile Bed. *Int'l Chem. Engr.*, 17:553-559, 1977.

## APPENDIX "A"

### DC-1 DROP COUNTER ENTRAINMENT DATA

TABLE A-1. DC-1 DROP COUNTER DATA FOR RUN NO. DC-1

Bin No.	Number Concentration (#/cm <sup>3</sup> )	Cum. Number Concentration (#/cm <sup>3</sup> )	Cum. Entrainment Volume (ml/Nm <sup>3</sup> )	Drop Diameter (μm)
1	0.95	0.95	$4.00 \times 10^{-6}$	1 - 3
2	1.17	2.12	$1.36 \times 10^{-4}$	3 - 9
3	0.53	2.65	$1.76 \times 10^{-3}$	9 - 27
4	0.09	2.74	$9.01 \times 10^{-3}$	27 - 81
5	0.07	2.81	$1.69 \times 10^{-3}$	81 - 243
6				>243

TABLE A-3. DC-1 DROP COUNTER DATA FOR RUN NO. DC-3

Bin No.	Number Concentration (#/cm <sup>3</sup> )	Cum. Number Concentration (#/cm <sup>3</sup> )	Cum. Entrainment Volume (ml/Nm <sup>3</sup> )	Drop Diameter (μm)
1	0.80	0.80	$1.42 \times 10^{-6}$	1 - 2
2	0.65	1.45	$1.06 \times 10^{-5}$	2 - 4
3	0.92	2.37	$1.15 \times 10^{-4}$	4 - 8
4	0.80	3.17	$8.30 \times 10^{-4}$	8 - 16
5	0.29	3.46	$2.90 \times 10^{-3}$	16 - 32
6	0.41	3.87		>32

TABLE A-2. DC-1 DROP COUNTER DATA FOR RUN NO. DC-2

Bin No.	Number Concentration (#/cm <sup>3</sup> )	Cum. Number Concentration (#/cm <sup>3</sup> )	Cum. Entrainment Volume (ml/Nm <sup>3</sup> )	Drop Diameter (μm)
1	0.43	0.43	$7.6 \times 10^{-7}$	1 - 2
2	0.54	0.97	$8.4 \times 10^{-6}$	2 - 4
3	0.85	1.82	$1.04 \times 10^{-4}$	4 - 8
4	0.58	2.40	$6.2 \times 10^{-4}$	8 - 16
5	0.18	2.58	$1.92 \times 10^{-3}$	16 - 32
6	0.27	2.85		>32

TABLE A-4. DC-1 DROP COUNTER DATA FOR RUN NO. DC-4

Bin No.	Number Concentration (#/cm <sup>3</sup> )	Cum. Number Concentration (#/cm <sup>3</sup> )	Cum. Entrainment Volume (ml/Nm <sup>3</sup> )	Drop Diameter (μm)
1	0.84	0.84	$3.52 \times 10^{-6}$	1 - 3
2	1.35	2.19	$1.57 \times 10^{-4}$	3 - 9
3	0.63	2.82	$2.08 \times 10^{-3}$	9 - 27
4	0.10	2.92	$1.00 \times 10^{-2}$	27 - 81
5	0.09	3.01	$2.00 \times 10^{-1}$	81 - 243
6	0.00			>243

TABLE A-5. DC-1 DROP COUNTER DATA FOR RUN NO. DC-5

Bin No.	Number Concentration (#/cm <sup>3</sup> )	Cum. Number Concentration (#/cm <sup>3</sup> )	Cum. Entrainment Volume (ml/Nm <sup>3</sup> )	Drop Diameter (μm)
1	1.36	1.36	$5.70 \times 10^{-6}$	1 - 3
2	2.31	3.67	$2.67 \times 10^{-4}$	3 - 9
3	0.92	4.59	$3.08 \times 10^{-3}$	9 - 27
4	0.17	4.76	$1.70 \times 10^{-2}$	27 - 81
5	0.11	4.87	$2.62 \times 10^{-1}$	81 - 243
6	0.00			>243

TABLE A-7. DC-1 DROP COUNTER DATA FOR RUN NO. DC-7

Bin No.	Number Concentration (#/cm <sup>3</sup> )	Cum. Number Concentration (#/cm <sup>3</sup> )	Cum. Entrainment Volume (ml/Nm <sup>3</sup> )	Drop Diameter (μm)
1	0.94	0.94	$1.66 \times 10^{-6}$	1 - 2
2	1.19	2.13	$1.68 \times 10^{-5}$	2 - 4
3	1.76	3.89	$2.00 \times 10^{-4}$	4 - 8
4	1.19	5.08	$1.08 \times 10^{-3}$	8 - 16
5	0.42	5.50	$3.04 \times 10^{-3}$	16 - 32
6	0.53	6.03		>32

TABLE A-6. DC-1 DROP COUNTER DATA FOR RUN NO. DC-6

Bin No.	Number Concentration (#/cm <sup>3</sup> )	Cum. Number Concentration (#/cm <sup>3</sup> )	Cum. Entrainment Volume (ml/Nm <sup>3</sup> )	Drop Diameter (μm)
1	0.82	0.82	$1.45 \times 10^{-6}$	1 - 2
2	1.01	1.83	$1.57 \times 10^{-5}$	2 - 4
3	1.65	3.48	$2.01 \times 10^{-4}$	4 - 8
4	1.06	4.54	$1.16 \times 10^{-3}$	8 - 16
5	0.33	4.87	$3.55 \times 10^{-3}$	16 - 32
6	0.46	5.33		>32

TABLE A-8. DC-1 DROP COUNTER DATA FOR RUN NO. DC-8

Bin No.	Number Concentration (#/cm <sup>3</sup> )	Cum. Number Concentration (#/cm <sup>3</sup> )	Cum. Entrainment Volume (ml/Nm <sup>3</sup> )	Drop Diameter (μm)
1	1.69	1.69	$7.10 \times 10^{-6}$	1 - 3
2	2.53	4.22	$2.93 \times 10^{-4}$	3 - 9
3	1.02	5.24	$3.40 \times 10^{-3}$	9 - 27
4	0.17	5.41	$1.70 \times 10^{-2}$	27 - 81
5	0.09	5.49	$2.18 \times 10^{-1}$	81 - 243
6	0.00			>243

TABLE A-9. DC-1 DROP COUNTER DATA FOR RUN NO. DC-9

Bin No.	Number Concentration (#/cm <sup>3</sup> )	Cum. Number Concentration (#/cm <sup>3</sup> )	Cum. Entrainment Volume (ml/Nm <sup>3</sup> )	Drop Diameter (μm)
1	0.98	0.98	$1.73 \times 10^{-6}$	1 - 2
2	1.02	2.00	$1.61 \times 10^{-5}$	2 - 4
3	1.80	3.80	$2.19 \times 10^{-4}$	4 - 8
4	1.46	5.26	$1.54 \times 10^{-3}$	8 - 16
5	0.54	5.80	$5.45 \times 10^{-3}$	16 - 32
6	0.81	6.61		>32

TABLE A-11. DC-1 DROP COUNTER DATA FOR RUN NO. DC-11

Bin No.	Number Concentration (#/cm <sup>3</sup> )	Cum. Number Concentration (#/cm <sup>3</sup> )	Cum. Entrainment Volume (ml/Nm <sup>3</sup> )	Drop Diameter (μm)
1	1.48	1.48	$6.2 \times 10^{-6}$	1 - 3
2	1.12	2.60	$1.3 \times 10^{-4}$	3 - 9
3	1.58	4.18	$5.0 \times 10^{-3}$	9 - 27
4	0.31	4.49	$3.1 \times 10^{-2}$	27 - 81
5	0.20	4.69	$4.8 \times 10^{-1}$	81 - 243
6	0.00			>243

TABLE A-10. DC-1 DROP COUNTER DATA FOR RUN NO. DC-10

Bin No.	Number Concentration (#/cm <sup>3</sup> )	Cum. Number Concentration (#/cm <sup>3</sup> )	Cum. Entrainment Volume (ml/Nm <sup>3</sup> )	Drop Diameter (μm)
1	1.84	1.84	$7.71 \times 10^{-6}$	1 - 3
2	2.35	4.19	$2.74 \times 10^{-4}$	3 - 9
3	1.34	5.53	$4.36 \times 10^{-3}$	9 - 27
4	0.27	5.80	$2.60 \times 10^{-2}$	27 - 81
5	0.17	5.97	$4.05 \times 10^{-1}$	81 - 243
6	0.00			>243

TABLE A-12. DC-1 DROP COUNTER DATA FOR RUN NO. DC-12

Bin No.	Number Concentration (#/cm <sup>3</sup> )	Cum. Number Concentration (#/cm <sup>3</sup> )	Cum. Entrainment Volume (ml/Nm <sup>3</sup> )	Drop Diameter (μm)
1	0.67	0.67	$1.19 \times 10^{-6}$	1 - 2
2	1.13	1.80	$1.71 \times 10^{-5}$	2 - 4
3	1.58	3.38	$1.96 \times 10^{-4}$	4 - 8
4	1.53	4.91	$1.58 \times 10^{-3}$	8 - 16
5	0.47	5.38	$4.98 \times 10^{-3}$	16 - 32
6	0.48	5.86		>32

TABLE A-13. DC-1 DROP COUNTER DATA FOR RUN NO. DC-13

Bin No.	Number Concentration (#/cm <sup>3</sup> )	Cum. Number Concentration (#/cm <sup>3</sup> )	Cum. Entrainment Volume (ml/Nm <sup>3</sup> )	Drop Diameter (μm)
1	0.26	0.26	$4.60 \times 10^{-7}$	1 - 2
2	0.47	0.73	$7.10 \times 10^{-6}$	2 - 4
3	0.94	1.67	$1.13 \times 10^{-4}$	4 - 8
4	0.72	2.39	$7.65 \times 10^{-4}$	8 - 16
5	0.24	2.63	$2.50 \times 10^{-3}$	16 - 32
6	0.24	2.87		>32

TABLE A-15. DC-1 DROP COUNTER DATA FOR RUN NO. DC-15

Bin No.	Number Concentration (#/cm <sup>3</sup> )	Cum. Number Concentration (#/cm <sup>3</sup> )	Cum. Entrainment Volume (ml/Nm <sup>3</sup> )	Drop Diameter (μm)
1	0.54	0.54	$2.27 \times 10^{-6}$	1 - 3
2	1.07	1.61	$1.23 \times 10^{-4}$	3 - 9
3	0.42	2.03	$1.4 \times 10^{-3}$	9 - 27
4	0.054	2.08	$5.85 \times 10^{-3}$	27 - 81
5	0.033	2.21	$8.00 \times 10^{-2}$	81 - 243
6	0.00			>243

TABLE A-14. DC-1 DROP COUNTER DATA FOR RUN NO. DC-14

Bin No.	Number Concentration (#/cm <sup>3</sup> )	Cum. Number Concentration (#/cm <sup>3</sup> )	Cum. Entrainment Volume (ml/Nm <sup>3</sup> )	Drop Diameter (μm)
1	0.69	0.69	$2.90 \times 10^{-6}$	1 - 3
2	1.16	1.85	$1.34 \times 10^{-4}$	3 - 9
3	0.50	2.35	$1.66 \times 10^{-3}$	9 - 27
4	0.08	2.43	$8.26 \times 10^{-3}$	27 - 81
5	0.06	2.50	$1.35 \times 10^{-1}$	81 - 243
6	0.00			>243

TABLE A-16. DC-1 DROP COUNTER DATA FOR RUN NO. DC-16

Bin No.	Number Concentration (#/cm <sup>3</sup> )	Cum. Number Concentration (#/cm <sup>3</sup> )	Cum. Entrainment Volume (ml/Nm <sup>3</sup> )	Drop Diameter (μm)
1	0.35	0.35	$6.20 \times 10^{-7}$	1 - 2
2	0.49	0.84	$7.53 \times 10^{-6}$	2 - 4
3	0.66	1.50	$8.21 \times 10^{-5}$	4 - 8
4	0.51	2.00	$5.44 \times 10^{-4}$	8 - 16
5	0.14	2.15	$1.55 \times 10^{-3}$	16 - 32
6	0.17	2.32		>32



TABLE A-17. DC-1 DROP COUNTER DATA FOR RUN NO. DC-17

Bin No.	Number Concentration (#/cm <sup>3</sup> )	Cum. Number Concentration (#/cm <sup>3</sup> )	Cum. Entrainment Volume (ml/Nm <sup>3</sup> )	Drop Diameter (μm)
1	0.37	0.37	$6.5 \times 10^{-7}$	1 - 2
2	0.30	0.67	$4.85 \times 10^{-6}$	2 - 4
3	0.39	1.06	$4.9 \times 10^{-5}$	4 - 8
4	0.42	1.48	$4.3 \times 10^{-4}$	8 - 16
5	0.08	1.56	$1.0 \times 10^{-3}$	16 - 32
6	0.10	1.66		>32

TABLE A-19. DC-1 DROP COUNTER DATA FOR RUN NO. DC-19

Bin No.	Number Concentration (#/cm <sup>3</sup> )	Cum. Number Concentration (#/cm <sup>3</sup> )	Cum. Entrainment Volume (ml/Nm <sup>3</sup> )	Drop Diameter (μm)
1	0.23	0.23	$9.6 \times 10^{-7}$	1 - 3
2	0.51	0.74	$5.9 \times 10^{-5}$	3 - 9
3	0.20	0.94	$6.7 \times 10^{-4}$	9 - 27
4	0.034	0.97	$3.5 \times 10^{-3}$	27 - 81
5	0.013	0.99	$3.2 \times 10^{-2}$	81 - 243
6	0.00			>243

TABLE A-18. DC-1 DROP COUNTER DATA FOR RUN NO. DC-18

Bin No.	Number Concentration (#/cm <sup>3</sup> )	Cum. Number Concentration (#/cm <sup>3</sup> )	Cum. Entrainment Volume (ml/Nm <sup>3</sup> )	Drop Diameter (μm)
1	0.42	0.42	$1.8 \times 10^{-6}$	1 - 3
2	0.74	1.16	$8.6 \times 10^{-5}$	3 - 9
3	0.24	1.40	$8.2 \times 10^{-4}$	9 - 27
4	0.035	1.44	$3.7 \times 10^{-3}$	27 - 81
5	0.023	1.46	$5.5 \times 10^{-2}$	81 - 243
6	0.00			>243

TABLE A-20. DC-1 DROP COUNTER DATA FOR RUN NO. DC-20

Bin No.	Number Concentration (#/cm <sup>3</sup> )	Cum. Number Concentration (#/cm <sup>3</sup> )	Cum. Entrainment Volume (ml/Nm <sup>3</sup> )	Drop Diameter (μm)
1	0.13	0.13	$2.3 \times 10^{-7}$	1 - 2
2	0.21	0.34	$3.2 \times 10^{-6}$	2 - 4
3	0.31	0.65	$3.8 \times 10^{-5}$	4 - 8
4	0.25	0.90	$2.6 \times 10^{-4}$	8 - 16
5	0.12	1.02	$1.1 \times 10^{-3}$	16 - 32
6	0.09	1.10		>32

TABLE A-21. DC-1 DROP COUNTER DATA FOR RUN NO. DC-21

Bin No.	Number Concentration (#/cm <sup>3</sup> )	Cum. Number Concentration (#/cm <sup>3</sup> )	Cum. Entrainment Volume (ml/Nm <sup>3</sup> )	Drop Diameter (μm)
1	0.58	1.58	$1.0 \times 10^{-6}$	1 - 2
2	0.44	1.02	$7.2 \times 10^{-6}$	2 - 4
3	0.65	1.67	$8.0 \times 10^{-5}$	4 - 8
4	0.46	2.13	$5.0 \times 10^{-4}$	8 - 16
5	0.10	2.23	$1.2 \times 10^{-3}$	16 - 32
6	0.11	2.34		>32

TABLE A-23. DC-1 DROP COUNTER DATA FOR RUN NO. DC-23

Bin No.	Number Concentration (#/cm <sup>3</sup> )	Cum. Number Concentration (#/cm <sup>3</sup> )	Cum. Entrainment Volume (ml/Nm <sup>3</sup> )	Drop Diameter (μm)
1	0.40	0.40	$1.7 \times 10^{-6}$	1 - 3
2	0.75	1.15	$8.7 \times 10^{-5}$	3 - 9
3	0.42	1.57	$1.4 \times 10^{-3}$	9 - 27
4	0.065	1.64	$6.8 \times 10^{-3}$	27 - 81
5	0.036	1.67	$8.7 \times 10^{-2}$	81 - 243
6	0.00			243

TABLE A-22. DC-1 DROP COUNTER DATA FOR RUN NO. DC-22

Bin No.	Number Concentration (#/cm <sup>3</sup> )	Cum. Number Concentration (#/cm <sup>3</sup> )	Cum. Entrainment Volume (ml/Nm <sup>3</sup> )	Drop Diameter (μm)
1	0.66	0.66	$2.8 \times 10^{-6}$	1 - 3
2	0.52	1.18	$6.2 \times 10^{-5}$	3 - 9
3	0.30	1.48	$9.8 \times 10^{-4}$	9 - 27
4	0.045	1.53	$4.7 \times 10^{-3}$	27 - 81
5	0.023	1.55	$5.6 \times 10^{-2}$	81 - 243
6	0.00			>243

TABLE A-24. DC-1 DROP COUNTER DATA FOR RUN NO. DC-24

Bin No.	Number Concentration (#/cm <sup>3</sup> )	Cum. Number Concentration (#/cm <sup>3</sup> )	Cum. Entrainment Volume (ml/Nm <sup>3</sup> )	Drop Diameter (μm)
1	0.13	0.13	$2.3 \times 10^{-7}$	1 - 2
2	0.25	0.38	$3.7 \times 10^{-6}$	2 - 4
3	0.61	0.99	$7.3 \times 10^{-5}$	4 - 8
4	0.49	1.48	$5.1 \times 10^{-4}$	8 - 16
5	0.16	1.64	$1.7 \times 10^{-3}$	16 - 32
6	0.14	1.78		>32

TABLE A-25. DC-1 DROP COUNTER DATA FOR RUN NO. DC-25

Bin No.	Number Concentration (#/cm <sup>3</sup> )	Cum. Number Concentration (#/cm <sup>3</sup> )	Cum. Entrainment Volume (ml/Nm <sup>3</sup> )	Drop Diameter (μm)
1	0.37	0.37	$6.5 \times 10^{-7}$	1 - 2
2	0.52	0.89	$8.0 \times 10^{-6}$	2 - 4
3	0.77	1.66	$9.5 \times 10^{-5}$	4 - 8
4	0.45	2.11	$5.0 \times 10^{-4}$	8 - 16
5	0.16	2.27	$1.7 \times 10^{-3}$	16 - 32
6	0.17	2.44		>32

TABLE A-27. DC-1 DROP COUNTER DATA FOR RUN NO. DC-27

Bin No.	Number Concentration (#/cm <sup>3</sup> )	Cum. Number Concentration (#/cm <sup>3</sup> )	Cum. Entrainment Volume (ml/Nm <sup>3</sup> )	Drop Diameter (μm)
1	0.73	0.73	$3.10 \times 10^{-6}$	1 - 3
2	1.32	2.05	$1.53 \times 10^{-4}$	3 - 9
3	0.51	2.56	$1.71 \times 10^{-3}$	9 - 27
4	0.067	2.63	$7.20 \times 10^{-3}$	27 - 81
5	0.032	2.66	$7.80 \times 10^{-2}$	81 - 243
6	0.00			>243

TABLE A-26. DC-1 DROP COUNTER DATA FOR RUN NO. DC-26

Bin No.	Number Concentration (#/cm <sup>3</sup> )	Cum. Number Concentration (#/cm <sup>3</sup> )	Cum. Entrainment Volume (ml/Nm <sup>3</sup> )	Drop Diameter (μm)
1	0.45	0.45	$1.9 \times 10^{-6}$	1 - 3
2	0.91	1.36	$1.02 \times 10^{-4}$	3 - 9
3	0.42	1.78	$1.4 \times 10^{-3}$	9 - 27
4	0.054	1.83	$5.9 \times 10^{-3}$	27 - 81
5	0.03	1.86	$7.3 \times 10^{-2}$	81 - 243
6				>243

TABLE A-28. DC-1 DROP COUNTER DATA FOR RUN NO. DC-28

Bin No.	Number Concentration (#/cm <sup>3</sup> )	Cum. Number Concentration (#/cm <sup>3</sup> )	Cum. Entrainment Volume (ml/Nm <sup>3</sup> )	Drop Diameter (μm)
1	0.53	0.53	$9.4 \times 10^{-7}$	1 - 2
2	0.52	1.05	$8.2 \times 10^{-6}$	2 - 4
3	1.07	2.12	$1.3 \times 10^{-4}$	4 - 8
4	0.57	2.69	$6.5 \times 10^{-4}$	8 - 16
5	0.21	2.90	$2.1 \times 10^{-3}$	16 - 32
6	0.19	3.10		>32

APPENDIX "B"  
TEST CONDITIONS AND PARTICLE DATA

TABLE B-1. TEST CONDITIONS AND PARTICLE DATA

MOBILE BED SCRUBBER: 1-STAGE  
 PACKING DIAMETER: 3.8 CM  
 SUPPORTING AND RETAINING GRIDS: HARDWARE SCREEN  
 AEROSOL: TITANIUM DIOXIDE

Run No.	$u_G$ (m/s)	$Q_G$ (m <sup>3</sup> /min)	$Q_L$ (l/min)	$\Delta P_w$ (cm W.C.)	$H_s$ (cm)	$H_d$ (cm)	$d_{pg}$ , $\mu m$		$\sigma_g$		$c_p$ , mg/DNm <sup>3</sup>		$\overline{P\overline{t}}$ (s)	$d_{pc}$ ( $\mu m$ )
							Inlet	Outlet	Inlet	Outlet	Inlet	Outlet		
C1-1	2.9	35.4	293	5.6	30	60	1.9	1.8	2.3	2.1	37.6	31.6	84.0	7.7
C1-2	2.9	35.4	293	5.6	30	60	2.0	2.1	2.1	1.9	78.6	60.2	76.6	8.6
C1-3	2.9	35.4	293	5.6	30	60	2.3	2.1	1.9	1.8	49.2	38.8	78.9	6.2
C1-4	2.9	35.4	293	5.6	30	60	2.0	2.2	2.0	1.8	71.8	58.9	82.0	7.5
C1-5	2.9	35.4	208	4.6	30	60	2.2	2.1	2.0	1.9	64.0	53.2	83.1	8.0
C1-6	2.9	35.4	197	4.8	30	63	2.3	2.5	2.2	1.9	143.8	97.3	67.7	9.5
C1-7	2.9	35.4	197	5.0	30	63	2.4	2.3	2.0	1.9	109.7	83.9	76.5	8.6
C1-8	2.9	35.4	197	5.2	30	58	2.0	2.0	1.9	1.8	54.3	44.4	81.8	7.6
C1-9	2.9	35.4	197	5.2	30	63	2.3	2.3	2.0	1.8	61.6	44.1	71.6	7.1
C1-10	2.2	26.9	227	5.1	30	58	1.8	2.0	1.7	1.6	33.6	30.1	89.6	8.0
C1-11	2.2	26.9	185	4.6	30	47	2.0	2.1	1.7	1.6	25.7	21.8	84.5	7.0
C1-12	2.2	26.9	185	4.6	30	47	2.6	2.7	1.7	1.6	24.9	18.4	73.9	8.6
C1-13	2.4	29.5	269	4.9	30	60	2.2	2.3	1.9	1.8	107.9	87.8	81.4	9.0
C1-14	2.4	29.5	269	4.9	30	60	2.1	2.2	2.0	1.8	128.1	103.5	80.8	10.5

TABLE B-2. TEST CONDITIONS AND PARTICLE DATA

MOBILE BED SCRUBBER: 2-STAGE  
 PACKING DIAMETER: 3.8 CM  
 SUPPORTING AND RETAINING GRIDS: HARDWARE SCREEN  
 AEROSOL: RED IRON OXIDE

Run No.	$u_G$ (m/s)	$Q_G$ (m <sup>3</sup> /min)	$Q_L$ (l/min)	$\Delta P_w$ (cm W.C.)	$H_s$ (cm)	$H_d$ (cm)	$d_{pg}$ , $\mu m$		$\sigma_g$		$c_p$ , mg/DNm <sup>3</sup>		$\overline{P\overline{t}}$ (s)	$d_{pc}$ ( $\mu m$ )
							Inlet	Outlet	Inlet	Outlet	Inlet	Outlet		
C2-1	3.1	37.9	136	5.3	15	32	1.8	1.9	1.9	1.8	52.0	36.1	69.4	7.9
C2-2	3.1	37.9	136	4.9	15	32	1.7	1.7	1.8	1.7	66.3	53.1	80.1	6.8
C2-3	2.6	31.2	136	5.0	15	30	1.9	1.9	1.9	1.8	57.5	38.0	66.1	7.4
C2-4	2.6	31.2	136	5.0	15	30	2.2	2.1	1.9	1.8	60.5	41.5	68.6	9.2
C2-5	2.6	31.2	136	5.0	15	30	1.9	2.0	2.0	1.9	75.9	58.6	72.2	9.8
C2-6	2.6	31.2	136	4.7	15	32	1.9	1.8	1.7	1.7	36.2	31.1	85.9	7.6
C2-7	2.0	24.0	136	4.8	15	30	2.1	2.1	1.9	1.8	69.1	49.1	71.1	9.6
C2-8	2.0	24.0	227	5.7	15	30	1.9	1.8	1.9	1.9	110.4	75.1	68.0	8.5
C2-9	2.0	24.0	227	5.7	15	30	2.3	2.3	2.0	1.9	97.4	73.2	75.2	9.0
C2-10	2.0	24.0	310	6.0	15	30	2.4	2.1	2.0	2.0	71.7	47.5	66.2	6.0
C2-11	2.0	24.0	136	8.9	30	43	1.9	1.8	2.2	1.8	49.3	28.1	57.0	3.6
C2-12	2.0	24.0	136	8.9	30	43	1.9	1.8	2.1	1.7	57.1	31.7	55.5	3.5
C2-13	3.1	37.9	136	9.4	30	60	2.4	2.4	2.0	1.8	165.3	94.9	57.4	5.5

TABLE B-3. TEST CONDITIONS AND PARTICLE DATA

MOBILE BED SCRUBBER: 2-STAGE  
 PACKING DIAMETER: 2.5 CM  
 RETAINING AND SUPPORTING GRIDS: HARDWARE SCREENS  
 AEROSOL: CUPOLA DUST

Run No.	$u_G$ (m/s)	$Q_G$ (m <sup>3</sup> /min)	$Q_L$ (l/min)	$\Delta P_w$ (cm W.C.)	$H_s$ (cm)	$H_d$ (cm)	$d_{pg}$ , $\mu m$		$\sigma_g$		$c_p$ , mg/DNm <sup>3</sup>		$\overline{P\overline{t}}$ (s)	$d_{pc}$ ( $\mu m$ )
							Inlet	Outlet	Inlet	Outlet	Inlet	Outlet		
C2-14	2.9	35.1	269	10.5	23	53	2.4	1.9	2.3	1.8	57.3	29.9	52.2	2.9
C2-15	2.9	35.1	269	10.2	23	53	1.9	1.8	2.5	1.9	77.8	33.2	42.7	2.9
C2-16	2.9	35.1	352	13.6	23	60	3.4	1.6	3.1	1.9	86.2	37.6	43.6	3.0
C2-17	2.9	35.1	352	13.5	23	60	2.5	1.9	2.2	2.0	49.1	21.6	44.0	2.7
C2-18	4.1	49.6	269	10.3	23	70	2.8	1.7	3.0	1.9	52.1	22.4	43.0	3.3
C2-19	4.1	49.6	269	10.0	23	70	2.6	1.6	2.7	1.9	64.6	26.8	72.4	3.1
C2-20	4.1	49.6	352	14.3	23	72	3.1	1.4	2.9	1.6	79.7	11.3	14.2	1.8
C2-21	4.1	49.6	307	12.6	23	72	2.9	1.4	2.7	1.9	98.1	26.4	26.9	1.7

TABLE B-4. TEST CONDITIONS AND PARTICLE DATA

MOBILE BED: 3-STAGE  
 PACKING DIAMETER: 3.8 CM  
 SUPPORTING AND RETAINING GRIDS: HARDWARE SCREEN  
 AEROSOL: RED IRON OXIDE

Run No.	$u_G$ (m/s)	$Q_G$ (m <sup>3</sup> /min)	$Q_L$ (l/min)	$\Delta P_w$ (cm W.C.)	$H_s$ (cm)	$H_d$ (cm)	$d_{pg}$ , $\mu$ m		$\sigma_g$		$c_p$ , mg/DNm <sup>3</sup>		$\overline{P_T}$ (%)	$d_{pc}$ ( $\mu$ m)
							Inlet	Outlet	Inlet	Outlet	Inlet	Outlet		
C3-1	2.6	31.2	227	8.4	15	32	2.2	2.0	2.0	1.9	66.7	47.8	71.7	5.2
C3-2	2.6	31.2	227	8.4	15	32	2.1	1.9	1.9	1.7	74.4	51.6	69.4	4.2
C3-3	2.6	31.2	310	10.4	15	38	2.1	1.9	1.9	1.8	58.7	37.8	64.4	4.3
C3-4	2.6	31.2	310	10.4	15	38	2.1	1.9	2.0	1.8	43.9	34.0	77.4	4.5
C3-5	3.1	37.9	310	10.9	15	44	2.1	2.0	2.0	1.7	74.3	45.3	61.0	4.1
C3-6	3.1	37.9	310	10.9	15	44	2.0	2.0	1.8	1.6	46.5	29.4	63.2	3.2
C3-7	3.1	37.9	310	10.9	15	44	2.3	2.2	2.1	1.7	41.7	23.8	57.1	3.8
C3-8	3.1	37.9	227	8.9	15	38	2.1	1.9	2.1	1.7	50.9	31.7	62.3	4.4
C3-9	3.1	37.9	227	8.9	15	38	2.1	1.8	2.0	1.7	53.0	36.7	69.2	3.8
C3-10	3.1	37.9	227	8.9	15	38	2.2	2.0	1.8	1.7	51.3	35.5	69.2	4.6
C3-11	3.1	37.9	136	7.7	15	35	2.0	2.0	2.0	1.7	63.5	48.7	76.7	5.2
C3-12	3.1	37.9	136	7.7	15	35	2.2	2.4	1.9	1.8	47.8	38.5	80.5	5.7
C3-13	3.1	37.9	136	7.7	15	35	2.7	2.5	1.9	1.8	81.1	53.7	66.2	4.3
C3-14	3.1	37.9	136	7.7	15	38	2.4	2.3	1.8	1.7	72.2	49.3	68.3	5.3
C3-15	2.8	34.3	136	8.3	15	35	2.3	2.2	1.7	1.7	99.3	65.5	66.0	5.0
C3-16	2.8	34.3	136	8.3	15	35	2.2	2.1	1.9	1.7	51.5	33.9	65.8	4.5
C3-17	2.8	34.3	227	9.2	15	38	2.6	2.3	2.0	1.8	71.3	43.1	60.4	4.6
C3-18	2.8	34.3	227	9.2	15	38	2.1	2.0	2.0	1.7	51.5	33.0	64.1	3.7
C3-19	2.8	34.3	310	11.2	15	43	2.8	2.1	2.1	2.0	102.0	50.8	49.8	2.7
C3-20	2.0	24.0	136	7.3	15	28	2.4	2.2	1.8	1.7	104.5	75.3	72.1	5.3
C3-21	2.0	24.0	136	7.3	15	28	2.3	2.2	1.9	1.8	122.7	82.1	66.9	6.0
C3-22	2.0	24.0	227	7.5	15	28	2.3	2.2	1.8	1.7	88.4	56.6	64.0	5.0
C3-23	2.0	24.0	227	7.5	15	28	2.6	2.1	1.9	1.8	81.0	49.5	61.1	3.8
C3-24	2.0	24.0	310	9.0	15	30	2.3	2.1	1.9	1.8	84.2	55.9	66.4	4.2
C3-25	2.0	24.0	310	9.0	15	30	2.2	2.0	1.8	1.7	96.7	46.6	48.2	2.5
C3-26	2.3	27.8	136	7.5	15	32	2.4	2.2	1.7	1.7	110.7	73.7	66.6	5.2
C3-27	2.3	27.8	136	7.5	15	32	2.4	2.1	1.9	1.7	127.0	79.0	62.2	4.1
C3-28	2.3	27.8	227	8.9	15	32	2.3	2.2	1.8	1.7	95.0	58.7	74.2	4.5
C3-29	2.3	27.8	227	8.9	15	32	2.1	2.0	1.6	1.6	128.1	79.1	61.7	4.1
C3-30	2.3	27.8	310	10.0	15	32	2.1	2.0	1.8	1.6	134.6	70.9	52.7	3.1
C3-31	2.3	27.8	310	10.0	15	32	2.1	1.9	1.9	1.8	92.7	67.6	72.9	4.5
C3-32	2.3	27.8	136	9.8	23	40	2.2	2.0	1.7	1.6	120.4	86.9	72.2	4.1
C3-33	2.3	27.8	136	9.8	23	40	2.1	1.9	1.9	1.7	115.1	82.4	71.6	4.2
C3-34	2.3	27.8	227	10.9	23	43	2.2	1.8	1.9	1.6	119.6	83.4	69.7	3.4
C3-35	2.3	27.8	227	10.9	23	43	2.1	2.0	1.8	1.6	138.9	87.1	62.7	3.4
C3-36	2.3	27.8	310	13.1	23	47	2.1	1.9	1.7	1.7	132.0	78.0	59.1	2.9
C3-37	2.3	27.8	310	13.1	23	47	2.2	2.0	1.8	1.6	122.7	67.1	54.7	2.8
C3-38	2.6	31.1	136	11.1	23	43	2.2	1.9	1.9	1.7	91.3	54.6	59.8	3.4

TABLE B-5. TEST CONDITIONS AND PARTICLE DATA

MOBILE BED SCRUBBER: 3-STAGE  
 PACKING DIAMETER: 3.8 CM  
 SUPPORTING AND RETAINING GRIDS: HARDWARE SCREEN  
 AEROSOL: FLY ASH

Run No.	$u_G$ (m/s)	$Q_G$ (m <sup>3</sup> /min)	$Q_L$ (l/min)	$\Delta P_w$ (cm W.C.)	$H_s$ (cm)	$H_d$ (cm)	$d_{pg}$ , $\mu$ mA		$\sigma_g$		$c_p$ , mg/DNm <sup>3</sup>		PF (%)	$d_{pc}$ ( $\mu$ mA)
							Inlet	Outlet	Inlet	Outlet	Inlet	Outlet		
C3-39	2.3	27.8	310	13.1	23	47	2.4	1.8	2.3	1.6	28.7	9.7	33.8	2.4
C3-40	2.3	27.8	310	13.1	23	47	2.7	2.0	3.4	2.2	31.4	12.0	38.2	3.2
C3-41	2.3	27.8	136	9.6	23	35	2.1	2.0	2.4	2.2	21.4	12.9	60.3	5.2
C3-42	2.3	27.8	136	9.6	23	43	2.3	1.7	2.8	2.0	27.7	12.6	45.5	3.0
C3-43	2.9	35.1	310	13.8	23	53	3.7	2.0	2.8	2.3	19.9	9.7	48.7	2.4
C3-44	2.9	35.1	310	13.8	23	53	2.4	1.9	2.4	2.5	48.1	29.0	60.3	2.4
C3-45	2.9	35.1	227	11.6	23	46	2.5	2.1	2.2	2.1	73.6	33.2	45.1	2.8
C3-46	2.9	35.1	227	11.6	23	46	2.2	2.1	2.4	2.2	45.4	24.0	53.2	3.1

TABLE B-6. TEST CONDITIONS AND PARTICLE DATA

MOBILE BED SCRUBBER: 3-STAGE  
 PACKING DIAMETER: 3.8 CM  
 SUPPORTING AND RETAINING GRIDS: HARDWARE SCREEN  
 AEROSOL: CUPOLA DUST

Run No.	$u_G$ (m/s)	$Q_G$ (m <sup>3</sup> /min)	$Q_L$ (l/min)	$\Delta P_w$ (cm W.C.)	$H_s$ (cm)	$H_d$ (cm)	$d_{pg}$ , $\mu$ mA		$\sigma_g$		$c_p$ , mg/DNm <sup>3</sup>		PF (%)	$d_{pc}$ ( $\mu$ mA)
							Inlet	Outlet	Inlet	Outlet	Inlet	Outlet		
C3-47	2.9	35.1	136	10.2	23	43	2.2	2.0	2.2	1.8	30.8	14.7	47.7	3.1
C3-48	2.9	35.1	136	10.2	23	43	2.3	2.1	2.4	2.0	65.3	28.6	43.8	2.9
C3-49	2.9	35.1	227	11.6	23	46	2.4	1.8	2.5	1.8	63.3	25.8	40.8	2.7
C3-50	2.9	35.1	310	14.2	23	46	2.6	1.8	2.4	1.9	38.0	15.9	41.8	2.4
C3-51	2.9	35.1	310	13.8	23	46	2.4	1.7	2.4	2.0	47.8	17.5	36.6	1.6
C3-52	2.3	27.8	310	13.6	23	47	2.0	1.5	2.4	1.9	90.3	35.6	39.4	2.2
C3-53	2.3	27.8	310	13.6	23	47	2.3	1.7	2.5	1.9	86.1	32.1	37.3	2.2
C3-54	3.9	47.0	227	12.5	23	53	3.8	2.1	2.6	1.9	18.1	6.4	35.4	2.7
C3-55	3.9	47.0	227	12.5	23	53	5.0	1.8	2.6	2.2	14.6	4.0	27.4	2.2
C3-56	3.9	47.0	227	12.5	23	53	2.8	2.1	2.2	1.9	34.9	17.5	50.1	2.5
C3-57	3.9	47.0	227	12.5	23	53	2.8	1.6	2.9	1.7	57.3	18.5	32.3	2.3
C3-58	3.9	47.0	310	14.3	23	62	2.8	1.5	2.5	2.1	23.3	11.3	48.5	2.4
C3-59	3.9	47.0	310	14.3	23	62	2.5	1.3	2.6	1.7	40.1	16.4	40.9	2.1
C3-60	3.9	47.0	136	9.7	23	50	2.2	1.8	2.8	1.8	24.7	14.8	59.9	3.9
C3-61	3.9	47.0	352	15.4	23	68	2.1	1.5	2.4	1.7	64.3	27.1	42.1	2.2
C3-62	3.9	47.0	352	15.4	23	68	2.0	1.5	2.5	2.3	82.0	40.3	49.1	2.1
C3-63	3.9	47.0	401	17.8	23	70	2.6	1.6	2.1	1.7	65.9	29.2	44.3	2.3
C3-64	3.9	47.0	401	17.1	23	70	2.5	1.3	3.1	1.7	60.9	23.7	38.9	2.2
C3-65	4.4	53.8	136	9.9	23	65	2.7	1.9	2.0	2.0	41.4	27.3	65.9	3.3
C3-66	4.4	53.8	136	10.6	23	65	2.2	1.7	2.6	2.0	47.2	28.8	61.0	3.6
C3-67	4.1	50.0	136	9.7	23	58	2.9	2.2	2.9	2.3	100.0	49.1	49.1	4.0
C3-68	4.1	50.0	136	9.5	23	58	2.6	1.8	3.3	2.1	90.8	41.3	45.5	3.4
C3-69	4.1	50.0	227	12.4	23	62	2.4	1.7	2.7	1.8	85.8	33.9	39.5	2.7
C3-70	4.1	50.0	227	11.9	23	62	2.5	2.0	2.5	2.1	96.1	38.1	39.6	2.2
C3-71	4.1	50.0	310	14.4	23	68	3.2	1.9	2.6	1.8	110.0	28.7	26.1	2.0
C3-72	4.1	50.0	310	14.6	23	68	3.2	1.8	2.6	1.7	59.0	16.9	28.6	1.9
C3-73	4.1	50.0	310	13.8	23	68	3.0	1.5	3.0	1.8	72.1	28.0	38.8	2.5

TABLE B-7. TEST CONDITIONS AND PARTICLE DATA

MOBILE BED SCRUBBER: 3-STAGE  
 PACKING DIAMETER: 5.1 CM  
 RETAINING AND SUPPORTING GRIDS: HARDWARE SCREEN  
 AEROSOL: CUPOLA DUST

Run No.	$u_G$ (m/s)	$Q_G$ (m <sup>3</sup> /min)	$Q_L$ (l/min)	$\Delta P_w$ (cm W.C.)	$H_s$ (cm)	$H_d$ (cm)	$d_{pg}$ , $\mu m$		$\sigma_g$		$c_p$ , mg/DNm <sup>3</sup>		$\bar{P}t$ (%)	$d_{pc}$ ( $\mu m$ )
							Inlet	Outlet	Inlet	Outlet	Inlet	Outlet		
C3-74	2.9	35.1	227	9.7	23	43	2.4	1.6	2.8	2.2	114.0	59.5	52.2	3.1
C3-75	2.9	35.1	269	10.1	23	43	2.5	1.7	2.8	2.1	114.0	56.6	49.6	3.3
C3-76	2.9	35.1	352	11.8	23	53	2.1	1.6	2.5	2.2	122.0	58.7	48.1	2.9
C3-77	2.9	35.1	352	11.8	23	53	2.1	1.8	2.3	1.9	136.1	54.6	40.1	2.2
C3-78	4.1	50.0	269	10.5	23	65	2.1	1.8	2.6	1.9	69.8	38.4	55.0	3.2
C3-79	4.1	50.0	269	10.8	23	65	2.5	2.9	1.7	1.9	69.0	31.4	45.5	3.1
C3-80	4.1	50.0	352	13.1	23	68	2.6	1.5	2.6	1.8	80.3	35.7	44.5	2.5
C3-81	4.1	50.0	352	13.2	23	68	2.5	1.6	2.9	2.1	64.8	32.4	50.0	2.7

TABLE B-8. TEST CONDITIONS AND PARTICLE DATA

MOBILE BED: 3-STAGE  
 PACKING DIAMETER: 3.8 CM  
 RETAINING AND SUPPORTING GRIDS: PLASTIC NETS  
 AEROSOL: CUPOLA DUST

Run No.	$u_G$ (m/s)	$Q_G$ (m <sup>3</sup> /min)	$Q_L$ (l/min)	$\Delta P_w$ (cm W.C.)	$H_s$ (cm)	$H_d$ (cm)	$d_{pg}$ , $\mu m$		$\sigma_g$		$c_p$ , mg/DNm <sup>3</sup>		$\bar{P}t$ (%)	$d_{pc}$ ( $\mu m$ )
							Inlet	Outlet	Inlet	Outlet	Inlet	Outlet		
C3-82	4.2	50.4	363	39.5	23	70	2.5	0.96	2.4	1.6	92.3	13.0	14.1	0.93
C3-83	4.2	50.4	322	31.2	23	70	4.8	1.2	3.1	1.4	150.3	8.2	5.5	*
C3-84	4.2	50.4	322	34.2	23	70	2.3	1.1	2.4	1.7	93.0	9.8	10.5	*
C3-85	4.2	50.4	322	33.0	23	70	2.9	1.0	2.5	1.8	105.0	16.4	15.6	0.96
C3-86	4.2	50.4	322	33.0	23	70	3.2	1.1	2.5	1.8	97.0	14.4	14.8	1.1
C3-87	4.2	50.4	280	21.3	23	70	2.0	1.2	2.6	2.0	128.0	38.6	30.2	1.1
C3-88	4.2	50.4	280	23.4	23	70	2.6	1.3	2.5	1.8	90.3	25.3	28.0	1.5
C3-89	4.1	49.6	280	25.9	23	70	2.5	1.1	2.8	1.9	96.2	12.3	12.8	*
C3-90	4.1	49.6	280	25.4	23	70	2.2	0.93	2.2	1.6	100.3	19.5	19.4	1.0
C3-91	4.2	50.4	237	18.3	23	66	2.3	1.4	2.6	1.9	106.0	41.3	39.0	2.0
C3-92	4.2	50.4	237	18.3	23	66	1.4	1.2	2.7	1.7	104.0	24.9	23.7	*
C3-93	2.1	25.5	237	14.5	23	43	1.6	1.3	2.7	1.7	160.0	93.0	58.1	2.7
C3-94	2.1	25.5	237	13.1	23	43	1.2	1.2	2.4	1.6	114.0	52.6	46.1	2.2
C3-95	2.1	25.5	280	15.1	23	47	1.1	1.2	2.8	1.6	120.0	50.7	42.3	2.2
C3-96	2.1	25.5	280	15.5	23	50	1.0	1.2	2.9	1.6	137.0	50.3	36.7	2.1
C3-97	2.1	25.5	322	16.8	23	55	1.1	1.3	3.3	1.4	190.0	63.2	33.3	2.1
C3-98	3.0	36.3	387	25.4	23	-	2.2	1.2	2.7	1.7	67.2	13.0	19.3	0.96
C3-99	3.5	42.6	269	18.3	23	-	2.0	1.5	2.5	1.9	52.9	18.2	34.5	1.7



TABLE B-9. SLURRY SCRUBBING TEST CONDITIONS AND PARTICLE DATA

MOBILE BED SCRUBBER: 3-STAGE

PACKING DIAMETER: 3.8 cm

SUPPORTING AND RETAINING GRID: HARDWARE SCREEN

AEROSOL: CUPOLA DUST

Run No.	$u_G$ (m/s)	$Q_G$ (m <sup>3</sup> /min)	$Q_L$ (l/min)	$\Delta P_w$ (cm W.C.)	$H_s$ (cm)	wt % in Slurry	$d_{pg}$ , $\mu m$		$\sigma_g$		$C_p$ , mg/DNm <sup>3</sup>		$\overline{P_t}$ (%)	$d_{pc}$ ( $\mu m$ )
							Inlet	Outlet	Inlet	Outlet	Inlet	Outlet		
S3-1	2.8	34	227	12.0	23	5	2.4	2.0	2.1	1.9	38.8	16.6	42.8	2.3
S3-2	2.8	34	310	14.1	23	5	2.4	1.6	2.3	1.9	37.9	13.5	35.6	1.9
S3-3	3.4	41	227	12.3	23	5	2.5	1.9	2.2	2.1	56.4	29.8	52.8	3.0
S3-4	3.4	41	310	14.3	23	5	2.5	1.7	2.2	1.8	45.5	21.9	48.1	2.6
S3-5	2.8	34	227	12.0	23	10	2.5	1.7	2.2	1.9	76.3	37.1	48.6	2.5
S3-6	2.8	34	227	12.0	23	10	2.6	1.8	2.3	1.8	83.0	34.5	41.6	2.7
S3-7	2.8	34	310	13.8	23	10	3.0	1.8	2.3	2.0	87.1	30.9	35.5	2.2
S3-8	3.4	41	227	12.3	23	10	3.0	1.9	2.6	1.9	73.9	28.6	38.7	2.7
S3-9	3.4	41	310	14.1	23	10	2.3	1.7	2.1	1.8	73.4	30.7	41.8	1.9
S3-10	2.8	34	227	12.0	23	10	--	--	--	--	--	0.2	--	--
S3-11	2.8	34	310	13.5	23	10	--	--	--	--	--	0.2	--	--
S3-12	3.4	41	227	12.6	23	10	--	--	--	--	--	0.3	--	--
S3-13	3.4	41	310	14.0	23	10	--	--	--	--	--	0.3	--	--
S3-14	2.8	34	227	11.7	23	10	--	--	--	--	--	0.2	--	--
S3-15	2.8	34	310	12.9	23	10	--	--	--	--	--	0.2	--	--
S3-16	3.4	41	227	12.2	23	10	--	--	--	--	--	0.3	--	--
S3-17	3.4	41	310	13.8	23	10	--	--	--	--	--	0.4	--	--

TABLE B-10. F/C SCRUBBING TEST CONDITIONS AND PARTICLE DATA

MOBILE BED: 3-STAGE

 $d_h = 3.8$  CM $H_s = 23$  CM

RETAINING AND SUPPORTING GRIDS: HARDWARE SCREEN

AEROSOL: CUPOLA DUST

Run No	$u_G$ (m/s)	$Q_G$ (m <sup>3</sup> /min)	$Q_L$ (l/min)	$\Delta P_w$ (cm W.C.)	Inlet Gas Temp.		Outlet Gas Temp °C	$q'$ g H <sub>2</sub> O/g DG	$d_{pg}$ , $\mu$ m		$\sigma_g$		$c_p$ , mg/DNm <sup>3</sup>		PF %	$d_{pc}$ $\mu$ m
					$T_{Db}$ , °C	$T_{Wb}$ , °C			Inlet	Outlet	Inlet	Outlet	Inlet	Outlet		
FC-1	2.8	34	273	12.6	17	-	17	0	2.0	1.9	1.9	1.5	74.4	51.6	69	2.9
FC-2	5.1	38	273	12.6	19	-	19	0	2.5	2.2	2.5	2.2	32.0	20.0	65	2.7
FC-3	5.4	41	273	12.6	20	-	20	0	2.1	1.9	2.1	1.7	41.7	28.7	57	2.5
FC-4	5.1	38	273	12.6	52	51	26	0.072	1.9	1.1	2.1	2.0	127.0	59.3	47	2.1
FC-5	5.1	38	273	12.6	52	51	26	0.072	2.6	1.2	2.7	2.0	136.0	47.2	35	2.0
FC-6	5.1	38	273	12.6	53	52	26	0.08	1.5	1.1	3.4	2.0	192.0	109.0	57	1.8
FC-7	5.1	38	273	12.6	62	58	28	0.11	1.1	0.84	3.4	2.5	166.0	91.9	55	1.7
FC-8	5.1	38	273	12.6	63	59	28	0.12	1.3	0.84	2.8	2.0	112.0	55.7	50	1.5
FC-9	5.1	38	273	12.6	66	63	29	0.15	1.6	0.98	4.3	3.5	73.2	37.1	51	1.5
FC-10	5.1	38	273	12.6	66	63	29	0.15	1.5	1.0	3.1	2.2	108.0	46.6	43	1.3
FC-11	5.1	38	273	12.9	66	63	29	0.16	1.3	0.82	3.3	2.4	133.0	58.8	44	1.2
FC-12	5.1	38	273	12.9	62	62	28	0.15	1.9	0.73	4.7	2.2	115.0	41.7	36	1.3
FC-13	5.1	38	273	12.9	63	63	28	0.17	1.4	0.78	3.2	2.1	135.0	46.4	34	1.0
FC-14	2.8	34	273	12.3	66	66	29	0.18	1.8	0.73	3.4	2.1	137.0	48.6	35	1.2
FC-15	2.8	34	273	12.6	66	66	29	0.18	1.9	0.79	2.9	1.9	100.0	28.7	29	1.1
FC-16	2.8	34	273	12.6	66	66	29	0.19	1.6	0.92	3.3	2.1	153.0	60.8	40	1.0
FC-17	5.1	38	273	12.6	66	66	29	0.18	1.6	0.96	3.1	2.3	122.0	47.7	39	1.1
FC-18	5.4	41	273	13.5	64	63	28	0.15	1.6	0.76	3.1	2.1	126.0	43.9	35	1.1
FC-19	5.4	41	273	13.5	64	62	29	0.14	1.7	0.82	3.5	2.2	132.0	43.6	33	1.1
FC-20	5.1	38	273	12.9	67	67	30	0.21	1.6	0.86	3.5	2.0	99.1	35.8	36	1.0
FC-21	5.4	41	273	13.5	63	63	29	0.16	1.7	0.78	2.9	2.1	52.1	17.2	33	1.1
FC-22	5.4	41	273	13.5	63	60	29	0.13	1.8	0.80	3.6	2.0	139.0	59.2	43	1.4

TABLE B-11. F/C SCRUBBING TEST CONDITIONS AND PARTICLE DATA

MOBILE BED: 3-STAGE

 $d_h = 3.8$  CM $H_s = 23$  CM

RETAINING AND SUPPORTING GRIDS: PLASTIC NET

AEROSOL: CUPOLA DUST

Run No	$u_G$ (m/s)	$Q_G$ (m <sup>3</sup> /min)	$Q_L$ (l/min)	$\Delta P_w$ (cm W.C.)	Inlet Gas Temp.		Outlet Gas Temp °C	$q'$ g H <sub>2</sub> O/g DG	$d_{pg}$ , $\mu$ m		$\sigma_g$		$c_p$ , mg/DNm <sup>3</sup>		PF %	$d_{pc}$ $\mu$ m
					$T_{Db}$ , °C	$T_{Wb}$ , °C			Inlet	Outlet	Inlet	Outlet	Inlet	Outlet		
FC-23	2.1	25	273	14.4	70	69		0.24	1.6	0.7	3.3	2.0	195.0	60.8	51	0.8
FC-24	2.1	25	273	14.4	70	68		0.23	1.6	0.65	3.4	2.0	120.0	23.7	19	0.8
FC-25	2.1	25	273	14.4	70	69		0.25	1.3	0.65	2.7	1.9	133.0	39.3	29	0.76
FC-26	2.5	31	273	15.0	69	67		0.17	1.2	0.8	4.2	2.2	226.0	110.0	48	1.3
FC-27	2.5	31	273	15.0	68	67		0.22	1.2	0.6	3.6	2.2	185.0	89.0	45	0.9

APPENDIX "C"

GRADE PENETRATION CURVES FOR  
COLD OPERATION MODE

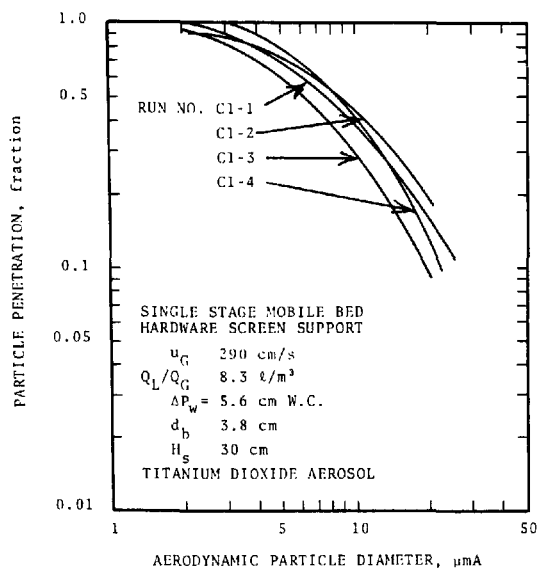


Figure C-1. Experimental grade penetration curves.

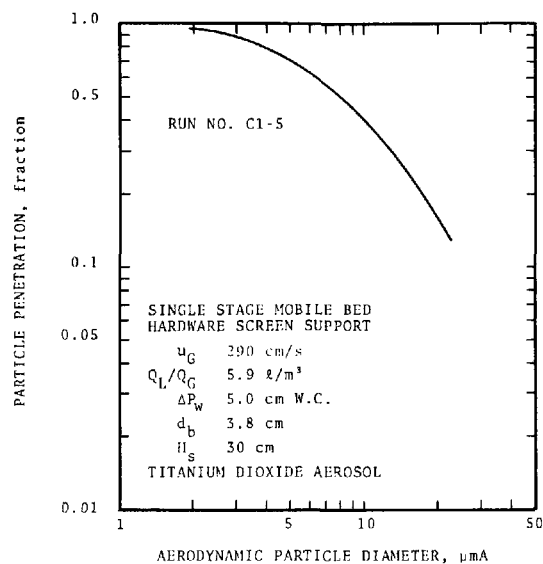


Figure C-2. Experimental grade penetration curve.

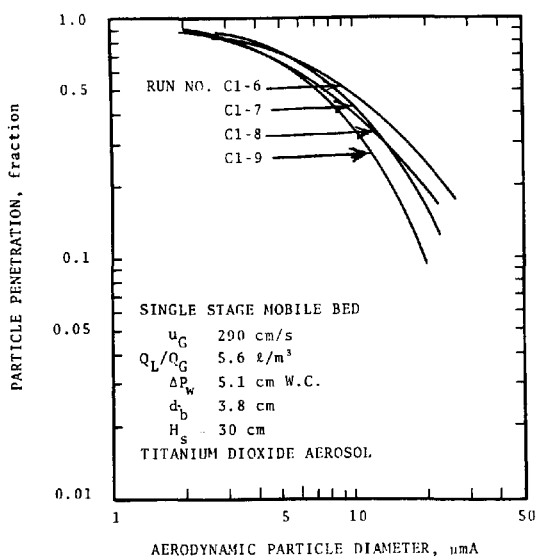


Figure C-3. Experimental grade penetration curves.

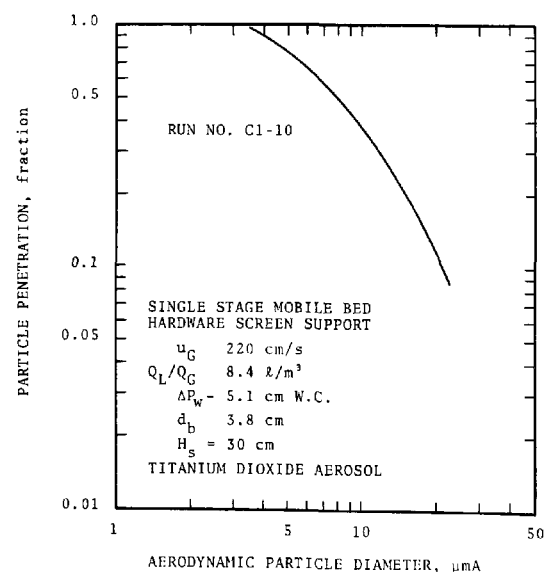


Figure C-4. Experimental grade penetration curve.

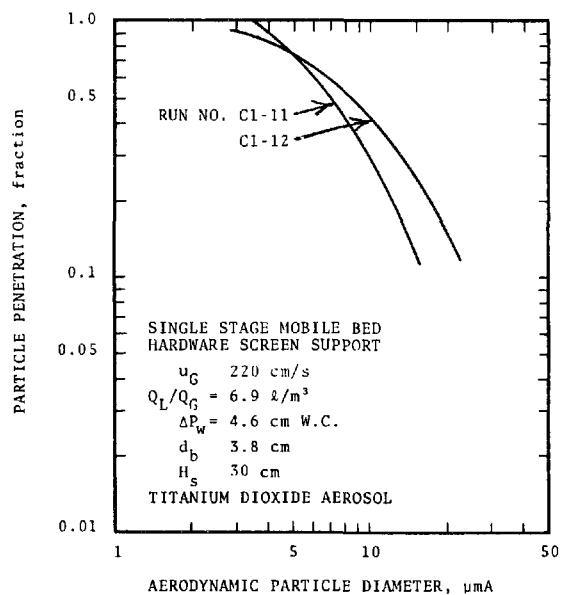


Figure C-5. Experimental grade penetration curves.

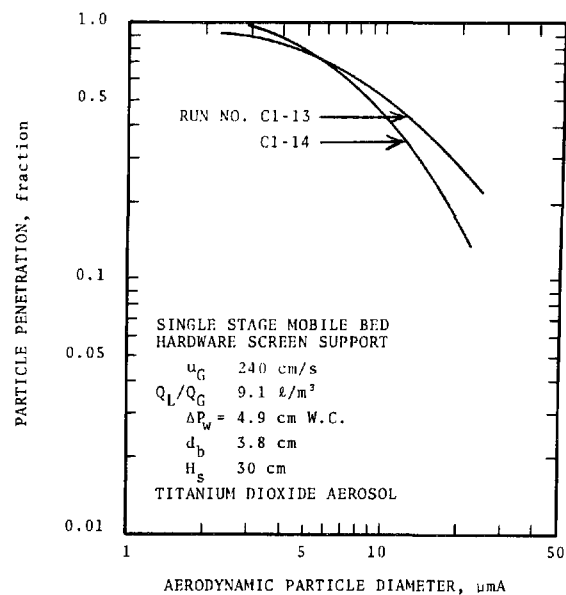


Figure C-6. Experimental grade penetration curves.

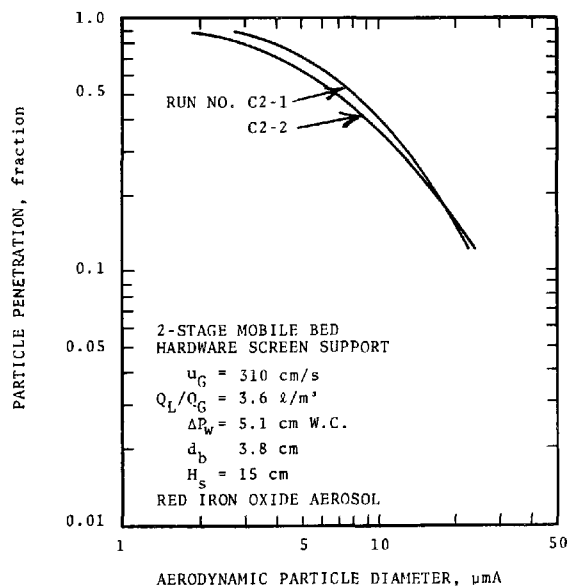


Figure C-7. Experimental grade penetration curves.

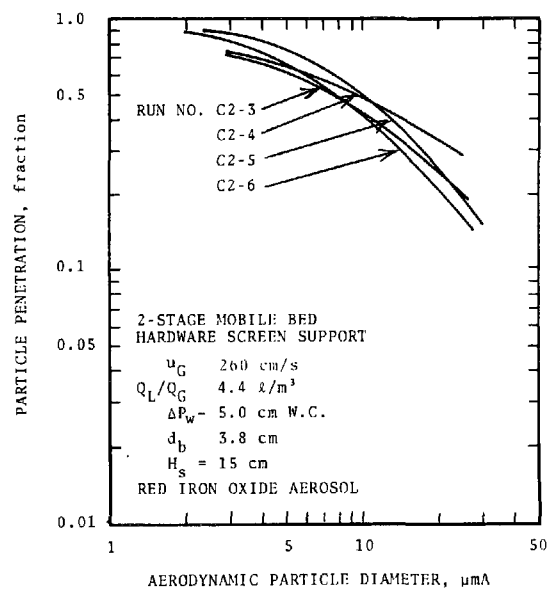


Figure C-8. Experimental grade penetration curves.

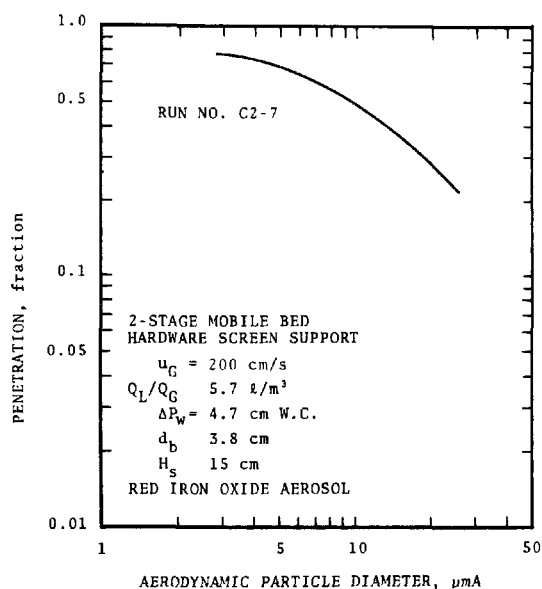


Figure C-9. Experimental grade penetration curve.

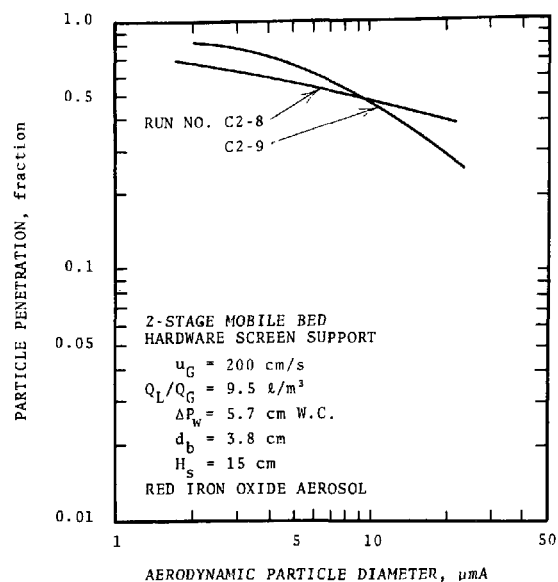


Figure C-10. Experimental grade penetration curves.

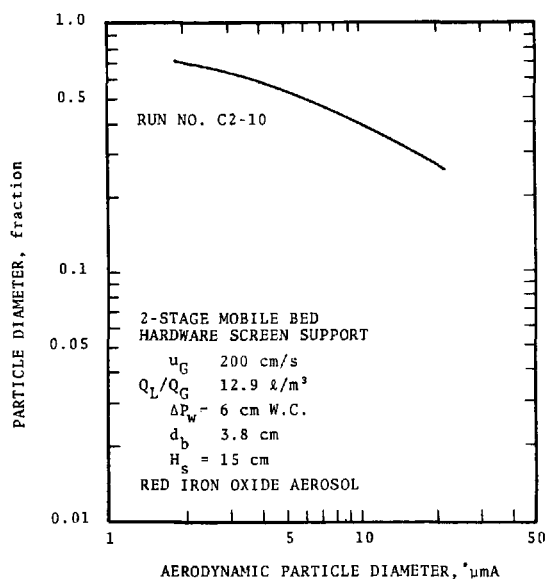


Figure C-11. Experimental grade penetration curve.

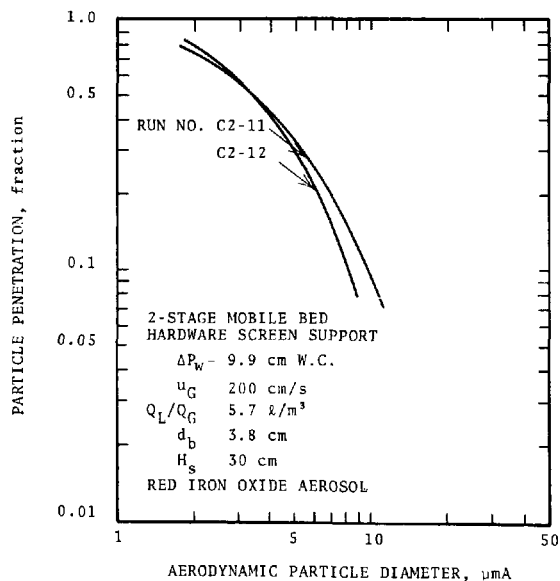


Figure C-12. Experimental grade penetration curves.

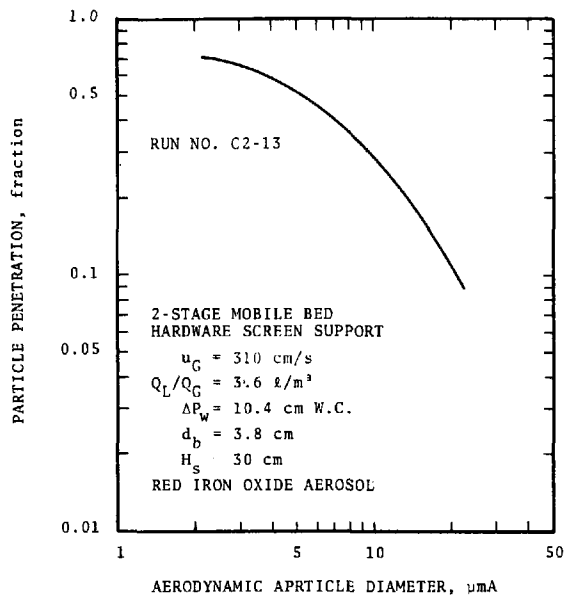


Figure C-13. Experimental grade penetration curve.

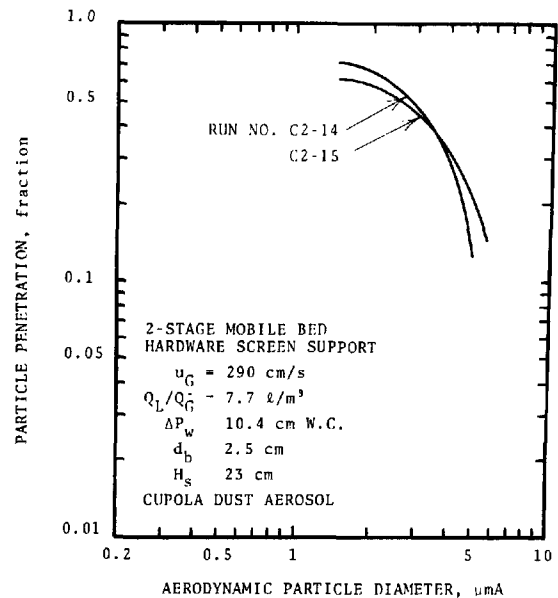


Figure C-14. Experimental grade penetration curves.

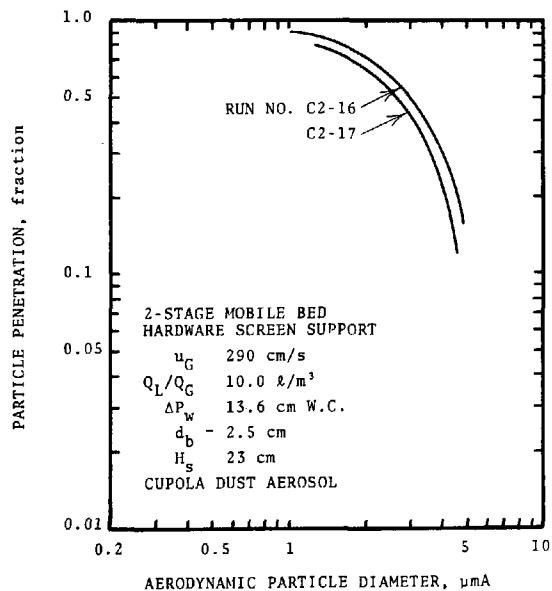


Figure C-15. Experimental grade penetration curves.

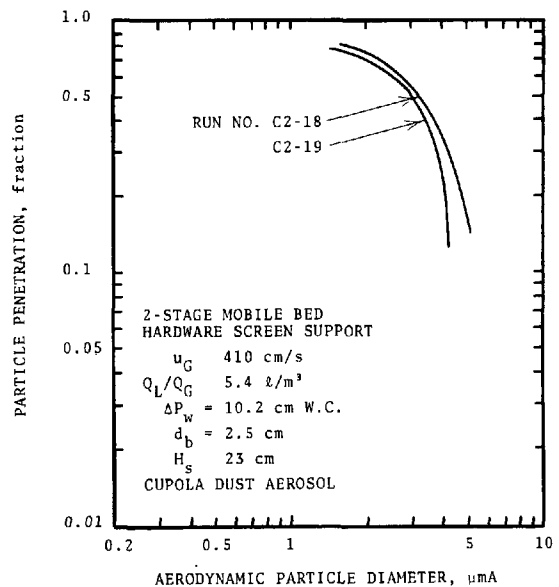


Figure C-16. Experimental grade penetration curves.

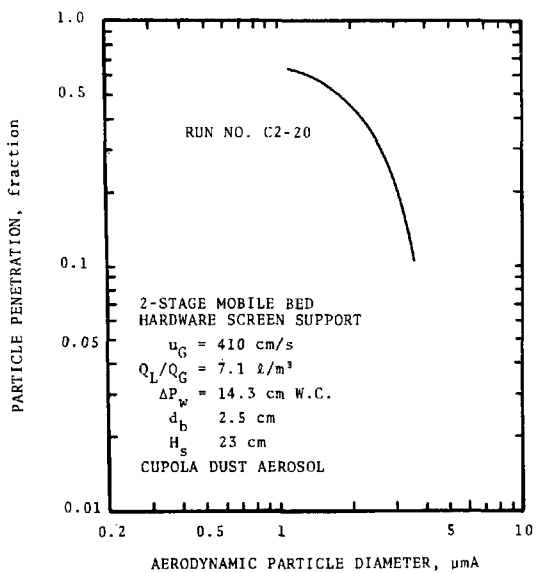


Figure C-17. Experimental grade penetration curve.

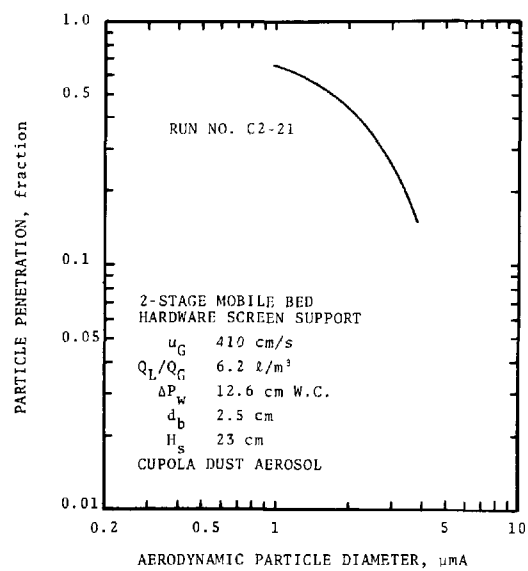


Figure C-17a. Experimental grade penetration curve.

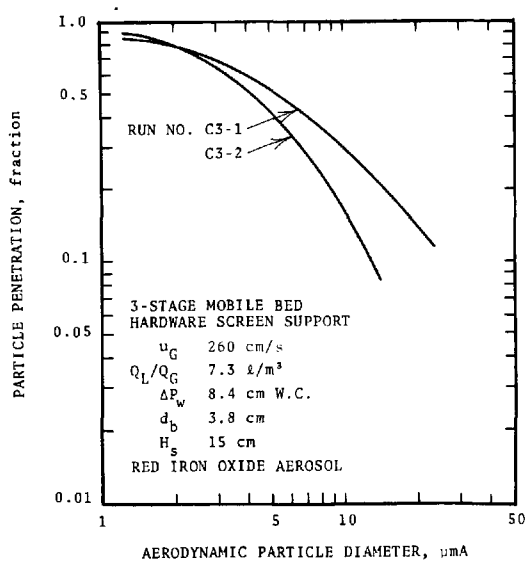


Figure C-18. Experimental grade penetration curves.

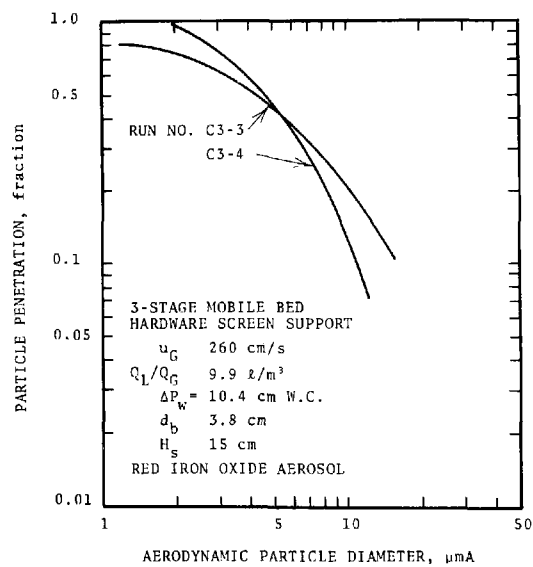


Figure C-19. Experimental grade penetration curves.



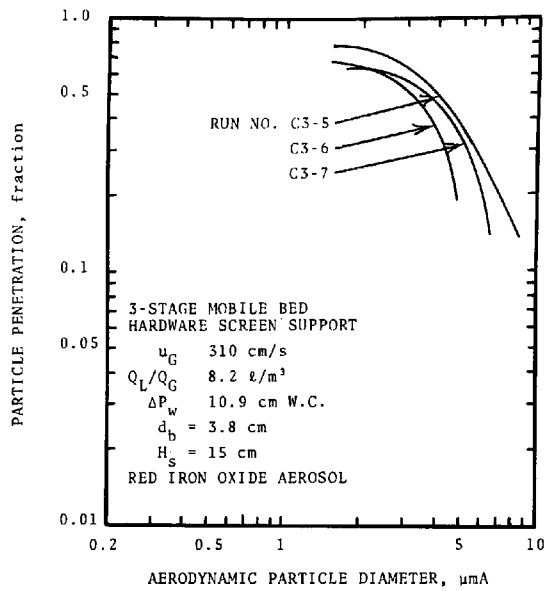


Figure C-20. Experimental grade penetration curves.

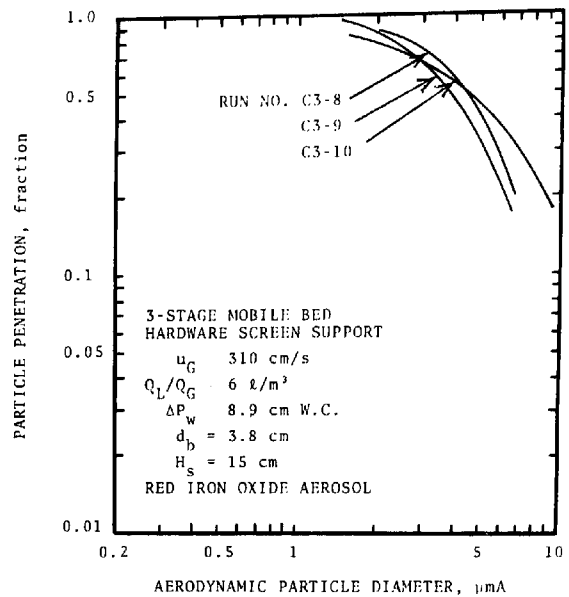


Figure C-21. Experimental grade penetration curves.

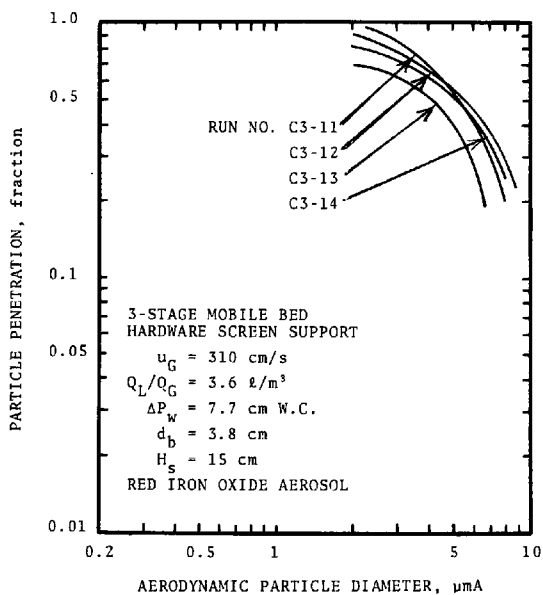


Figure C-22. Experimental grade penetration curves.

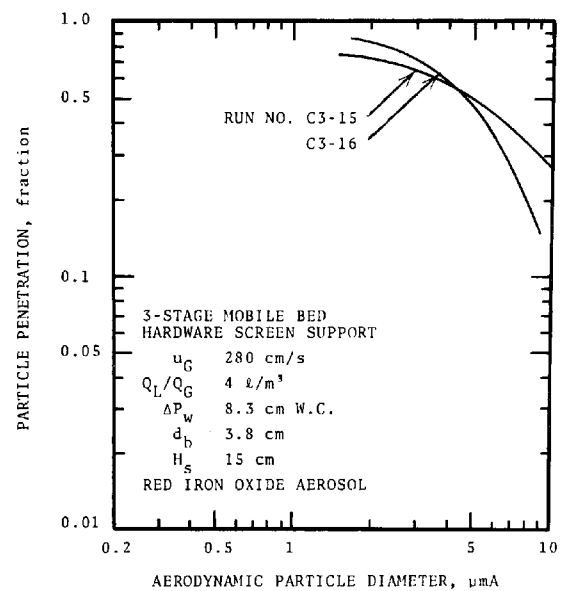


Figure C-23. Experimental grade penetration curves.

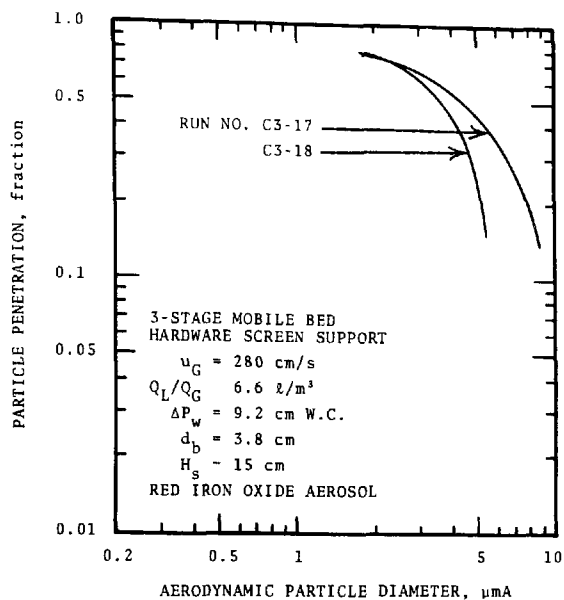


Figure C-24. Experimental grade penetration curves.

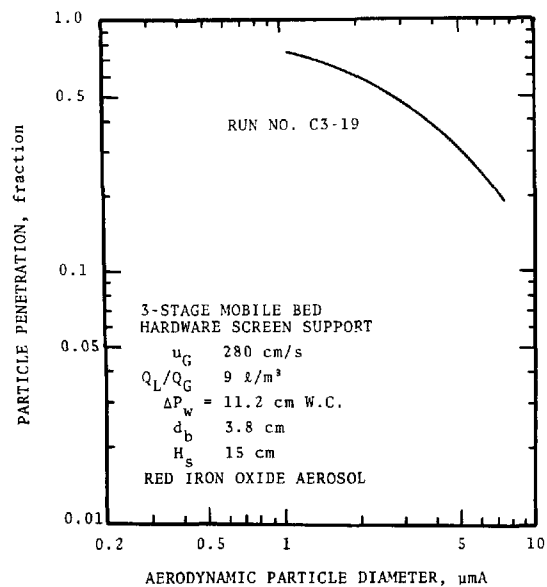


Figure C-25. Experimental grade penetration curve.

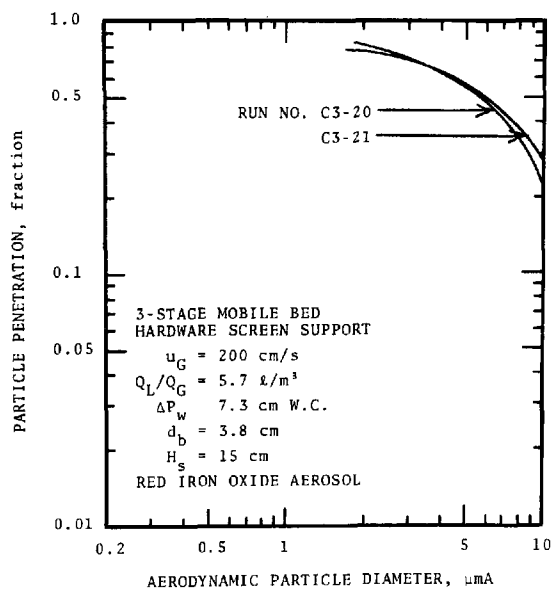


Figure C-26. Experimental grade penetration curves.

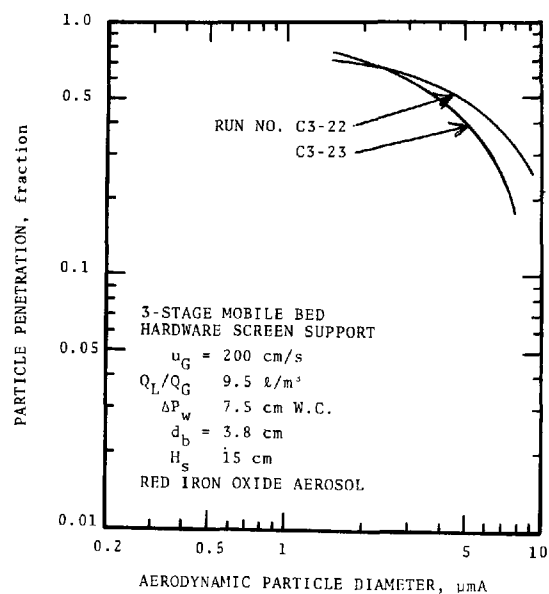


Figure C-27. Experimental grade penetration curves.

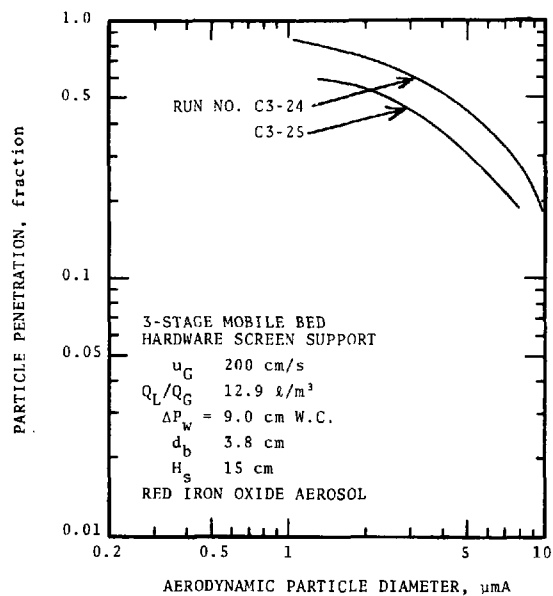


Figure C-28. Experimental grade penetration curves.

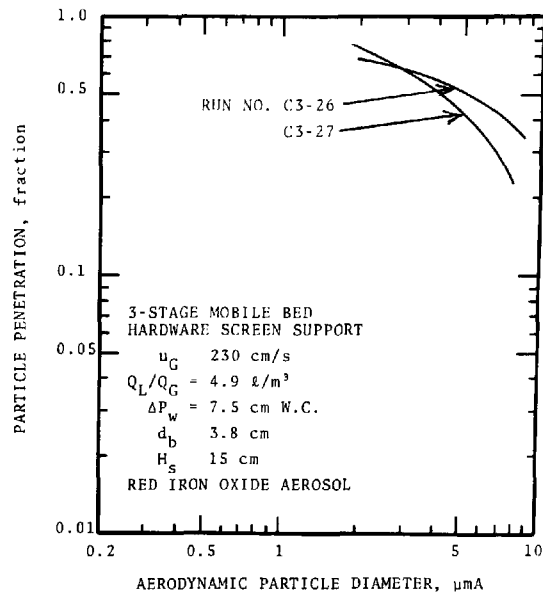


Figure C-29. Experimental grade penetration curves.

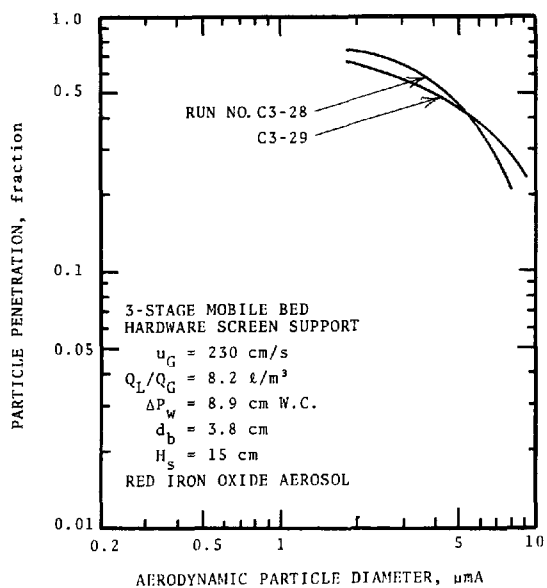


Figure C-30. Experimental grade penetration curves.

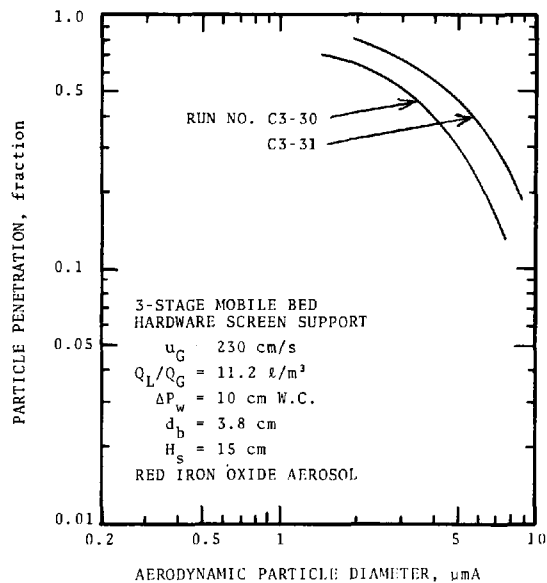


Figure C-31. Experimental grade penetration curves.

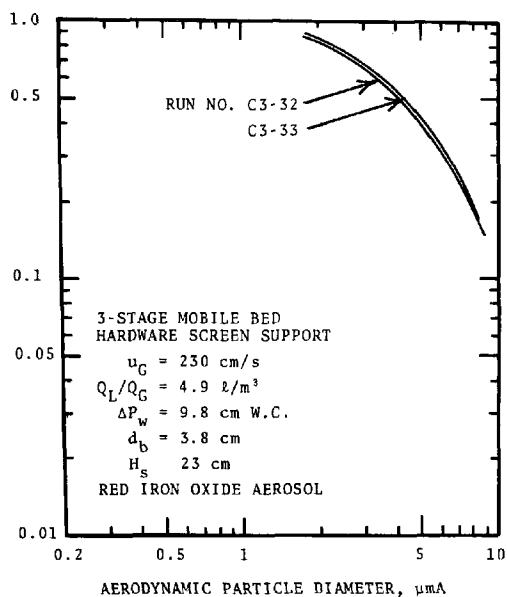


Figure C-32. Experimental grade penetration curves.

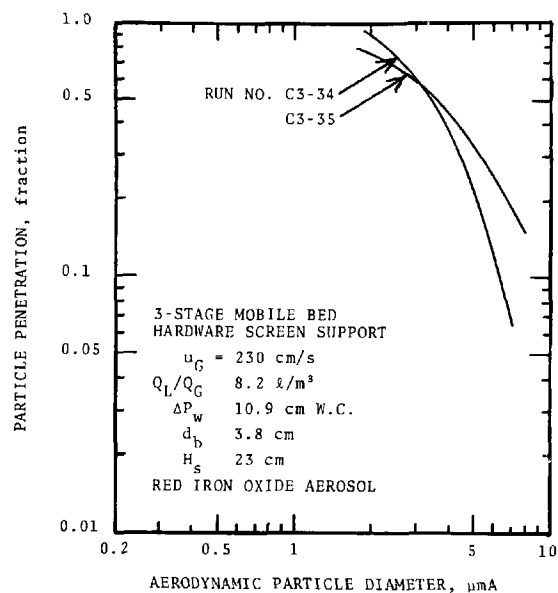


Figure C-33. Experimental grade penetration curves.

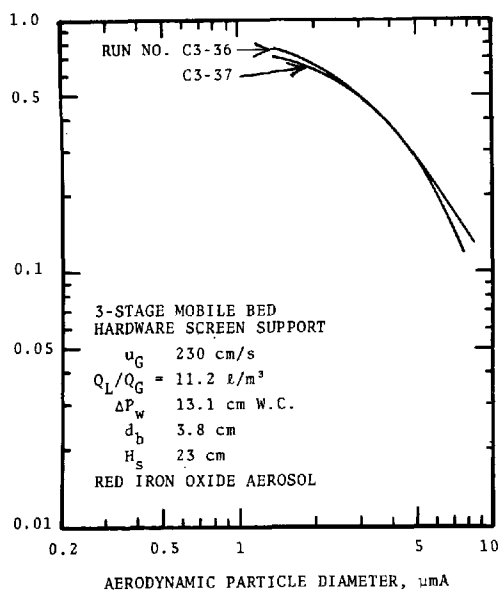


Figure C-34. Experimental grade penetration curves.

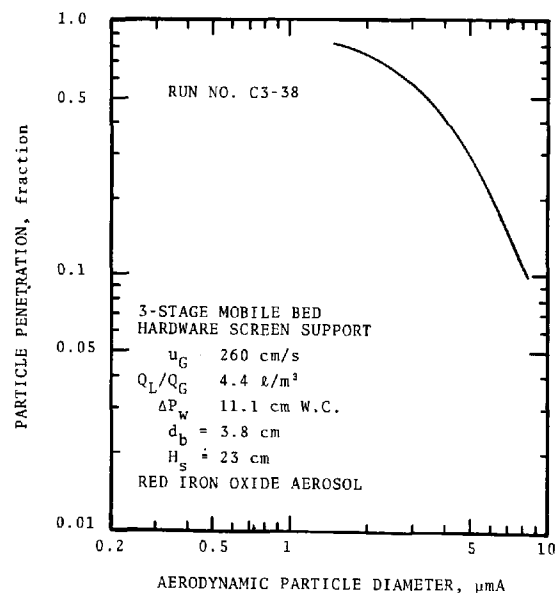


Figure C-35. Experimental grade penetration curve.

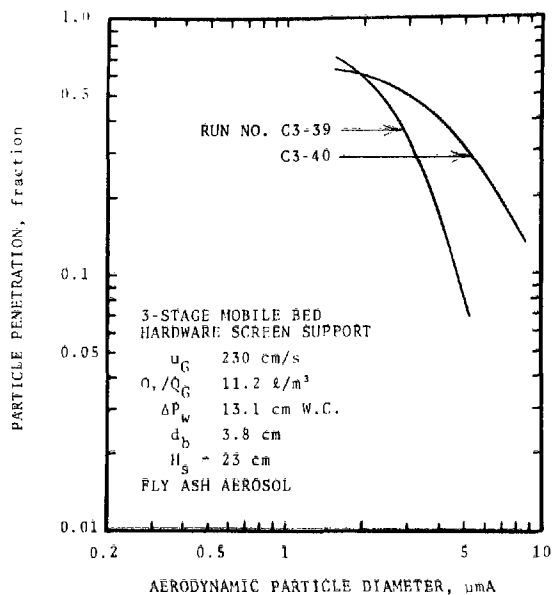


Figure C-36. Experimental grade penetration curves.

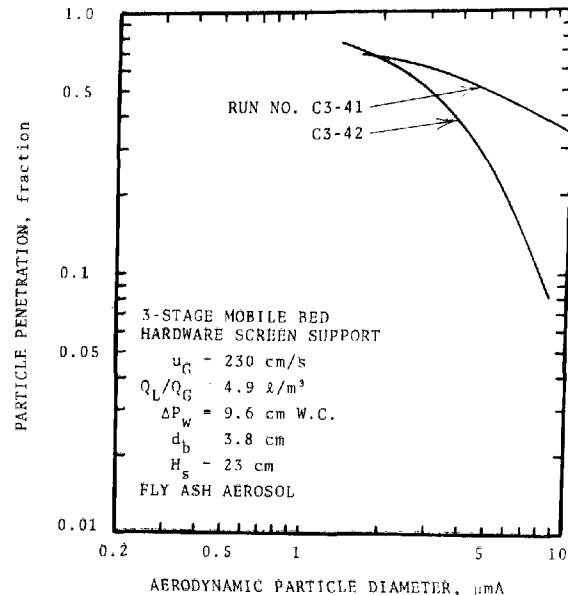


Figure C-37. Experimental grade penetration curves.

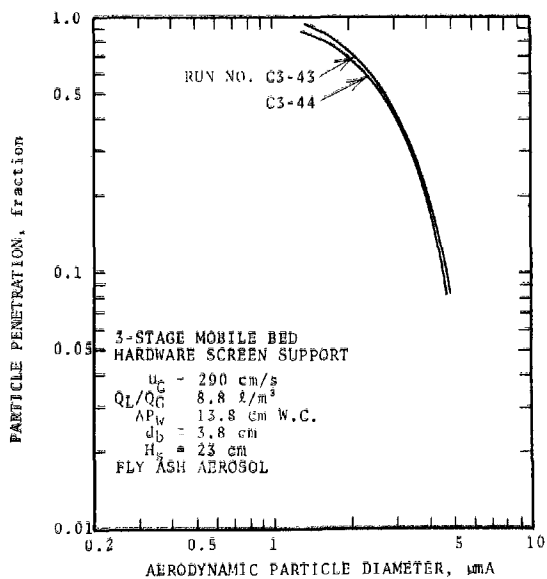


Figure C-38. Experimental grade penetration curves.

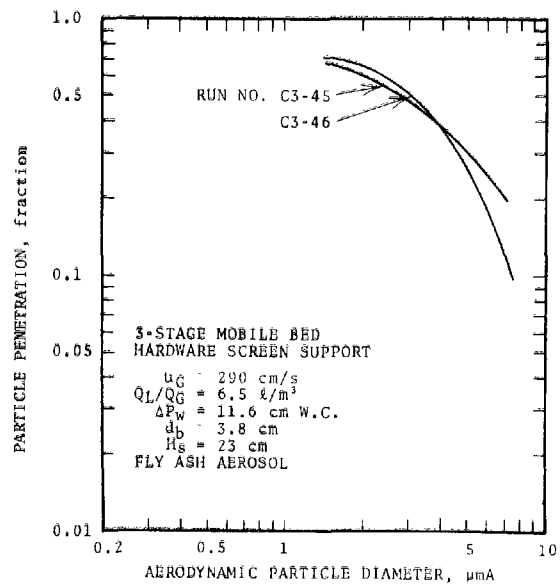


Figure 39. Experimental grade penetration curves.

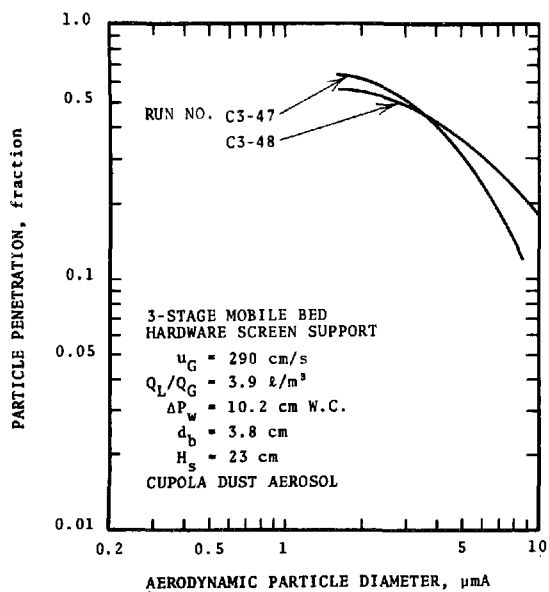


Figure C-40. Experimental grade penetration curves.

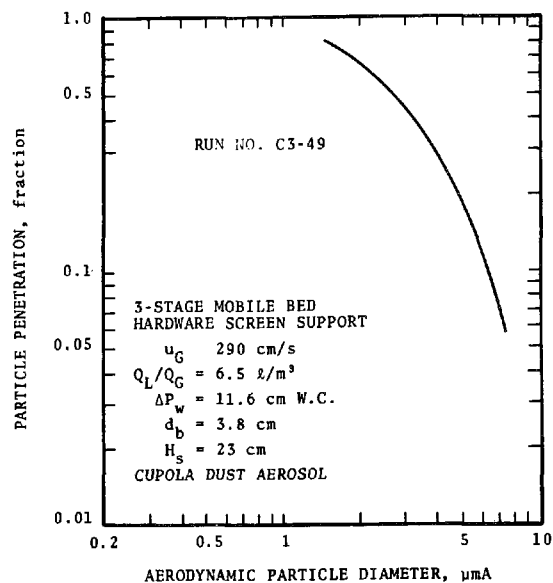


Figure C-41. Experimental grade penetration curve.

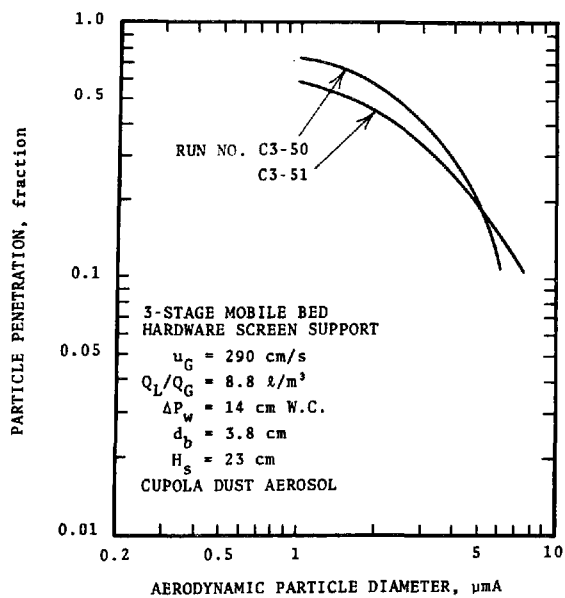


Figure C-42. Experimental grade penetration curves.

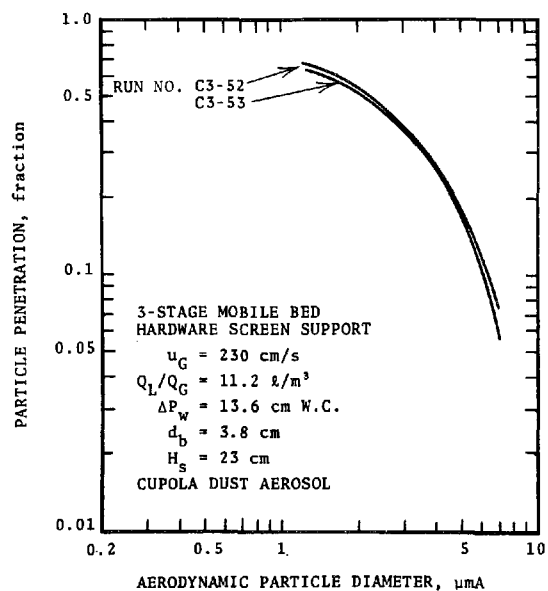


Figure C-43. Experimental grade penetration curves.

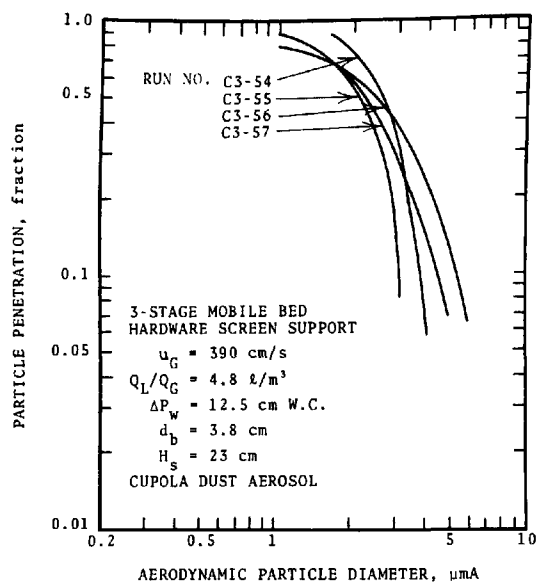


Figure C-44. Experimental grade penetration curves.

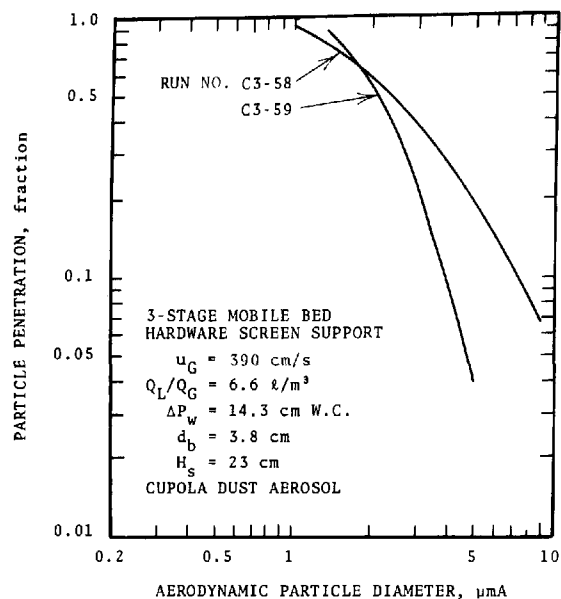


Figure C-45. Experimental grade penetration curves.

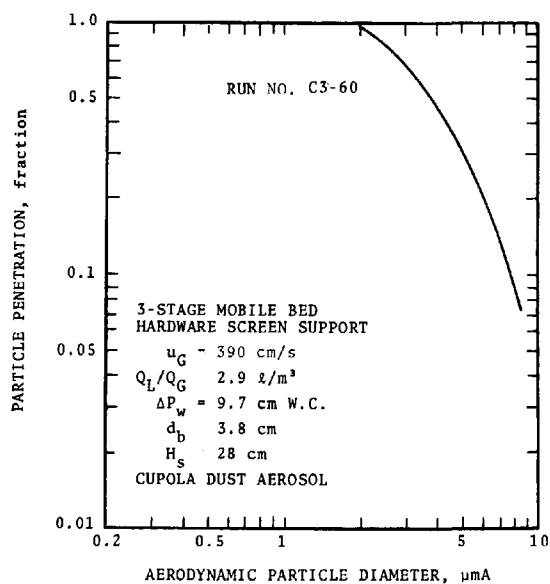


Figure C-46. Experimental grade penetration curve.

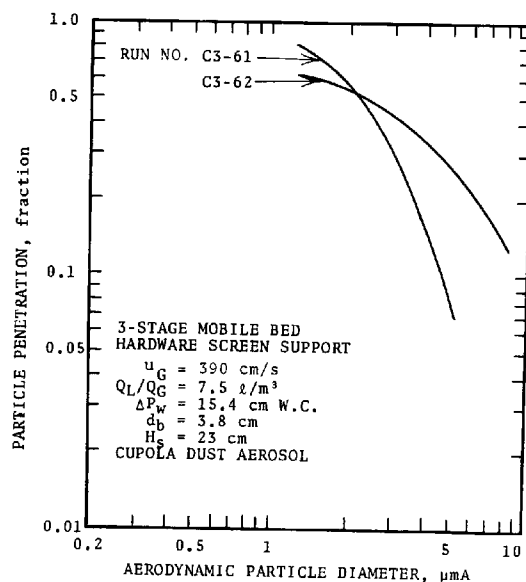


Figure C-47. Experimental grade penetration curves.

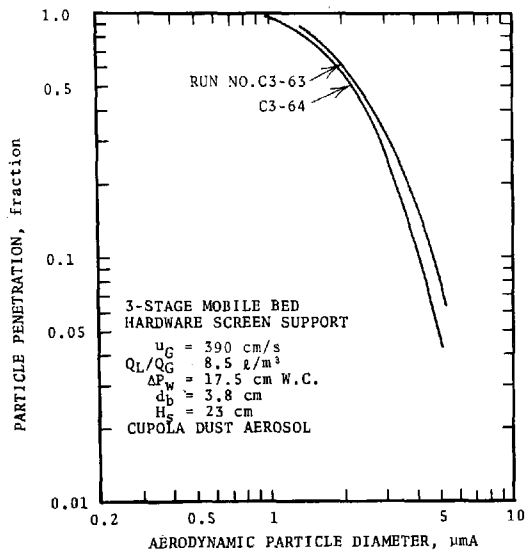


Figure C-48. Experimental grade penetration curves.

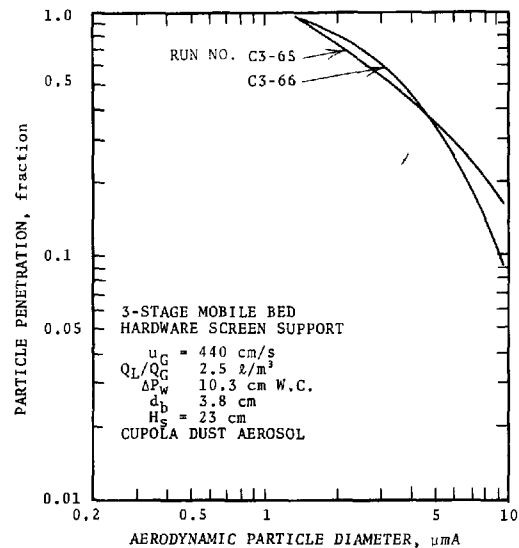


Figure C-49. Experimental grade penetration curves.

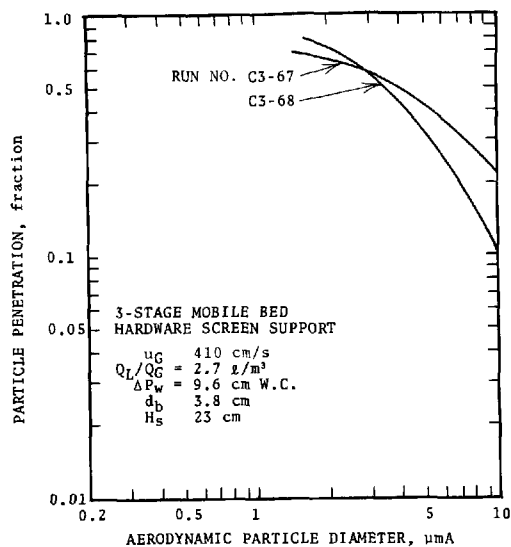


Figure C-50. Experimental grade penetration curves.

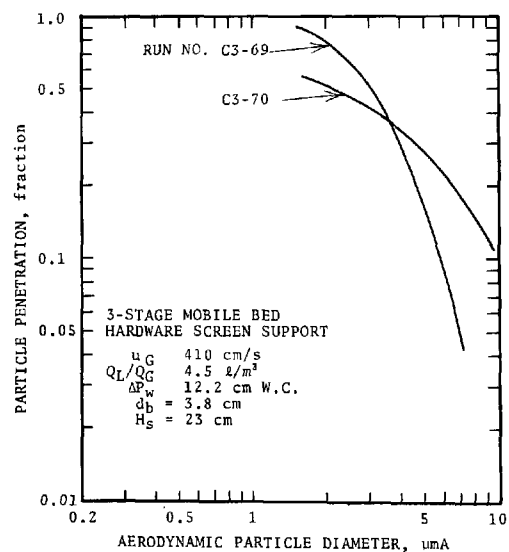


Figure C-51. Experimental grade penetration curves.



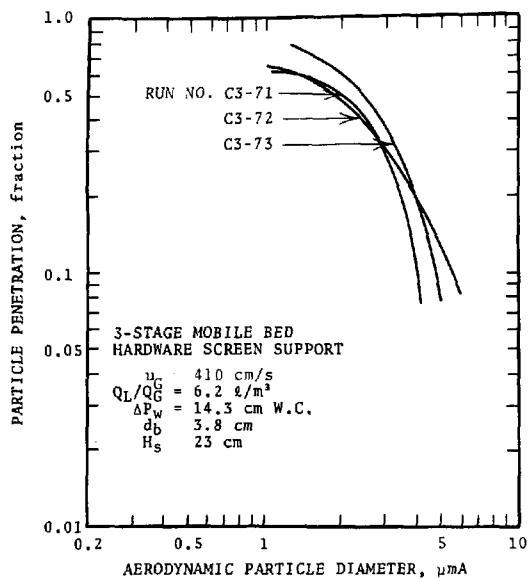


Figure C-52. Experimental grade penetration curves.

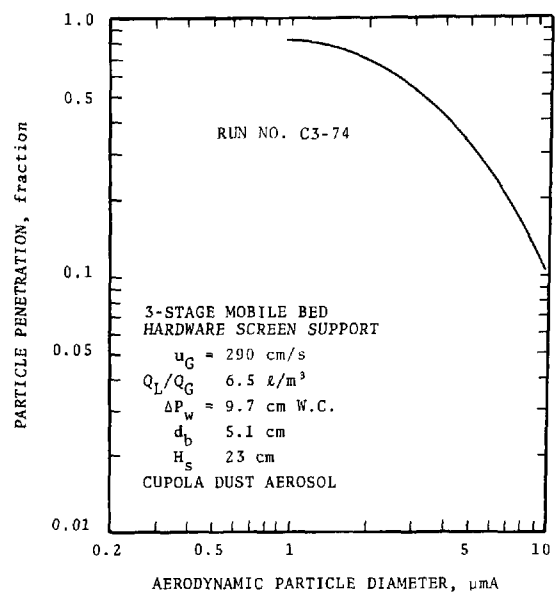


Figure C-53. Experimental grade penetration curve.

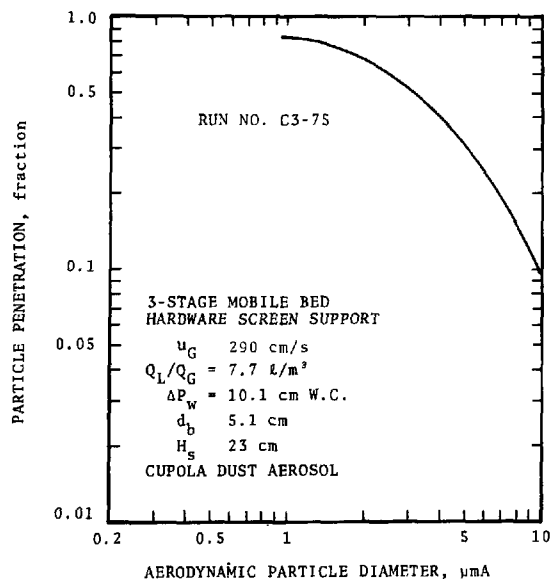


Figure C-54. Experimental grade penetration curve.

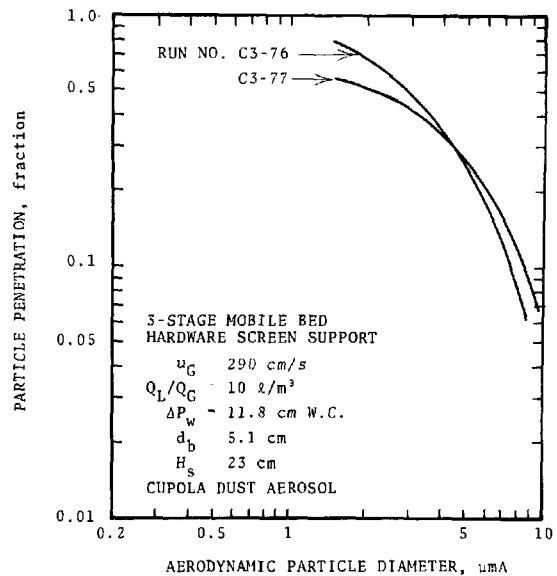


Figure C-55. Experimental grade penetration curves.

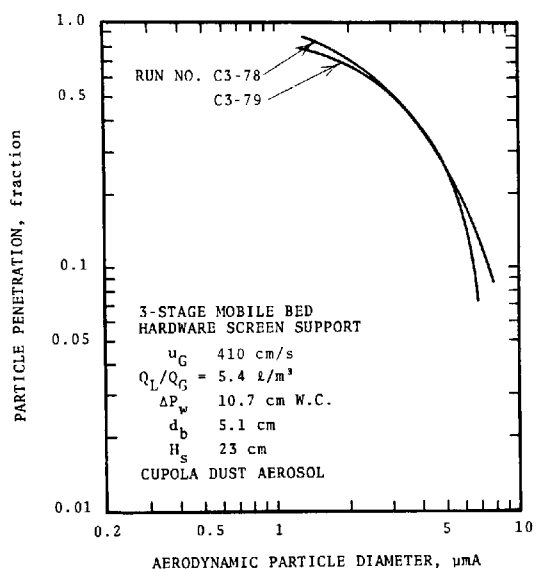


Figure C-56. Experimental grade penetration curves.

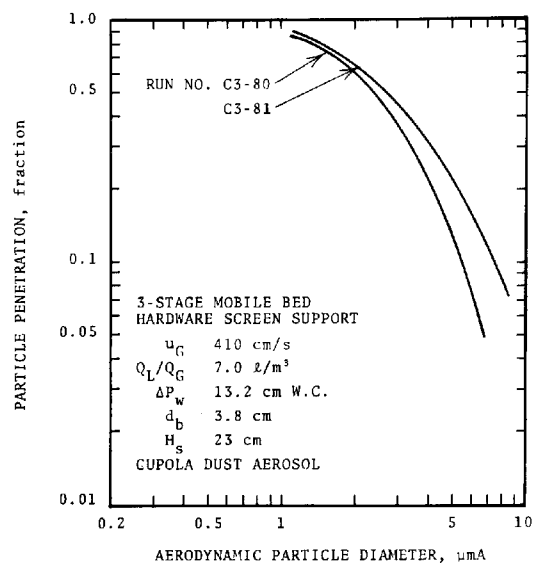


Figure C-57. Experimental grade penetration curves.

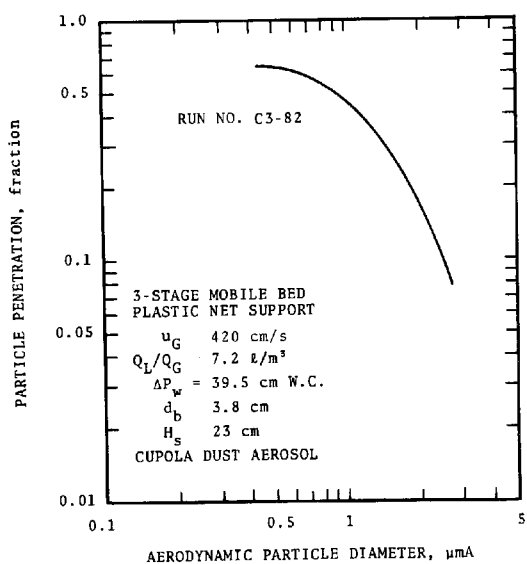


Figure C-58. Experimental grade penetration curve.

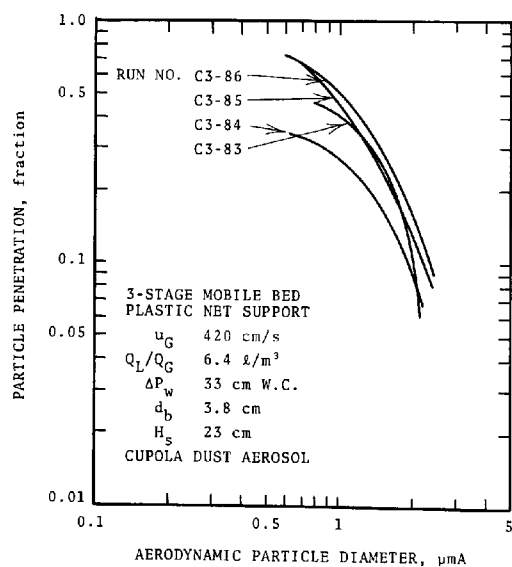


Figure C-59. Experimental grade penetration curves.

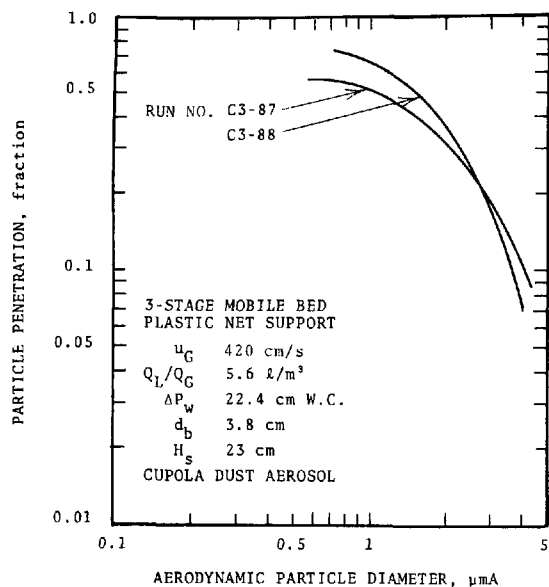


Figure C-60. Experimental grade penetration curves.

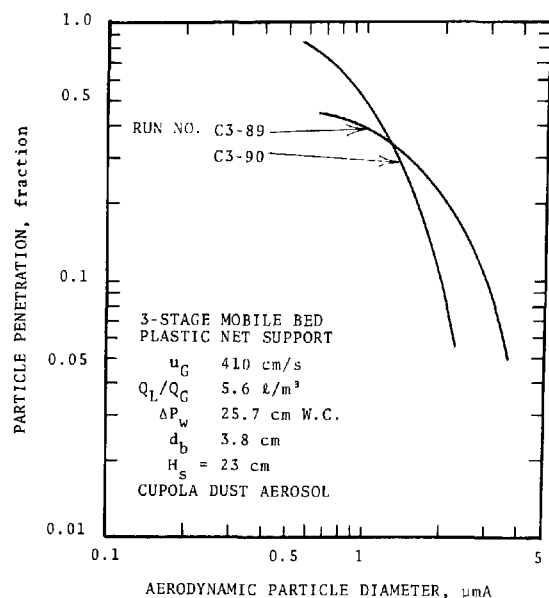


Figure C-61. Experimental grade penetration curves.

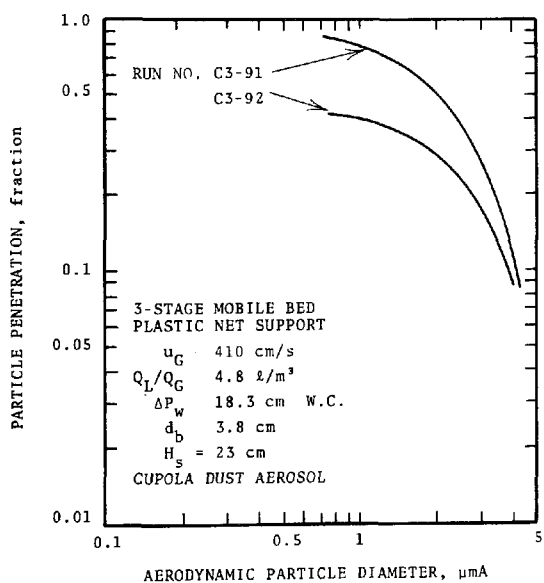


Figure C-62. Experimental grade penetration curves.

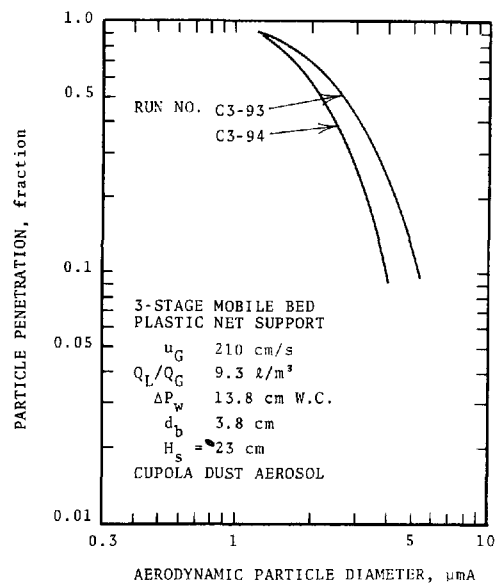


Figure C-63. Experimental grade penetration curves.

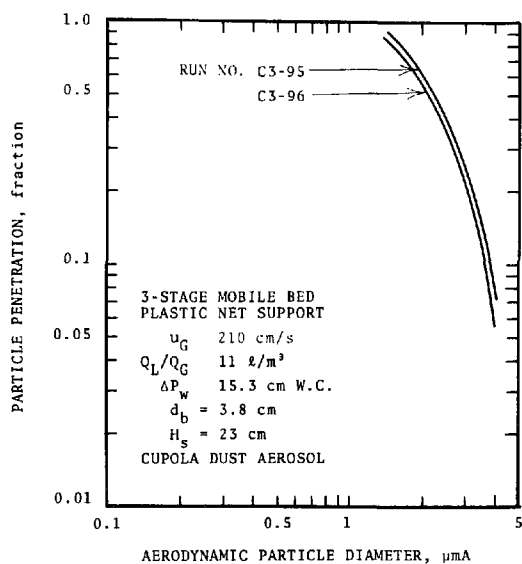


Figure C-64. Experimental grade penetration curves.

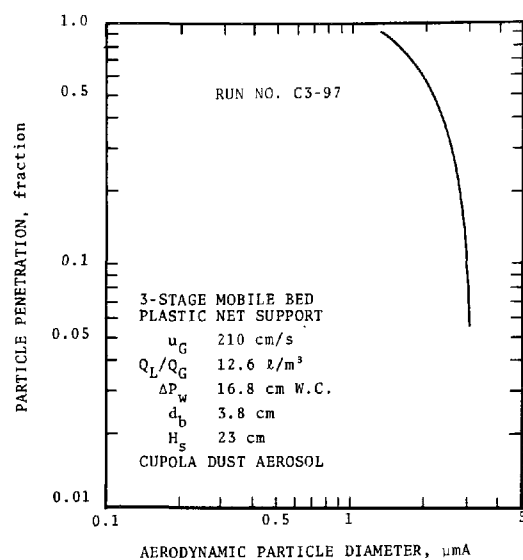


Figure C-65. Experimental grade penetration curve.

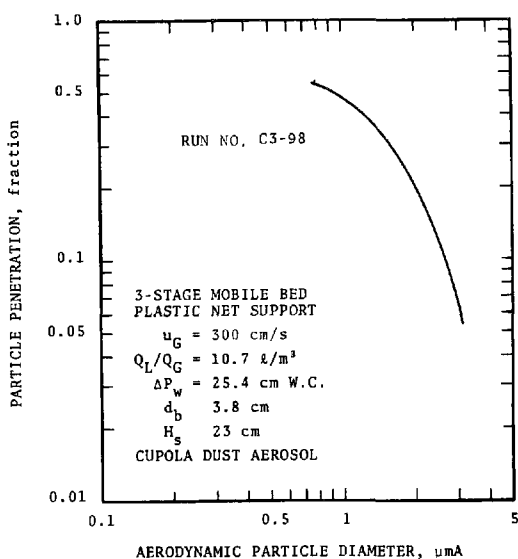


Figure C-66. Experimental grade penetration curve.

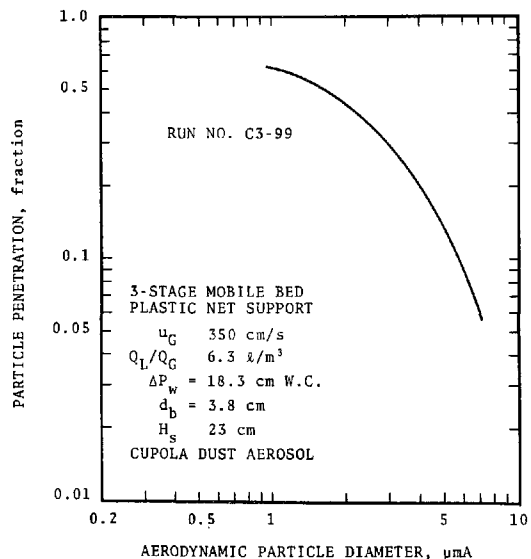


Figure C-67. Experimental grade penetration curve.

APPENDIX "D"

SLURRY SCRUBBING PENETRATION CURVES

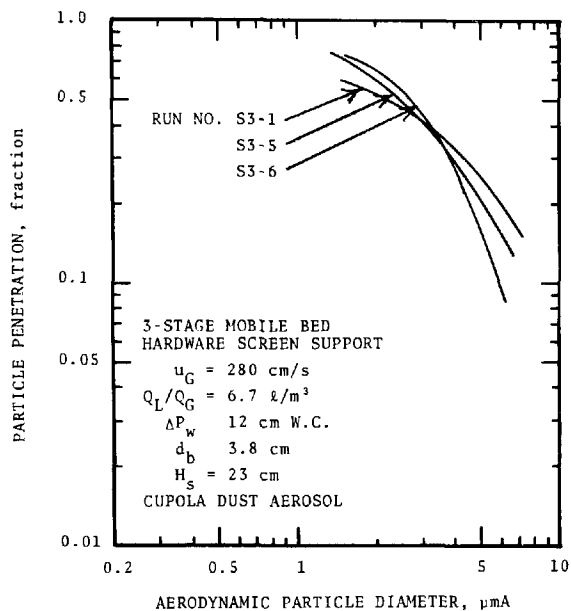


Figure D-1. Experimental penetration curves.

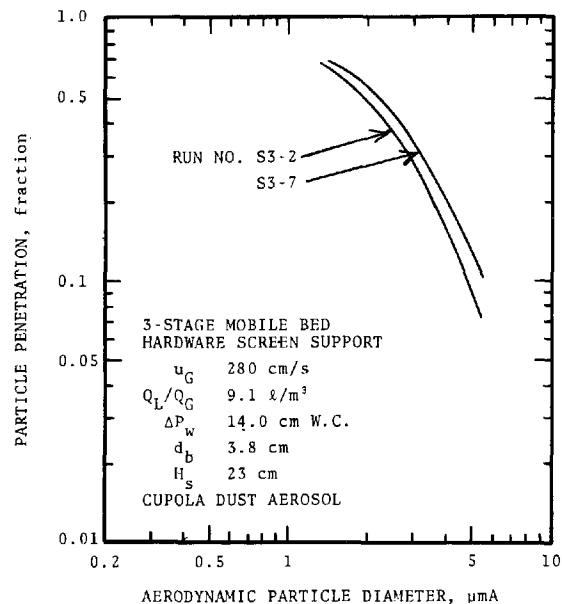


Figure D-2. Experimental penetration curves.

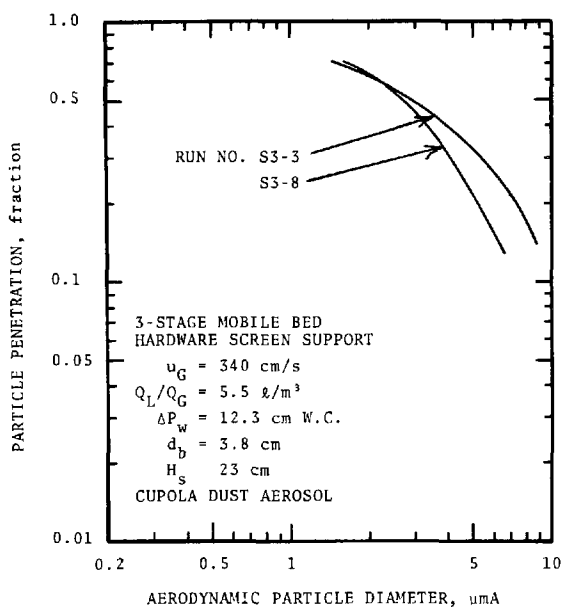


Figure D-3. Experimental penetration curves.

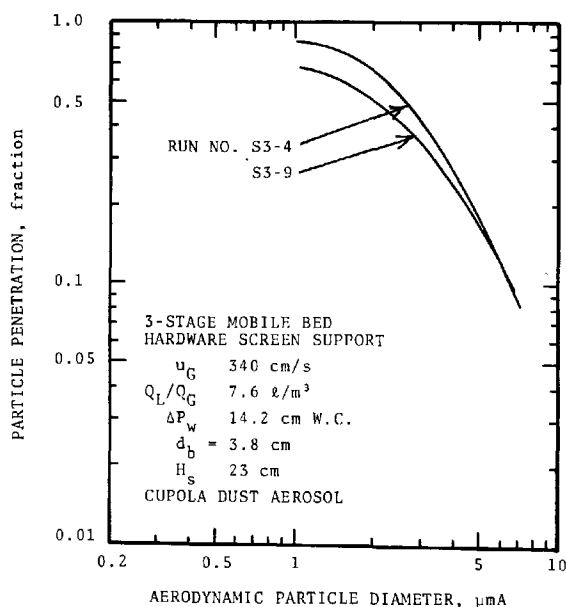


Figure D-4. Experimental penetration curves.

APPENDIX "E"  
GRADE PENETRATION CURVES FOR F/C RUNS

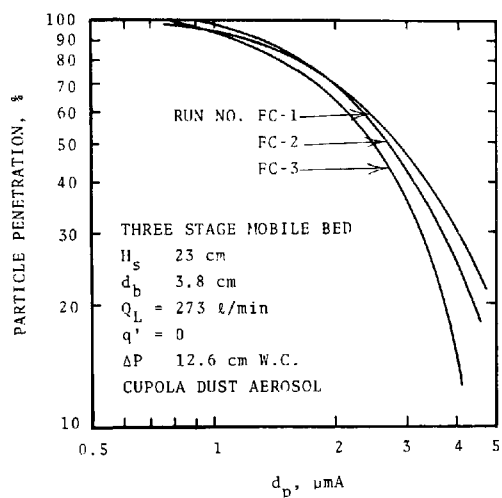


Figure E-1. The penetration curve for Runs No. FC-1, FC-2 and FC-3.

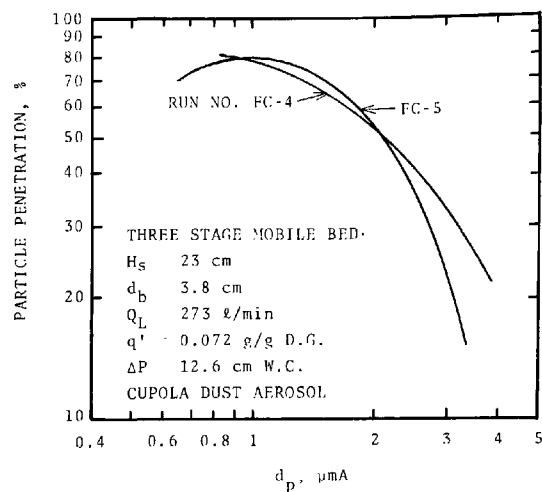


Figure E-2. The penetration curve for Runs No. FC-4 and FC-5.

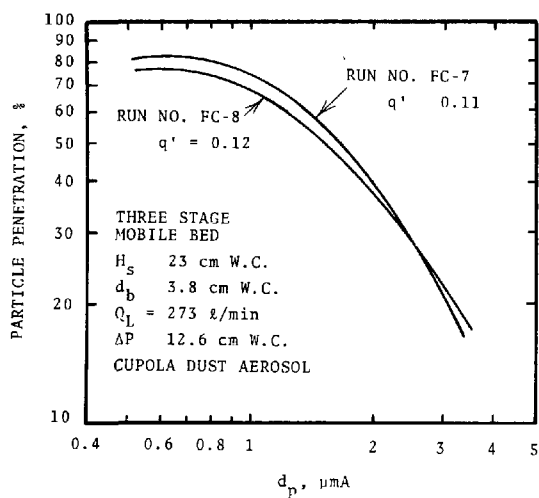


Figure E-4. The penetration curve for Runs No. FC-7 and FC-8.

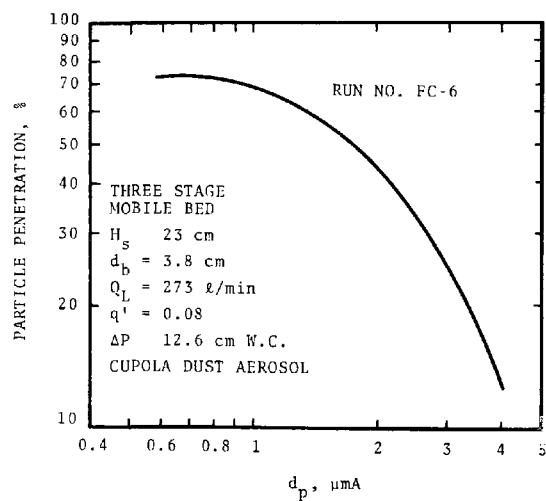


Figure E-3. The penetration curve for Run No. FC-6.



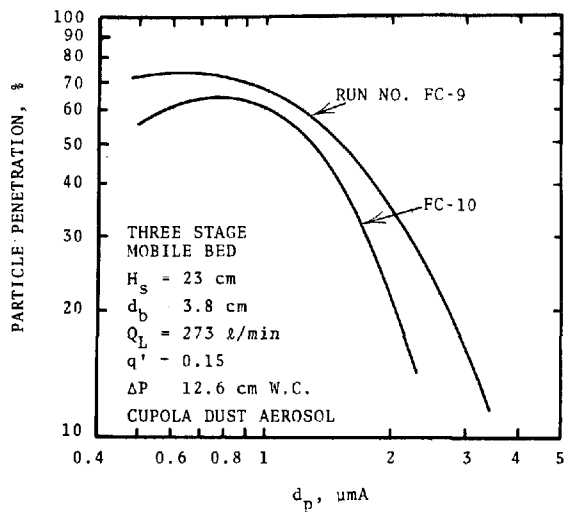


Figure E-5. The penetration curve for Runs No. FC-9 and FC-10.

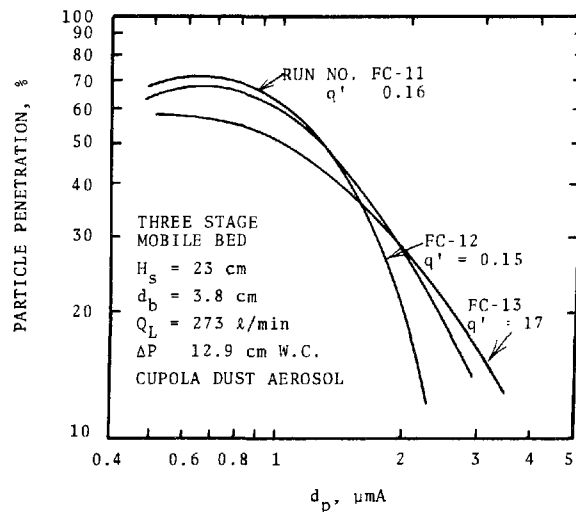


Figure E-6. The penetration curve for Runs No. FC-11, FC-12 and FC-13.

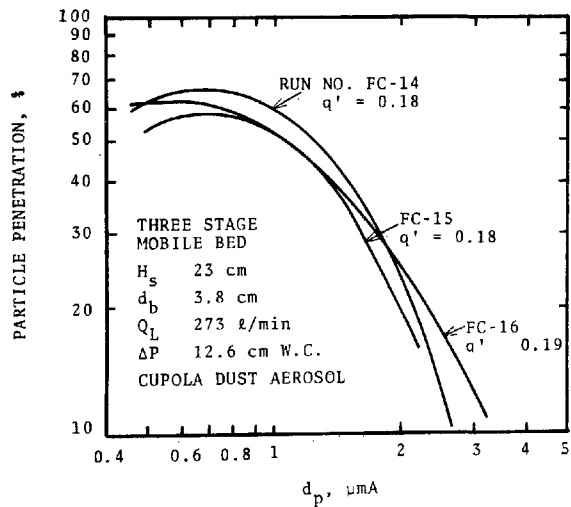


Figure E-7. The penetration curve for Runs No. FC-14, FC-15 and FC-16.

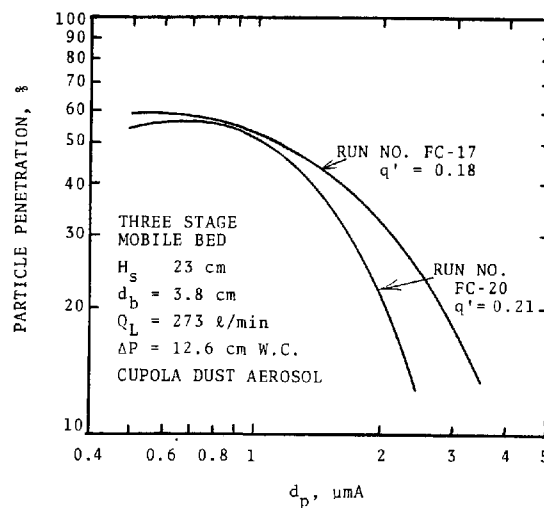


Figure E-8. The penetration curve for Runs No. FC-17 and FC-20.

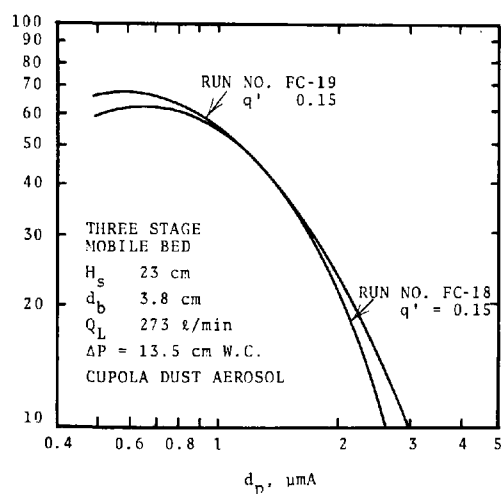


Figure E-9. The penetration curve for Runs No. FC-18 and FC-19.

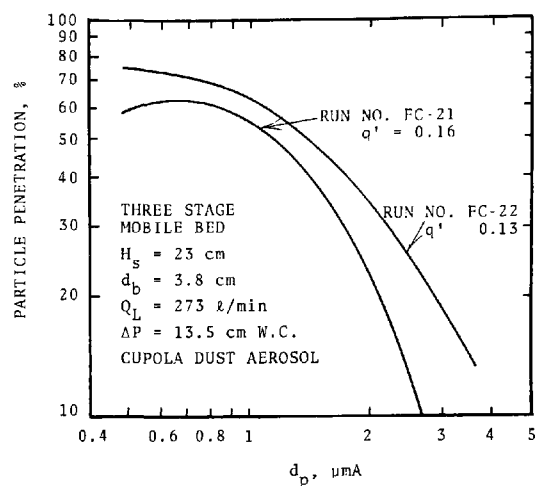


Figure E-10. The penetration curve for Runs No. FC-21 and FC-22.

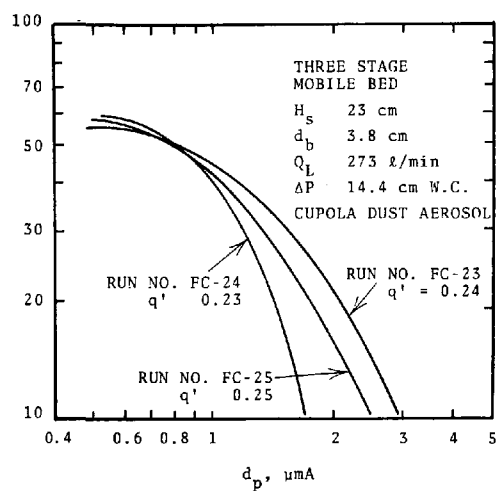


Figure E-11. The penetration curves for Runs No. FC-23, FC-24 and FC-25.

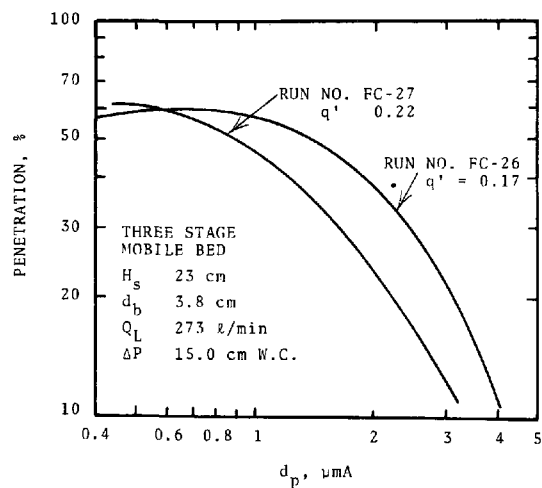


Figure E-12. The penetration curves for Runs No. FC-26 and FC-27.

# **TECHNICAL REPORT DATA**

*(Please read Instructions on the reverse before completing)*

1. REPORT NO. <b>EPA-600/7-79-071</b>		2.		3. RECIPIENT'S ACCESSION NO.	
4. TITLE AND SUBTITLE <b>Mobile Bed Flux Force/Condensation Scrubbers</b>				5. REPORT DATE <b>February 1979</b>	
				6. PERFORMING ORGANIZATION CODE	
7. AUTHOR(S) <b>S. C. Yung, R. Chmielewski, and S. Calvert</b>				8. PERFORMING ORGANIZATION REPORT NO.	
9. PERFORMING ORGANIZATION NAME AND ADDRESS <b>Air Pollution Technology, Inc. 4901 Morena Boulevard, Suite 402 San Diego, California 92117</b>				10. PROGRAM ELEMENT NO. <b>EHE624A</b>	
				11. CONTRACT/GRANT NO. <b>68-02-2124</b>	
12. SPONSORING AGENCY NAME AND ADDRESS <b>EPA, Office of Research and Development Industrial Environmental Research Laboratory Research Triangle Park, NC 27711</b>				13. TYPE OF REPORT AND PERIOD COVERED <b>Final; 11/75 - 12/78</b>	
				14. SPONSORING AGENCY CODE <b>EPA/600/13</b>	
15. SUPPLEMENTARY NOTES <b>IERL-RTP project officer is Dale L. Harmon, MD-61, 919/541-2925.</b>					
16. ABSTRACT <b>The report gives results of an experimental determination of fine particle collection in mobile bed scrubbers. Particle collection efficiency increased greatly as the gas-phase pressure drop increased. With no water vapor condensation, the performance capability of a mobile bed scrubber is less than that of a gas-atomized spray scrubber with the same pressure drop. Compared to packed bed and sieve plate scrubbers, the mobile bed scrubber has better efficiency when the pressure drop is above 20 cm W.C. Limestone in the scrubber liquid has no effect on particle collection. When the mobile bed scrubber was used as a flux force/condensation (FF/C) scrubber, it had better performance characteristics than sieve plate and spray scrubbers with condensation. However, its capability is inferior to a FF/C system consisting of a condenser and venturi scrubber. Design equations reported in the literature are inadequate to predict the collection efficiency and pressure drop of the mobile bed scrubber. The study developed new correlations to predict particle collection and pressure drop.</b>					
17. KEY WORDS AND DOCUMENT ANALYSIS					
a. DESCRIPTORS		b. IDENTIFIERS/OPEN ENDED TERMS		c. COSATI Field/Group	
Pollution Scrubbers Dust Aerosols Flux Density Condensing		Pollution Control Stationary Sources Mobile Bed Scrubbing Particulate Flux Force/Condensation		13B 07A, 13I 11G 07D 14B	
18. DISTRIBUTION STATEMENT  <b>Unlimited</b>		19. SECURITY CLASS (This Report) <b>Unclassified</b>		21. NO. OF PAGES <b>261</b>	
		20. SECURITY CLASS (This page) <b>Unclassified</b>		22. PRICE	